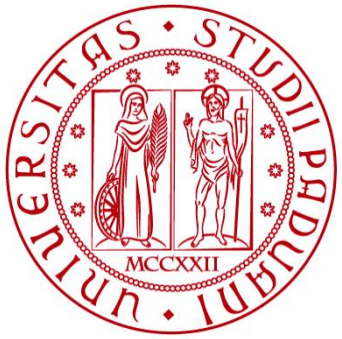

UNIVERSITÀ DEGLI STUDI DI PADOVA

Sede Amministrativa: Università degli Studi di Padova

Dipartimento di Scienze Chimiche

Dottorato in Scienze e Ingegneria dei Materiali - PhD School in Materials Science and Engineering

XXIX CICLO

Development of Innovative Ceramic Materials for ElectroCatalysis

Coordinatore: Ch.mo Prof. Gaetano Granozzi

Supervisore: Ch.mo Prof. Alessandro Martucci

Dottorando: Andrea Paduano

“Nothing is impossible! Not if you can imagine it. That's what being a scientist is all about!”

Prof. H. Farnsworth

Summary

1. Introduction

In this chapter we will briefly outline in which context the argument of this thesis has been developed and the main motivations. The main goal is the development of innovative ceramic powders that should be used as anodic supports for electrocatalysis.

1.1. Direct Ethanol Fuel Cells

A rapid transition from fossil to more sustainable energy sources is mandatory in the next years. Fuel cells (FCs) represent a promising and flexible technology to convert the chemical energy stored in fuels into electricity with a high efficiency, applicable both in stationary and mobile applications. Hydrogen is often discussed as the energy carrier of choice for use in FCs, and hydrogen based FCs (H-FCs) represent the most efficient and clean FCs, since the exhaust is solely water. However, there are some serious hurdles for the application of H-FCs: hydrogen is not a natural resource and it is normally produced by hydrocarbon steam reforming or by water electrolysis. The latter represents a significant waste of primary energy, only sustainable if electricity from renewable sources is available. Moreover, issues regarding hydrogen storage and distribution need to be solved, especially in the transportation sector. Hence, there is a need for the implementation of alternative energy carriers into FCs.

Bioethanol is an attractive alternative energy carrier [1], especially when it is not produced at the expense of food production, e.g. by fermentation of lignocellulose, which uses crop or wood as precursors [2-6]. Bioethanol is produced by converting biomass into sugars, which are then fermented to ethanol (EtOH). The process of hydrolysis separates most of the water from EtOH, leaving an end product that is generally about 95% EtOH and 5% water. Such a composition is optimal for the direct use of bioethanol as energy carrier for FCs (to be reminded that in the case that bioethanol is used as a fuel for standard engines, the water has to be removed with the consequent costs). Use of bioethanol results in a neutral carbon footprint, i.e. the carbon dioxide (CO_2) emitted during its use is offset by the absorption from the atmosphere during its growth. It is considered an alternative to petroleum and diesel and its popularity is emerging as a fuel for cars, particularly well established in Brazil. Bioethanol has a number of advantages over conventional fuels. It comes from a renewable and not from a finite resource, such as crops. These crops are specifically grown for energy use and include corn, maize and wheat crops, waste straw, willow

and popular trees, sawdust, reed canary grass, cord grasses, Jerusalem artichoke, myscanthus and sorghum plants. There is also on-going research and development into the use of municipal solid wastes to produce EtOH.

Therefore, development of efficient FCs exploiting a direct conversion of the chemical energy stored in EtOH into electricity would have a tremendous impact on FC technology and commercialization.

The Direct Ethanol Fuel Cell (DEFC) in principle would have many advantages with respect to H-FCs:

- The energy density of EtOH (8 $kJkg^{-1}$) is higher than that of hydrogen and comparable to gasoline;
- EtOH is a liquid at room temperature and relatively non-toxic, which allows for a simple storage and use;
- The DEFC can in principle directly convert EtOH to CO_2 (Ethanol Oxidation Reaction, EOR) without reforming: breaking down EtOH molecules to produce CO_2 would release far more electrons (a total of 12 per molecule) and generate higher currents (see Figure 1.1);

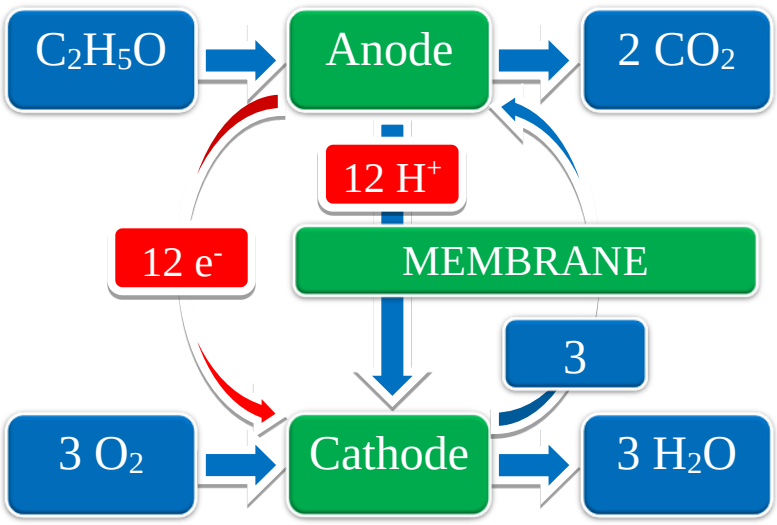

Figure 1.1: Schematic drawing of the conversion of EtOH (C_2H_5OH) into CO_2 in a DEFC.

However, existing catalysts convert EtOH into acetic acid and acetaldehyde, a process that releases just a couple of electrons per EtOH molecule, hence generates low currents. For a complete EtOH oxidation to CO_2 at the anode, the carbon-carbon bond needs to be broken, which requires both higher operating temperatures (in the 150- 200°C range, often referenced as intermediate-*T*) [7] and the use of appropriate catalysts.

Thence, for an efficient design of a DEFC a number of questions still have to be addressed, mainly because the technological solutions so far optimized for standard hydrogen polymer electrolyte membrane (PEM) FCs (which usually operate at low temperature 60 – 120°C) are not directly transferable to DEFC [8]s.

To this end the contribution from the methods and tools of the emerging field of Nanoscience&Nanotechnology can play a relevant role. When the catalyst is dispersed into nanodimensional objects (i.e. nanoparticles, NPs), the nano-catalyst becomes much more efficient due to the higher intrinsic specific surface area, and due to the new active chemisorption sites peculiar for the NPs themselves. The big challenge is the stabilization of the nano-catalysts, which have a low intrinsic stability. In this context, the interaction with the catalyst support plays a major role, both for the stabilization of the nano-catalyst and for the innovative chemical properties induced by the nano-catalyst/support interaction. It is commonly recognized that also the catalyst support plays a pivotal role in both activity and durability of the nano-catalyst itself.

Besides being stable (chemically and electrochemically in the operating potential and temperature ranges and in the used electrolyte) and conductive, the support should be specifically tailored to avoid degradation of the active catalyst due to events such as metal dissolution, sintering, as well as agglomeration induced by temperature and electrochemical potential [9]. In general, a well-matched physicochemical and electronic metal-support interaction is beneficial to improve both the activity and durability of the catalyst. It is noteworthy that according to the DOE (Department Of Energy, USA) the targeted durability for PEM-FCs systems is 5 kh and 60-80 kh for mobile applications and stationary applications, respectively [10]. Reaching these values when operating at intermediate-*T* becomes even more difficult using standard carbon-based supports [11]. Thus alternative support materials are required in order to increase the electrode lifetime for intermediate-T DEFCs.

The best methodological route to face such challenges is to adopt a rational design of the nano-catalyst/support assembly aiming at *efficient electrodes*, mainly based on an approach where the outcome of rigorous studies on *model electrodes* are capitalized to implement efficient *real electrodes* to be properly tested under realistic working conditions.

Another pivotal point for a widespread FC commercialization relies on reducing (or even avoiding) the noble metal loading in the catalyst without compromising FC performance. State-of-the-art catalysts for both anode- and cathode-side are based on noble metals, especially platinum. Among the components in a PEM-FC, Pt-based electrodes contribute to ca. 55% of the total costs [12].

As an example, in the automotive field, a FC stack needs the power of about 100 kW. A state-of-the-art Pt/C electrode has a Pt specific power density of about 0.5 $g_{Pt}kW^{-1}$ (grams of Pt per kW), and thus 50 g Pt are needed for the required FC stack [13]. Precious metals like Pt are expensive (~30 € per g_{Pt} on 10.05.2017), but even more critical is the fact that the Pt resources are limited and they are confined outside of EU in countries that are not extremely politically stable. The annual production of Pt is currently estimated to some 220 t with a clear trend for further increase. Short supply coupled with an expected increasing demand, is likely to cause prices to rise in the future.
Considering these facts, it is highly strategic to investigate alternative catalyst materials where the precious metal is reduced or completely avoided.

1.2. DECORE: An European project

The arguments reported above were at the basis of an European Project called DECORE (**D**irect **E**lectro**C**hemical **O**xidation **R**eaction of **E**thanol: optimization of the catalyst/support assembly for high temperature operation) [14], which started on January 2013 under the coordination of the University of Padova (Prof. Granozzi). The main general goal of DECORE is to achieve the fundamental knowledge needed for the development of a FC electrode, which can operate efficiently (both in terms of activity and selectivity) as the anode of a DEFC in the intermediate-T range. Such a technology is still lacking in the market. The choice for EtOH as an alternative energy source was founded on the abundance of bioethanol, and on the relatively simpler storage and use with respect to other energy carriers. The intermediate-T is required for an efficient and selective total conversion of EtOH to CO_2, so exploiting the maximum number of electrons in the DEFC. DECORE is exploring the use of fully innovative supports (based on titanium oxycarbide, TiO_xC_{1-x}) and nano-catalysts (based on group 6 metal carbides, MC_x, M=Mo, W), which have never been tested in literature as anodes for DEFCs. The new support is expected to be more durable than standard carbon supports at the targeted temperature [11, 15]. The innovative nano-catalysts would be noble-metal free, so reducing Europe's reliance on imported precious metals. To tailor the needed materials, the active role of the support and nano-catalyst will be studied at atomic level. Demonstrating an activity of such nano-catalyst/support assembly at intermediate-T would open a novel route where DEFCs with strongly reduced production costs would have an impact on a fast industrialisation. The power range for the envisioned application is of the order of hundreds of Watts,

i.e. the so called distributed generation, having an impact for devices such as weather stations, medical devices, signal units, auxiliary power units, gas sensors and security cameras.

1.3. MAX phases: the meeting point for metals and ceramics

Another support can be searched amongs a new class of ceramic materials, called MAX Phases, with interesting properties because they show typical behaviors from the metals beside ceramic attributes. The MAX Phases form a large family of ternary carbides with the general formula $\mathbf{M}n_{+1}\mathbf{AX}n$, where n = 1–3, **M** is an early transition metal, **A** is an A-group element (mostly IIIA and IVA), and **X** is C and/or N. They show electrical and heat conductivity, ductility and thermal shock resistance like metals but at the same time they have high temperature tolerance and acid and corrosion resistance. They were already utilized in harsh environments, like gas burner nozzles or high current contacts, but, despite the promising characteristics the spreading is very limited because of their very high prices that don't justify the exceptional properties. A new use as anodic support is tested for the first time, showing that new ceramic materials could be used for non-standard applications in the electrocatalysis field at intermediate-T. The development of reaction synthesis methods from less-expensive precursor powders, such as TiO2 instead of pure titanium and TiC would constitute a major breakthrough.

1.4. Thesis outline

In this work we followed two different branches, corresponding to two different type of ceramic powder. Firstly we tried to obtain TiO_xC_{1-x} powders with defined stoichiometry and large surface area (i.e. >100 m^2g^{-1}), with the objective of employing it as the anode in the DECORE DEFC. In order to obtain high porosity and an acceptable stoichiometric control, in the present work we have adopted two different molecular approaches: one starts from a nanostructured template made of elemental carbon, (Cabot Corp. XC 72 [16] and Ensaco 350G [17]), that is impregnated with a titanium dioxide precursors; the other uses organic precursors as the source for both carbon and titanium dioxide. In the first approach the porosity is determined by the carbon template, in the second one by the production of gaseous by-

products from the precursors. The obtained powders were decorated with various nanoparticles to study the electrocatalytic behavior for the oxidation of ethanol. The two approaches and the decoration are described in Chapter 3.2, and each is followed by the experimental results and analysis. The characterization techniques employed to study the synthesized samples are introduced in Chapter 2. At the end of each Chapter we summarized the overall achievements obtained through this experimental work, and try and outline the possible outcomes and directions for the future research activity.

The second branch we explored consists in the vast family of MAX phases. We focused our studies on three compositions, trying to synthetize them with high purity and reproducibility. In a first time we tried to adapt the organic precursors used before tailoring them to the new requirements, but this path proved to be unsuccessful. Afterwards we walked the more conventional path of solid state sintering, adapting the various parameters to our needs. These powders were decorated with nanoparticles and the electrochemical properties were briefly investigated. The two paths and the obtained results are described in Chapter 4.

2. Characterization Metods

XRD

In order to determine with precision the composition of the solid solution of TiO_xC_{1-x} and to identify unwanted phases, the most usefull technique is X-Ray Diffraction (XRD).

For the X-ray diffraction we used two different diffractometers. For samples available in small amounts (< 1 gram) we used a Philips PW 1729, configured with a glancing angle geometry, while for samples available in larger amounts we used a Bruker D8 Advance with a Bragg-Brentano geometry.

For the glancing angle measurements, the sample was first ground in a mortar and then homogeneously distributed on a microscopy glass slide partially covered with double sided tape. This particular sample holder configuration determined the presence of a characteristic background pattern that can be seen in Figure 2, due to the glass support and the tape.

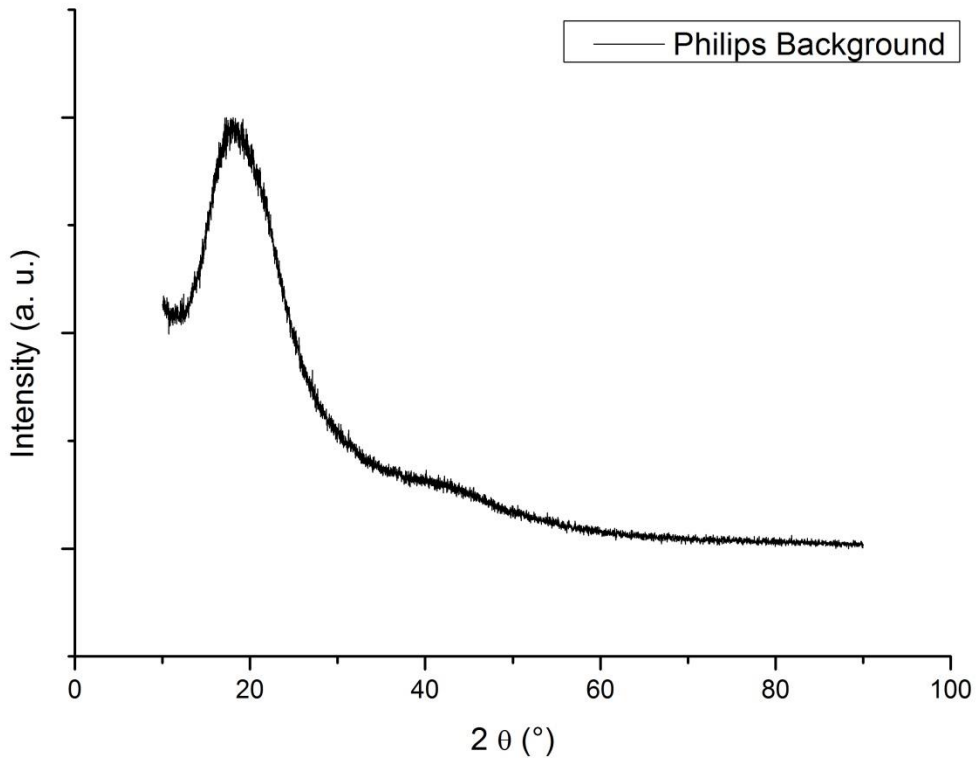

Figure 2, glass slide and double sided tape used as powder support for Philips diffractometer

When the sample weighted more than 1 gram we used the Bruker diffractometer. The sample was first ground and then put on an aluminium sample holder. Then the powder was gently pressed and the surface smoothed with the help of a laboratory spatula.

The composition of each sample is determined from XRD data. TiO_xC_{1-x} is a solid solution of the two different cubic phases (Fm-3m) of TiO and TiC. The dependence of the cell parameter of the solid solution on the relative oxygen and carbon content, presents significant deviations from the ideal linear behavior described by Vegard's law. In literature such behavior was discussed by Neumann et al. [18]. Taking their work as reference, we determined a non-linear function that well fits (R^2 = 0,999) their experimental data in the whole compositional range.

From this curve, we determined the fit function, as can be seen in Figure 3.

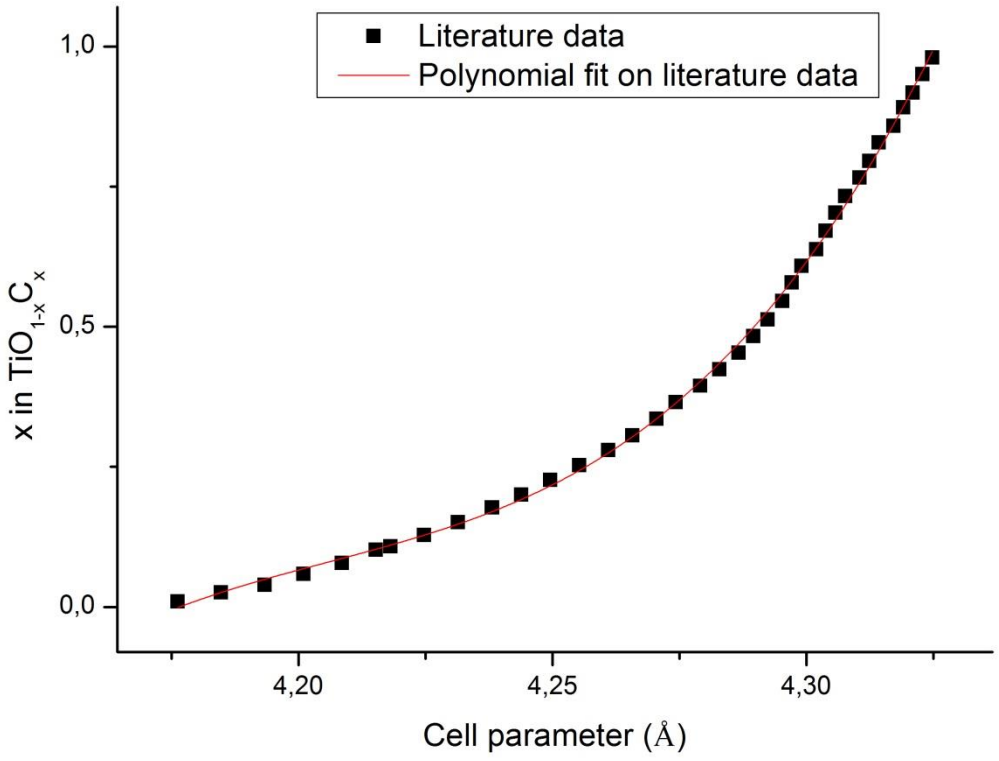

Figure 3, experimental curve [18] and fitted function for C content vs. cell parameter in TiO1-xCx

Moreover the cell parameter for TiO varies experimentally with the oxygen content, as stoichiometric TiO is difficult to obtain due to the tendency to lose O_2, thus becoming TiO_{1-x}, with$0 < x < 0,05$ and the formation of vacancies.

The cell parameter calculated by the diffractograms can be used to estimate the relative content of O and C in the TiO_xC_{1-x} powder. We used a 3rd order polynomial fit on the data found in literature with the following formula:

$$x = A_0 + A_1 y + A_2 y^2 + A_3 y^3$$

with x the relative C fraction in $TiO_{1-x}C_x$, while A_0, A_1, A_2, A_3 are parameters optimized in order to reduce R^2. In Table 1 the values and relative errors of the parameters are reported.

	A_0	A_1	A_2	A_3
Value	-27808.6	19829.91	-4714.02	373.5891
Error	1814.508	1279.744	300.8444	23.57304

Table 1,values and errors for the fitting parameters of equation $x = A_0 + A_1 y + A_2 y^2 + A_3 y^3$

The cell parameter can be calculated from the peak position 2θ, using Bragg's law:

$$n\lambda = 2d \sin\theta$$

$$d = \frac{n\lambda}{2 \sin\theta}$$

where d is the interlayer distance. The typical pattern of TiC or TiO shows five characteristic peaks, each corresponding to a defined crystallographic plane that arises from the [111], [200], [220], [311] and [222] planes. With n=1, the cell parameter d_{cell} is derived from the interlayer distance. For the cubic Fm-3m lattice:

$$for\ the\ [111]\ peak: d_{cell} = \frac{\sqrt{3}\lambda}{2 \sin\theta}$$

$$for\ the\ [200]\ peak: d_{cell} = \frac{\lambda}{\sin\theta}$$

$$for\ the\ [220]\ peak: d_{cell} = \frac{\sqrt{2}\lambda}{\sin\theta}$$

$$for\ the\ [311]\ peak: d_{cell} = \frac{\sqrt{11}\lambda}{2\sin\theta}$$

$$for\ the\ [222]\ peak: d_{cell} = \frac{\sqrt{3}\lambda}{\sin\theta}$$

The five characteristic peaks for the TiO_xC_{1-x} phase are located in the surrounding of five different angles, that are ~36°, ~42°, ~61°, ~73° and ~77°.

The MAX phases, instead, don't show stoichiometric shifts in composition; the presence of one phase or another can be evaluated by the presence of the different peaks, ascribable to each phase.

SEM

For the morphology and surface analysis we used a Zeiss Supra 35VP FEG SEM. The samples were loaded in the microscope chamber on copper supports with carbon tape. The microscope was set to an accelerating voltage of 10 kV.

BET

For the surface area analysis we used a Quantachrome Nova 1200E. For each analysis 50 mg of ground samples were loaded in the glass analysis vial. The surface area of our samples is determined with gas absorption using Brunauer–Emmett–Teller (BET) theory [19]. For the pore distribution, DFT simulation with the best fitting function were performed with the software supplied with the machine.

DTA/TGA

For the thermogravimetric analysis we used a Netzsch STA 409. Few mg of each analysed samples were loaded on the Netzsch alumina crucible. The analyses were conducted in air or controlled Argon atmosphere depending on the analysis type.

FTIR

For the analysis in the infrared range we used a Jasco FT/IR 620, a Fourier transformate IR. We used anhydrous KBr to make pellets incorporating our samples or used ATR configuration.

RAMAN

For a more complete analysis of the chemical bonding of our samples we used laser Raman microspectroscopy (Renishaw inVia Raman Microscope) using a 514 nm (green) argon ion laser at 25 kW.

Cyclic Voltammetry

For an electrochemical study of the behavior of the samples, we used an Autolab PGStat 101 potentiostat with the correlated software to control the measure parameters or a Nordic Electrochemistry ECi-200 potentiostat with the EC4 software. A platinum wire was used as counter electrode, while for the reference electrode we used a standard hydrogen electrode (SHE or RHE) or a saturated calomel electrode (SCE).

3. Titanium oxycarbide ceramics

3.1. Introduction

The titanium oxycarbide is a ceramic material made by a solid solution of TiO and TiC with variable stoichiometry (TiO_xC_{1-x}, with $0 \leq x \leq 1$). It shows particular properties, all due to the mixing and union of the different phases. In fact, it has the corrosion resistance proper of TiC [20] but it has also the electrical conductivity of the TiO; therefore, it is a promising candidate for an anodic support of a fuel cell [21].

It can be synthetized in different ways to obtain a powder with defined stoichiometry and large specific surface area (>100 m^2g^{-1}). The main strategies with the typical reactions are listed here after

- $TiO_2 + C \rightarrow TiO_xC_{1-x} + xCO$

  An immediate solution is based on the solid state reaction of elemental carbon and titanium dioxide. In fact, the reaction follows a more complex pathway as TiO_2 upon heating in inert atmosphere [22] undergoes first the loss of oxygen and then at higher temperatures the carburization starts following the next reactions:

$$TiO_2 \rightarrow TiO + \frac{1}{2}O_2$$

$$TiO + C \rightarrow TiO_xC_{1-x}$$

  Instead of elemental carbon and titanium dioxide [23, 24], different carbon based materials [25-29] and titania precursors can be used. The carbon source can also act as a template for high surface area powders and it is possible to achieve a mixing at the nanoscale level between the precursors.

- $xTiO + yTiC \rightarrow TiO_xC_y$

  An alternative path can be the reaction of titanium monoxide and titanium carbide [18, 30]. The main disadvantage of this reaction is that large surface areas are not easily achievable [31-33] due to the scarce availability of nanosized powders of said precursors, sintering effects during the thermal treatment required for the reaction to proceed, and the difficulty in post-synthetic milling of the powders because of their intrinsic hardness.

- $TiC + O_2 \rightarrow TiO_xC_y + CO$

  This reaction [34-37] should be feasible in principle but it's kinetically difficult, and requires particular reaction conditions (high vacuum, oxygen plasma) that make it a quite unpractical alternative.

- $TiO_2 + CH_4 \rightarrow TiO_xC_y + H_2O + CO$

  The reaction between titanium dioxide and methane [38, 39], or other hydrocarbons like ethan, propane or ethylene [40], is an interesting way to synthesize oxycarbides. In order to obtain high specific surface areas, the titania substrate has to act as the templating agent and therefore to be highly porous. Furthermore, the carburization of the substrate takes place at high temperatures and proceeds very fast, yielding TiO_xC_{1-x} powders with high carbon content.

Based on preliminary results obtained in my Master Thesis, we started to investigate the feasibility of the first reaction path, using carbon black as carbon source and templating agent. Then we started to develop a new path that promised better results, both in stoichiometry control both in achievable surface areas, using methyl cellulose and a titanium complex. We further investigated and improved the two synthesis paths, changing reagents or refining the conditions and parameters of the reactions. We tried to use different carbon precursors as templating agent in order to increase the specific surface area and different titania precursors to have better wettability and impregnation. We also tried to improve the yet promising methyl cellulose path, including in the solution different metals' precursors as platinum or tungsten and trying different drying paths.

Firstly we focused on the synthesis of $TiO_{0.5}C_{0.5}$, as it should be the best compromise regarding acid resistance and electric conductivity.

Once found the best conditions for an optimal product, we investigated also how the titanium oxycarbide behave in a half cell if decorated with catalyst nanoparticles. Commercial catalysts are made of pure platinum or gold deposited on carbon supports, but the goal of the DECORE project is to find a cheaper alternative with different metals as molybdenum or tungsten and a more stable support. We searched for a path to grow nanoparticles on the surface of the titanium oxycarbide, using platinum or platinum alloys in order to check the stability of TiOC in the oxidative ambient of the half cell, meanwhile the research of new and cheaper catalysts is not part of this work.

Several paths were investigated: from the simplest one that consist in the addition of some platinum precursor before the carburization, to the one that is the classical "polyol synthesis" [41, 42], that involves the reduction of platinum and other metals complexes during the heating in ethylene glycol. Another path is an evolution of the polyol because it uses the microwaves as heating agent [43], changing the way the heat is transferred to the solution. This path assures shorter reaction times and higher rates, giving as result nanoparticles with better dimensional dispersion.

Once the nanoparticles were synthetized on the surface of TiO_xC_{1-x}, the powders were tested in a half cell in the expected working conditions at the university of Copenhagen with the help of the group of the professor Matthias Arenz. Various Pt:Sn ratios were made and used, trying to find the best alloy for the oxidation of ethanol. We concentrated not only on the power that can be extracted from the half cell but also on the resistance of the substrate and the nanoparticles. Further studies are needed to investigate the resistance to numerous cycles thoroughly.

3.2. Precursors

3.2.1. Carbon Black

We chose to use carbon black (CB) because of various reasons: it has high specific surface area and can be used as templating agent for the creation of porous ceramics, it is widely available and cheap, and can be easily impregnated with different titania precursors.

The first carbon precursor was the Cabot XC72, a commonly used support for electrochemical application. It has high surface area, in the range of 250 m^2g^{-1}, and a narrow pore distribution, as can be seen in Figure 4.

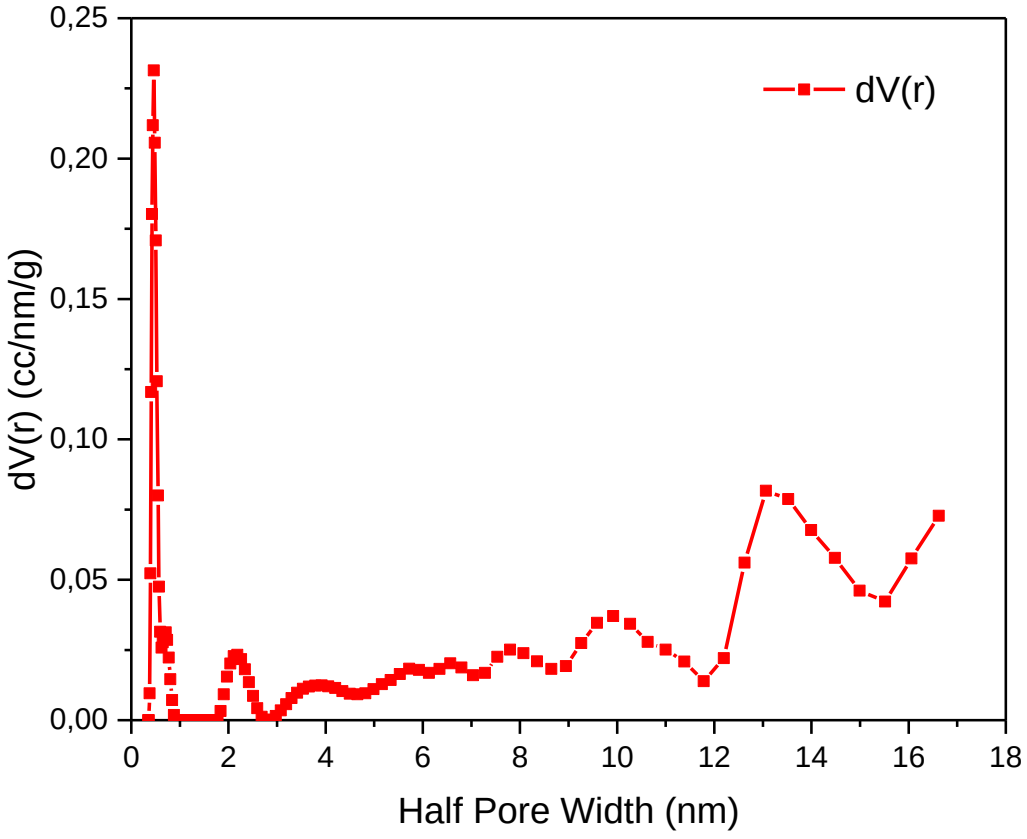

Figure 4, DFT extrapolation of pore distribution for Cabot XC72

The first samples were prepared with titanium isopropoxide (TiPO), a commonly used alkoxide of titanium with formula $Ti(OCH(CH_3)_2)_4$. Titanium isopropoxide readily reacts with water undergoing hydrolysis, as shown in the following reaction:

$$Ti(OCH(CH_3)_2)_4 + 4H_2O \rightarrow Ti(OH)_4 + 4(CH_3)_2CHOH$$

It is enough stable to be handled in air, upon impregnation of XC-72 by TiPO, the latter is partially hydrolyzed by physisorbed and atmospheric moisture to $Ti(OH)_x(OiPr)_{4-x}$, with the concurrent formation of isopropanol as the reaction byproduct [44]. The subsequent drying step had the multiple effect of removing the as-formed isopropanol, promoting the oxolation and condensation reactions, and further increasing the hydrolysis of the remaining alkoxide groups by the oxolation water. Previous work [45] has shown that the potential evaporation of TiPO at room temperature is insignificant. Due to his molar weight of 284,215 g/mol and density of 0,96 g/mL, for each gram of CB the minimum C:Ti ratio is 6,67:1, which would imply according to the stoichiometry of the carburization reaction the full conversion of TiO_2 to TiC. To overcome this stoichiometric limit, the CB powder undergoes multiple impregnation and drying steps in order to reach the wanted C:Ti ratio.

The impregnation and the following drying step are made putting the CB powder in a small plastic vial and the maximum amount of TiPO is added. Then the vial is properly sealed and vigorously shacked in order to wet all the powder. The drying step is conducted in oven at 60°C in air to accelerate the evaporation of isopropanol. Once dry the powder can be impregnated again to reach the desired C:Ti ratio; for $TiO_{0.5}C_{0.5}$ it is 2:1.

It is likely that this repetitive process resulted in concentration of Ti in the pores and hence consequent concentration of TiO_x at these sites. It is possible that this resulted in the counter-intuitive effect of creating a TiO_x-rich core surrounded by a carbonaceous shell at the lower C/Ti ratios. Owing to the potentially large size of the resultant oxide-rich core, carbon reduction and diffusion could be prevented from reaching the interior, leaving a hypostoichiometric (oxide higher than TiO) oxide-rich domain both resistant to reduction and carburization and subject to densification and grain growth. This outcome then would be expected to generate a duplex microstructure.

After the necessary impregnation and drying steps the powder is heat treated in order to start the carburization of the titanium dioxide. The treatment is conducted in a Lenton Furnaces tubular oven, within an alumina tube with argon atmosphere. The first attempts were conducted in order to find the most suitable temperature to conduct the carburization [46], searching the lowest possible temperature.

After several samples we deducted that the ideal C:Ti ratio of 2:1 is not sufficient to guarantee the carburization of TiO_2 to $TiO_{0,5}C_{0,5}$ as expected. As can be seen in Figure 5, the main peaks of TiO_xC_{1-x} are present, but there are also small peaks due to non-stoichiometric titanium oxides.

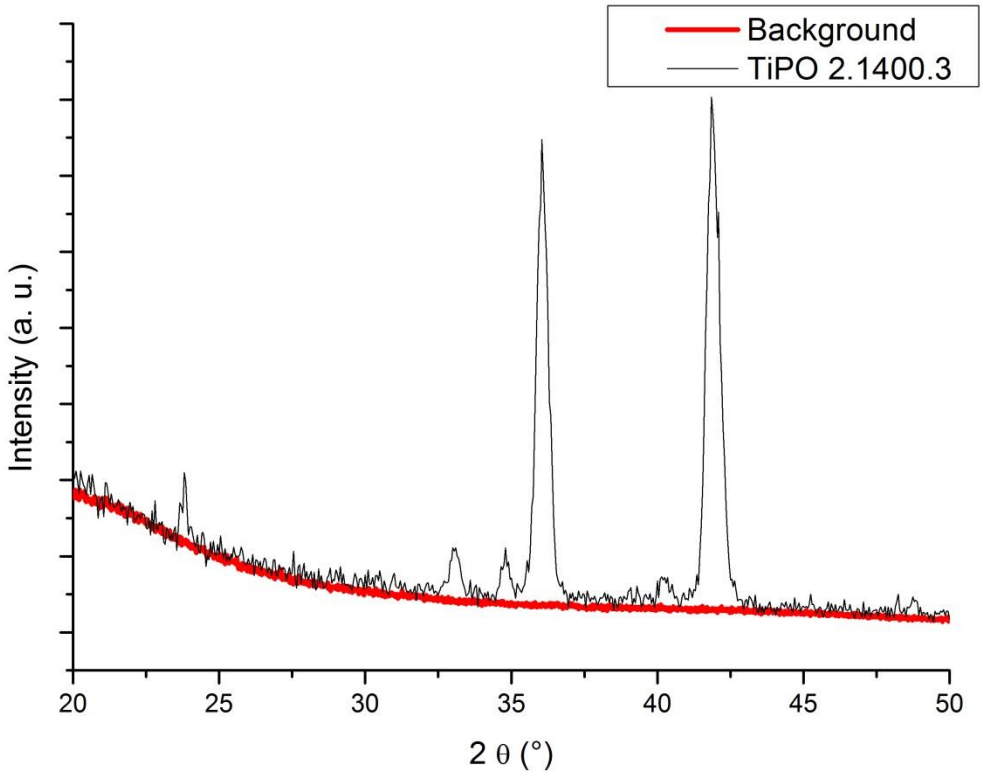

Figure 5, XRD pattern of XC72 impregnated with titanium isopropoxide, C:Ti ratio 2:1, treated at 1350°C for 3 hours

Analyzing the position of the titanium oxycarbide diffraction peaks the cell parameter was estimated to be 4.308 Å[1] and the oxygen content 28%. The carburization was uncompleted because there wasn't a perfect mix between CB and TiPO, leading to areas rich in TiO_2 that underwent a partial reduction during the heat treatment.

After several batches, we made an attempt with an even more rich content of TiO_2. The impregnation route was improved using a vacuum oven in order to dry up completely the samples between one impregnation and the other. With this renewed route we prepared two identical samples, with a C:Ti ratio

[1] Altough Ångstrom (Å) is not an SI unit, it is still commonly and extensively used in crystallography. The following cell parameters will be expressed in Å

of 1.75:1. The two samples were heat treated in different times, to check if the samples don't undergo time dependent alterations.

The XRD pattern of the first sample, heat treated as soon as possible after the preparation, is shown in Figure 6.

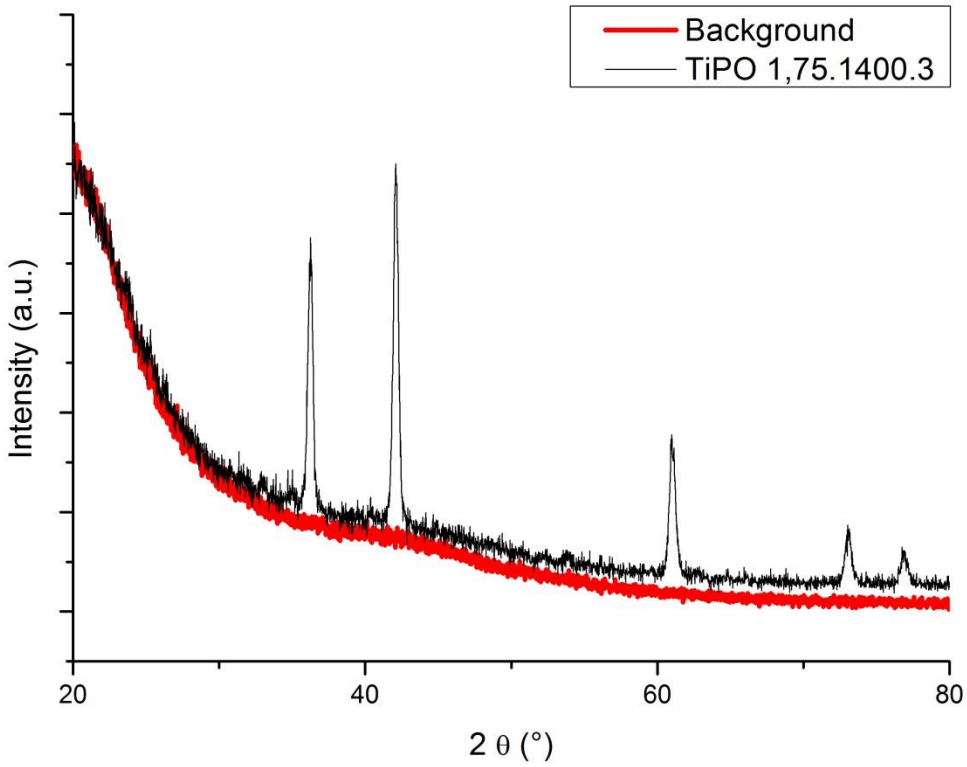

Figure 6, XRD pattern of XC72 impregnated with titanium isopropoxide, C:Ti ratio 1,75:1, treated at 1350°C for 3 hours

The first peak lies at 36.24°, revealing a cell parameter equal to 4.288 Å. Using the correlation between composition and cell parameter found in literature, the oxygen content can be valued at 51%, or, in other word, the stoichiometry is $TiO_{0.51}C_{0.49}$.

The second sample was heat treated three weeks later, and the diffractogram is in Figure 7.

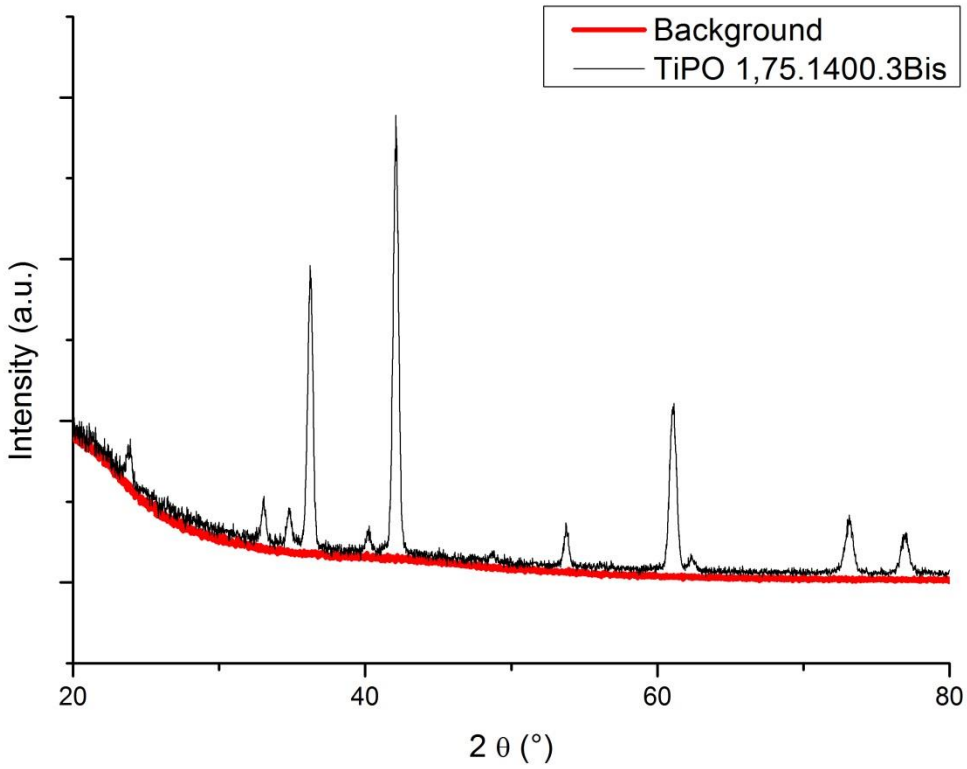

Figure 7, XRD patter of XC72 impregnated with titanium isopropoxide, C:Ti ratio 1.75:1, treated at 1350°C for 3 hours after 3 weeks

As can be easily seen, there are small peaks referable to sub-stoichiometric titanium oxides. The exact cause of that is not clear, perhaps is due to a non-perfect seal of the tube furnace. In any case the first peak of the TiOC phase lies at 36.24°, like the one of the previous sample.

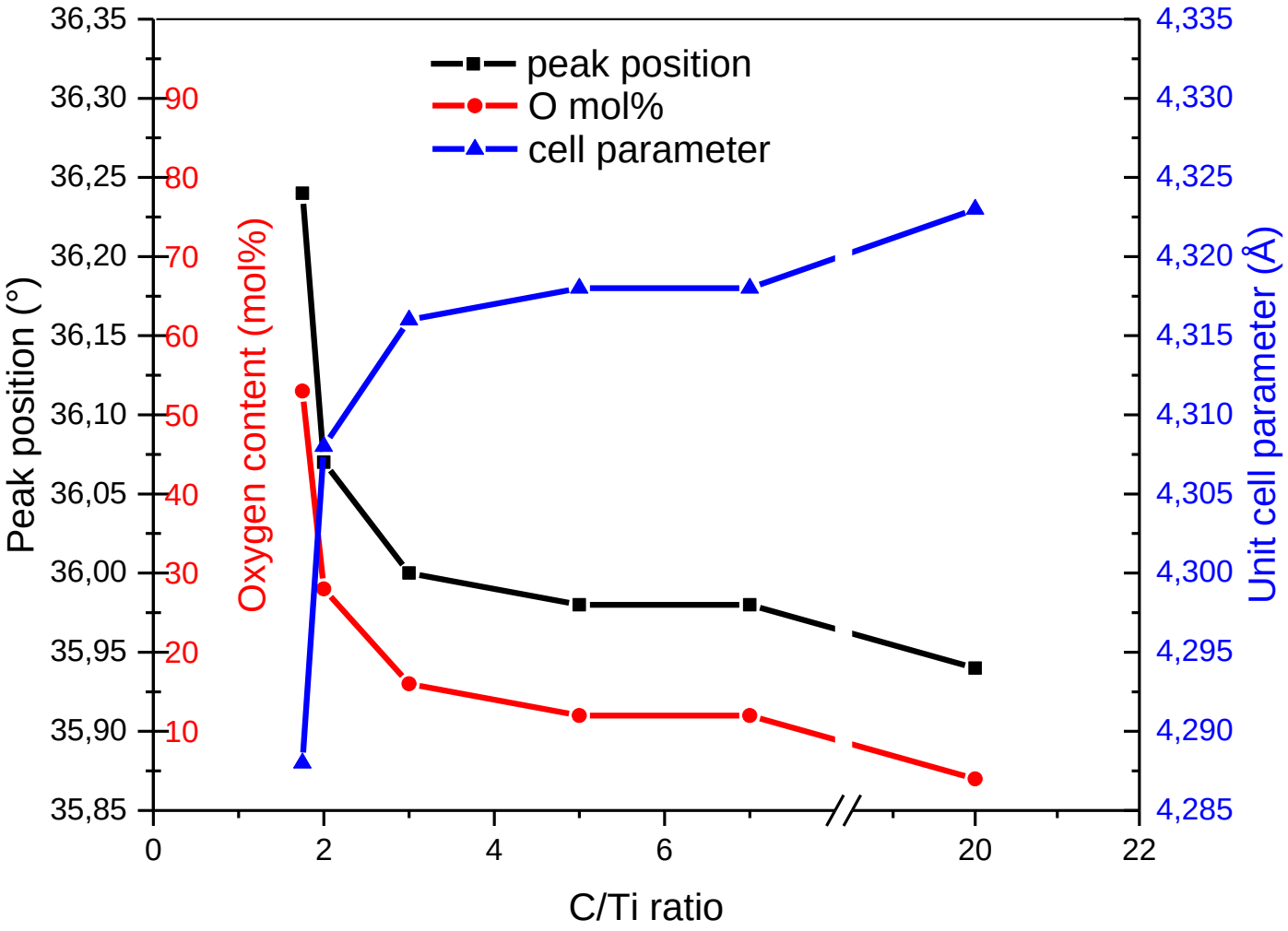

Figure 8, oxygen content, (111) peak position, and unit cell parameter as a function of initial C/Ti ratio for TiOxCy powders following firing (0.4 L min-1 Ar; 3 h at 1400°C)

Including the results obtained in the thesis work, Figure 8 shows the effects of C/Ti ratio on the calculated oxygen atomic percent, (111) peak position and the unit cell parameter. These data indicate that the processing procedures used in the present work allow relatively precise control of the initial and final C/Ti ratios for values ≥2.

For good catalytic properties, the powder has to have a good surface area, about 100 m^2g^{-1}. The CB as is has ca. 250 m^2g^{-1}. The sample prepared from CB and TIPO with 6.67 C:Ti ratio at 1350°C for 3 hours, after the thermal treatment, has a surface area equal to 102 m^2g^{-1}.

A possible contribution to such an elevated porosity might come from the presence of residual carbon species, that would be particularly detrimental for assessing the electrochemical properties of the powder for catalytic applications. To verify the presence and nature of said species, we employed Raman

spectroscopy on the C/Ti 7 sample, before and after firing, along with references of the pure XC-72 and the glass slide substrate. The results are reported in Figure 9. From the spectra analyses it is possible to observe that the characteristic G and D bands of carbon materials [47] at ~1590 cm^{-1} and at ~1380 cm^{-1} are visible for the XC-72 before and after the impregnation with TiPO [47, 48]. However, after firing, the two bands disappear, suggesting that in the carburized powder there are negligible traces of amorphous carbon or graphitic products.

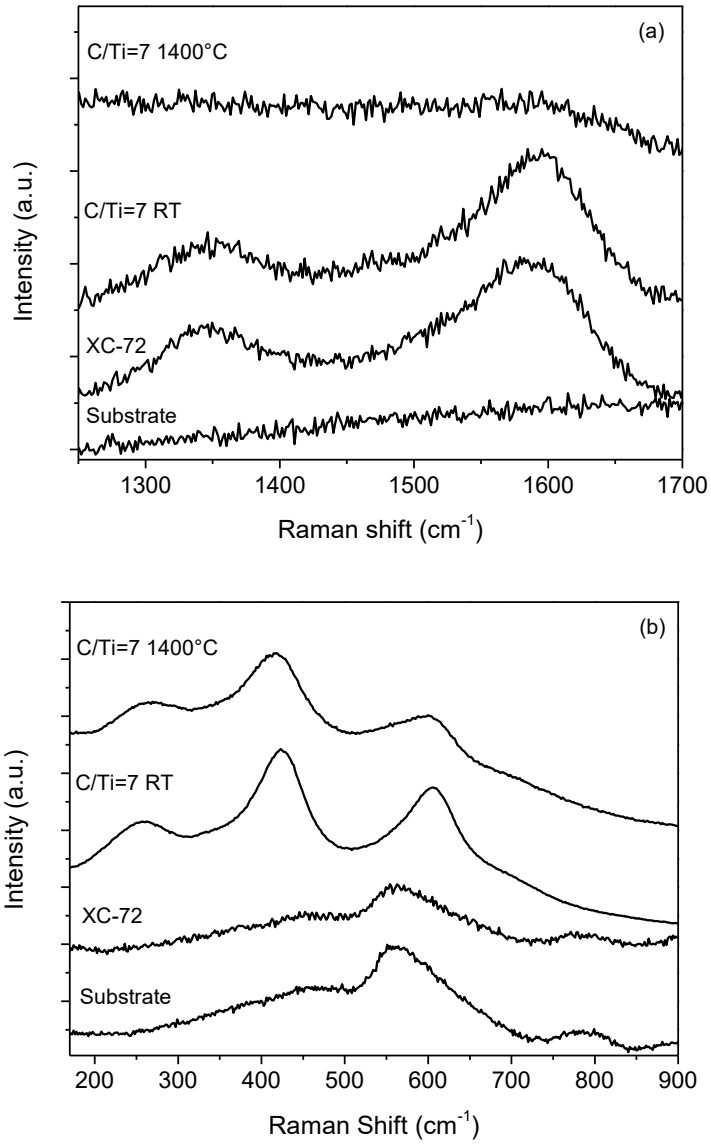

Figure 9, Raman spectra for TiOxCy powders prepared from a starting precursor ratio C/Ti = 7. (a) high frequency region, showing the presence of peaks related to C species for the XC-72 and pre-treatment impregnated sample; (b) low frequency region, showing the presence of Ti-O-C bonds in the impregnated sample, before and after firing

In the low frequency region the analyses of the spectra is more difficult, due to the different contribution of Ti-O-C and Ti-O-H bonds [47, 49]. In the sample of pure XC-72 there are no relevant peaks,

meanwhile after the impregnation three peaks appear at ~260, ~420 and ~600 cm^{-1}. These peaks can be referred to amorphous Ti-O_x and Ti-OH weakly bonded to C. After the heat treatment the position of these peaks is slightly shifted, in agreement with the formation of TiOC, as observed with XRD analysis.

The morphology of our samples was investigated using a scanning electron microscope (SEM) combined with Energy Dispersive X-ray spectroscopy (EDX). The morphology analysis was conducted on the last sample made. We chose this one because it shown in the XRD the presence of numerous peaks ascribable to non-stoichiometric titanium oxides. With this SEM analysis we wanted to investigate if it was possible to physically separate the TiOC phase from the oxide ones. In Figure 10 and Figure 11 the morphology of this sample can be observed.

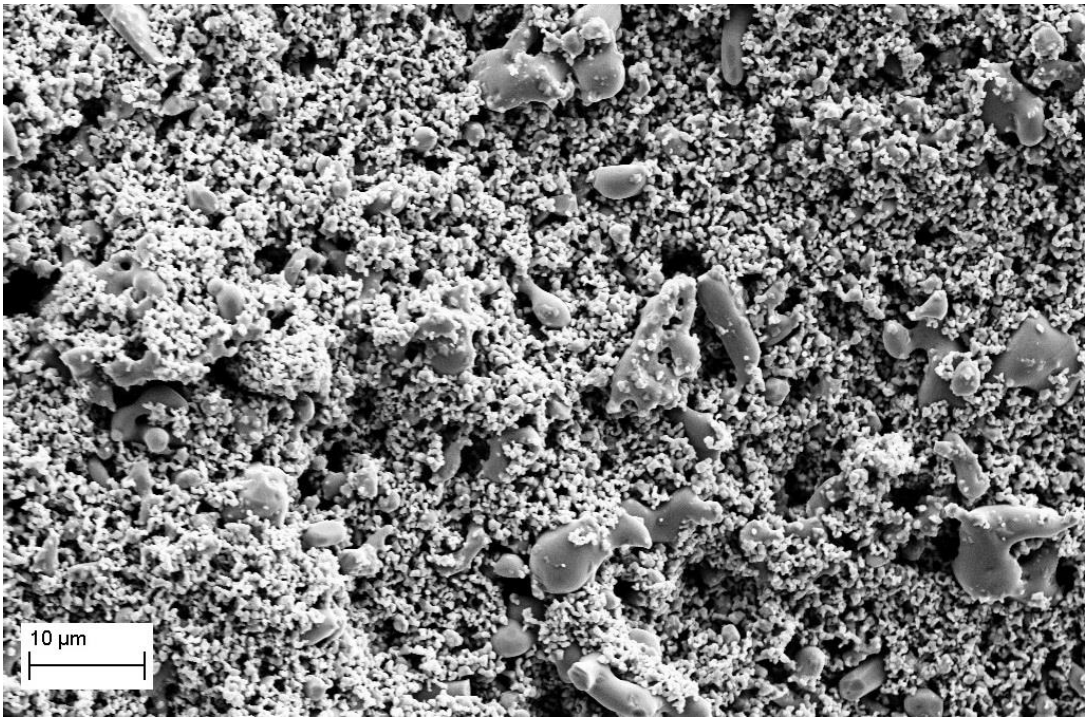

Figure 10, SEM image of XC72 impregnated with titanium isopropoxide, C:Ti ratio 1,75:1, treated at 1350°C for 3 hours

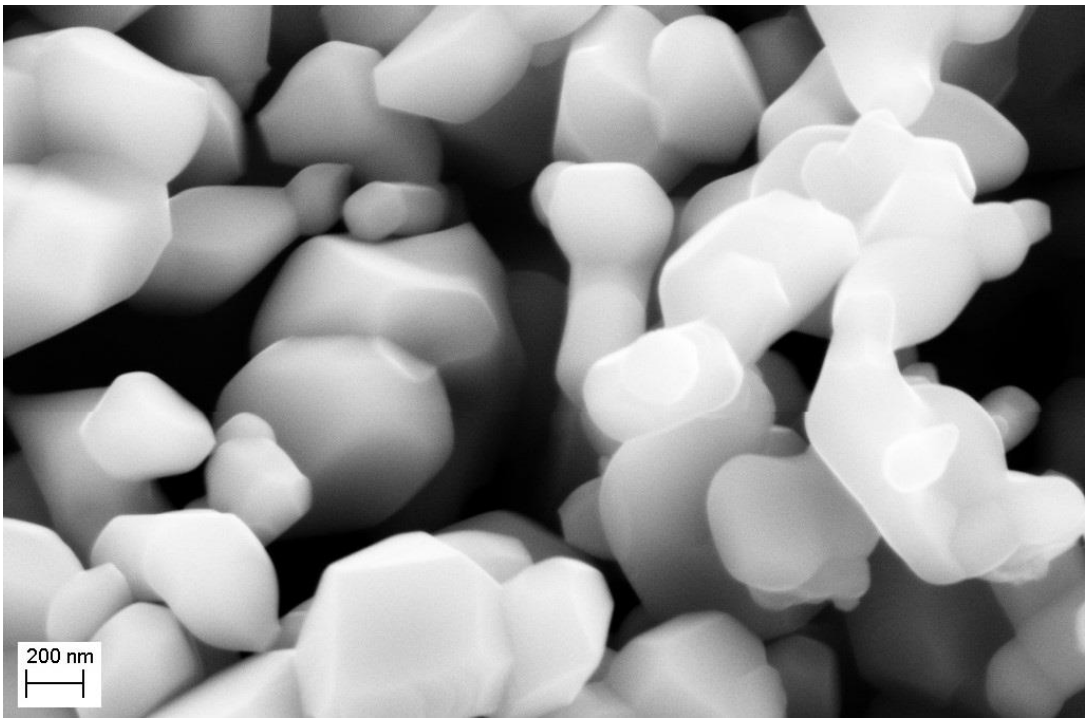

Figure 11, SEM image of XC72 impregnated with titanium isopropoxide, C:Ti ratio 1,75:1, treated at 1350°C for 3 hours

As can be seen in these figures, the powder displays two different phases, the first one constituted by small and even distributed particles, the second one by bigger and smooth particles. EDX analysis was made on the two different phases: for the bigger particles it was found that they are compound of titanium and various quantity of oxygen, suggesting that they are non-stoichiometric titanium oxides, as seen in XRD; the smaller particles are made of titanium, oxygen and carbon. The quantity of oxygen is ~1.5 times the quantity of carbon, that slightly differ from the stoichiometry evaluated from XRD, $TiO_{0.51}C_{0.49}$.

From this batch we obtained good results, both in terms of final stoichiometry and reproducibility, beside the initial lower C:Ti ratio. This particular ratio, that exceeds the ideal 2:1 for a 50-50 composition, was chosen to avoid low oxygen content because, as proven with the previous samples, the final stoichiometry is always lower than the expected one. This behavior could be strange at a first glance, but can be partially explained. The maximum amount of liquid that the XC72 can adsorb is 3.5 mL per gram, that correspond to a C:Ti ratio of 6.67:1. With additional impregnations to lower that ratio, the TiO_2 precursor is not able to penetrate perfectly inside the carbon particles, and tends to hydrolyze at the surface. So the particles grew up with a core-shell like configuration, and during the heat treatment the titanium dioxide has to diffuse in the carbon core. Another determining factor is how the impregnation is conducted, because it can lead to a non-perfect mixture of the TiO_2 precursor. This last factor is not easily controllable and

represents the biggest disadvantage of this approach, because takes different days and it is not completely reproducible because of the complexity of the impregnation steps with a moisture sensitive precursor.

In conclusion, we found that carbon black can provide a good base for porous titanium oxycarbides because it represents a good templating agent and carbon source. However, the XC72 has several criticalities that cannot lead to an excellent quality level of the final oxycarbide porous powders. A different grade of carbon black is required, with higher wettability and surface area.

Following the previous studies, a new carbon source was searched and Timcal Ensaco 350G was selected for its very high porosity and surface area. Moreover it is one of the most used in commercial fuel cells and it was already used by the industrial partner of the European project DECORE, Elcomax. Like the XC72, also the Ensaco 350G is a commercial grade conductive CB used for inks, polymer reinforcement and electro-catalytic support.

The surface area is much greater than the XC72's one, from the producer it is stated to be around 770 m^2g^{-1} [50]. From BET measurements, we found that it has a specific surface area of 800 m^2g^{-1}, with a very narrow pore distribution around 0.4 nm and a broader one around 2 nm, as it can be seen in Figure 12. The DFT model that we used for the best fit of the experimental data is for round pores, suggesting that they are very thin capillary.

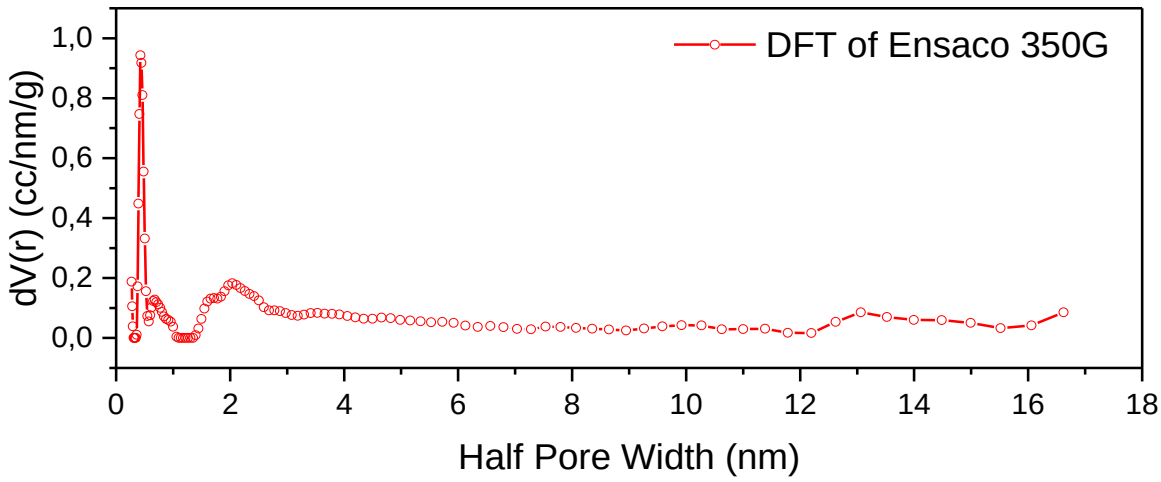

Figure 12, DFT analysis of Ensaco 350G

Considering these facts, we decided to substitute the XC72 with the Ensaco 350G, using the same impregnation and drying route. The quantity of titanium alkoxide that can be soaked by the Ensaco is

much bigger, exceeding the ideal volume needed to reach a C:Ti ratio of 2:1. In this way a faster impregnation and drying is possible.

The very first attempt was conducted using a proper quantity of titanium isopropoxide in order to reach the wanted C:Ti ratio of 2:1. The impregnation was conducted in air mixing the wetted carbon black in a closed vial and shaking it vigorously. When the powder is uniformly mixed and wetted, the drying step is conducted at 60°C for reducing the necessary time. After the complete evaporation of the titanium alkoxide's hydrolyzation byproducts the powder exhibited a greyish color, due to the mixing of the black color of the carbon and the white one from the titanium oxides.

The resulting powder is then put in the tubular furnace in an alumina vessel. The tube is washed with a flow of Argon of 0.4 L/min for an hour to remove nearly all the traces of air (having the tube an internal volume of 2 liters, after an hour the residual quantity of air is ~0.25%, that is expelled and/or consumed during the first phases of the following heat treatment) and then heated up to 1350°C with a heating ramp of 10°C/min. During the heat treatment, the argon flow is maintained constant in order to remove the reaction byproducts [51]. The top temperature is hold for 3 hours and then the furnace is let to cool down to room temperature naturally. The heat-treated powder is hand ground in a mortar to reduce the dimension of the particles before XRD analysis.

The results from this analysis are promising but some problems must be addressed, as can be seen in Figure 13. The main peaks of the TiO_xC_{1-x} are present among different peaks from non-stoichiometric titanium oxides. These can be due by a non-complete and -even mix of the precursors or by the drying process. Another possibility is the presence of air, and thus oxygen, in the tube, conducting to the formation of multiple oxides.

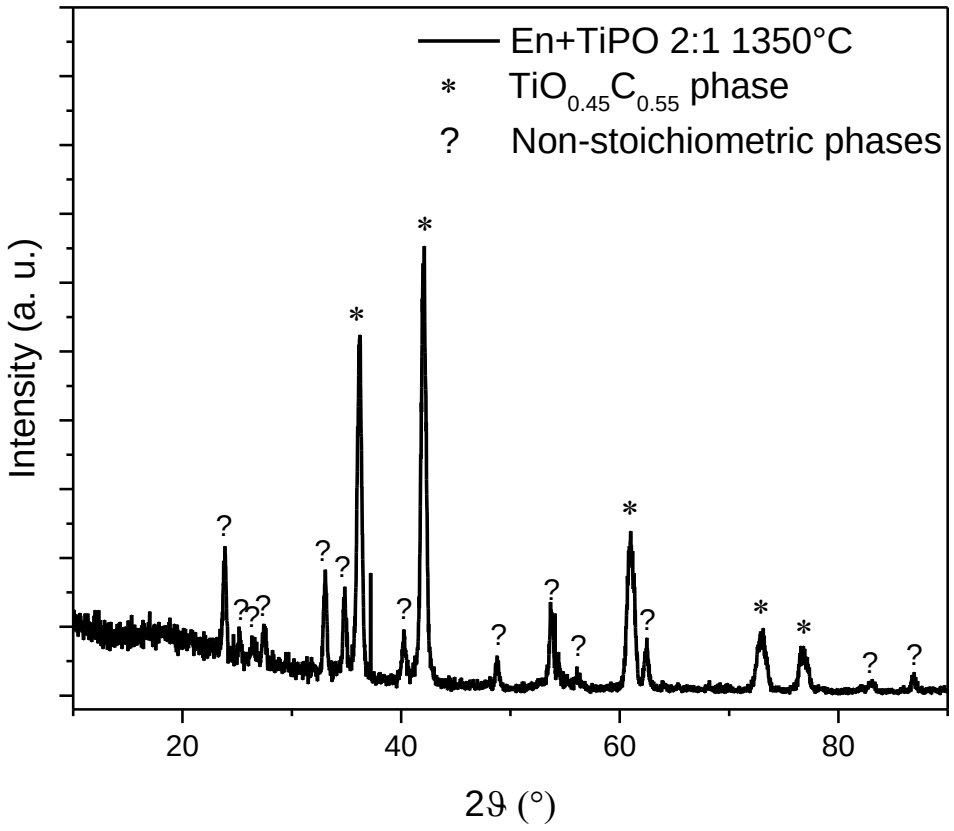

Figure 13, XRD patter of Ensaco+TiPO 2:1, 1350°C 3hrs

Another sample was prepared with the same C:Ti ratio but with a more accurate mixing and a longer drying step. It was again with a C:Ti ratio of 2:1, mixed with a tumbler several times waiting 5 minutes between the shakes in order to let to settle down the powder and the titanium alkoxide and left to dry at 60°C for 48 hours.

After these steps the powder is placed in the middle of the tube in an alumina vessel. The argon was flown for 2 hours in order to remove the air inside and the heat treatment was conducted in the same way, with a heating ramp of 10°C/min up to 1350°C. This temperature was hold for 3 hours before the natural cooling down to room temperature. After the treatment, the resulting powder was hand ground in the mortar before XRD analysis. The resulting pattern can be seen in Figure 14.

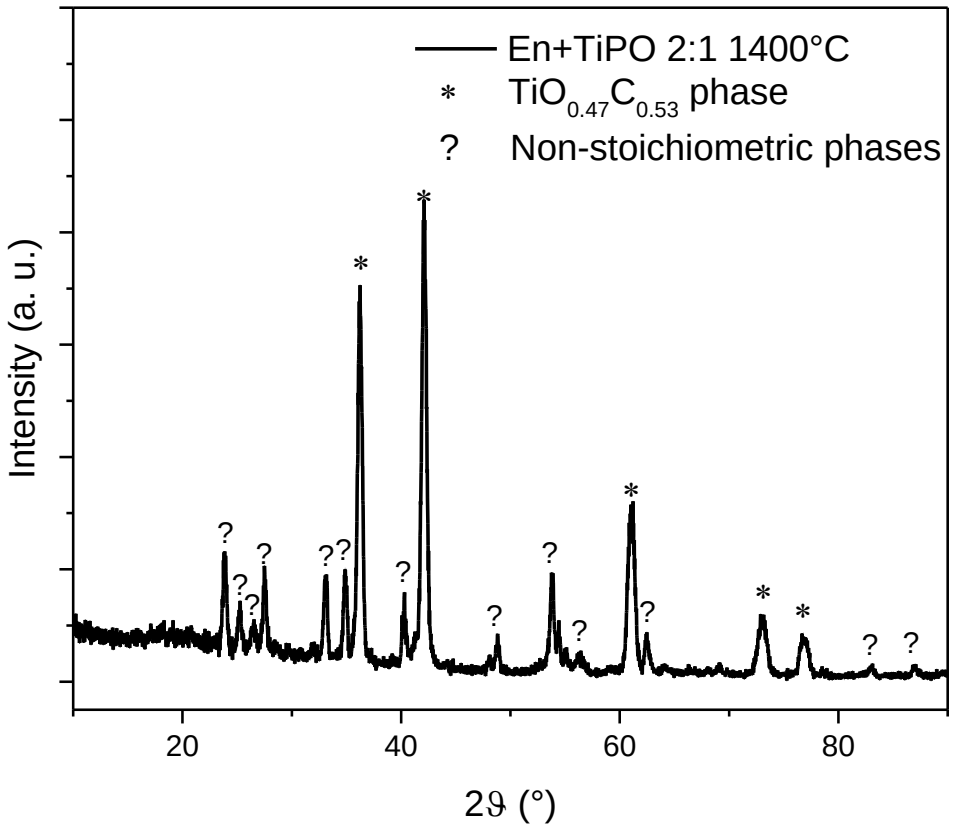

Figure 14, XRD patter of Ensaco+TiPO 2:1, 1350°C 3hrs with better preparation

Also, for this sample there are present the same oxides peaks, as can be seen in the comparison in Figure 15 with the first sample. As can be noted the peaks are in the same positions, meaning that the more accurate mixing step and longer drying weren't very effective to limit the formation of unwanted titanium oxides' phases. This consideration is very important because it means that a different hydrolyzation method is required to have an intimate mixing of carbon black and titanium isopropoxide, and eventually also a different heat treatment for the complete carburization.

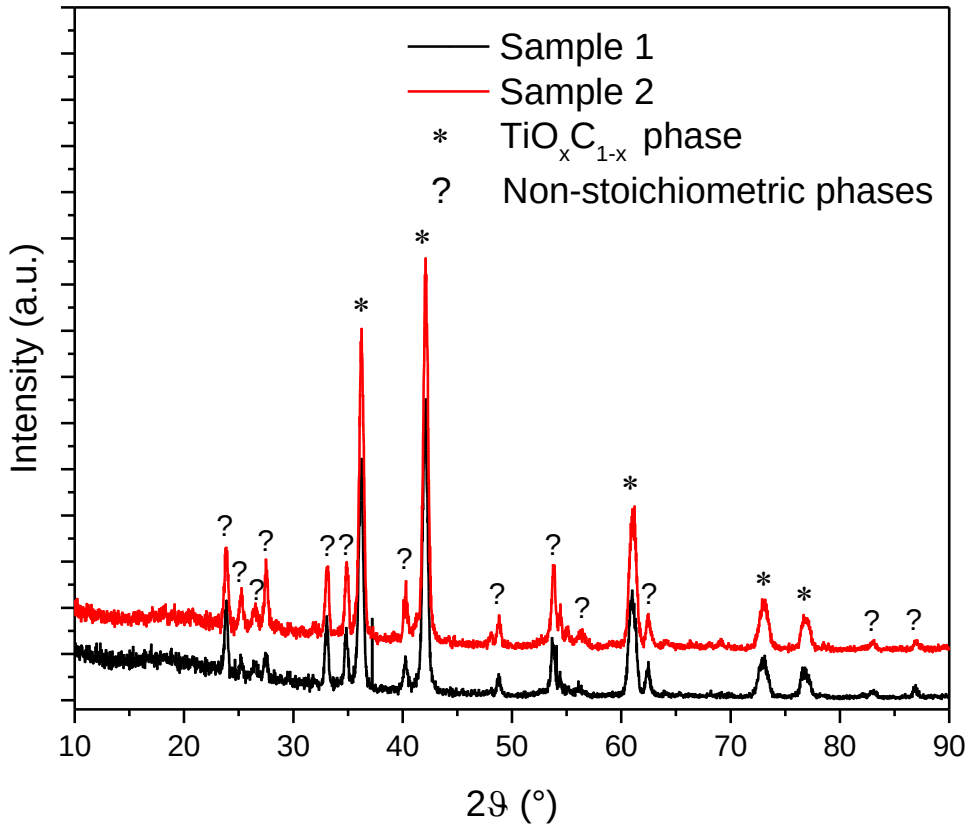

Figure 15, XRD patterns of different samples of En+TiPO 2:1, 1350°C 3hrs

After these first two samples the work focused on understanding the single parameters that can influence the final result, separating the whole process in three different steps: the hydrolyzation phase, the heat treatment and the raw starting materials.

For the hydrolyzation step different routes were followed in order to try to eliminate the unwanted titanium oxides' traces.

The first method we tried was to hydrolyze and dry the powder at higher temperature, 120°C. In this way we hoped to maintain the titanium alkoxide still inside the carbon pores during the evaporation stage, because the drying step requires only 4 to 5 hours to be complete, instead of 48 hours. The carburization treatment was kept the same, with a heating ramp of 10°C/min up to 1350°C, a dwell of 3 hours and then the furnace was let to cool down naturally. The pattern acquired with the XRD is shown in Figure 16.

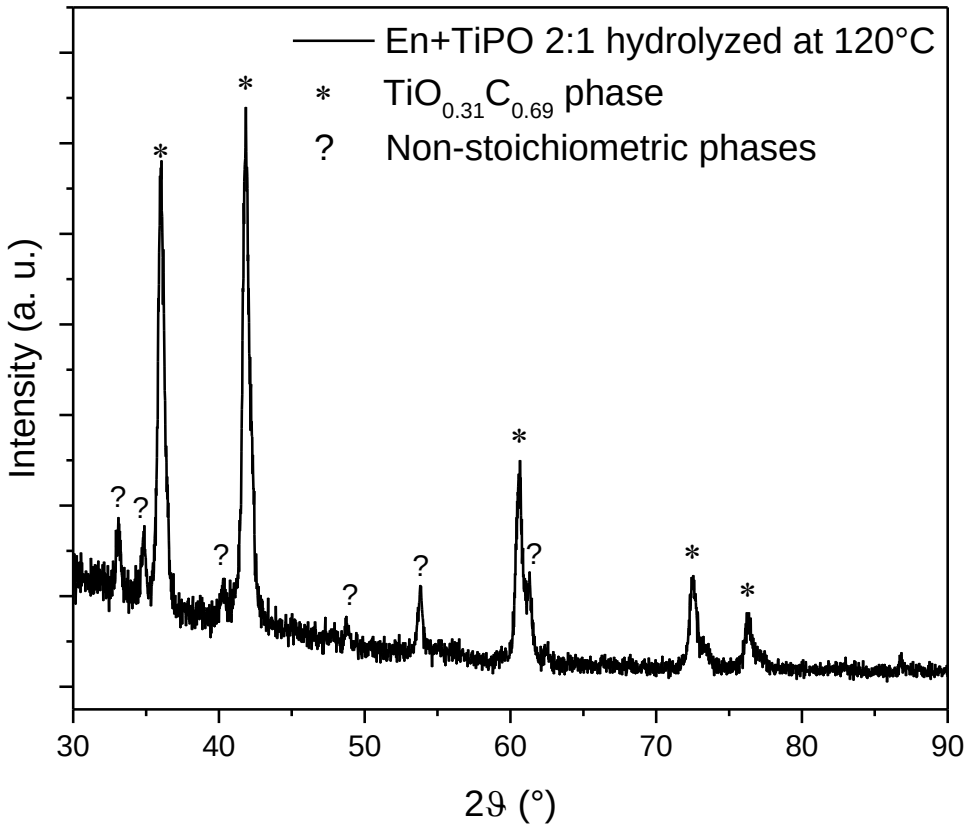

Figure 16, XRD pattern of Ensaco+TiPO 2:1, 1350°C 3hrs with 120°C hydrolyzation

As can be seen the number and intensity of the unwanted peaks are decreased, even if still relevant. The hypothesis we formulated behind this behavior is that the titanium alkoxide is too reactive and cannot fulfill the pores of the Ensaco before the complete hydrolyzation. With the next route, we tried to understand if this is true or not.

Because the titanium alkoxide we use is very sensitive to the ambient moisture, we decided to remove this variable using a glove box. In the glove box, we are able to create the desired atmosphere, controlling the gas inside and the moisture. We used only argon gas to make the atmosphere inert and molecular sieves to remove as most as possible the residual moisture within the chamber. In this way, we reached a relative humidity of 3-5%, that can be non-relevant for our impregnation times.

The Ensaco and the titanium propoxide is loaded in the chamber using a pre-chamber where a slight vacuum is made with the aid of a vacuum pump to remove the air and then is filled with Argon. This procedure is executed three times, to remove as much as possible air and moisture.

Inside the main glove box chamber the carbon black is impregnated with the wanted amount of alkoxide to reach a C:Ti ratio of 2:1. After the impregnation, the wetted powder is mixed with a magnetic stirrer for an hour, to have a better homogeneity. In order to control the hydrolyzation step, we have to introduce some water. We preferred to pour an acidic solution directly into the impregnated powder rather than increase the relative humidity. The acidity is needed to neutralize the surface charges of the carbon black and have better results, letting the water to completely wet the powder. An HCl solution with a pH=4-5 is used, adding it dropwise to the still wet Ensaco powder under heavy stirring. The quantity of water solution is chosen to be twice the molar quantity of the titanium propoxide. For our test we used 0.5g of Ensaco, 6.168mL of titanium propoxide and 0.72mL of HCl solution. After all the water is added, the powder is mixed for two hours in order to complete the hydrolyzation of the titanium propoxide and then it is removed from the glove box and put in an oven at 60°C to remove all the byproducts, mainly constituted by alcohol.

As the water is dropped on the impregnated powder, heat is generated and increasing the amount of water a light white fog floats on the top of the sample, due to the high temperatures that locally are reached that create an aerosol of water and titanium oxide. This phenomenon will induce a small drift of the results from what we expected, but the quantity of aerosol is so small that it can be not considered for our aims.

After 24 hours in the oven, the dried powder is heat treated as the previous samples, i.e. with a heating ramp of 10°C/min up to 1350°C, a dwell of 3 hours and then natural cooling.

In Figure 17 the XRD pattern of this sample is reported.

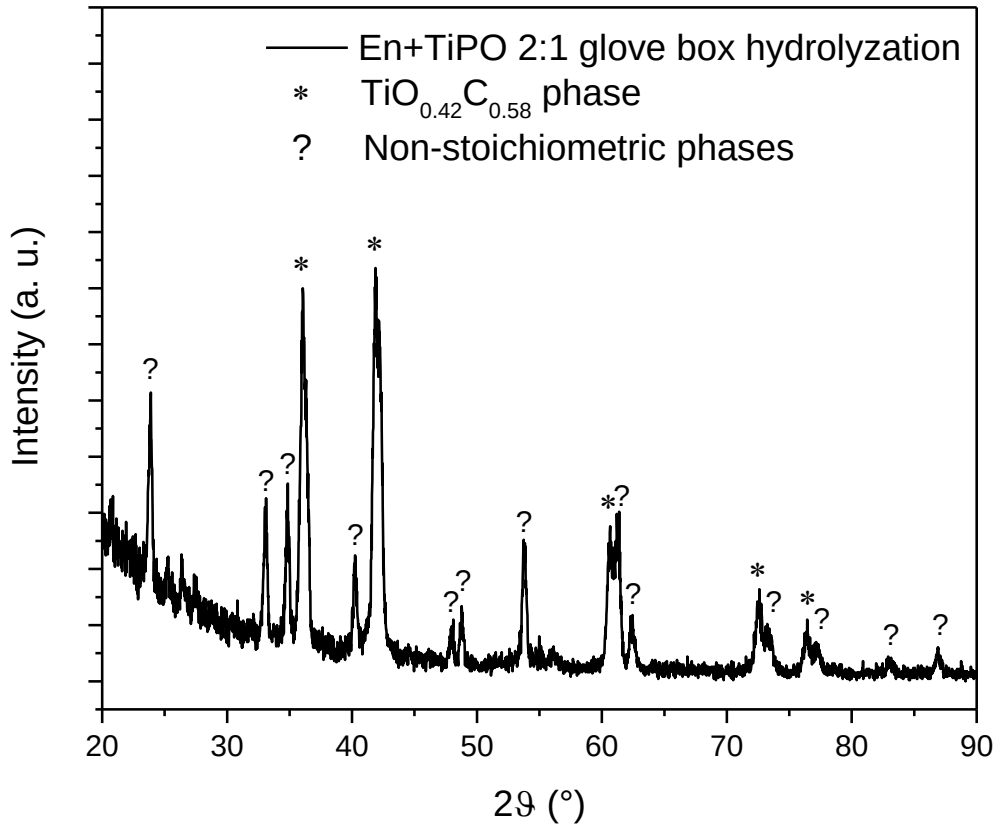

Figure 17, XRD pattern of Ensaco+TiPO 2:1, glove box hydrolyzation, 1350°C 3hrs

As can be noted, there are still a lot of unwanted phases that contaminate the final result.

After all these tests, we guessed that the main problem is not how the titanium alkoxide hydrolyze when it wets the carbon black, but how it wets it. The Ensaco pores are very thin, in the range of 0.8 – 4 nm, as we reported before with the BET analysis. Given the very small size of them, the titanium alkoxide probably cannot penetrate all the pores because of the trapped air inside.

The idea behind the following route was to remove completely the air inside the pores of the Ensaco. A simple way to make this is to lower the pressure around the carbon black powder and then impregnate it with the titanium alkoxide. This method will be called from now on *vacuum hydrolyzation*. To be more specific about our internal protocol, the needed amount of Ensaco is put inside a two-necked flask. One neck is connected to the vacuum pump and the other is sealed with a rubber septum, allowing the introduction of a needle syringe. Firstly, the vacuum is applied for 30 minutes with the powder inside gently mixed with a magnetic stirrer. After that the right amount of titanium isopropoxide is collected

with the syringe and slowly dropped on the black carbon through the rubber septum in order to wet completely the powder without compromising the vacuum inside the flask. When the powder is fully wetted a stoichiometric amount of distilled water is added in order to start the hydrolyzation, because there isn't the natural atmospheric humidity. When the Ensaco is completely dried, it is heat treated in the same way as the previous samples.

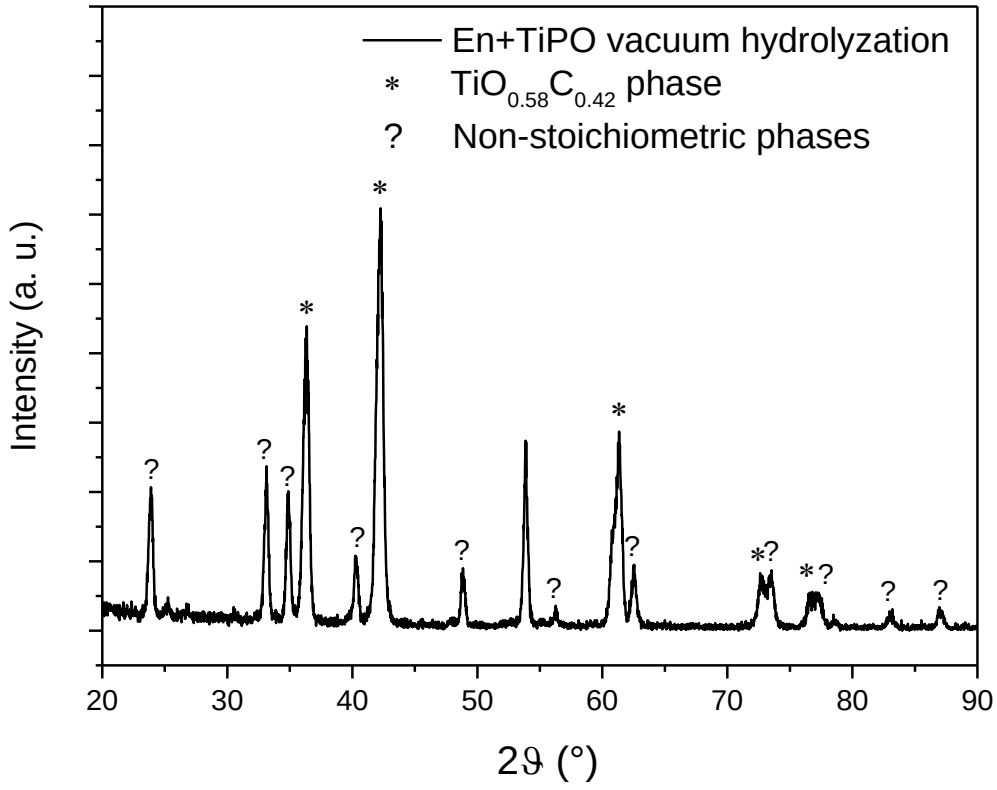

Figure 18, XRD pattern of Ensaco+TiPO 2:1, 1350°C 3hrs with vacuum hydrolyzation

With this method, the *vacuum hydrolyzation*, the problem of unwanted oxide phases is not resolved; we obtained worst results than the previous sample, as can be seen in Figure 18 and Figure 19. In the second figure also a right shift of the titanium oxycarbide phase can be noted, meaning that an oxygen-richer stoichiometry is reached. The exact reasons behind this shift aren't fully understood, the most consistent hypothesis is that at 120°C part of the evaporating byproducts of the hydrolyzation flies away with a small amount of titania, leading to a higher C:Ti ratio.

After these unsuccessful attempts we investigated how the titanium propoxide wets the powder. For this purpose we impregnated the Ensaco with a higher C:Ti ratio, equal to 3.15:1 to see if with a smaller

amount of titanium alkoxide the carbon grains get fully covered with a thin patina of titania or only the pores get flooded.

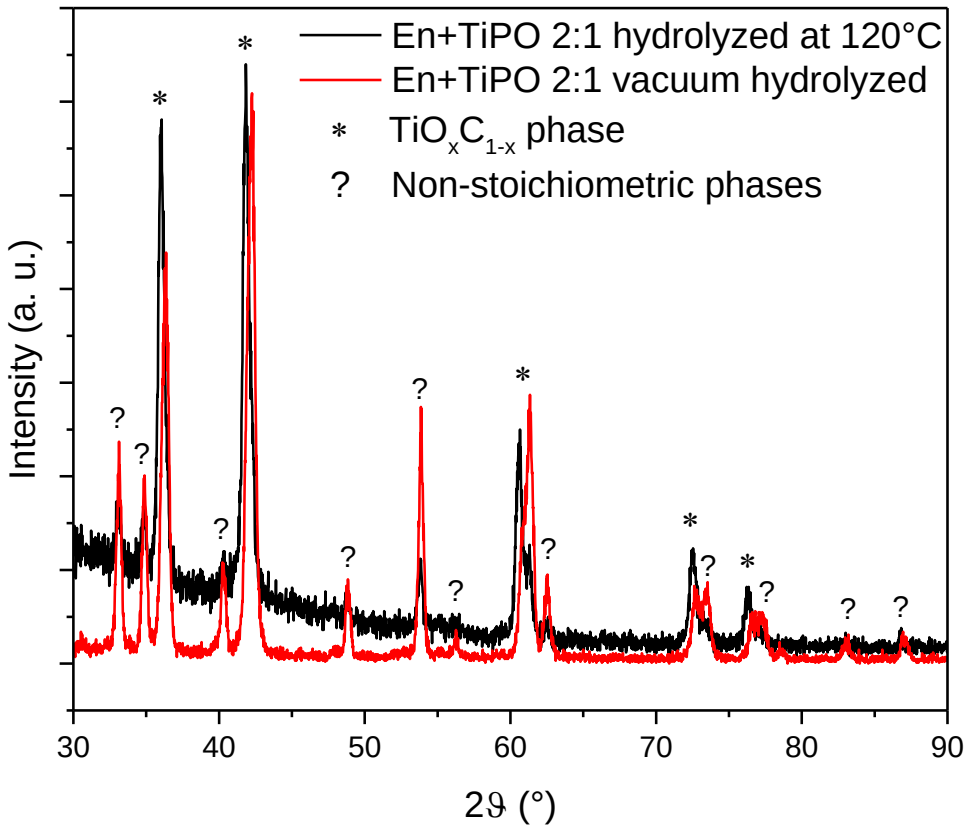

Figure 19, XRD pattern of Ensaco+TiPO 2:1, 1350°C 3hrs with vacuum and 120°C hydrolyzation

After the usual heat treatment, we used a stereo microscope in order to investigate the surface of the obtained powder at low magnifications. In Figure 20 two broken grains can be recognized, on top left corner and on the center bottom. As can be noted, the grains present a core-shell like structure, where the surface is coated with titanium oxycarbide meanwhile the inner part is still largely carbon.

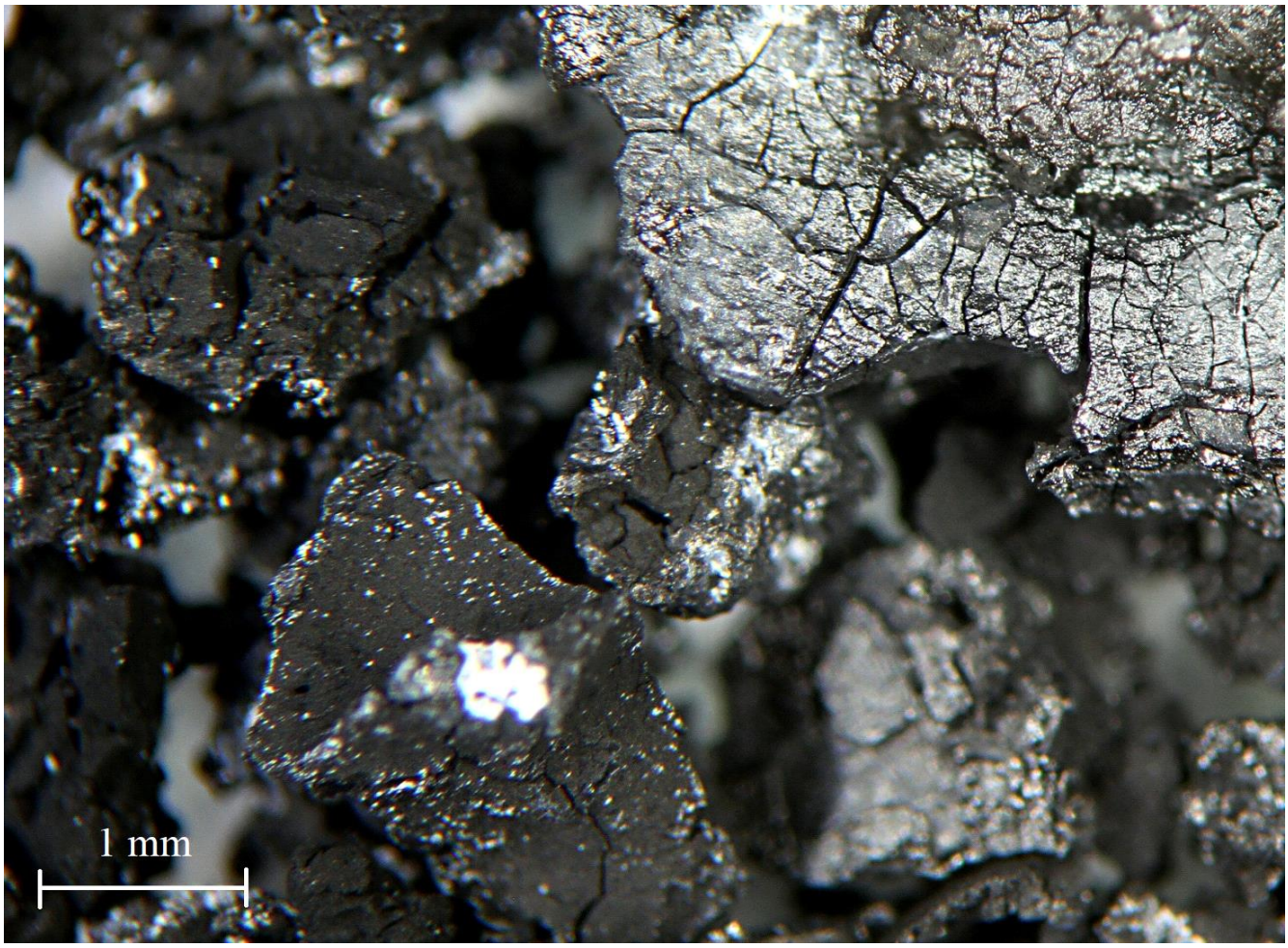

Figure 20, stereo microscope image of Ensaco+TiPO 3,15:1, 1350°C 3 hrs

With this result in mind, we tried to improve the impregnation using a multi-step procedure in order to let the titanium alkoxide to better penetrate the pores of the carbon black, reducing the reactivity and the viscosity of the titanium isopropoxide. To wet completely the powder, the needed amount of titanium propoxide is diluted with iso-propoxide to the same volume as pure alkoxide. After the impregnation, the sample is let to dry at 60°C and hydrolyze in atmosphere. We still reach a C:Ti ratio of 2:1, but dividing the impregnation in two or three steps, heat treating the dried powder every time between the different steps with the usual heat treatment.

The first sample is made with two impregnation, reaching with the first one a C:Ti ratio of 2:0.5, and then the desired 2:1. The results after the two heat treatments are resumed in Figure 21.

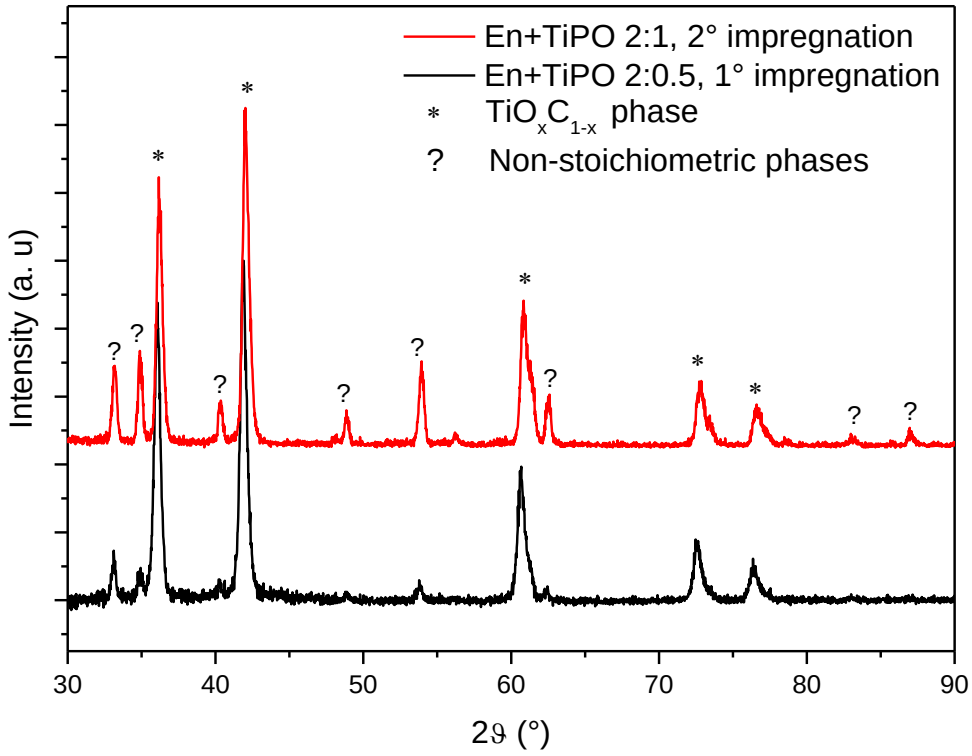

Figure 21, XRD pattern of Ensaco+TiPO 2:1, after the 1st and 2nd impregnation of diluted TiPO

As can be easily noted the peaks of the TiO_xC_{1-x} shift to higher angles, due to the titania-richer C:Ti obtained with the second impregnation, that mirrors the stoichiometry of the titanium oxycarbide, that changes from $TiO_{0.37}C_{0.63}$ to $TiO_{0.54}C_{0.46}$. Unluckily the unwanted non-stoichiometric oxides' peaks increase their intensity, meaning that the titanium isopropoxide didn't wet well the inner pores of the CB.

The second attempt with three different steps of impregnation conducted to similar results, as can be seen in Figure 22. The TiO_xC_{1-x} peaks shift to higher angles, changing the stoichiometry from $TiO_{0.28}C_{0.72}$ to $TiO_{0.43}C_{0.57}$ and finally to $TiO_{0.48}C_{0.52}$, but there is also the increment of intensity of the titanium oxides. This method proved to be not so good to reduce the quantity of unwanted phases with the usual heat treatment, because the titanium propoxide doesn't penetrate well the internal pores of the carbon black after the first carburization. The most probable cause is that the pores get fully filled with the first impregnation, not allowing the following impregnations to penetrate the carbon grain and, instead, making a shell cover that leads to non-stoichiometric phases.

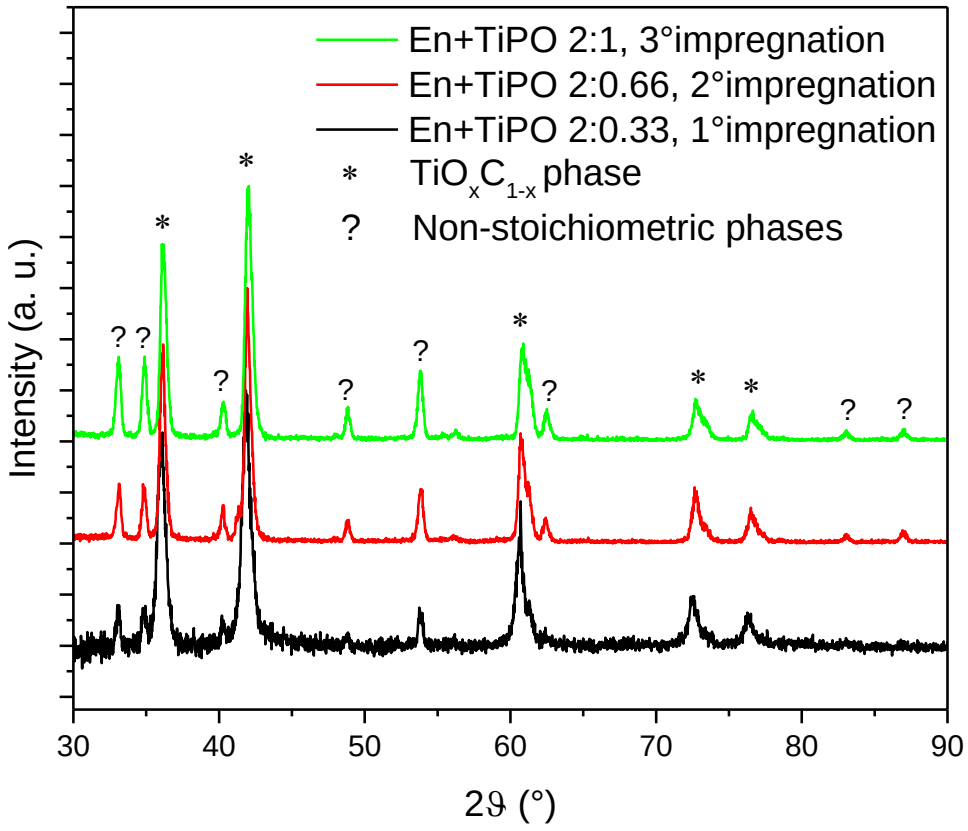

Figure 22, XRD pattern of Ensaco+TiPO 2:1, after the 1st, 2nd and 3rd impregnation of diluted TiPO

These phases are non-stoichiometric because the temperature which we work at are very high and the diffusion coefficients become relevant, letting the titanium oxides and carbon to react in-between the layers of the core-shell like carbon grains.

The natural conclusion that can be reached from this consideration is that a longer heat treatment should be used to let the titanium oxides to diffuse completely in the carbon black and have a complete carburization. We tested also different temperatures in order to understand if the treatment can be shortened or not.

The first test we made with different treatment time was conducted with a sample prepared with the glove box procedure. The C:Ti ratio is retained equal to 2:1, only the heat treatment is different. The dried and not carburized powder is firstly treated at 1350°C for 3 hours, like a normal heat treatment. After the first one the sample is analyzed with XRD and the treated again in the same condition two times in order to achieve a total of 9 hours of heat treatment. The XRD patterns are exposed in Figure 23.

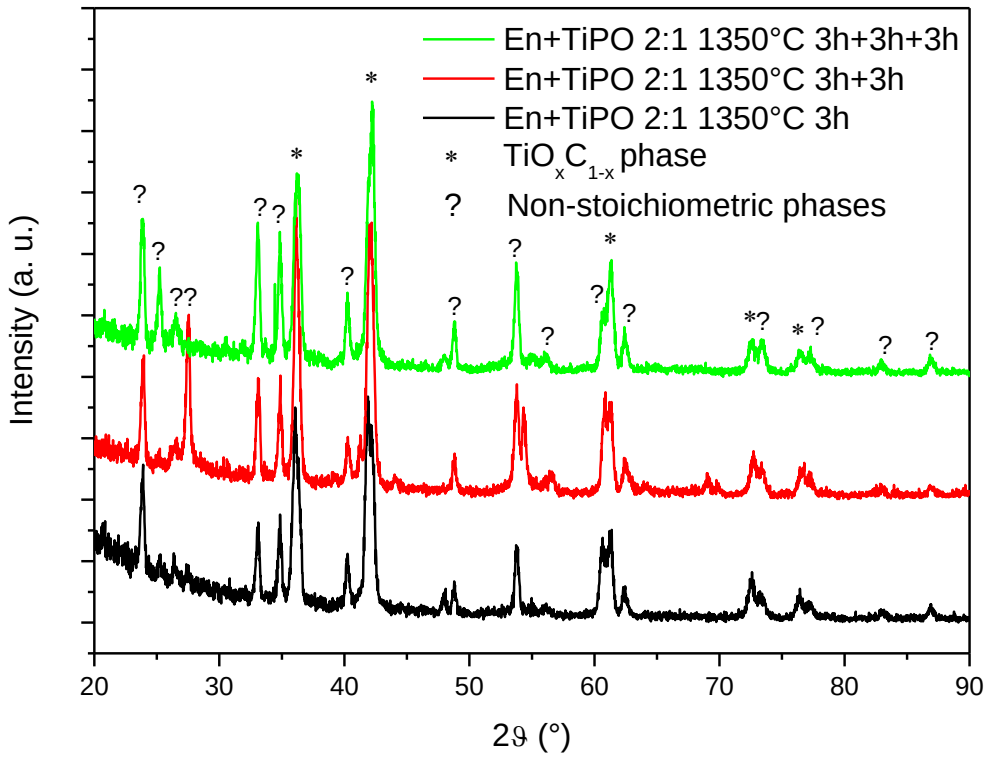

Figure 23, XRD patterns of Ensaco+TiPO 2:1, hydrolyzed in glove box with different time of heat treatment

As can be seen, changing the time of heat treatment doesn't solve the problem of unwanted phases, at most they change slightly composition but the quantity of them doesn't decrease significantly. This can be due to the too low diffusion coefficients of carbon and titanium oxides, that don't permit a complete diffusion and reaction of the different chemical species. In Table 2 we reassumed the peaks' positions and the composition of the three samples. All the values for all the peaks are not listed because most of the oxycarbide peaks were superimposed by non-stoichiometric phases' peaks, not allowing the position analysis. Consequently the cell parameters and oxygen contents aren't very precise, but they are meant to represent only the trend of the samples that underwent different heat treatments.

Sample name	***1st peak position (°)***	***2nd peak position (°)***	***3rd peak position (°)***	***4th peak position (°)***	***5th peak position (°)***	***Cell parameter (Å)***	***Oxygen content (mol%)***
1350°C 3h	36.13	n. a.	n. a.	n. a.	n. a.	4.3009	37
1350°C 3+3h	36.18	42.09	n. a.	n. a.	n. a.	4.2918	48
1350°C 3+3+3h	36.23	42.14	n. a.	n. a.	n. a.	4.2865	53

Table 2, peak positions, cell parameter and oxygen content of Ensaco+TiPO 2:1, glove box hydrolyzation, 1350°C 3hrs, 3+3hrs, 3+3+3hrs

We tried also to change the temperature of carburization, searching if higher temperatures lead to significant changes in diffusion coefficients or if, at lower temperatures, different titanium oxide phases are created with a higher reactivity.

The first test was conducted at 1300°C for 6 hours. The XRD pattern is visible in Figure 24. It can be clearly noted that at this temperature the oxides' phases are still present. However also the titanium oxycarbide is present, meaning that the carburization starts at lower temperatures than expected. The peak positions, cell parameter and oxygen content are reported in Table 3.

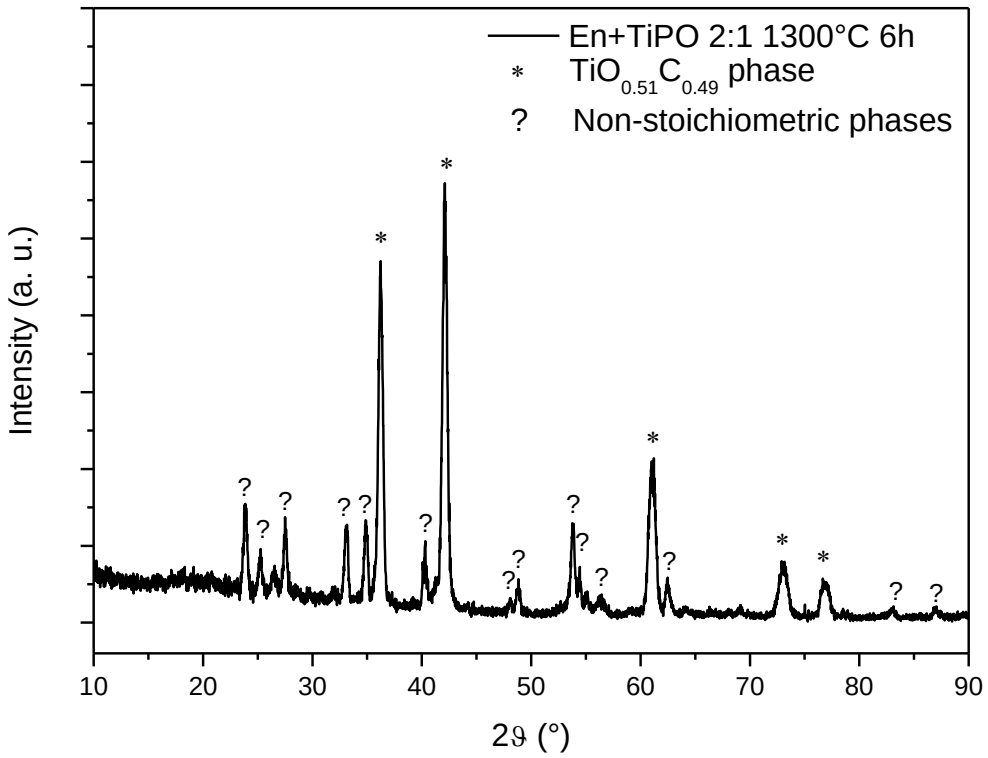

Figure 24, XRD pattern of Ensaco+TiPO 2:1, glove box hydrolyzation, 1300°C 6hrs

1st peak position (°)	***2nd peak position (°)***	***3rd peak position (°)***	***4th peak position (°)***	***5th peak position (°)***	***Cell parameter (Å)***	***Oxygen content (mol%)***
36.24	42.11	61.06	73.04	76.87	4.2889	51

Table 3, peak positions, cell parameter and oxygen content of Ensaco+TiPO 2:1, glove box hydrolyzation, 1300°C 6hrs

This sample shown a composition very close to the expected one. This means that at 1300°C the carburization of the titanium oxide already takes place, but the temperature is too low to have a proper diffusion that allows the complete reaction of all the precursors.

The next sample comes from the same batch of the previous one, but with a different heat treatment. We incremented the temperature, reaching 1450°C, 100°C more than the standard treatment. In Figure 25 the XRD pattern is shown. There aren't traces of unwanted oxides' phases, representing a remarkable goal after several attempts.

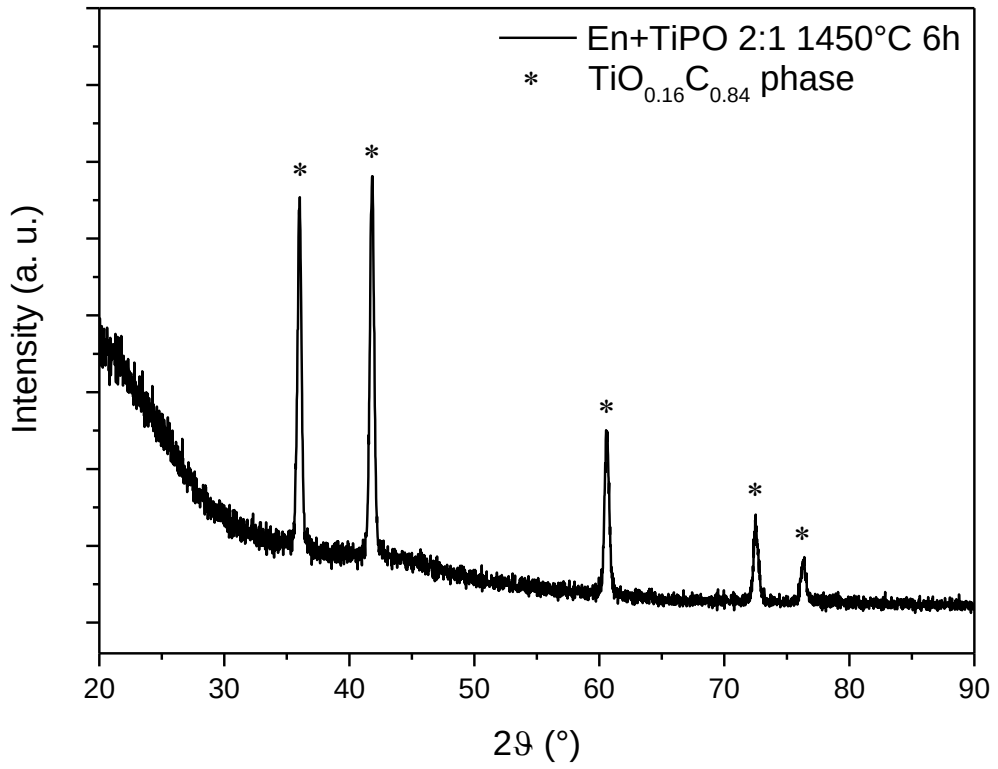

Figure 25, XRD pattern of Ensaco+TiPO 2:1, glove box hydrolyzation, 1450°C 6hrs

In Table 4 the positions of the peaks, the cell parameter and the oxygen content of the titanium oxycarbide are reported.

1st peak position (°)	***2nd peak position (°)***	***3rd peak position (°)***	***4th peak position (°)***	***5th peak position (°)***	***Cell parameter (Å)***	***Oxygen content (mol%)***
36.01	41.82	60.60	72.53	76.32	4.3162	16

Table 4, peak positions, cell parameter and oxygen content of Ensaco+TiPO 2:1, glove box hydrolyzation, 1450°C 6hrs

The oxygen content leads to a different composition from the desired one, $TiO_{0.16}C_{0.84}$ against the theoretical $TiO_{0,50}C_{0,50}$. The reason is that from the phase diagram [52] at higher temperature TiC is favored over the oxides' phases, leading to a near depletion of oxygen in the ceramic.

To better understand the influence of temperature and time, we treated the precursors from the same batch at 1350°C but for a longer time, 12 hours. The XRD pattern is shown in Figure 26.

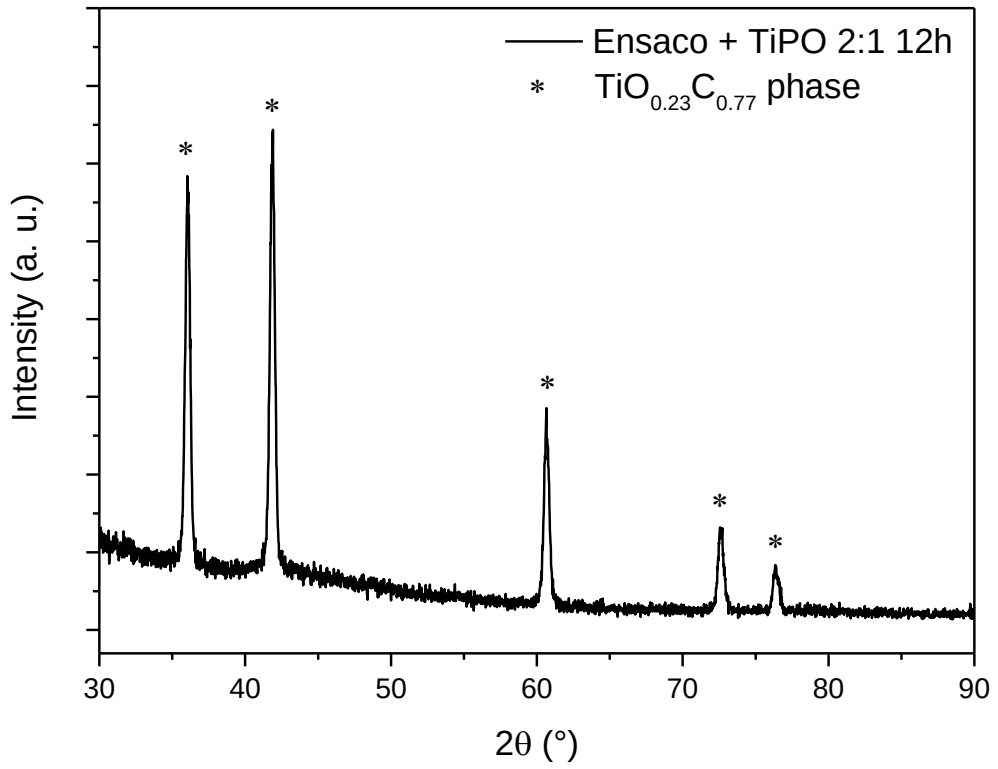

Figure 26, XRD pattern of Ensaco+TiPO 2:1, glove box hydrolyzation, 1300°C 12hrs

The peak positions and composition are reported in Table 5.

1st peak position (°)	***2nd peak position (°)***	***3rd peak position (°)***	***4th peak position (°)***	***5th peak position (°)***	***Cell parameter (Å)***	***Oxygen content (mol%)***
36.06	41.86	60.67	72.62	76.40	4.3116	23

Table 5, peak positions, cell parameter and oxygen content of Ensaco+TiPO 2:1, glove box hydrolyzation, 1350°C 12hrs

As can be seen in the XRD pattern there are no traces of unwanted non-stoichiometric oxides, only the five peaks of the titanium oxycarbide are present. From an analysis of the peaks' positions we deducted that the stoichiometry of the ceramic is $TiO_{0.23}C_{0.77}$, far from the expected one. With this set of measurements, we understood that at 1300°C the carburization starts but the diffusion coefficients are too low to have a complete reaction of the precursors in useful times. At 1350°C the diffusions between species become relevant, but the TiC phase is favored over the oxycarbide. Indeed it can be noticed that,

treating the sample for 12 hours, the oxygen content in the titanium oxycarbide drops to very low levels, comparable to that founded at higher temperatures where, obviously, the titanium carbide is the prevalent phase. But treating the samples for shorter times, the oxycarbide is formed and with subsequent treatment the stoichiometry can be adjusted thanks to the higher diffusion coefficient.

The right heat treatment is therefore a balance between kinetics and thermodynamics factors, that tend to compete. From our experiences we saw that the heat treatment at 1350°C for 6 hours is the best combo among the infinite possibilities for having the desired stoichiometry, but it is mandatory to have precursors that are natively bonded together in order to avoid the formation of unwanted phases that requires the extension of the treatment. With this condition satisfied, perhaps it is possible to change the parameters in order to reach a faster carburization. All the results from the different temperatures and times are reassumed in Table 6.

In Figure 27 and Figure 28 there are shown all the XRD pattern acquired varying the time or temperature of the heat temperature, meanwhile in Figure 29 the stoichiometric composition calculated from the 1st peaks of all the samples is plotted with the aid of a colored surface. Summarizing the results obtained from the previous set of data, the best parameters of time and temperature to obtain TiO_xC_{1-x} without non-stoichiometric phases are 6 hours at 1350°C.

Sample name	***1st peak position (°)***	***2nd peak position (°)***	***3rd peak position (°)***	***4th peak position (°)***	***5th peak position (°)***	***Cell parameter (Å)***	***Oxygen content (%)***
1300°C 6h	36.24	42.11	61.06	73.04	76.87	4.2889	51
1350°C 3h	36.13	n. a.	n. a.	n. a.	n. a.	4.3009	37
1350°C 3+3h	36.18	42.09	n. a.	n. a.	n. a.	4.2918	48
1350°C 3+3+3h	36.23	42.14	n. a.	n. a.	n. a.	4.2865	53
1350°C 12h	36.06	41.86	60.67	72.62	76.40	4.3116	23
1450°C 6h	36.01	41.82	60.60	72.53	76.32	4.3162	16

Table 6, peak positions, cell parameter and oxygen content of Ensaco+TiPO 2:1, glove box hydrolyzation, treated at different temperatures and times

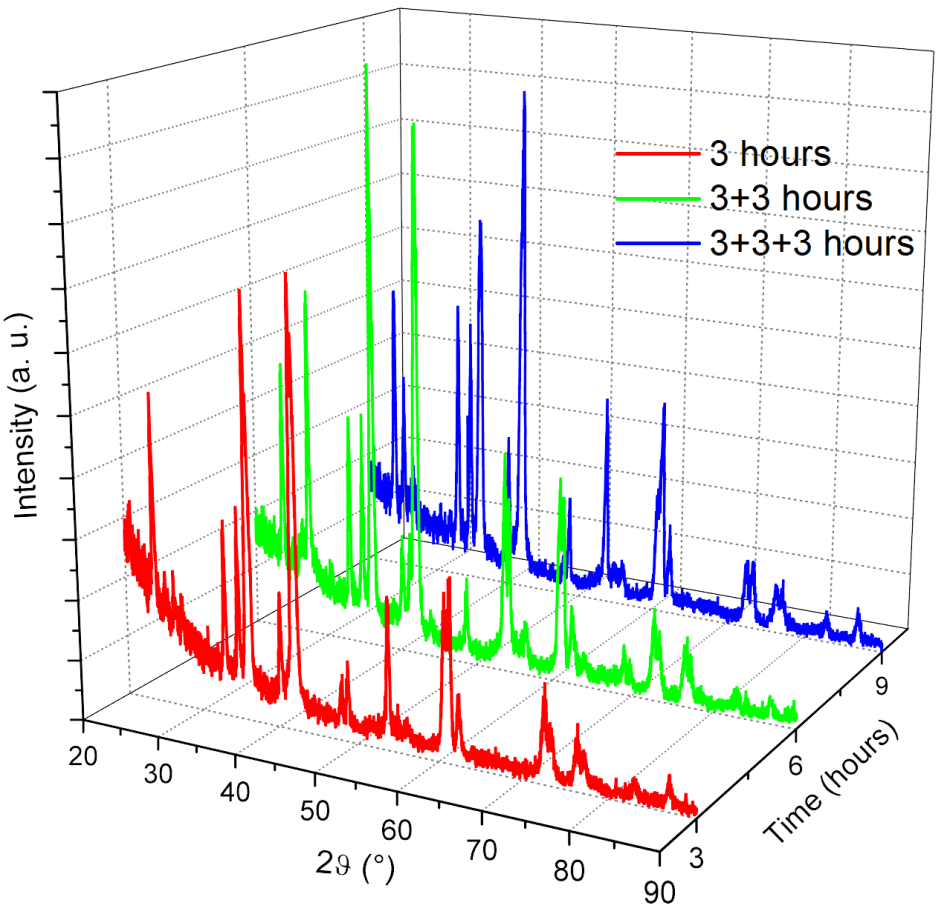

Figure 27, XRD pattern of Ensaco+TiPO 2:1, hydrolyzed in glove box with different time of heat treatment.

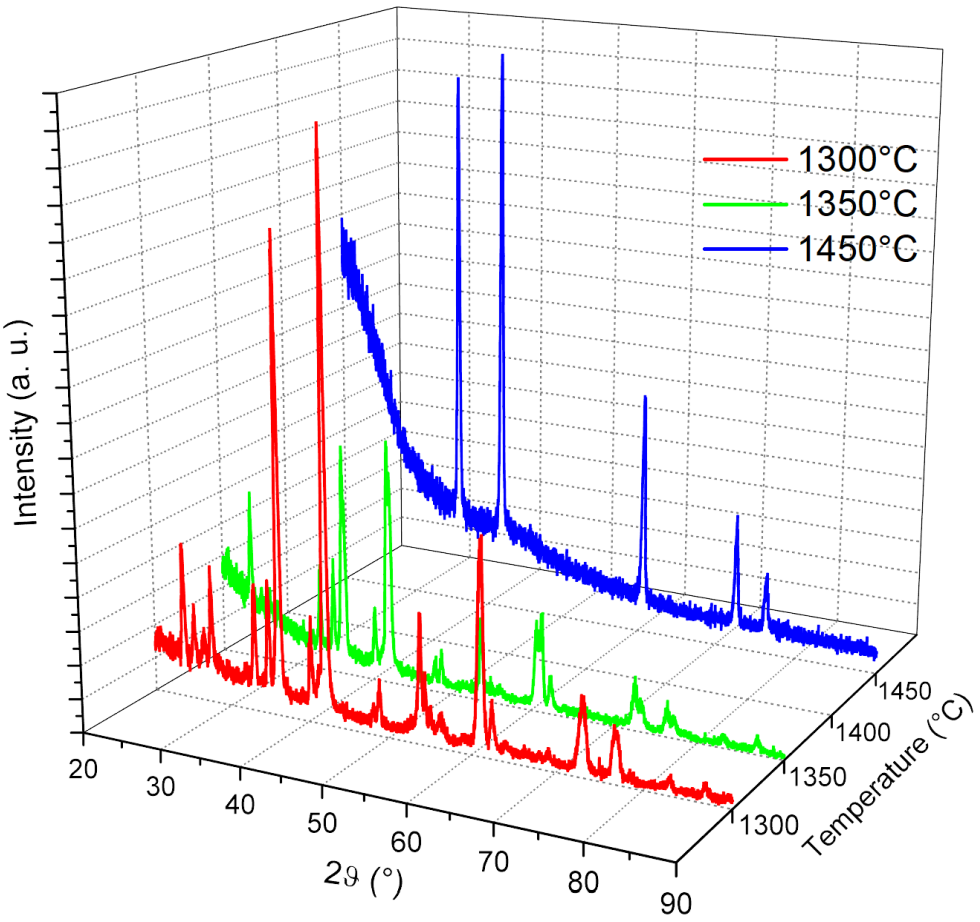

Figure 28, XRD pattern of Ensaco+TiPO 2:1, hydrolyzed in glove box with different temperatures of heat treatment.

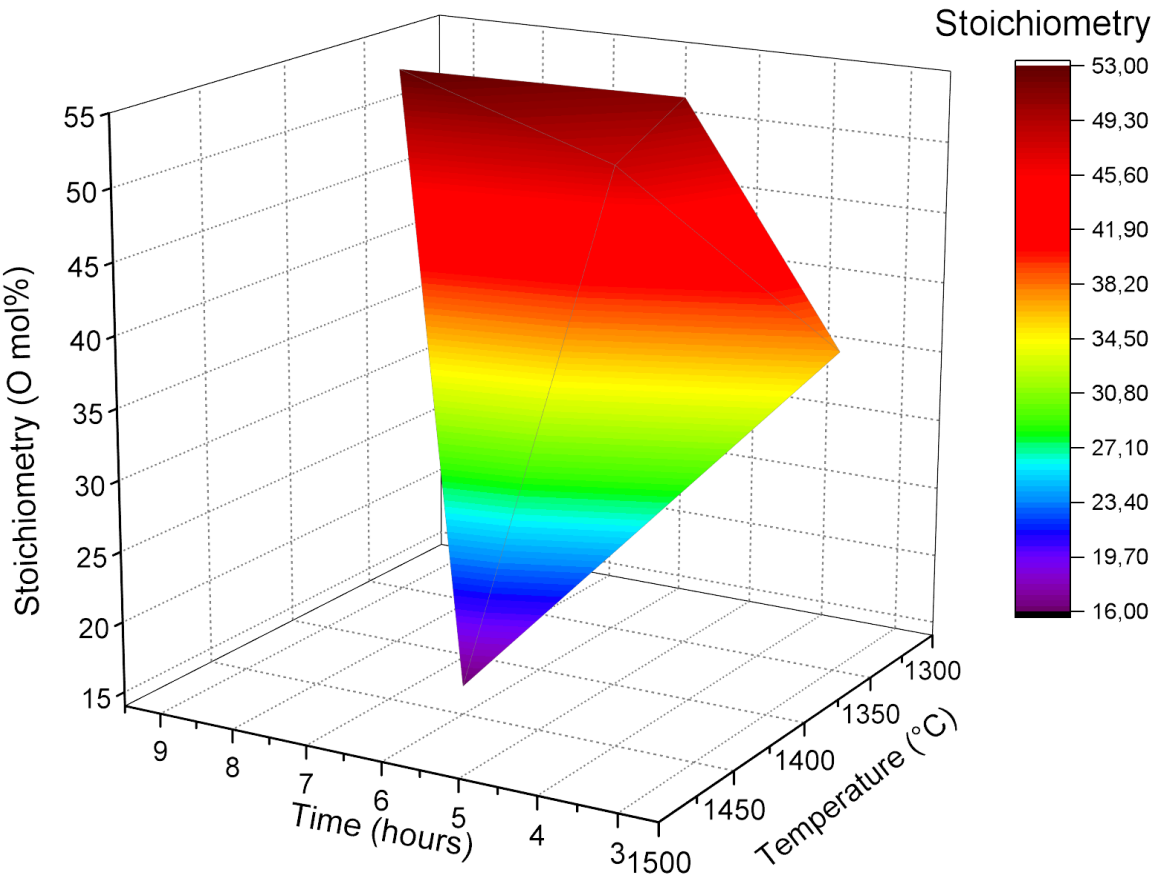

Figure 29, 1st peak positions of all the samples heat treated at different temperatures and for different times.

After this set of experiments, we investigated the precursors, focusing especially on the Ensaco 350G. We tried to understand if the carbon black was in sort way responsible to the undesired results. So we dried the powder in a laboratory furnace at 150°C for 12 hours in order to remove all the possible moisture stuck inside the small pores. The weight loss was equal to 13.06%. This rather high value means that not only moisture is present but probably also some byproducts from the synthesis stage that can interact with the titanium alkoxide and interfere with the carburization.

In order to evaluate the presence of contaminants in the CB, FTIR measurements were performed on the as received Ensaco CB. As can be noted in Figure 30, there are a lot of organic-related peaks indicating the presence of contaminants from amine and amide groups (3630 and 3730 cm^{-1}) and CH and CH_2 groups (2850 and 2920 cm^{-1}). They are probably related to the synthesis of the carbon black, with an incomplete carburization of the precursors.

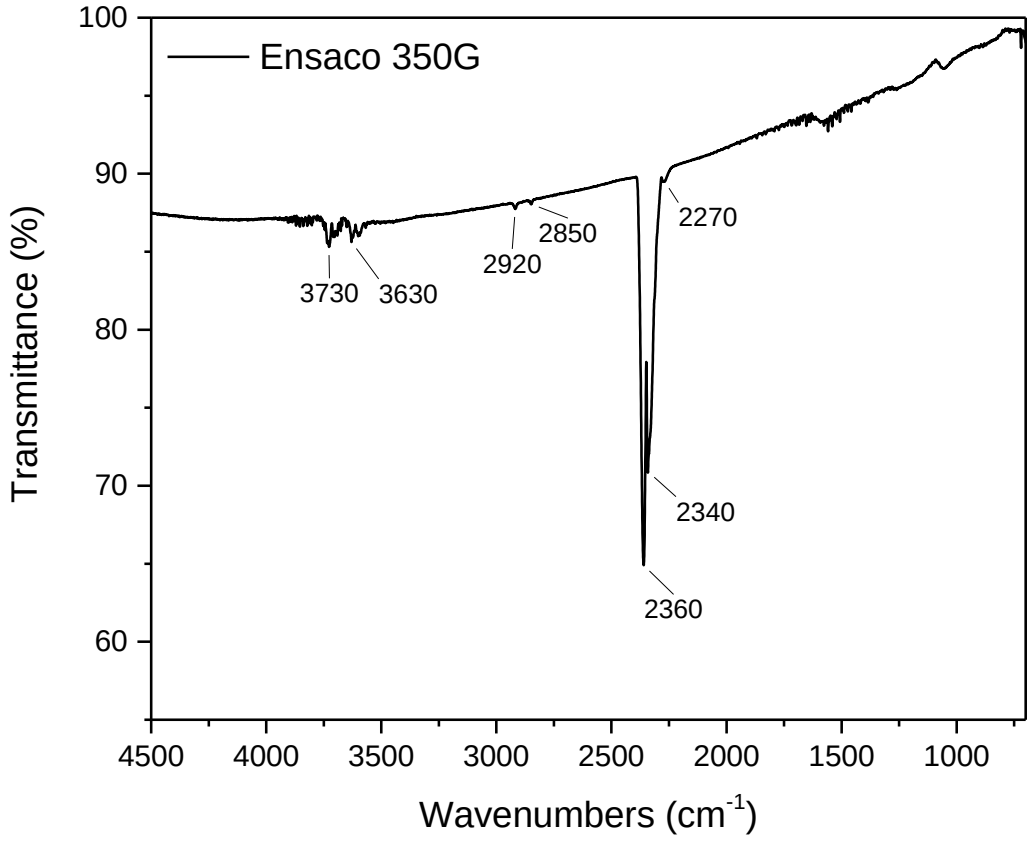

Figure 30, FTIR spectrum of Ensaco 350G

The most intense peaks at 2340 and 2360 cm^{-1} are probably due to CO_2, from the reaction of the surface with air. They can be found also in FTIR spectrum of XC72, in Figure 31.

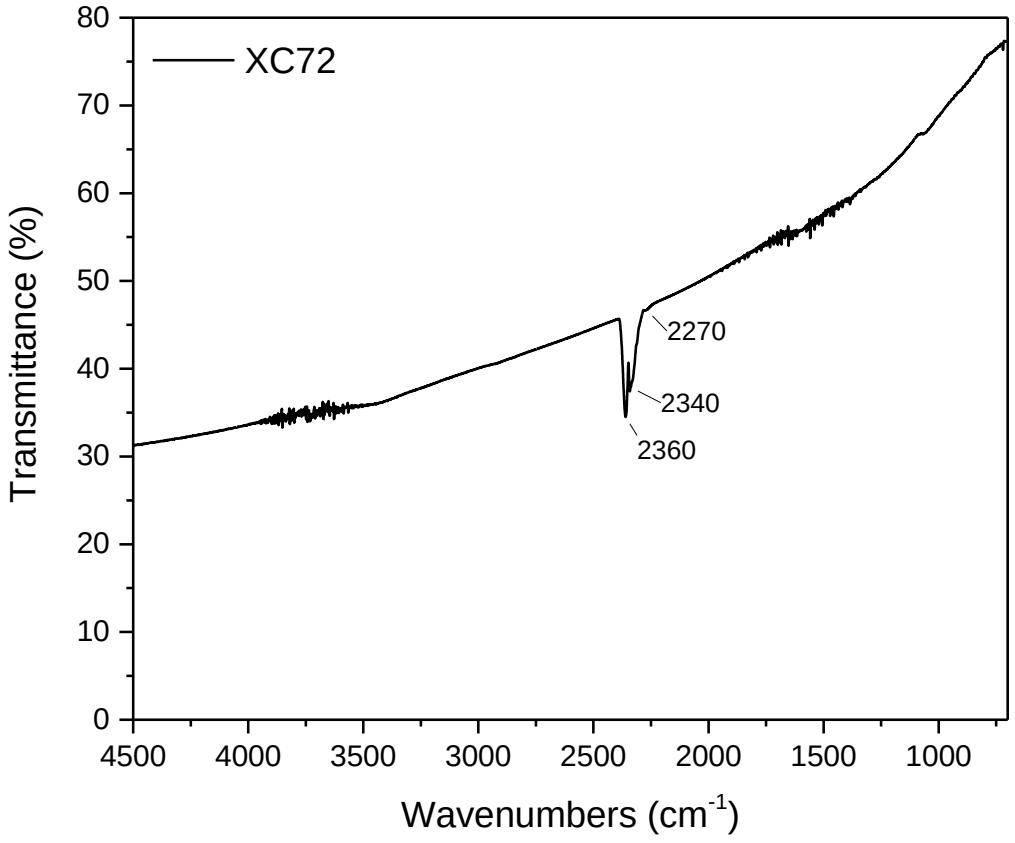

Figure 31, FTIR spectrum of XC72

We also evaluated the weight loss of the CB after heat treatments at 150°C for 4 hours, finding out the the weight loss was ~10%. This means that the Ensaco 350G isn't uniform in composition, and before impregnation and carburization it needs some thermal treatment in order to remove the contaminants and have an even batch.

We tried several different treatments changing temperature, atmosphere and time. As said, we started with a mild treatment at 150°C in air, but from FTIR we found out the presence s of residual organic phases, mainly due to alkanes group (peaks at 2850 and 2920 cm^{-1}), while the amine and amide peaks are disappeared, as can be seen in Figure 32. The absence of the peaks at 2340 and 2360 cm^{-1} are ascribed to the background subtraction, that was made with XC72 for this sample, while for the others the background was air.

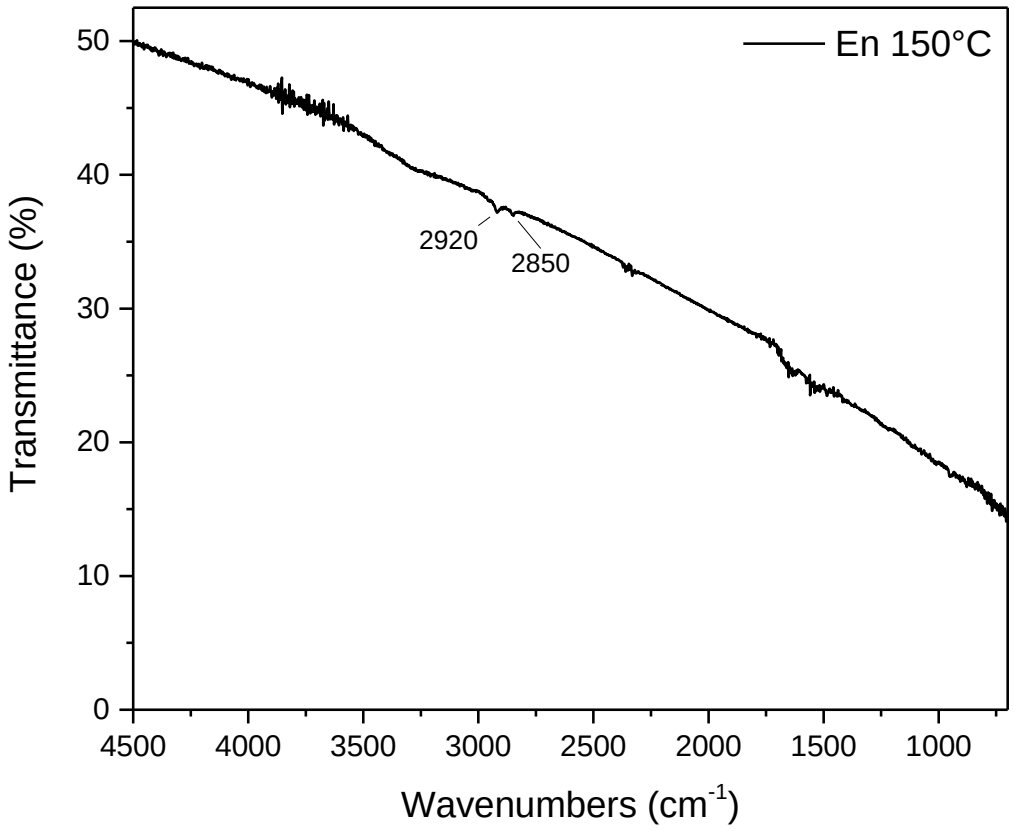

Figure 32, FTIR spectrum of Ensaco 350C treated at 150°C for 4 hours in air

So we maintained the temperature at 150°C but applying vacuum to remove all the volatile composites. After 24 hours, the weight loss was equal to 1.97%, a value that is very low compared to that collected with the previous treatment in air. This can be explained with the different mechanism that undergo in the two atmospheres. In air it is possible that pyrolysis occurs, with complex organic molecules that reacts with oxygen or nitrogen and give simpler and volatile compounds. In vacuum, in absence of oxygen and nitrogen, only amine and amide groups reacted as confirmed by FTIR in Figure 33, explaining the smaller loss.

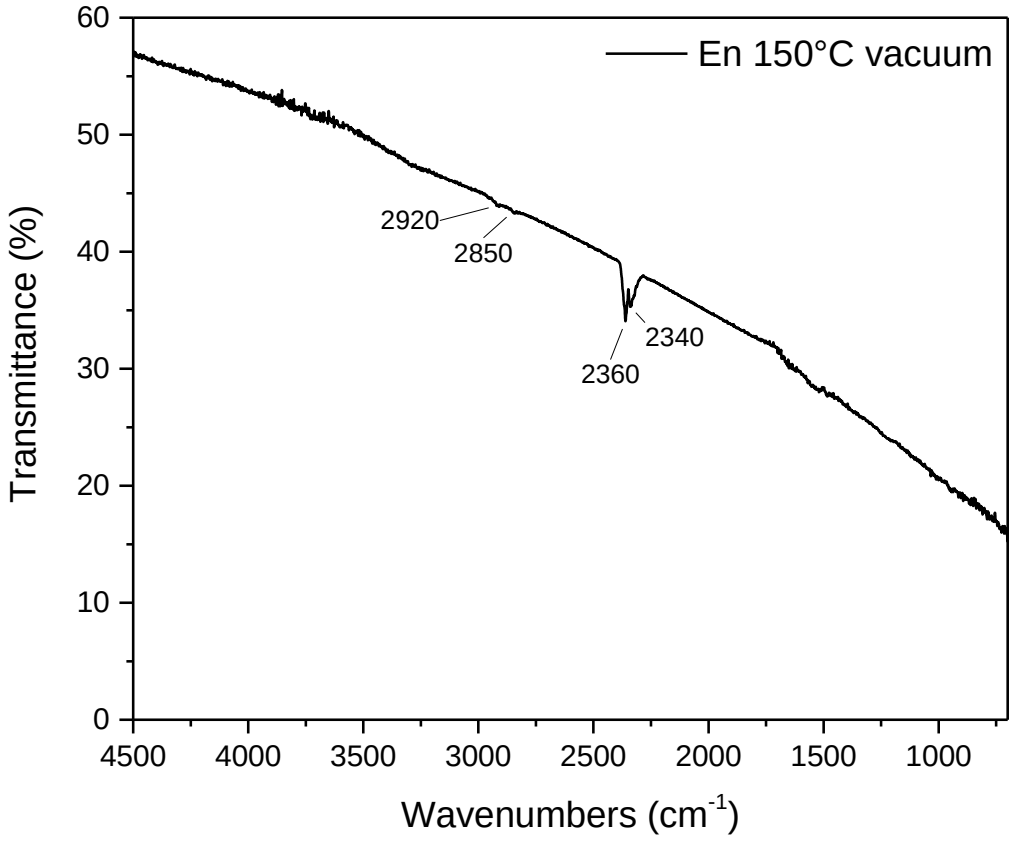

Figure 33, FTIR spectrum of Ensaco 350G treated at 150°C for 24 hours in vacuum

Increasing the temperature to 200°C, still in vacuum, we lost 1.99% of weight, a value that looks very similar to the previous one. This is another evidence for the explanation of the mechanism that starts at these temperatures.

The next treatment was conducted at 400°C in a different atmosphere, composed by pure argon, in a tubular furnace, because the vacuum oven doesn't permit to modify the gas atmosphere. For our purpose this atmosphere isn't very different from vacuum, because the Ar is a noble gas that doesn't react at this temperature. The only change is that volatile molecules that are produced with the thermal degradation are less prone to go to gas phase due to the presence of the pressure. After 6 hours of treatment, we recorded a weight loss of 1.98%, very close to the results collected in vacuum. From the FTIR spectrum in Figure 34, the two peaks at 2850 and 2920 cm^{-1} are still visible.

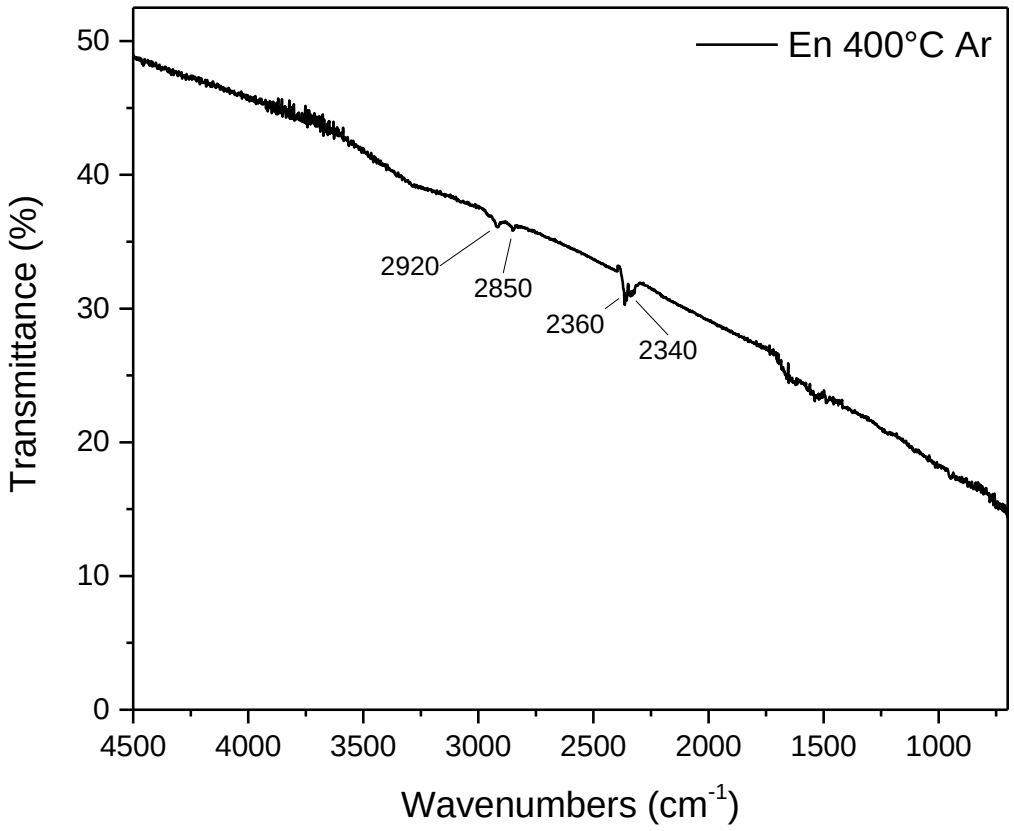

Figure 34, FTIR spectrum of Ensaco 350G treated at 400°C for 6 hours in argon

The final treatment was the combination of two, with a first step at 400°C in Ar and a second one at 150°C in vacuum, both for 6 hours. We didn't apply vacuum at 400°C in the tubular furnace because at that time we hadn't the necessary equipment to change the atmosphere and we needed to transfer the powder from the tubular furnace to the vacuum oven. We did this second step in order to remove all the small molecules that can be volatile at 200°C, losing 2.49% in weight at the end of the treatments. From FTIR spectrum in Figure 35, the CH and CH_2 groups are still present.

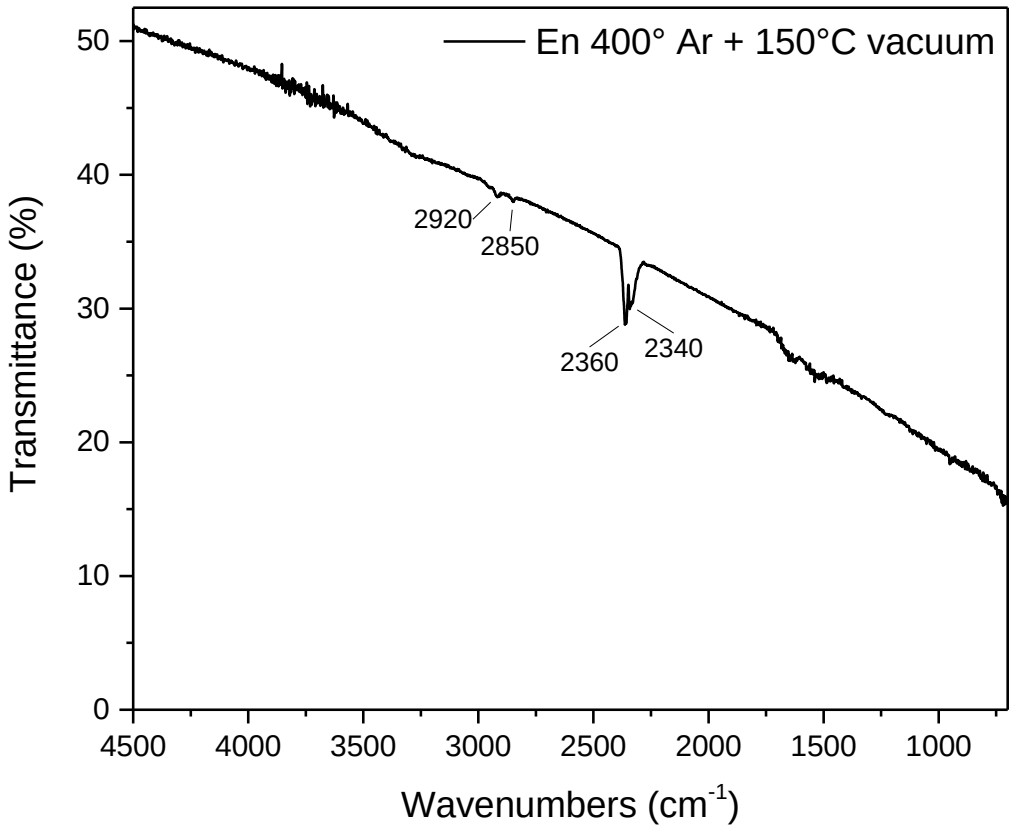

Figure 35, FTIR spectrum of Ensaco 350G treated at 400°C for 6 hours in Ar and at 150°C for 6 hours in vacuum

For a more complete view of the reactions that occur during the complete heat treatment we did DTA-TGA measurements both for the pure Ensaco and the Ensaco impregnated with titanium isopropoxide.

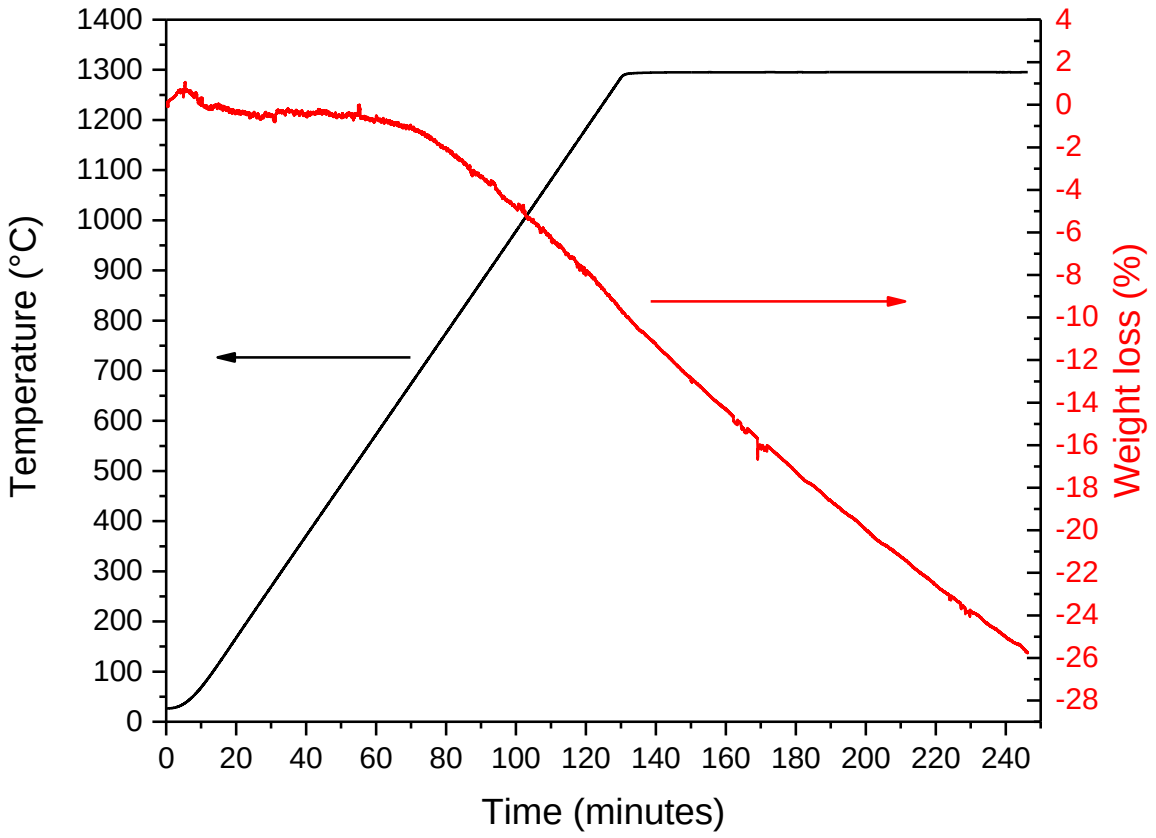

Figure 36, TGA plot of Ensaco treated up to 1300°C with a heating ramp of 10°C/min in Ar

In Figure 36 the TGA plot of pure Ensaco is reported. The heating program consists in a ramp of 10°C/min in Ar atmosphere and dwelling the top temperature of 1300°C for 3 hours. Unluckily the TGA instrument encountered a problem holding the inert atmosphere inside, allowing the argon to escape and letting in some air. This problem was resolved only after several months. It is possible to see that the weight loss, when ~700°C are reached, starts to increase in a linear way, meaning that inside the measure chamber the CB was undergoing a slow but complete oxydation.

Looking to the left section of Figure 36 where low temperatures are reached, we can anyway understand something. The weight loss is not so relevant, increasing slowly in 1 hour from ~1% to ~2%. That confirm the powder is not pure, with a small percentage of impurities that can be removed with treatments at moderate temperatures.

In Figure 37 the TGA plot of the impregnated Ensaco is reported. The problem encountered with the previous measure is not present, allowing the measure to be completed after 3 hours at 1300°C.

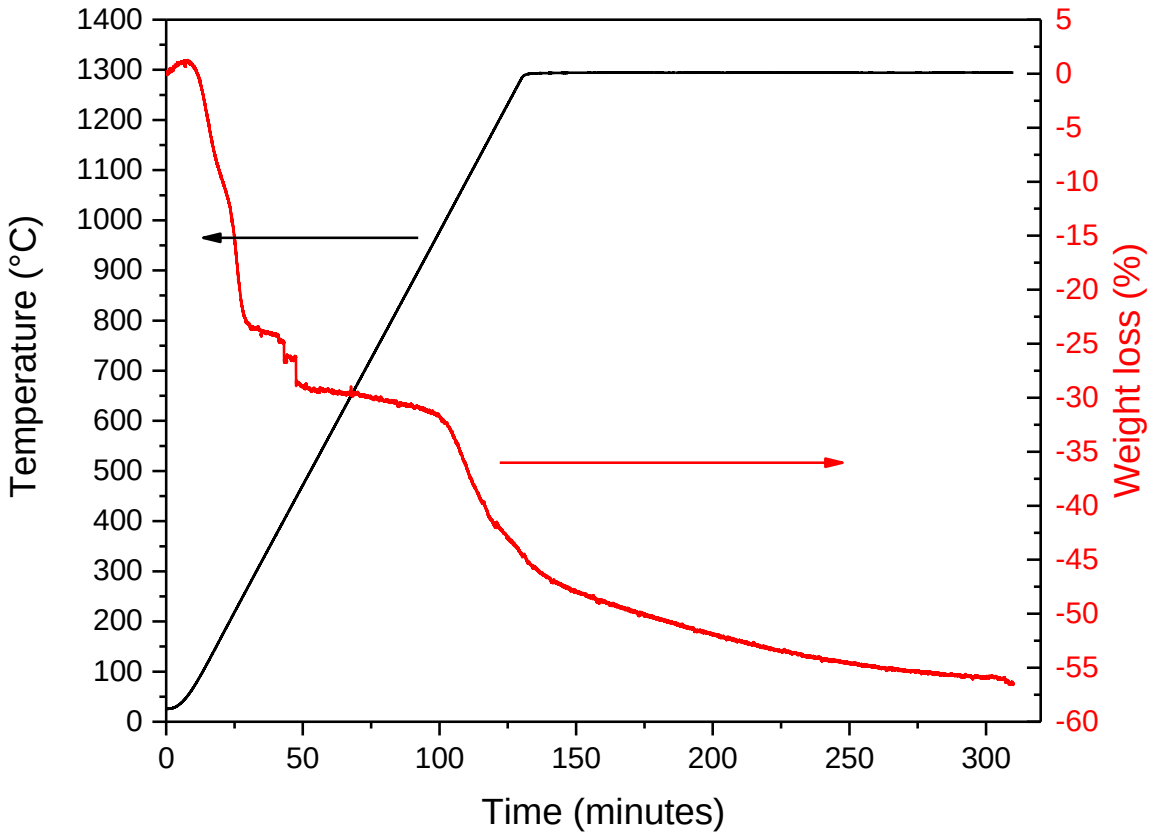

Figure 37, TGA plot of Ensaco+TiPO 2:1 treated up to 1300°C with a heating ramp of 10°C/min in Ar

The TGA curve can give a lot of information about the processes that occur during the heat treatment. It can be divided into three different sectors, the first one from room temperature up to 400-500°C, the second one from 500°C to ~1000°C and the latter one from 1000°C up to the top temperature.

In the first sector a steep weight loss happens, due to the evaporation of the byproducts produced from the degradation of the titanium propoxide, consisting mainly in propanol. The small steps are due to more complex byproducts. The second sector is instead pretty stable where the titanium alkoxide is fully converted in titanium dioxide but the temperature is too low to start the carburization. Only at temperatures higher than ~1000°C, corresponding to the start of the third sector, the carburization starts, initially involving only the contact layer between oxide and carbon, slowing down a little because of the diffusive processes that allows the complete carburization of the sample.

With these considerations in mind, we tried to obtain the wanted target (high purity, controlled stoichiometry and large surface area) with pre-treating the Ensaco before the impregnation and carburization.

We used for comparison the vacuum impregnation on two samples of CB, one treated at 200°C in vacuum for 24 hours, the other at 400°C in Argon for 6 hours and then at 150°C in vacuum for other 6 hours. In Figure 38 and Figure 39 the XRD patterns obtained from the two samples are shown, respectively. As can be easily noted, the non-stoichiometric oxides phases are still present. This leads to the conclusion that, albeit the Ensaco being pure after the pre-treatments, the problem cannot be related to the carbon source and other methods have to be used to reach the desired phase purity.

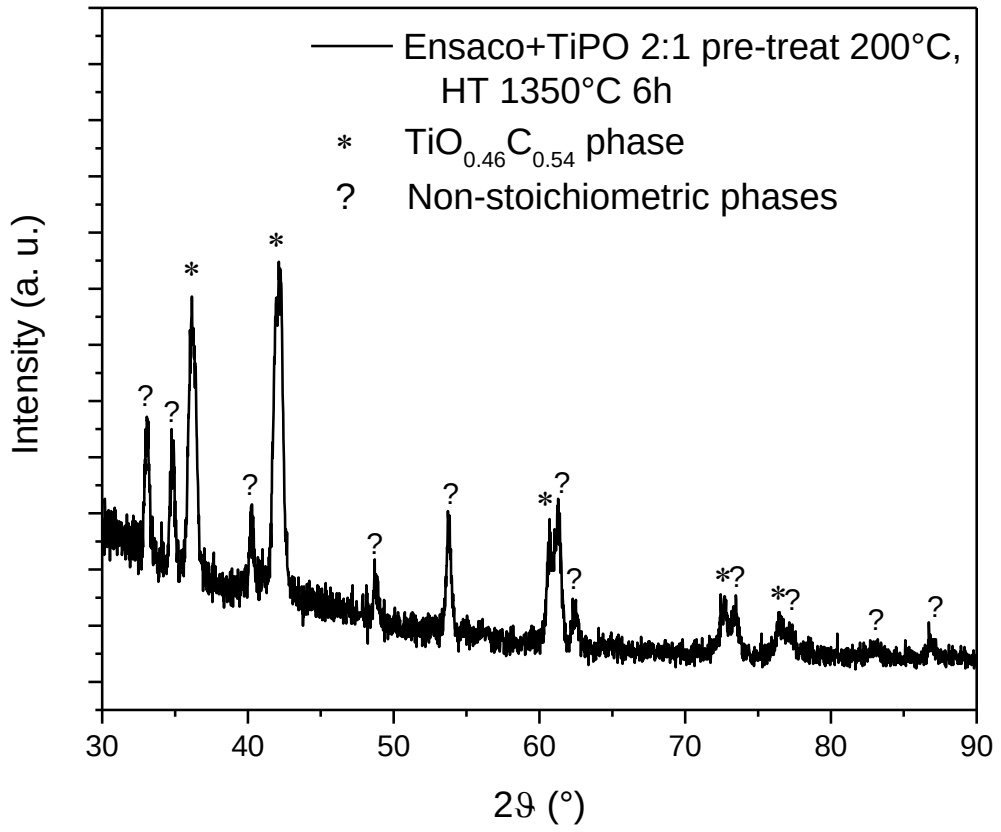

Figure 38, Ensaco+TiPO 2:1, pretreated at 200°C for 6 hours in vacuum, heat treated at 1350°C for 6 hours in Argon

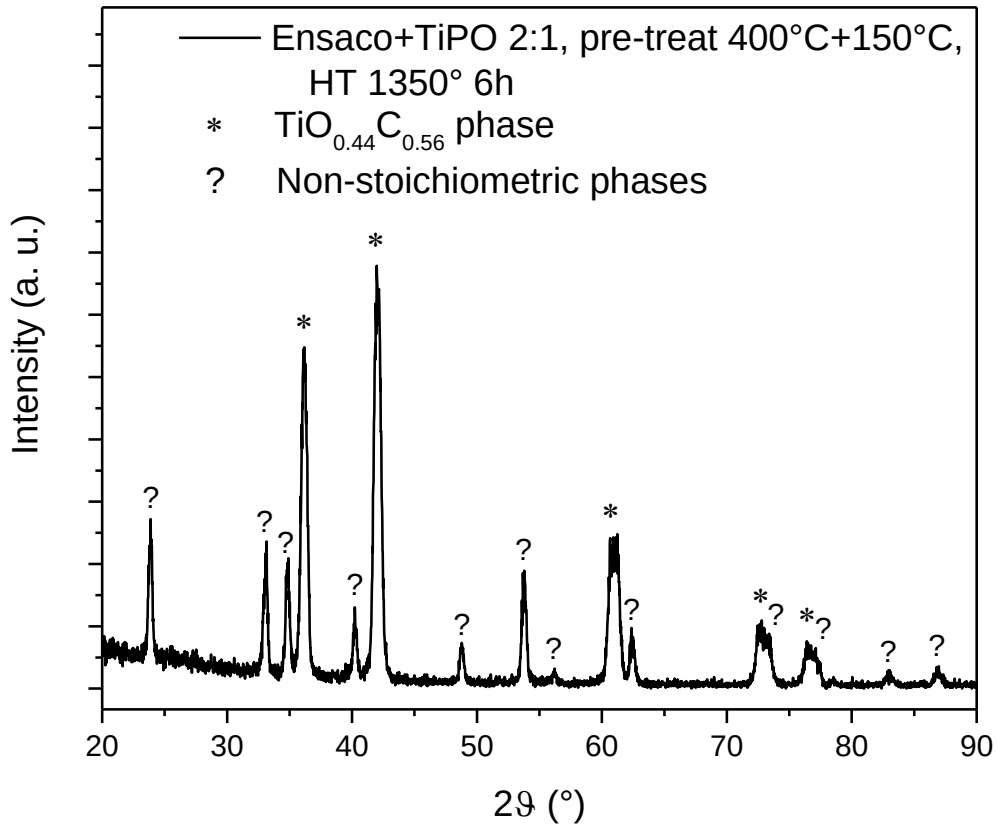

Figure 39, Ensaco+TiPO 2:1, pretreated at 400°C for 6 hours in Ar and at 150°C with vacuum for 6 hours, heat treated at 1350°C for 6 hours in Argon

Understanding that the non-stoichiometric phases cannot be removed before the heat treatment, we tried to remove them after. The titanium oxides can commonly be dissolved with an acidic solution of chloridic acid or sulfuric acid.

For the first test, we made a water solution with HCl at a pH=4 and soaked an already made titanium oxycarbide sample in the solution for different times. We left the powder in the solution for 2, 4 and 6 hours straight and recorded an XRD pattern after each interval. The results are shown in Figure 40.

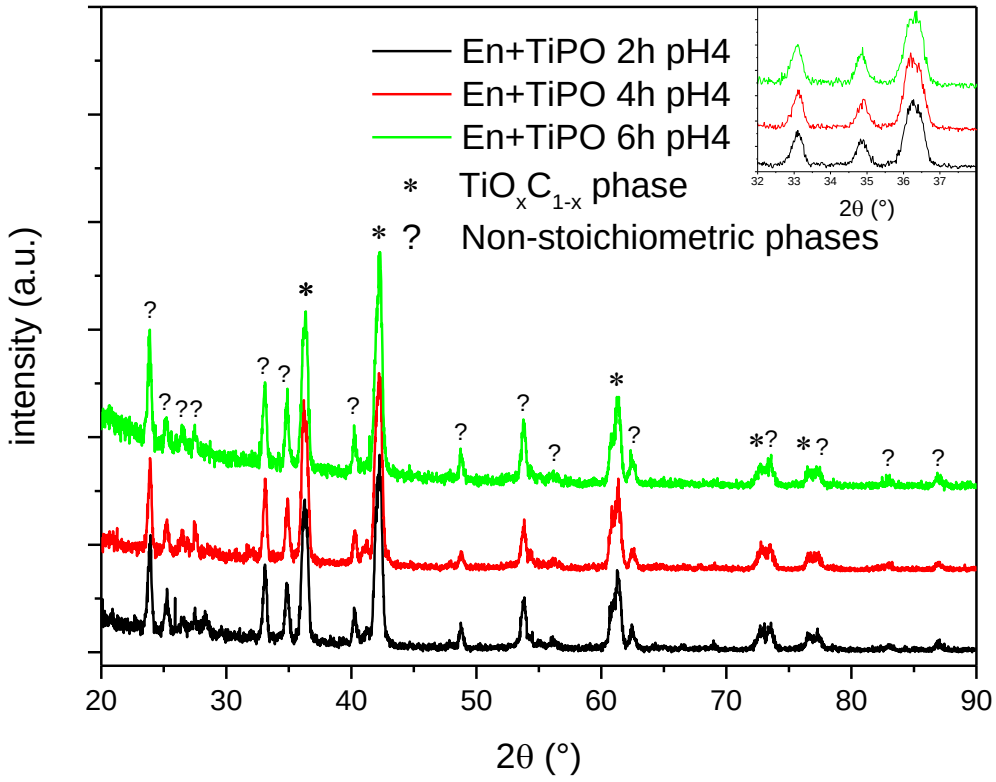

Figure 40, XRD patterns of titanium oxycarbide soaked in an HCl solution at pH=4 for 2, 4 and 6 hours

The samples show the same peaks of both the non-stoichiometric phases and the titanium oxycarbide, although the latter are not modified. This means that the acid is too diluted to sort some effect, so we tested another solution of HCl with a pH=1. We increased also the time of the treatment to 18 hours. The results from the XRD analysis are shown in Figure 41, meanwhile in Figure 42 there is a zoom on the position of the two main peaks of the titanium oxycarbide.

As can be easily seen in the first figure, the non-stoichiometric phases are nearly completely removed, albeit small traces are still present. In the second figure, it can be noted that the two main peaks of the same sample after and before the acidic treatment aren't in the same position, meaning that the HCl has attacked not only the oxides but also the titanium oxycarbide lowering the oxygen content, as reported in Table 7.

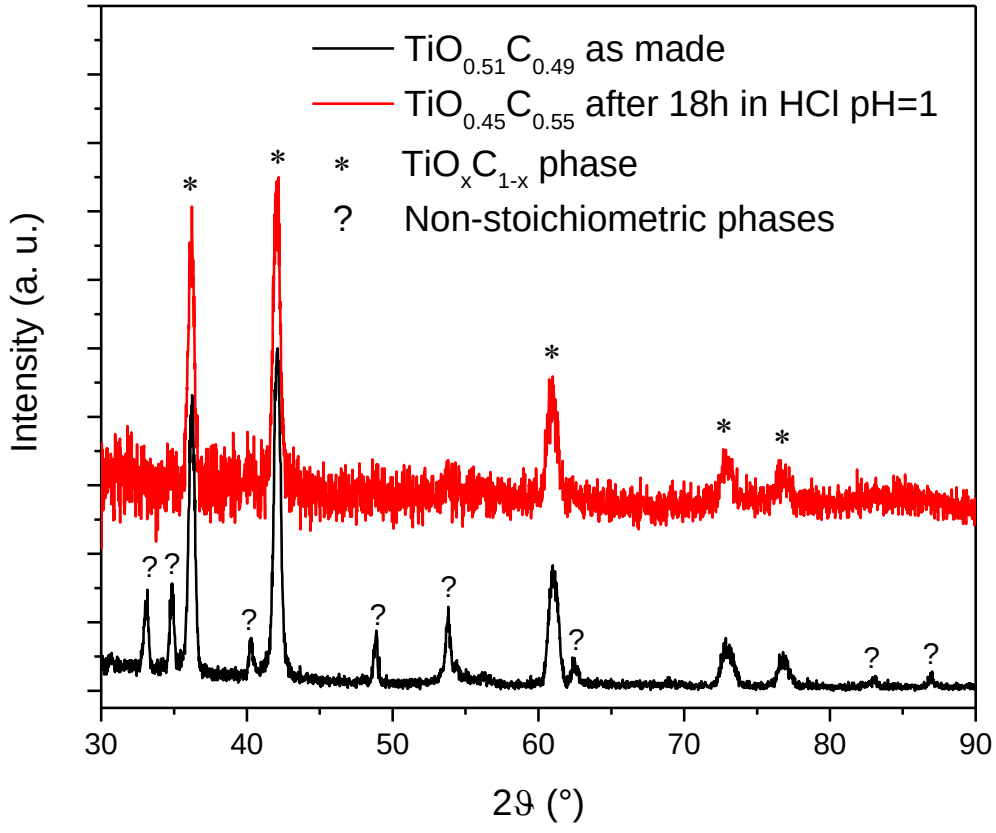

Figure 41, XRD patterns of titanium oxycarbide before and after the HCl solution at pH=1 treatment for 18 hours

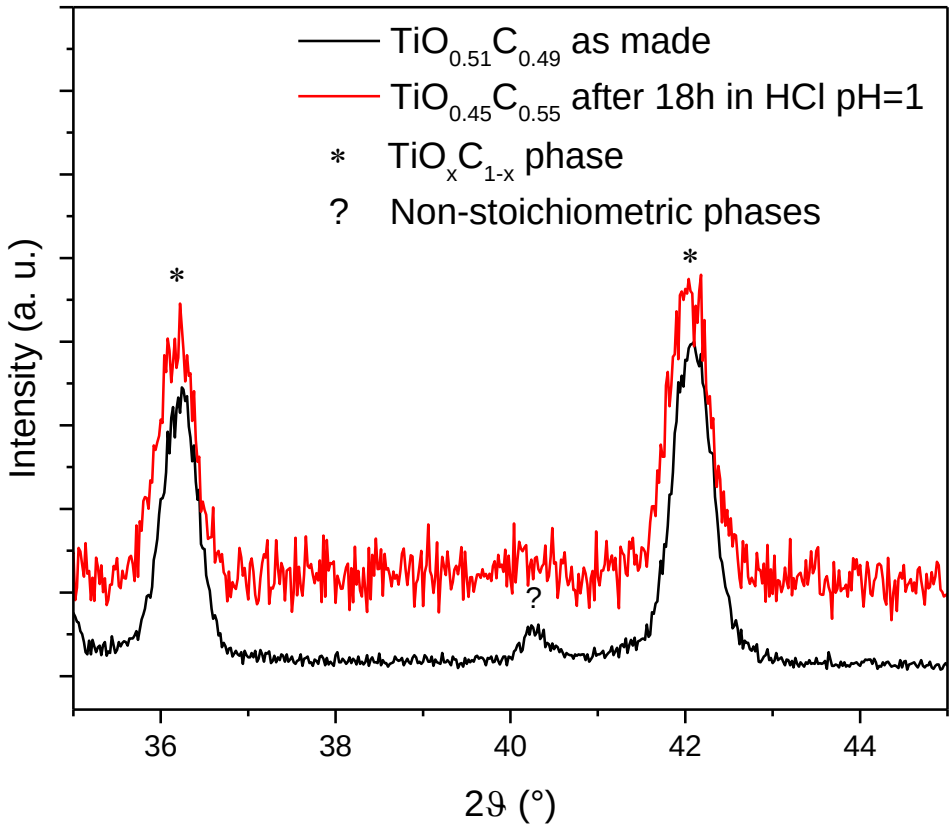

Figure 42, zoom on the two main peaks from XRD patterns of titanium oxycarbide before and after the HCl solution at pH=1 treatment for 18 hours.

Sample	***1st peak position (°)***	***2nd peak position (°)***	***Cell parameter (Å)***	***Oxygen content (mol%)***
Before	36.24	42.11	4.2889	51
After	36.18	42.04	4.2942	45

Table 7, peak position, cell parameter and oxygen content of the titanium oxycarbide before and after the treatment with HCl solution at pH=1 for 18 hours

The HCl solution is too aggressive against the titanium oxycarbide, meaning that such a treatment is not suitable for our purposes.

We decided then to use phosphoric acid (H_3PO_4). We made a solution in water with a pH=1 and treated the same sample in the new solution for 12 hours to evaluate the behavior of this acid. In Figure 43 the XRD patterns are reported.

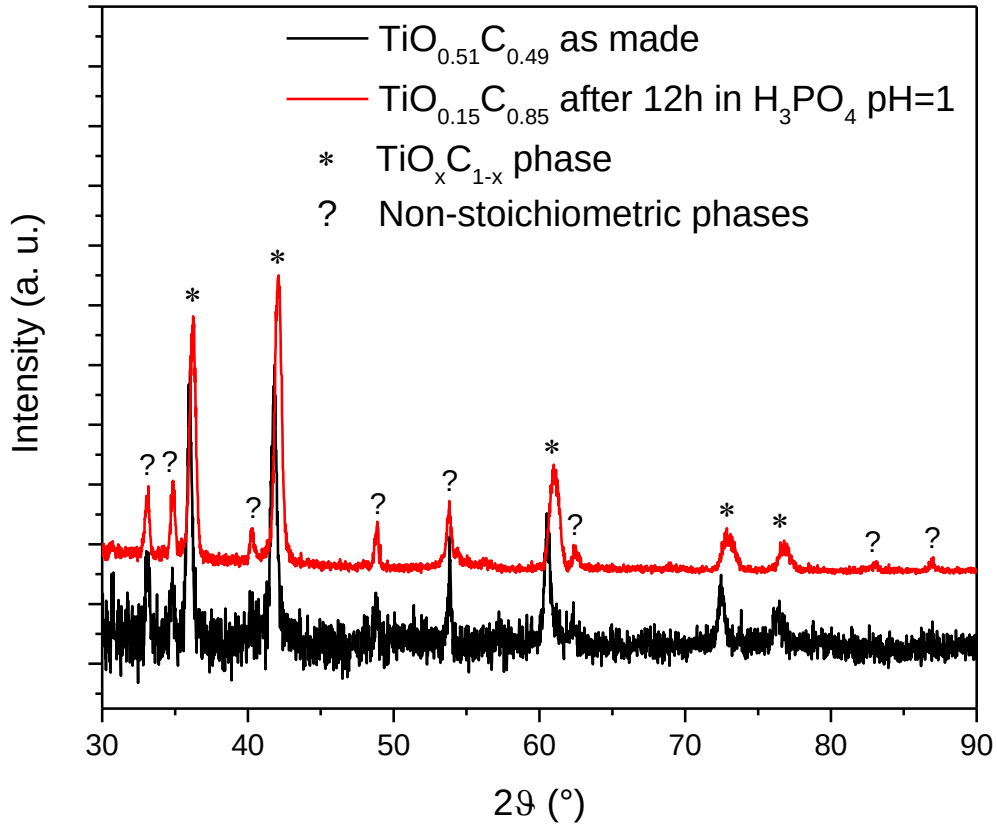

Figure 43, XRD patterns of titanium oxycarbide before and after the H_3PO_4 solution at pH=1 treatment for 12 hours.

It can be steadily seen that the main peaks of the oxycarbide peaks are completely shifted toward higher angles, meaning that the stoichiometry is poorer in oxygen, as reported in Table 8.

Sample	***1st peak position (°)***	***2nd peak position (°)***	***Cell parameter (Å)***	***Oxygen content (mol%)***
Before	36.24	42.11	4.2889	51
After	36.00	41.79	4.3168	15

Table 8, peak position, cell parameter and oxygen content of the titanium oxycarbide before and after the treatment with H_3PO_4 solution at pH=1 for 12 hours

With this treatment the results are worse than the expected ones, not only because the stoichiometry changes completely but also because the non-stoichiometric phases aren't removed from the sample. The removal of the unwanted phases with acids cannot be completed without undermining the titanium oxycarbide.

Considering all the tests that were made, a major change is needed in order to fulfill the objectives that are aimed, namely a high purity, large surface area and controllable stoichiometry. After changing the hydrolyzation parameters, the heat treatment and purity of the carbon black, the only thing that can be modified is the titanium precursor.

Because of the small diameter of the pores of the Ensaco 350G, we investigated the feasibility of use of a smaller molecule that could act as titanium oxide precursor. There are two possibilities: the first one is the use of a smaller and simpler titanium alkoxide, like titanium methoxide o titanium ethoxide; the second one is using titanium halides, as titanium tetrachloride. Both the two families suffer for a common problem, that is the high reactivity in air. We preferred to use titanium ethoxide because it represents a good compromise between reactivity and molecular dimension, meanwhile the titanium chloride, albeit having smaller molecules, is too reactive releasing hydrochloric acid when exposed to the ambient moisture and generating a great amount of heat.

In order to lower the reactivity of the titanium ethoxide (TiEtO) we diluted it in pure ethanol, also because the volume of alkoxide for a C:Ti ratio of 2:1 is too low to wet completely the powder. The first test was conducted in the easiest way possible, i.e. impregnating the Ensaco with a solution of TiEtO and ethanol, mixing it until all the powder is evenly wet and then drying and hydrolyzing the precursors in an oven at 60°C for 24 hours. After all these steps, the sample is put in the tubular furnace under a constant flow of argon and heated to 1350°C with a ramp of 10°C/min. The dwell time of the higher temperature was set to 6 hours, representing the same carburization routine used for the previous samples.

When the temperature inside the tubular furnace reaches ambient values after natural cooling, the sample is removed and analyzed preliminary with the XRD, which pattern is reported in Figure 44.

The results are very promising because the unwanted phases are greatly reduced, only few small peaks are visible. This means that the titanium alkoxide with smaller molecules is able to penetrate better the Ensaco, creating an intimate mix that doesn't create a core-shell like structure.

Albeit the good preliminary results more tests have been performed in order to corroborate this thesis.

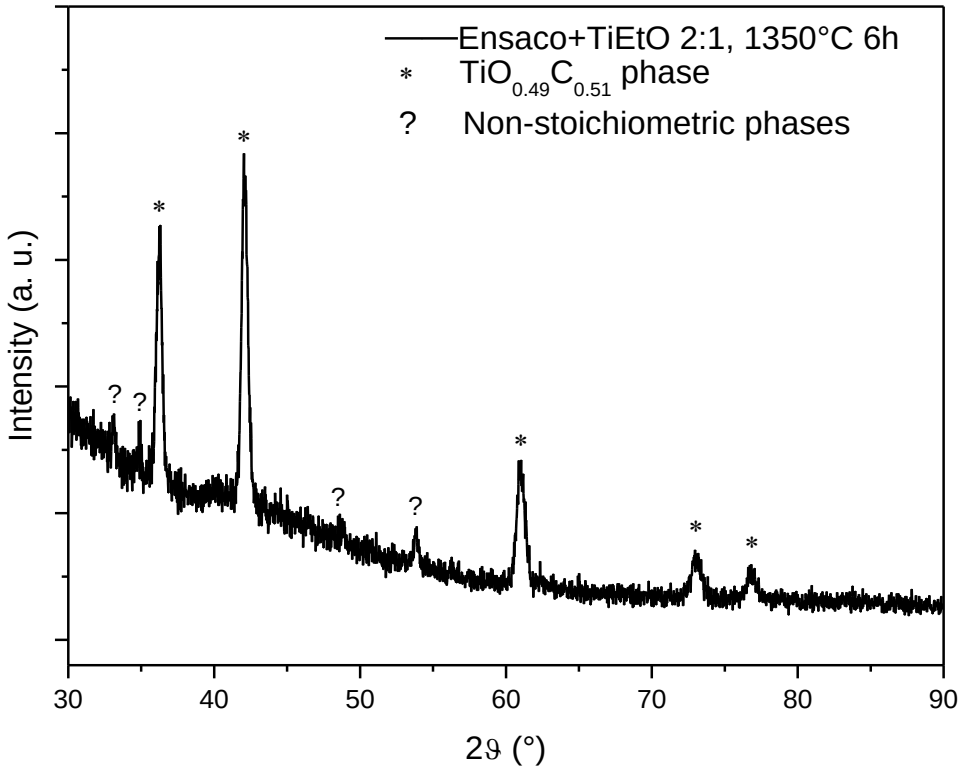

Figure 44, XRD pattern of Ensaco+TiEtO 2:1, air hydrolyzation, 1350°C for 6 hours.

After the first one, two more samples were prepared in the same way to check if it was only a fortunate coincidence.

The two new samples are made exactly with the same procedure, diluting the titanium ethoxide in pure ethanol for better wetting properties. After the hydrolyzation in air at 60°C for 24 hours, the powders were placed inside the tubular furnace for the carburization step.

The acquired XRD patterns are reported in Figure 45. The patterns show a good reproducibility, with only very small peaks from other phases. This means that the quantity of non-stoichiometric phases is very small, but there are still traces of them.

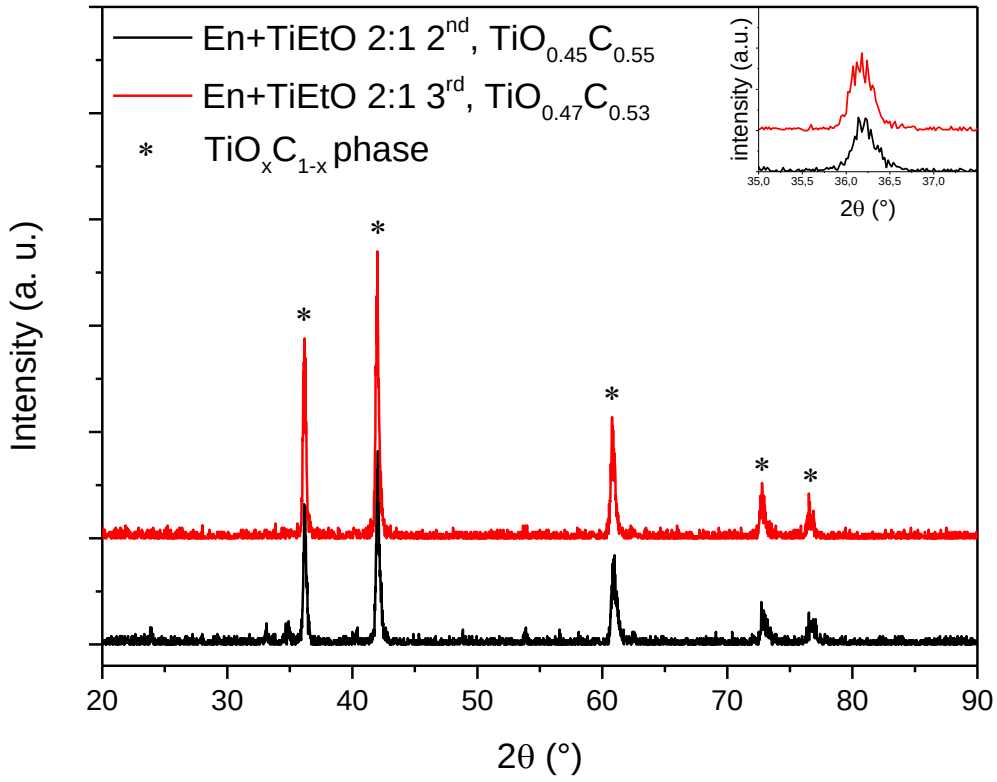

Figure 45, XRD patterns of Ensaco+TiEtO 2:1, 1350°C 6 hours, 2nd and 3rd sample.

Minding all the test made before to achieve the best combination of hydrolyzation and carburization parameters, we tried to change one at a time for eliminate as much as possible the traces of non-stoichiometric phases.

The first variation was made with the impregnation and subsequent hydrolyzation. We used again the glove box hydrolyzation to achieve a controlled and more precise result. Within an atmosphere of argon, the Ensaco was impregnated with the diluted titanium ethoxide and, when well mixed, a proper quantity of acidic water with pH=4-5 was added dropwise. After two hours the powder is removed from the glove box and dried in an oven at 60°C in order to remove the remaining ethanol and all the byproducts of the hydrolyzation, that are mainly ethanol and water.

The carburization step for the first “glove box” sample was the same as used for the previous samples, that means a top temperature of 1350°C for 3 hours with a heating ramp of 10°C/min and natural cooling.

The XRD pattern of the carburized sample is reported in Figure 46.

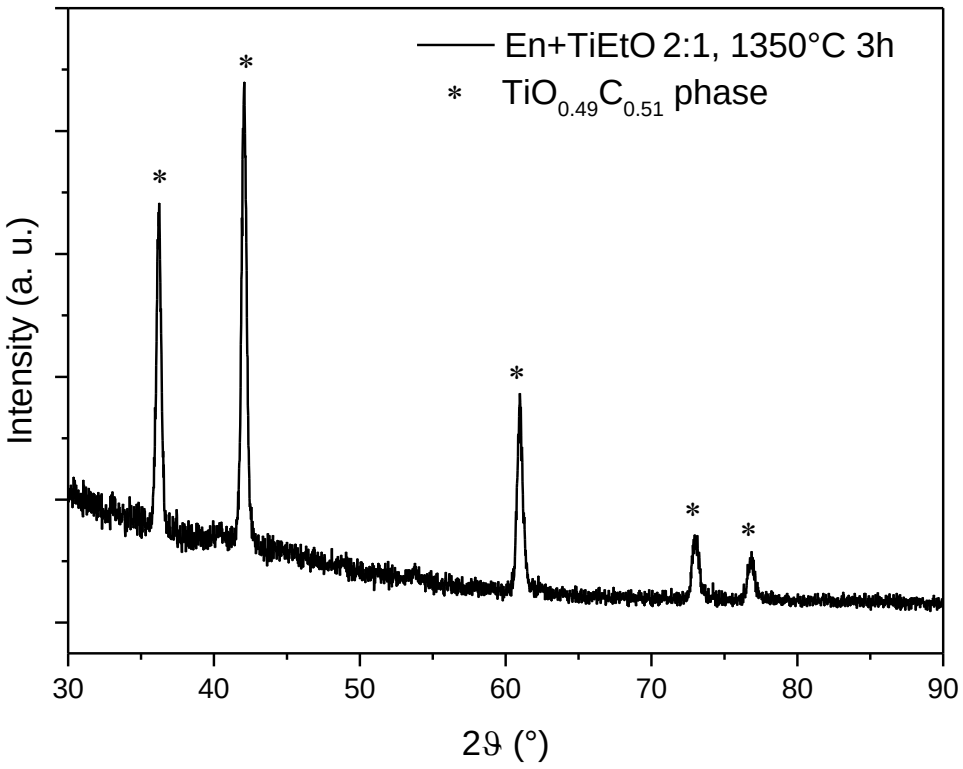

Figure 46, XRD pattern of Ensaco+TiEtO 2:1, glove box hydrolyzation, 1350°C for 3 hours.

We analyzed also the peak position in order to discover the stoichiometry of the titanium carbide, that are summarized in Table 9.

1st peak position (°)	***2nd peak position (°)***	***3rd peak position (°)***	***4th peak position (°)***	***5th peak position (°)***	***Cell parameter (Å)***	***Oxygen content (mol%)***
36.22	42.07	60.98	73.08	76.83	4.2911	49

Table 9, peak positions, cell parameter and oxygen content of Ensaco+TiEtO 2:1, glove box hydrolyzation, 1350°C 3hrs

The oxygen content is exactly the searched one because the value has an error of ±2%. Near all the unwanted phases are disappeared because there are no recognizable peaks but the five of the titanium oxycarbide. This is a great goal because all the hydrolyzation problem are resolved, leading to a perfectly mixed solid solution of TiO and TiC.

We tried to enhance the synthesis lowering by 50°C the carburization temperature, in order to have a final product that, within an industrial point of view, can be more convenient. The used hydrolyzation method is the same, the glove box routine, meanwhile the heat treatment was conducted at 1300°C for 3 hours before natural cooling. The result from the XRD measurements is reported in Figure 47.

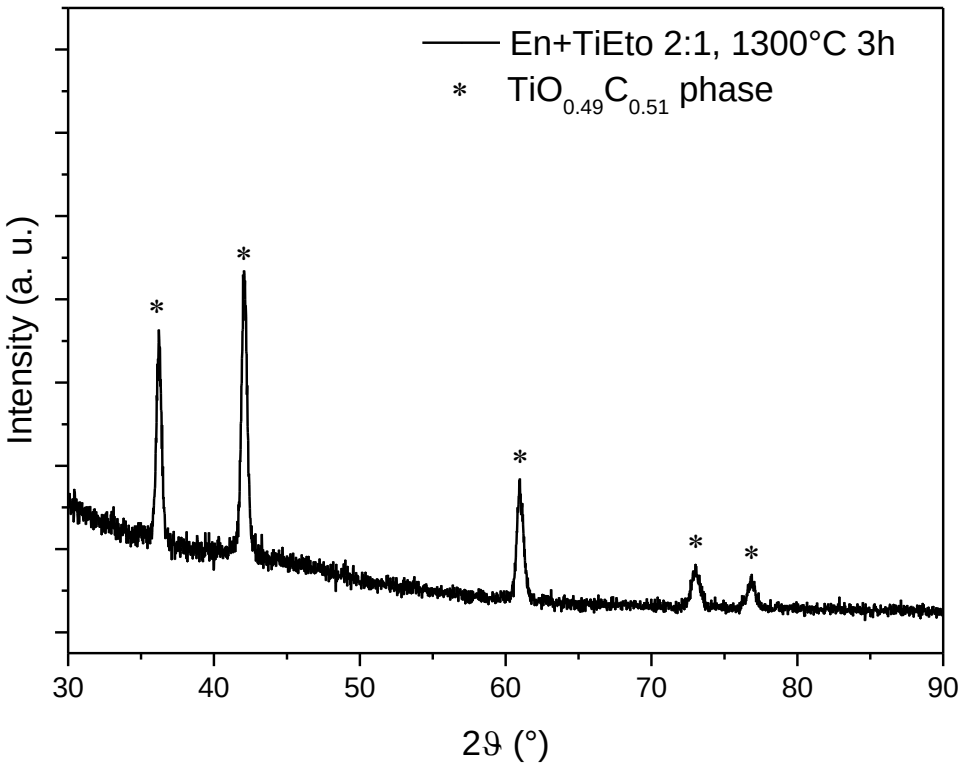

Figure 47, XRD pattern of Ensaco+TiEtO 2:1, glove box hydrolyzation, 1300°C for 3 hours.

Lowering the temperature, the formation of unwanted phases hasn't taken place, leading only to titanium oxycarbide. The peak positions and oxygen content are reported in Table 10.

1st peak position (°)	***2nd peak position (°)***	***3rd peak position (°)***	***4th peak position (°)***	***5th peak position (°)***	***Cell parameter (Å)***	***Oxygen content (mol%)***
36.23	42.08	61.00	73.02	76.85	4.2908	49

Table 10, peak positions, cell parameter and oxygen content of Ensaco+TiEtO 2:1, glove box hydrolyzation, 1300°C 3hrs

As can be seen, the positions of the peaks slightly differ from the previous sample, but without compromising the final result. This is a big achievement, because with a better and more intimate mixing

of the precursors the carburization can be conducted at lower temperatures without sacrificing the purity or composition.

The next step was to establish the surface area in order to determine if the obtained titanium oxycarbide is suitable or not as support in a fuel cell. As said before, the minimum requirement is 100 m^2g^{-1}. From the BET analysis the results are very surprising, but not in a good way. The surface area is calculated to be 12 m^2g^{-1}, far away from the expected values and only a small fraction of the starting value for the pure Ensaco (800 m^2g^{-1}). The pore distribution is not completely changed, as can be seen in Figure 48.

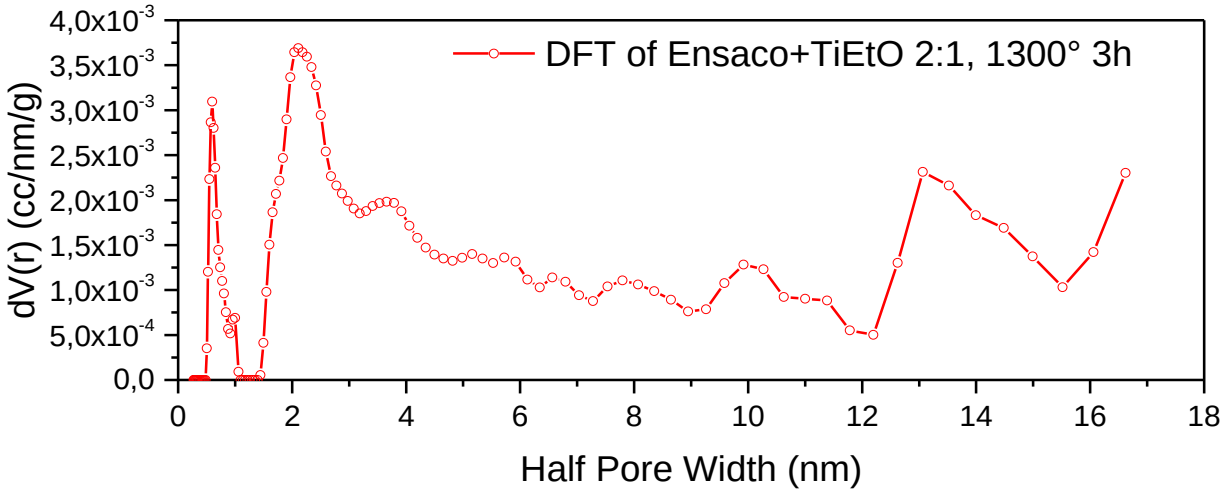

Figure 48, DFT analysis of Ensaco+TiEtO 2:1, 1300°C 3 hours

Now the pores have the same radius, but their volume is decreased by a factor of ~66. The DFT model that fitted best the experimental points suggests that the pores still have round shape, with similar diameter but different depth.

In order to understand the reasons behind the dramatic lowering of surface area we treated pure Ensaco, not impregnated, with the carburization routine, heating it with a ramp of 10°C/min up to 1300°C for 3 hours. After the treatment the powder was analyzed again with BET for verifying if it is the typical behavior of this carbon black.

The isotherm plot and the DFT pore distribution are shown in Figure 49 and Figure 50.

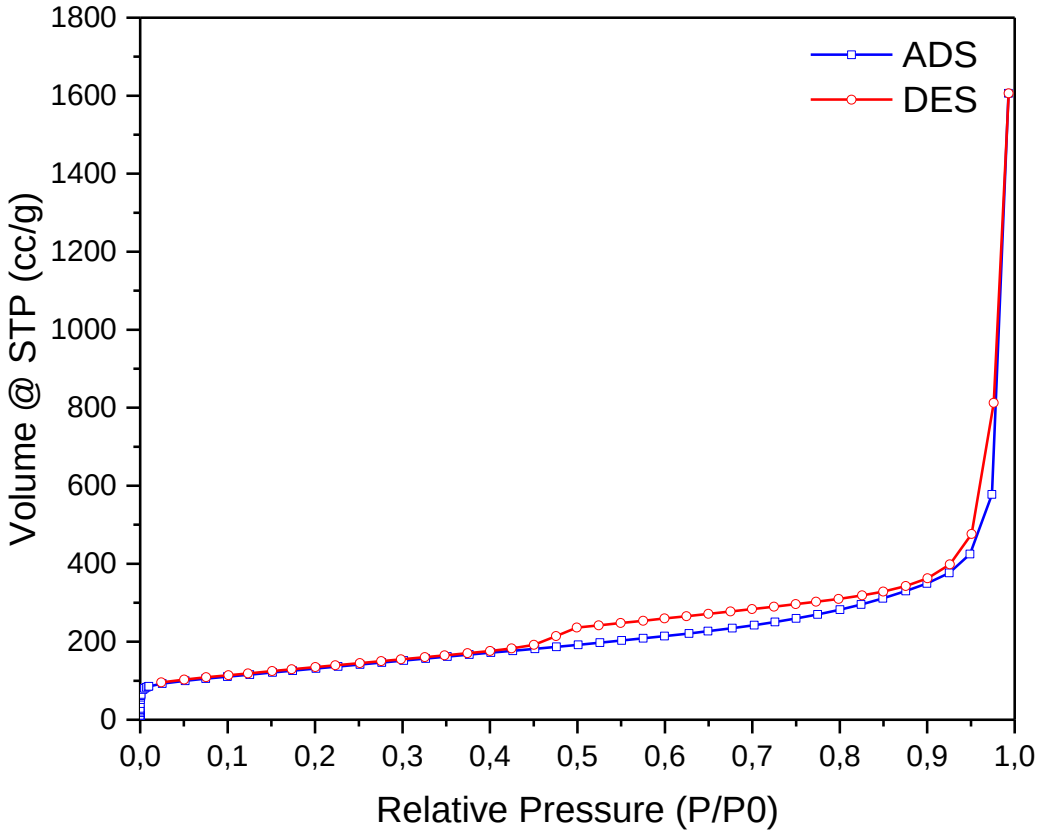

Figure 49, isotherm plot of pure Ensaco, 1300°C 3 hours

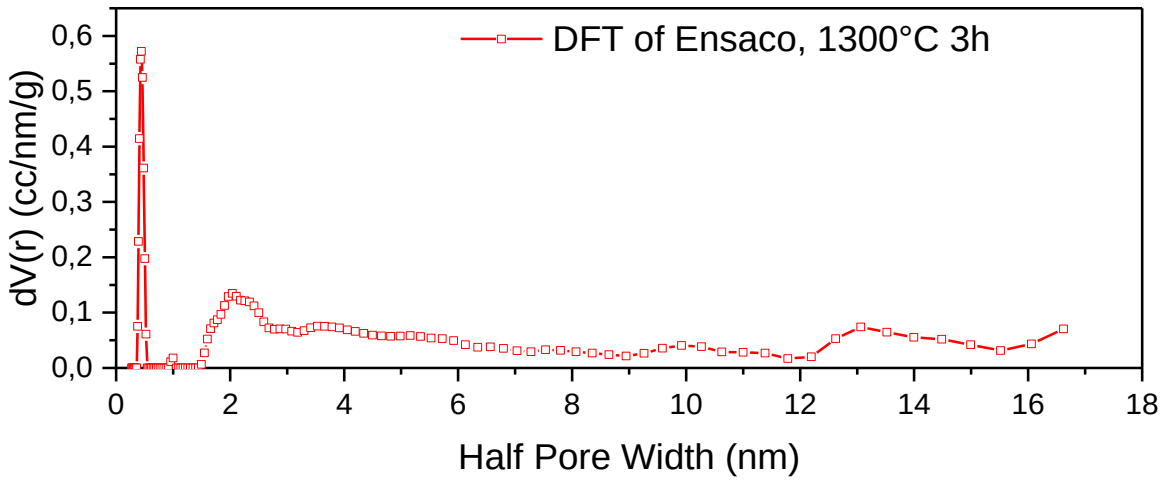

Figure 50, DFT analysis of pure Ensaco 2:1, 1300°C 3 hours

The surface area from the BET is 475 m^2g^{-1}, almost half of the pure Ensaco (800 m^2g^{-1}).

In Figure 51 and Figure 52 a comparison of the different isotherm plots and DFT analyses is presented.

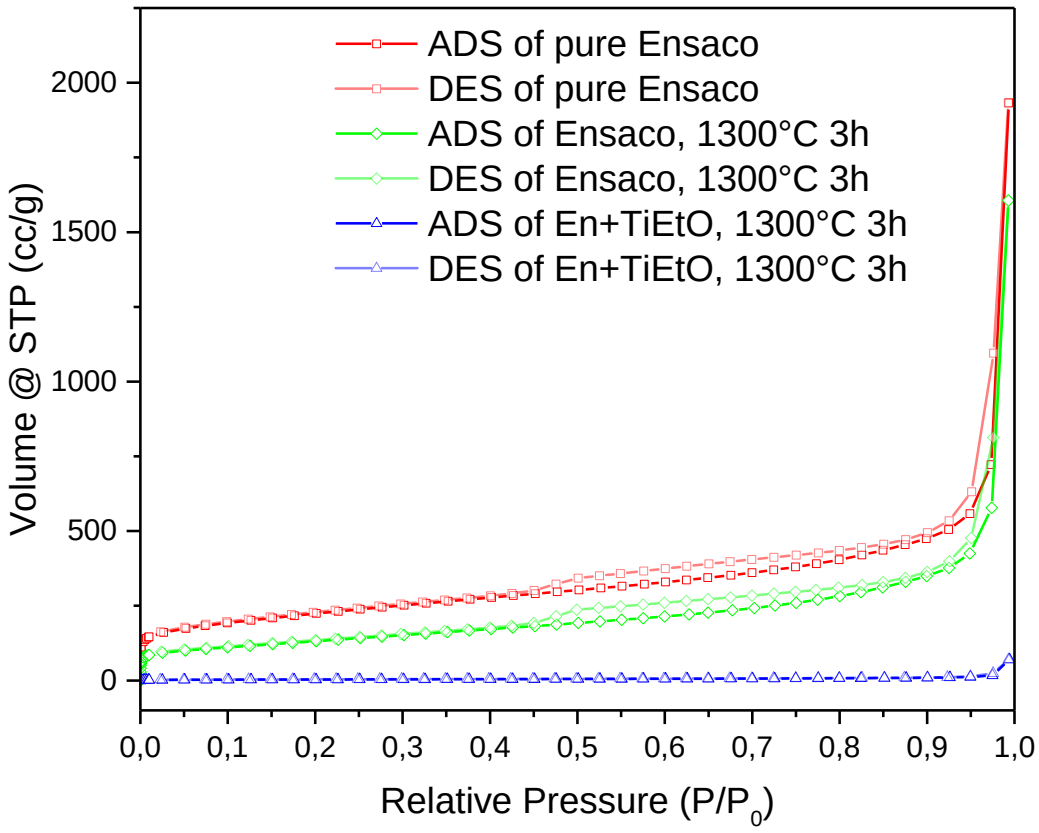

Figure 51, isotherm plots comparison of pure Ensaco, pure Ensaco treated at 1300°C for 3 hours and Ensaco+TiEtO treated at 1300°C for 3 hours

As can be seen in the first image, the isotherm plots of the treated and non-treated Ensaco are pretty similar. The isotherm plot of the Ensaco+TiEtO is very low, reflecting the small surface area of the titanium oxycarbide.

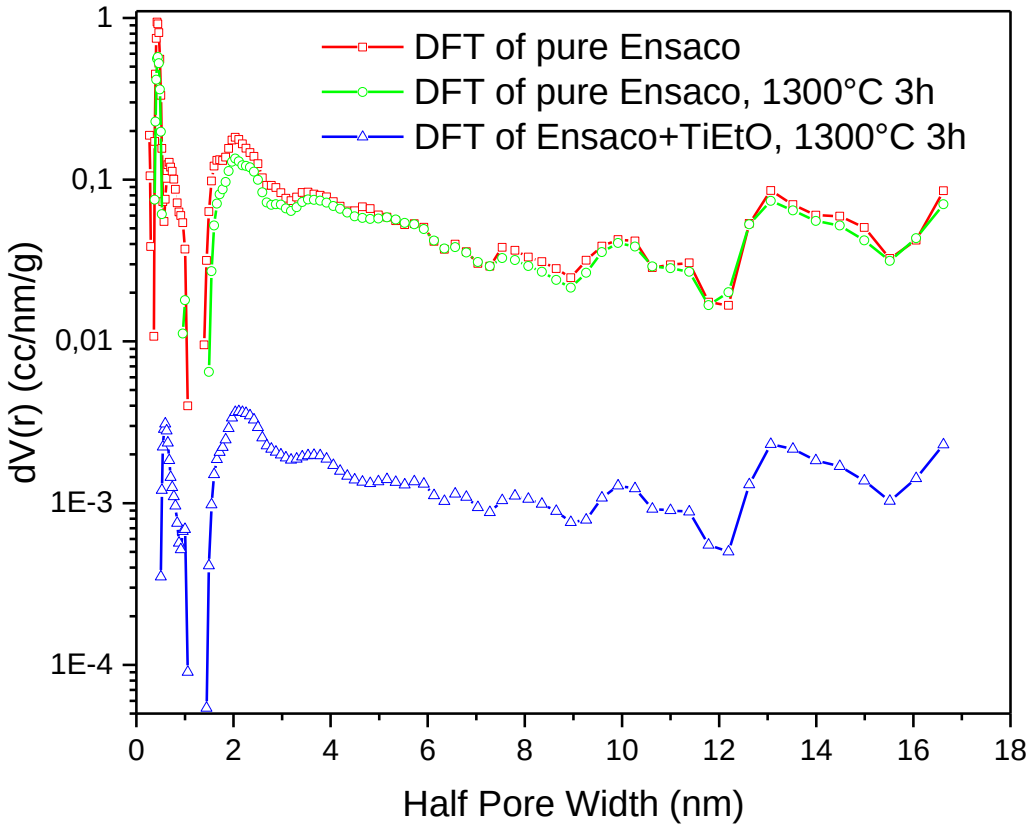

Figure 52, DFT analysis' comparison of pure Ensaco, pure Ensaco treated at 1300°C for 3 hours and Ensaco+TiEtO treated at 1300°C for 3 hours. Note the logarithmic scale

The DFT analyses enlighten that the pores' dimensions and distribution are very similar through all the samples, albeit with a drift. This means that the powder grains retain the same morphology after the heat treatment, losing only the depth of the pores that can be estimated to be round capillary from the used DFT model.

We prepared new samples in order to check if the previous results were due to only coincidence or they are systematic. We made two samples in slightly different ways: the first one was impregnated and hydrolyzed in air, without the aid of the glove box and water to accomplish a perfect and stable mix. The second one was conducted again in the glove box.

The XRD pattern for the first sample is presented in Figure 53, for the second sample in Figure 54.

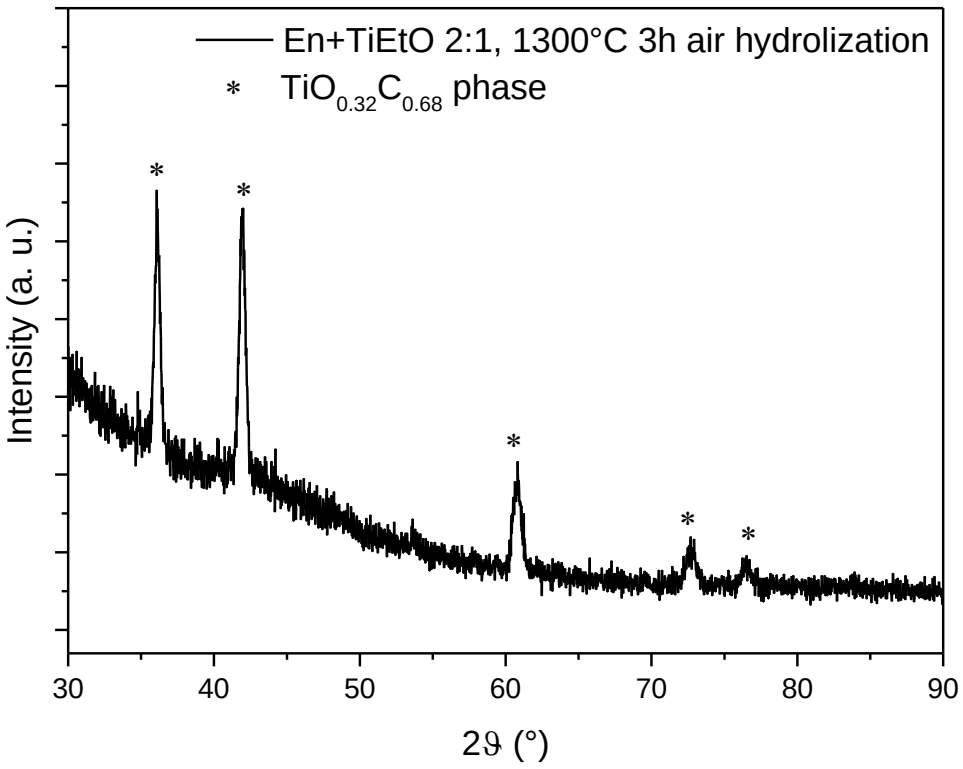

Figure 53, XRD pattern of Ensaco+TiEtO 2:1, air hydrolyzation, heat treated at 1300°C for 3 hours

As can be noted the two patterns look very similar, showing the five characteristic peaks of the titanium oxycarbide without traces of unwanted phases. The peaks are not in similar positions, as summarized in Table 11.

Sample name	*1st peak position (°)*	*2nd peak position (°)*	*3rd peak position (°)*	*4th peak position (°)*	*5th peak position (°)*	*Cell parameter (Å)*	*Oxygen content (%)*
Air hydrolization	36.11	41.95	60.78	72.71	76.52	4.3052	32
Glove box hydrolyzation	36.24	42.09	61.03	73.01	76.84	4.2902	49

Table 11, peaks' position, cell parameters and oxygen content of Ensaco+TiEtO hydrolyzed in air and hydrolyzed in glove box, both heat treated at 1300°C for 3 hours

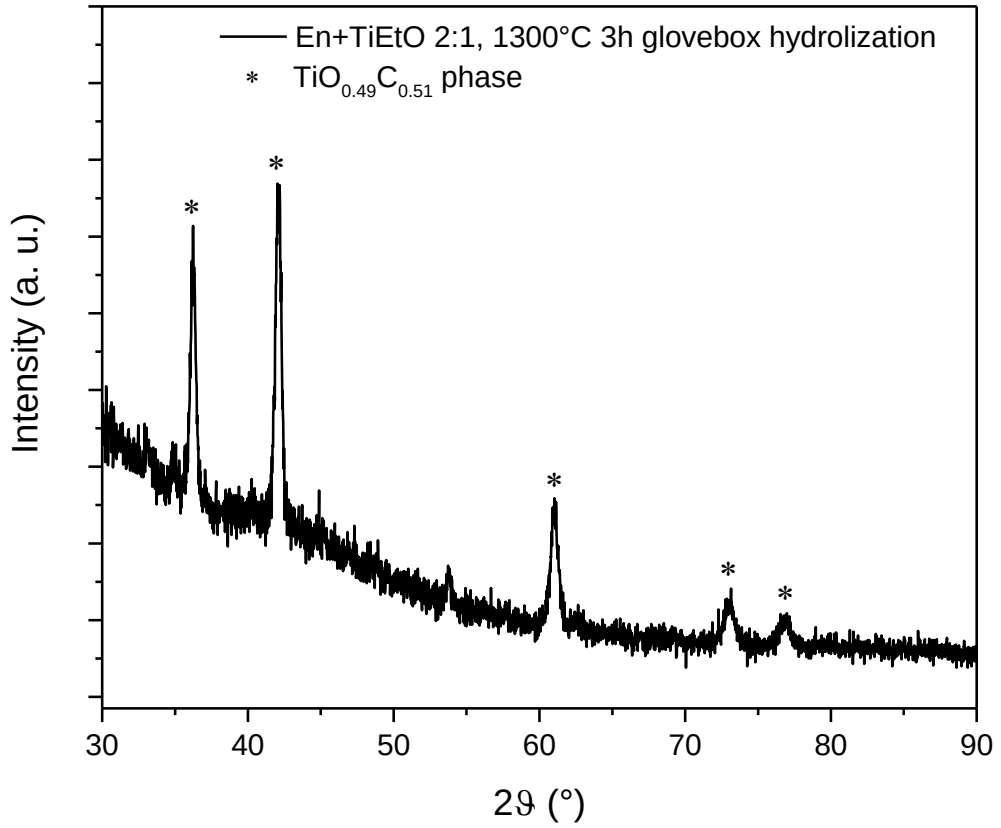

Figure 54, XRD pattern of Ensaco+TiEtO 2:1, hydrolyzed in glove box, heat treated at 1300°C for 3 hours

The different peaks positions are related to the different method used for impregnation and hydrolyzation, confirming that the TiEtO is very sensitive to the moisture and encounters a very fast hydrolyzation,

blocking the complete and intimate impregnation of the Ensaco powder. From BET analyses, we obtained again very low specific surface area, similar to the previous ones: for the air hydrolyzed sample we obtained 13 m^2g^{-1}, meanwhile for the glove box hydrolyzed one 14 m^2g^{-1}. This means that the occlusion of the pores seems to be inevitable, albeit very good purities were achieved. The geometry of the pores and the depth of them simplify the impregnation of the carbon black, acting otherwise as growing centers that reduces greatly the usable surface area.

Considering all the obtained results, a major leap towards bigger surface areas is needed. A radical change of point of view will follow, because from an already porous material that acts like a template we will migrate to a polymer that works both as carbon precursor and as porogenous agent.

Before other experiments we investigated the feasibility of growing platinum nanoparticles on the surface of the titanium oxycarbide, because if better results couldn't be achieved we made out how to use the powder actively for electrocatalytic tests.

The cost of platinum is fairly high and the quantity of it in a fuel cell can represent an important factor in the final price. In order to reduce the quantity and have similar or better performances, one possibility is to use nanoparticles of the noble metal, because the surface-volume ratio rapidly raises when reducing the mean diameter of the particles. When the diameter is in the range of the tens of nanometers, the available surface for electrochemical reaction is dramatically increased, allowing for a smaller quantity of platinum.

Normally there are different ways to deposit platinum nanoparticles (NPs) on the surface. The simplest one is to buy commercially available suspensions and dry them on the surface of the investigated support. Another is CVD or PVD, that is very easy and straightforward but they are limited to planar or regular surfaces, not for powder. Wet chemistry allows to create nanoparticles on every support, letting to adjust the mean diameter and the quantity. However it needs to manage more synthesis parameters, such as temperature, concentrations, atmosphere and the choice of the most suited reagents.

We firstly used a pretty simple way to decorate the surface of the titanium oxycarbide, introducing the chosen platinum precursor during the impregnation of the carbon black. Then the powder is hydrolyzed and heat treated. For the first test we used a platinum precursor that can have a double purpose, a water solution of hexachloroplatinic acid. It acts as platinum precursor and also as water source for the hydrolyzation of the titanium propoxide, representing a very clever reagent for our reaction. We call this method "one-step".

Summarizing the procedure for the preparation of the sample, we impregnated the Ensaco with titanium propoxide in vacuum and then we added a mixture of water and hexachloroplatinic acid solution in order to reach a ratio of 2:1 between total water and titanium alkoxide and a molar percentage of Pt of 5 in confront of the titanium oxycarbide. When the powder is dried, following the previous method used for the so-called vacuum hydrolyzation, it is put in the tubular furnace for the heat treatment at 1350°C for 6 hours, with a heating ramp of 10°C/min followed by natural cooling after the dwell time. The powder is then ground by hand and analyzed by XRD, which pattern is shown in Figure 55.

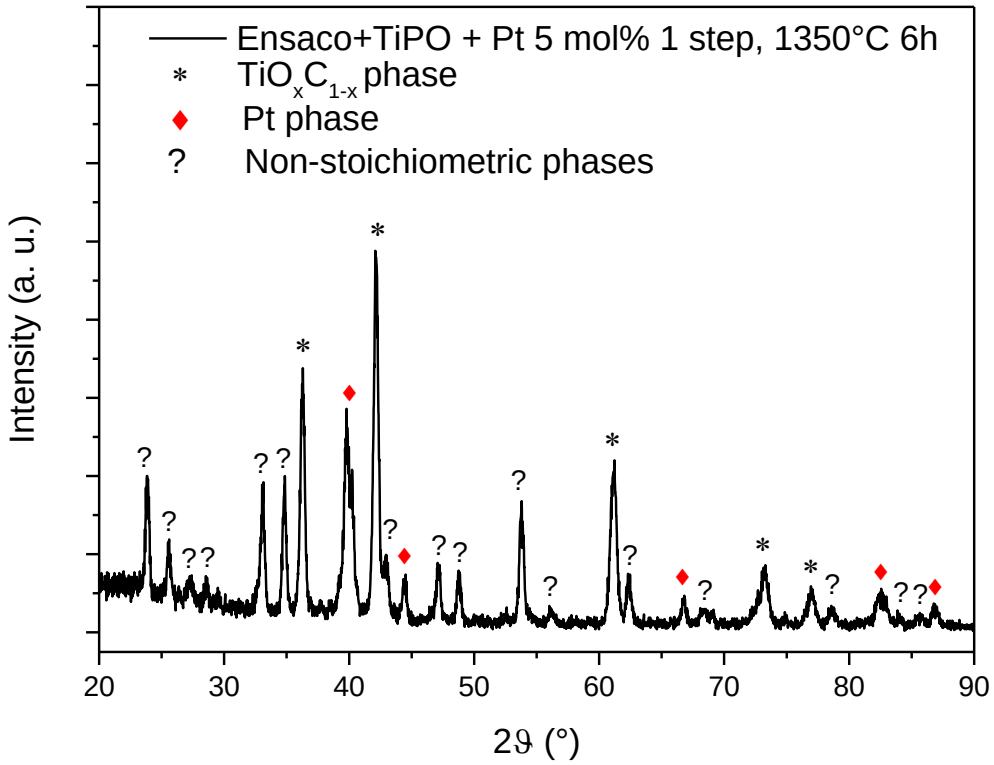

Figure 55, XRD pattern of Ensaco+TiPO with the addition of 5 mol% of Pt, vacuum hydrolyzed and treated at 1350°C for 6 hours

The platinum's peaks are clearly visible among the non-stoichiometric oxides and the oxycarbide. Analysing the width of the main peak and using the Scherrer equation [53], we can roughly estimate the diameter of the NP to be around 11 nm (assuming the NPs monocrystalline). From the SEM images, as seen in Figure 56, the presence of NPs is confirmed, albeit a complete analysis of the dimensions of them is not possible due to the small dimensions and the low number of them in the

image. However the mean diameter can be estimated to be in the range of 20nm, slightly bigger that the calculated one from XRD.

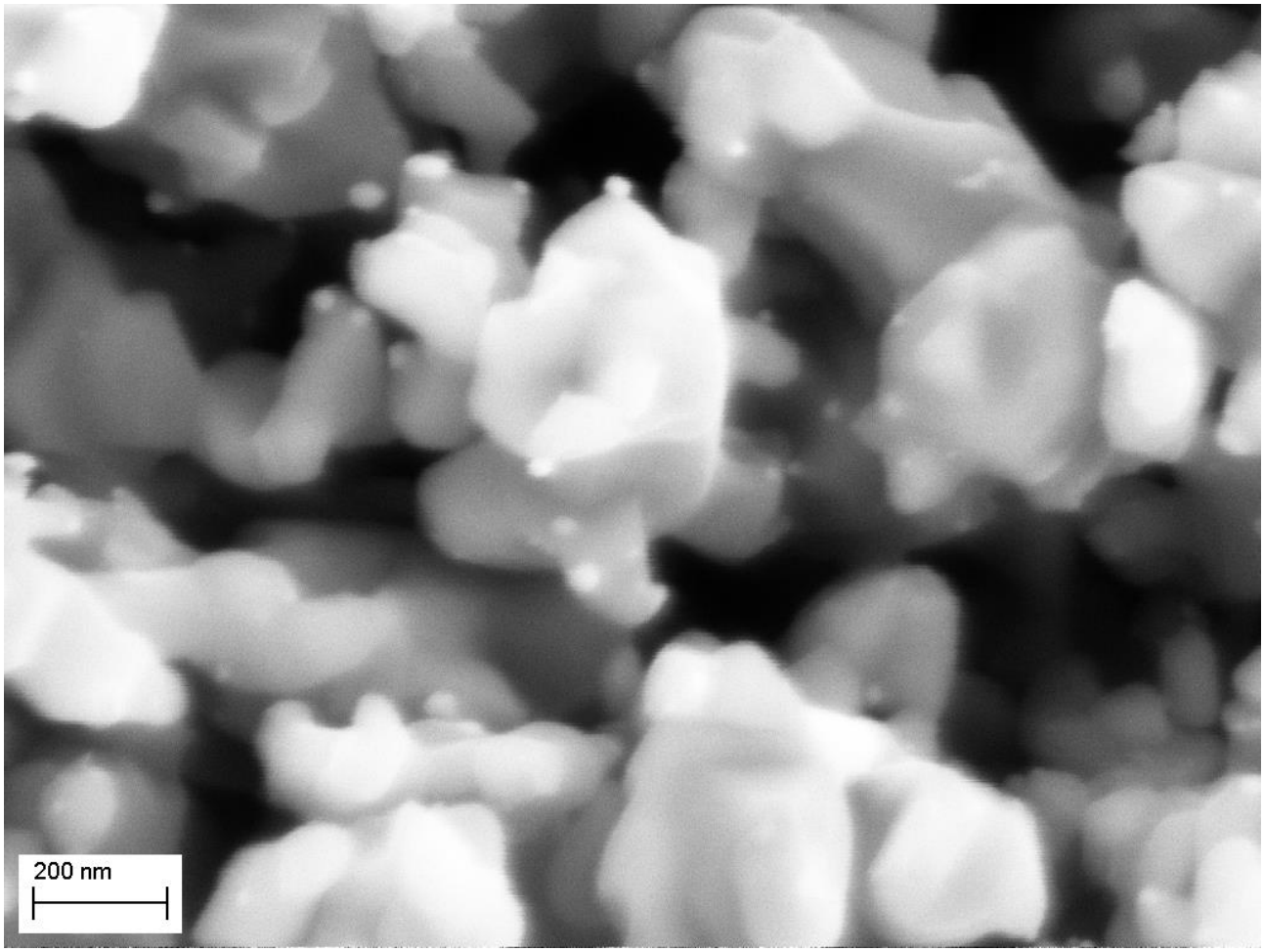

Figure 56, SEM image of Ensaco+TiPO+Pt 5 mol%, 1 step, 1350°C for 6 hours

We tried also another route to decorate titanium oxycarbide because with the one-step method, the real concentration of platinum at the surface of the powder grains is lower than the expected. This is because the platinum precursor is added to the CB wetted with titanium propoxide, so the nanoparticles during the heat treatment grow not only on the surface but wherever the solution is penetrated with the probability that an account of platinum is trapped inside the oxycarbide. The high temperature also favors the agglomeration of the nanoparticles, increasing the dimensions of them and lowering the surface area.

The new method will be called 2 steps, because the titanium oxycarbide is made firstly in the usual way and then the Pt NPs will be added. The addition is made diluting the hexachloroplatinic acid solution in a proper quantity of water, in order to fully wet the already carburized powder. Then the water is removed

applying low heat and when it is completely evaporated the powder is treated at 500°C in Argon for half an hour. In this way the possibility to decrease the surface concentration of the nanoparticles is very small and the dimensions of them is expected to be smaller. We took both XRD pattern and SEM images, as the previous sample, shown in Figure 57 and Figure 58, respectively.

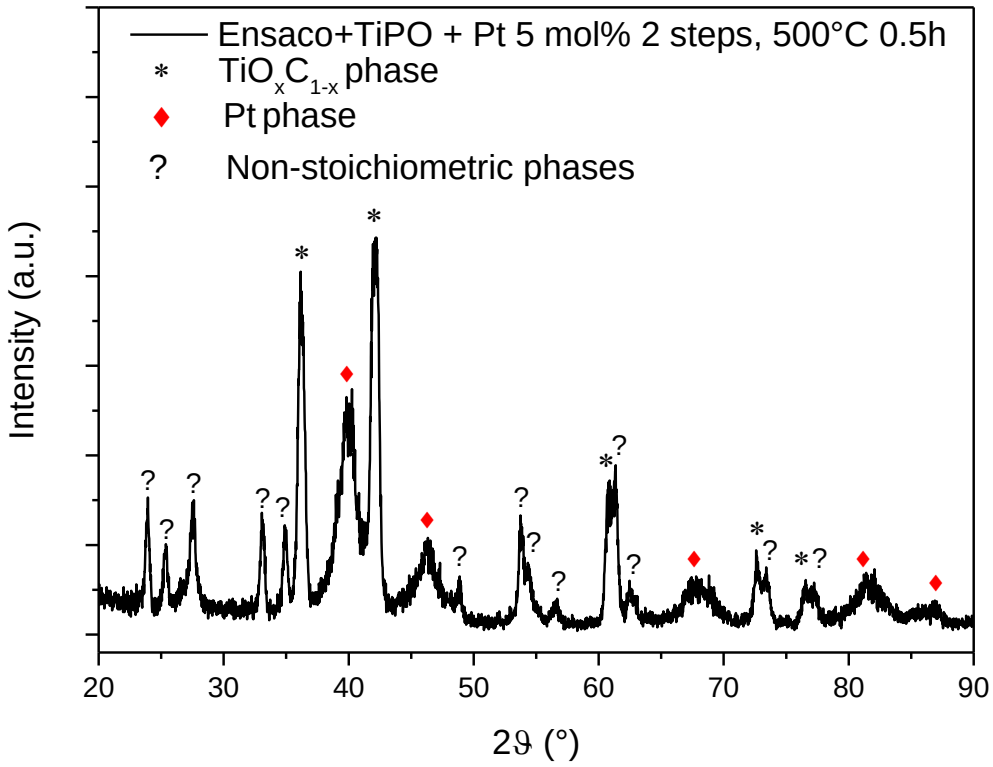

Figure 57, XRD pattern of Ensaco+TiPO with the addition of 5 mol% of Pt, vacuum hydrolyzed and treated at 500°C for 0.5 hours

The two images are taken with the same parameters of the previous ones and show little differences. In the XRD pattern the peaks related to Pt are larger, meaning that the dimensions of the nanoparticles are smaller. It is confirmed by the SEM image, that highlights smaller and more evenly distributed dots. Using the Scherrer equation the diameter of the nanoparticles is calculated to be around 5 nm.

From the SEM image in Figure 58 it is possible to see a larger amount of nanoparticles, smaller in diameter but with a more broad diameter distribution, with respect to the previous one-step samples, although a precise analysis is not possible.

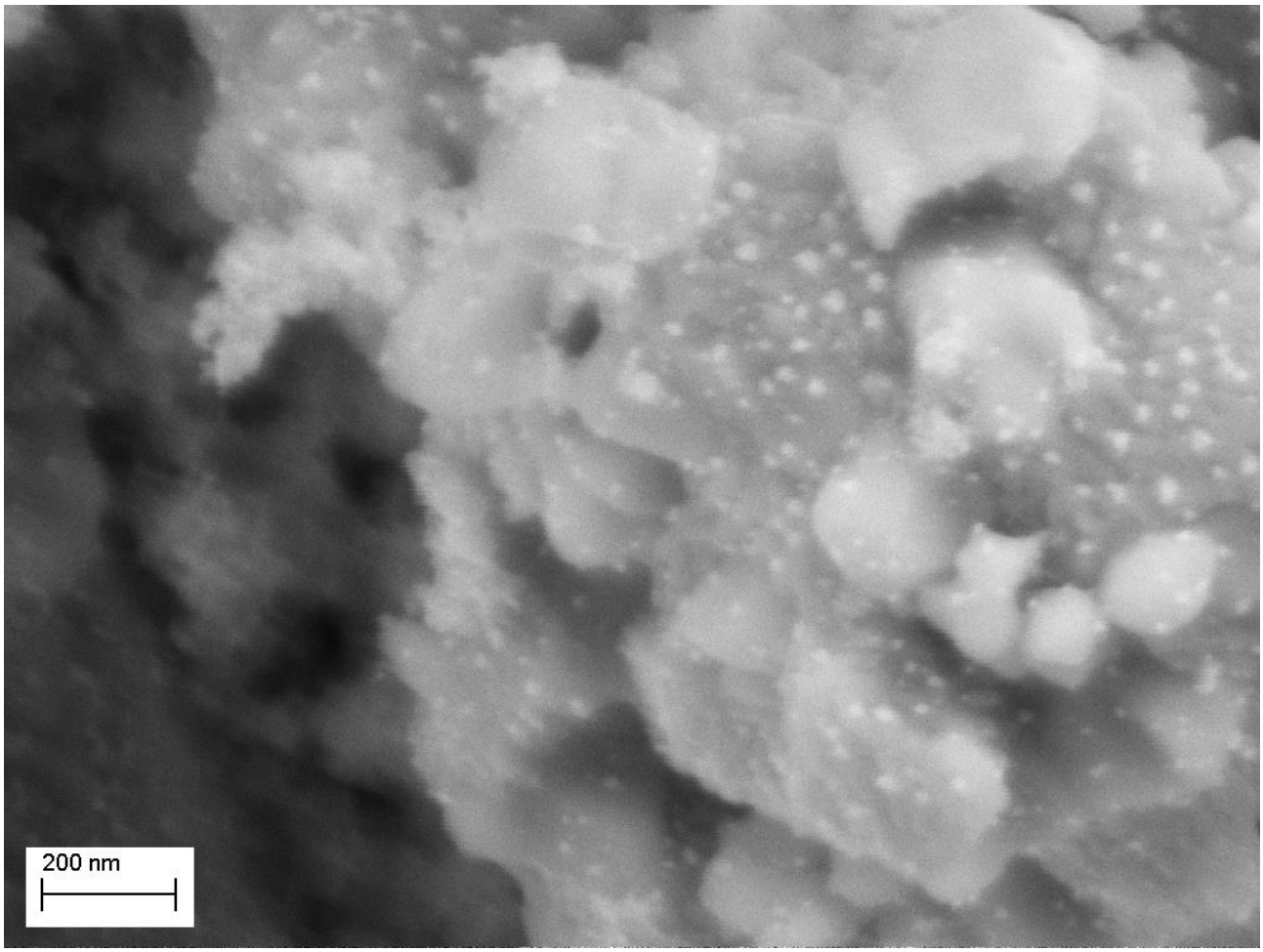

Figure 58, SEM image of Ensaco+TiPO+Pt 5 mol%, 2 steps, 500°C for 0,5 hours

Comparing the two synthesis methods, as done in Figure 59 and Figure 60, the differences are clearly visible.

In the XRD patterns (Figure 59), the broader dimensions of the Pt NPs in the 2 steps sample are easily noted, especially for the peak at 46.30°. The width of the peaks corresponds only to the crystallite size, that could be different from the dimensions of the nanoparticles, as seen by SEM.

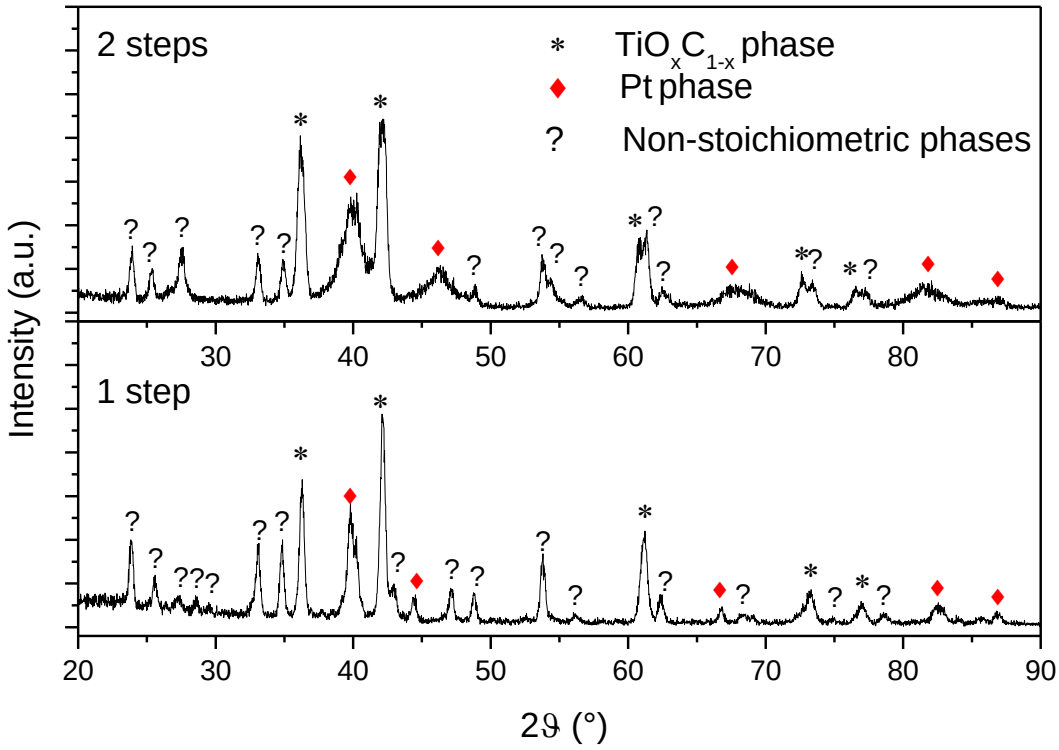

Figure 59, XRD patterns comparison of Ensaco+TiPO+Pt 5 mol%, 1 step and 2 steps

The comparison of the SEM images reveals different morphologies and distribution of the NPs. In the sample made with 2 steps the NPs are smaller and more numerous, meanwhile in the image of the 1 step sample few and bigger NPs are visible. This is due, respectively, to the dispersion of a fraction of the NPs in the oxycarbide substrate and the higher temperature of the heat treatment that promotes the Ostwald ripening and growth in dimension.

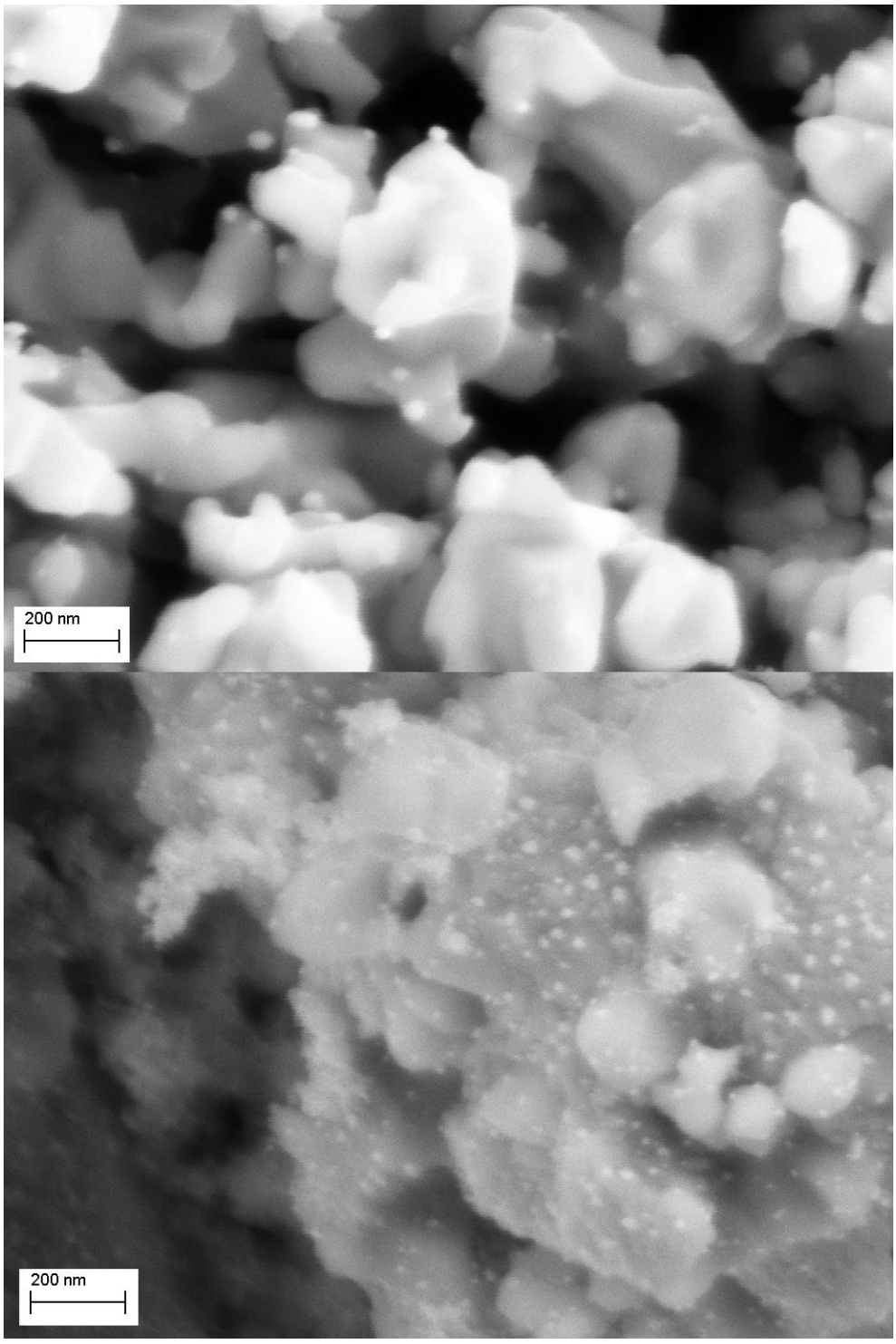

Figure 60, SEM images comparison of Ensaco+TiPO+Pt 5 mol%, 1 step (upper) and 2 steps (lower)

From literature results [42, 54-68], for ethanol oxidation in the working condition of the designed fuel cell, there are better materials than pure platinum, especially the alloys of platinum with tin. In this way

the total amount of metallic platinum can be lowered with the cheaper tin, increasing at the same time the performances of the catalyst. For our studies we used the most simple and straightforward route for synthetizing Pt-Sn nanoparticles, i.e. reducing the platinum and tin precursors in an ethylene glycol bath [57, 64, 68, 69] but substituting the common CB with the titanium oxycarbide as support.

We tried to make two slightly different nanoparticles, as described in literature [57]: the first treatment aimed to synthetize Pt_xSn_y nanoparticles, meanwhile with the second we tried to create Pt/SnO_2 core-shell nanoparticles.

For the Pt_xSn_y NPs we chose a stoichiometric ratio between platinum and tin of 3:1. The NPs load was 5 mol%, directly synthetized on the titanium oxycarbide obtained from the Ensaco and titanium ethoxide. Albeit the small surface area, we chose these samples because they didn't show crystalline unwanted phases and they have a precise stoichiometry around $TiO_{0.5}C_{0.5}$.

The XRD pattern is shown in Figure 61. The peaks related to the $TiO_{0.5}C_{0.5}$ phase are still completely visible and four new peaks can be attributed to the Pt_3Sn alloy. From the peak width, the mean crystallite diameter can be estimated to be ~6 nm.

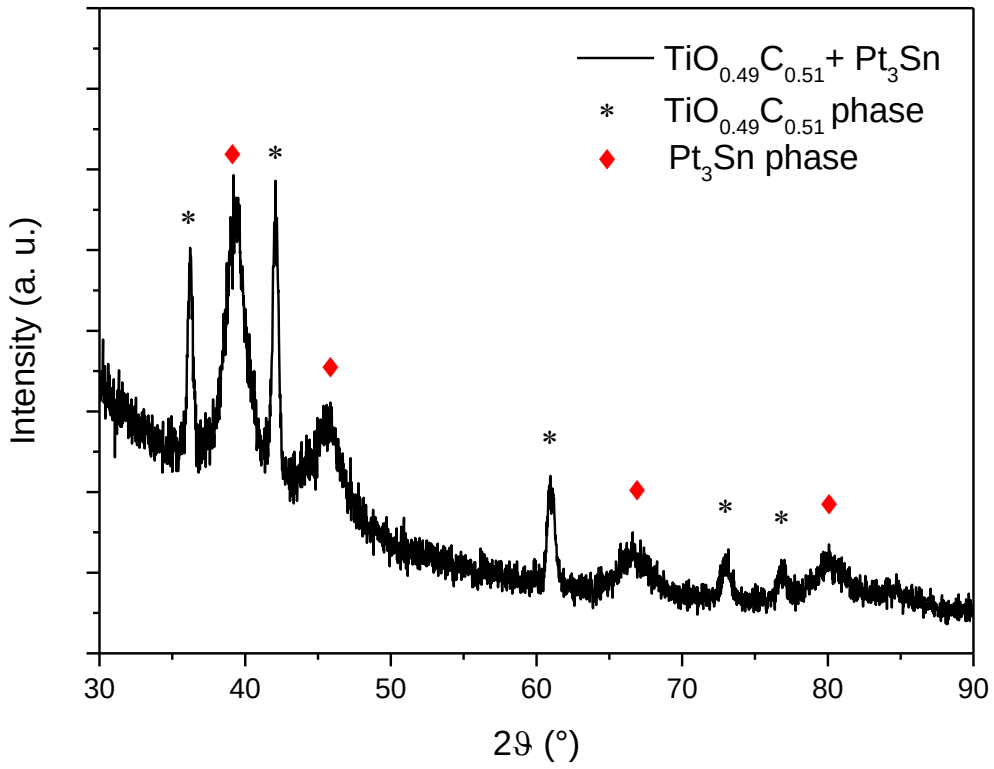

Figure 61, XRD pattern of TiOC from En+TiEtO decorated with Pt_3Sn nanoparticles

For the core-shell nanoparticles we maintained the Pt:Sn ratio of 3:1, but in this case the inner core is made of tin oxide and the shell of pure platinum. The XRD pattern is reported in Figure 62. The peaks of the core-shell nanoparticles are in the same position of the peaks from the previous sample, because the Pt shell, during the synthesis, reacted with the tin oxide core making a Pt_3Sn alloy. Again, from the analysis of the peak width, the crystallite dimension is estimated to be ~6 nm.

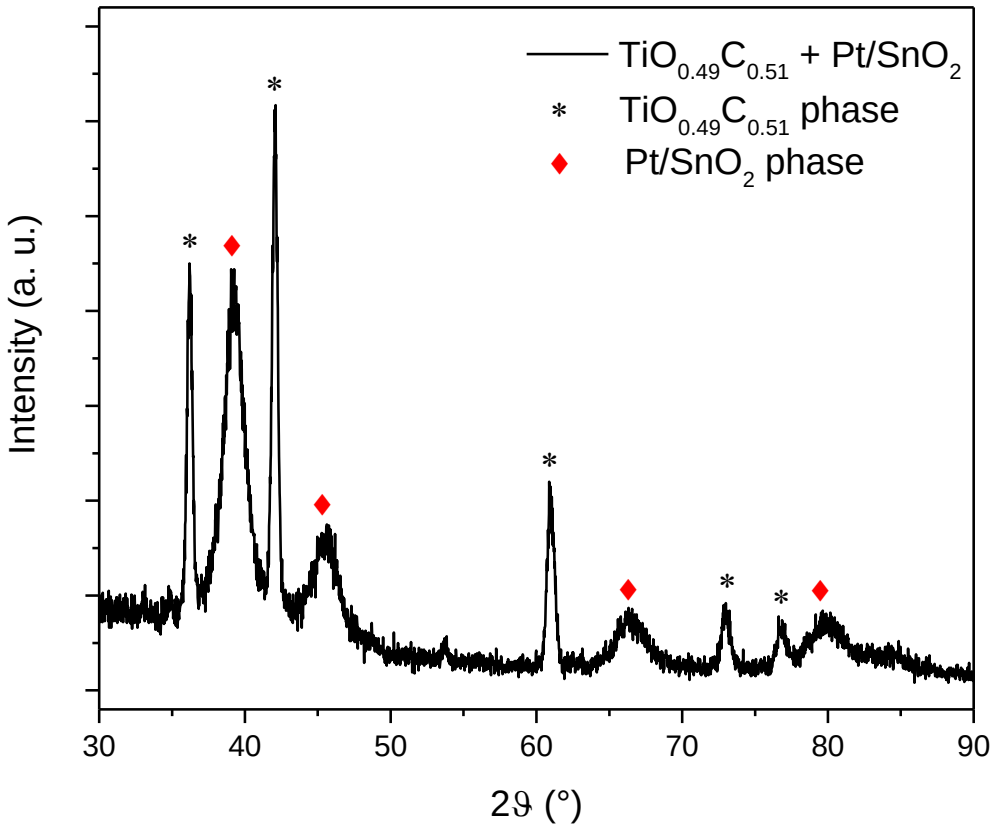

Figure 62, XRD pattern of TiOC from En+TiEtO decorated with Pt/SnO_2 nanoparticles

Because we weren't sure if the alloying of the platinum shell was an accident we tried to make again the same sample, whom XRD pattern is reported in Figure 63. The peaks are the same, confirming the hypothesis that the external platinum shell reacts with the tin oxide core making an alloy. The core seems to be amorphous, because there aren't detectable peaks of the crystalline phase, or it isn't oxidized and it has reacted completely with the shell. In Figure 64 there is a comparison for the three sample, the first with Pt-Sn alloy, the second two with the core-shell nanoparticles, and the TiO_xC_{1-x} used as substrate, made from the Ensaco impregnated with TiEtO in glove box.

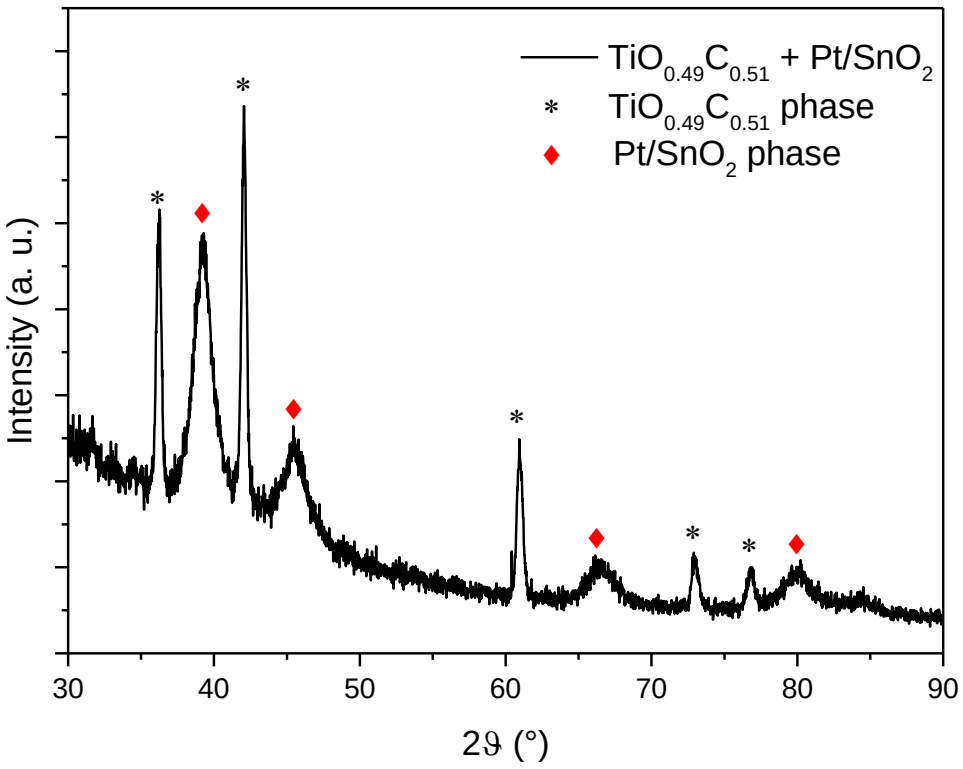

Figure 63, XRD pattern of TiOC from En+TiEtO decorated with Pt/SnO_2 nanoparticles

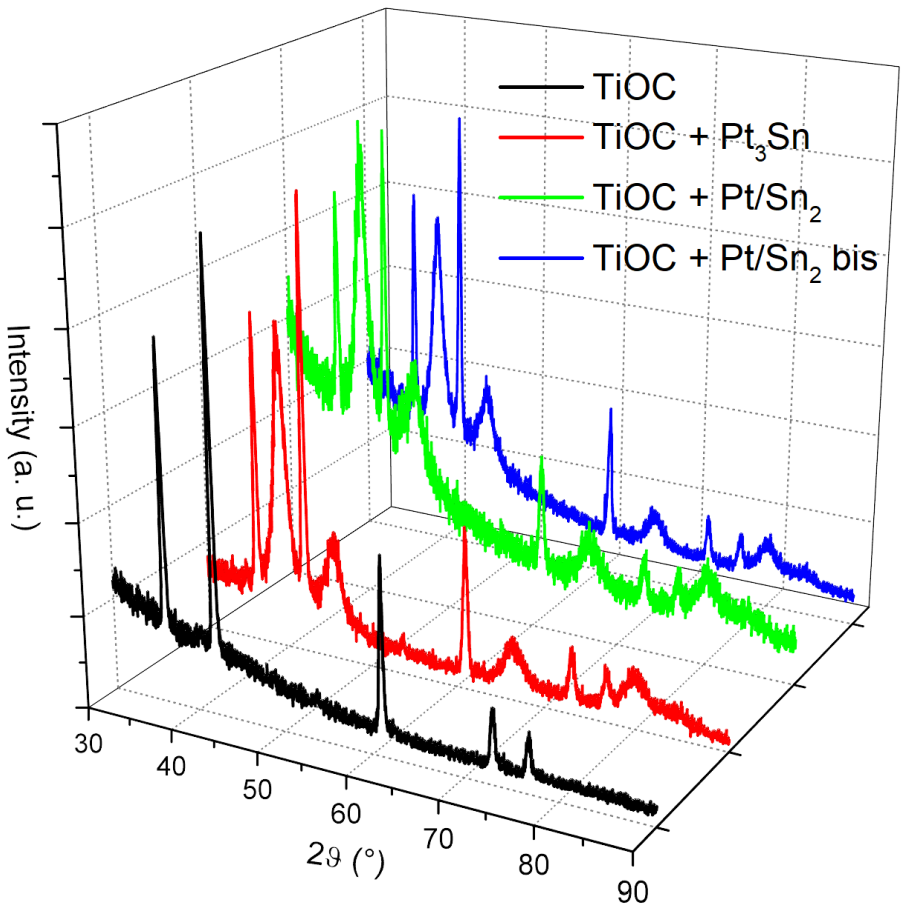

Figure 64, comparison of XRD patterns obtained from TiO_xC_{1-x}, TiO_xC_{1-x} decorated with Pt_3Sn NPs and TiOC decorated with Pt/SnO_2 core-shell NPs made twice

As can be noted from the last figure, the peaks of the $TiO_{0.49}C_{0.51}$ phase aren't changed with the different syntheses, because the temperature of the treatment is too low to induce some change in the crystalline structure and stoichiometry of the titanium oxycarbide. The only difference amongst the three samples with Pt_3Sn or Pt/SnO_2 NPs is the area of the platinum alloy peaks. This means that different loadings of crystalline alloy are present, probably due to the slightly different condition occurred during the synthesis or small error during the preparation of the samples. However, these small drifts can be considered physiological, because the amounts of reagents are very small, in the range of few milligrams for each.

After these considerations, the proposed method for decorating the titanium oxycarbide with platinum alloy nanoparticles could be valid for future samples.

3.2.2. Methyl cellulose

After the results obtained with the carbon black, which is used both as template and carbon source, we decided to change completely perspective in order to obtain better results in stoichiometric control, crystalline purity and surface area.

Before, the porosity was due only to the pores already present in the chosen carbon black, leading to better results with the Cabot XC72 with respect to the Ensaco 350G. In this way, the specific surface area could be at the best slightly smaller than the starting value of the template.

In order to revise the synthesis, instead of starting with a porous material that can only decrease its specific surface area (especially considering the high temperature needed for the carburization process), we chose a bulk material with almost none surface area that develops pores during the carburization treatment. The synthesis route would be still the carburization of the titanium dioxide, but with a different approach.

There are several organic precursors that can be used as carbon sources and develop pores during a heat treatment, like the one used for aerogels or active carbons. These materials are known for their high porosity and low density, but the commonly used precursors and syntheses are not cheap, fast or harmless. The aim of the following experiments will be the search of the best precursor that has low price, is not harmful and easy to manipulate.

In literature [29, 32, 70-72] several attempts for the synthesis of porous titanium carbide were conducted, but everybody looked for pure TiC, without traces of oxygen, because it is considered an undesired contamination that compromises the hardness of the material. After the evaluation of different polymers, we chose to use methylcellulose (MC). The methylcellulose is a common polymer derived mainly by wood, used extensively in the food and cosmetic industry. We chose it for its water solubility, that permits an intimate mixing with the titanium complex, and high carbon gain after the heat treatment. In literature [73, 74] it is reported that it undergoes a complete and clean degradation under inert atmosphere during a thermal treatment. From our tests, the carbon residue after a treatment at 1300°C for 3 hours is 10 weight%. The appearance of the methylcellulose is a white and soft powder. A particularity of this polymer is that it has a lower critical solution temperature: above ~55°C the MC is soluble with high concentrations in water, but when the critical temperature is passed, it becomes completely insoluble. This is very useful because the powder when put in water tends to make agglomerations with a dry core

that are very difficult to disaggregate, leading to a non-uniform suspension. In order to obtain a gel, the water has to be heated at temperatures higher than 60°C and, under vigorous stirring and the MC has to be added slowly. In this way, a suspension of the powder is made, and after cooling to room temperature, a uniform gel is formed. The gel can be subsequently dried applying modest heat and vacuum. The obtained polymer is pale yellow with a plastic consistence.

During the master thesis period, we investigated the best way to add titanium dioxide to the solution, founding two different way: the first one involved a colloidal suspension of nanoscale titania; the second a titania diethanolamine complex (DEATi). After abandoning the colloidal titania we investigated deeper the DEATi route during the PhD thesis. The titanium diethanolamine complex is very useful because of its stability and its high solubility in water, which leads to an excellent mixing with the MC. The reaction involved in the synthesis of DEATi is very simple and with high yields [75]. The preparation of DEATi is conducted as follows: titanium isopropoxide (TiPO, 97 wt%, Sigma Aldrich) is stirred with diethanolamine (DEA, ≥98 wt%, Sigma Aldrich) with a 1:4 molar ratio in a closed flask with a nitrogen atmosphere. The reaction is slightly exotherm, generating little heat. Once the temperature is dropped again at room temperature, the pale yellow solution is subsequently heated up to 180°C for 1 hour to remove completely the byproducts, mainly consisting in 2-propanol. The viscous liquid can be stored for several weeks without any change in composition or color in a closed flask. For the preparation of the green with methylcellulose and DEATi, the latter is diluted 4 times the initial volume with doubly distilled water, and heated to 60 °C before slowly adding the desired amount of methylcellulose under vigorous stirring. Once a homogeneous suspension is obtained, the solution is allowed to cool down slowly under stirring, until a highly viscous fluid is formed, with a pale yellow color and a translucent appearance. When cooled, it can be dried in vacuum oven at 50°C overnight to obtain a plastic polymer that appears like a yellow soft, non-sticky material, which can easily be ground to a finer powder with the aid of a mechanical grinder. The polymer can be stored at room temperature for only few days, because the DEATi tends to percolate from the methylcellulose network and change the starting stoichiometry. The XRD pattern for the polymer is reported in Figure 65, where crystalline phases cannot be recognized exept for a broad peak around 24° that is characteristic to MC [73].

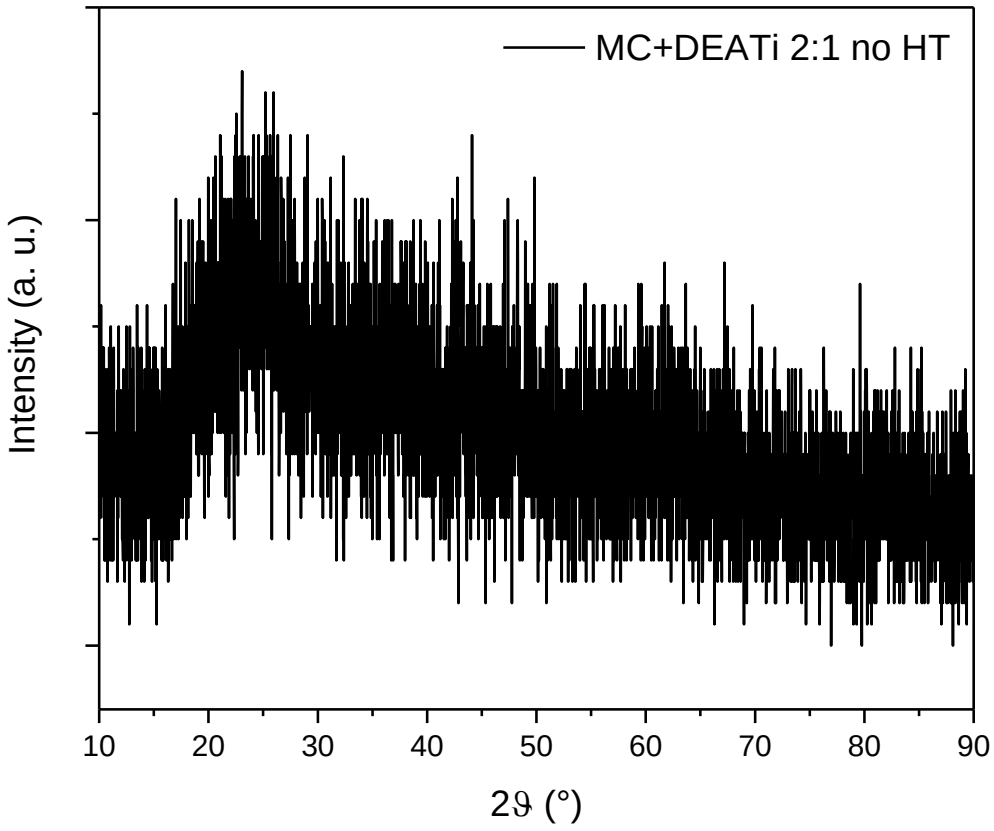

Figure 65, XRD pattern of MC+DEATi 2:1 before the heat treatment

The heat treatment consists in the carburization process used for the carbon black: the sample is put in an alumina vessel inside tubular furnace. An argon flow of 0.4 L/min is let to flux for an hour before starting the treatment, for eliminating residual oxygen. Then heat is applied following a heat ramp of 10°C/min reaching 1300°C. The top temperature is hold for 3 hours and then the oven is let to cool down naturally.

The first attempts made revealed that that route is very promising, with three different samples that don't show unwanted peaks and have only small drifts from the desired stoichiometry. They were made with a C:Ti ratio of 2:1 that should lead to a stoichiometry equal to $TiO_{0.5}C_{0.5}$. The results from the first samples are reassumed in Table 12.

Sample	*Cell parameter (Å)*	*Oxygen content (mol%)*
1	4.300	0.39 ± 0.02
2	4.284	0.56 ± 0.02
3	4.295	0.44 ± 0.02

Table 12, cell parameters and oxygen content for 3 samples of MC+DEATi

As can be seen from the last column, the stoichiometry of the first samples were not exactly uniform, but they had not traces of oxides' phases.

Starting from these preconditions, we made several different samples in order to find the best way to obtain reproducible results. Firstly, we investigated the dwell time influence on the stoichiometry, varying the time from 1 to 6 hours, with an intermediate step of 3 hours.

The XRD pattern of the samples treated for only one hour is reported in Figure 66. It can be seen that, despite the short time of treatment, the sample does not show other peaks except titanium oxycarbide. The peaks' positions, cell parameters and oxygen content are reported in Table 13.

1^{st} peak position (°)	*2^{nd} peak position (°)*	*3^{rd} peak position (°)*	*4^{th} peak position (°)*	*5^{th} peak position (°)*	*Cell parameter (Å)*	*Oxygen content (mol%)*
36.31	42.18	61.14	73.21	77.05	4.2815	58

Table 13, peak positions, cell parameter and oxygen content for MC+DEATi 2:1 heat treated at 1300°C for 1 hour

The stoichiometry is not the expected one, because the treatment took place in a too short time, not allowing the complete carburization of titanium oxide. It is however important to notice that, albeit the short time, unwanted oxide phases were not formed, meaning that all the precursor for the titanium dioxide reacted uniformly and the carburization already started.

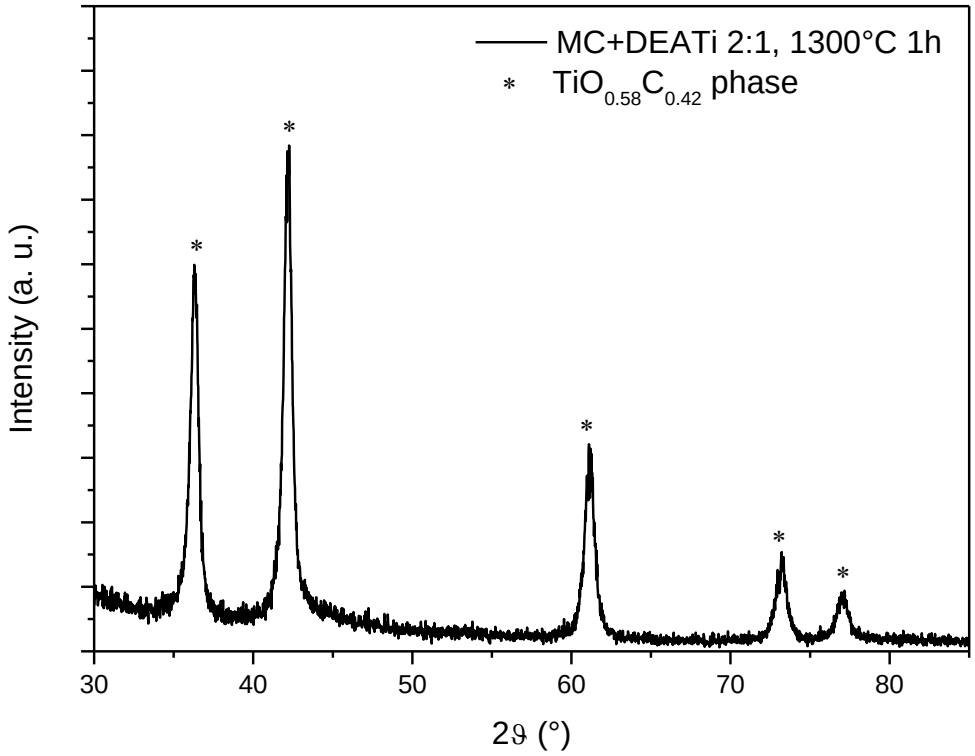

Figure 66, XRD pattern of MC+DEATi 2:1 heat treated at 1300°C for 1 hour

With the same non-treated MC+DEATi we made another treatment for 3 hours. The XRD pattern is shown in Figure 67. The peaks' positions, cell parameters and oxygen content are reported in Table 14.

1st peak position (°)	***2nd peak position (°)***	***3rd peak position (°)***	***4th peak position (°)***	***5th peak position (°)***	***Cell parameter (Å)***	***Oxygen content (mol%)***
36.26	42.13	61.07	73.11	76.95	4.2864	53

Table 14, peak positions, cell parameter and oxygen content for MC+DEATi 2:1 heat treated at 1300°C for 3 hours

The stoichiometry now is very close to the expected $TiO_{0.5}C_{0.5}$, meaning that the titanium oxides started to carburize with the residual carbon thanks to larger diffusion.

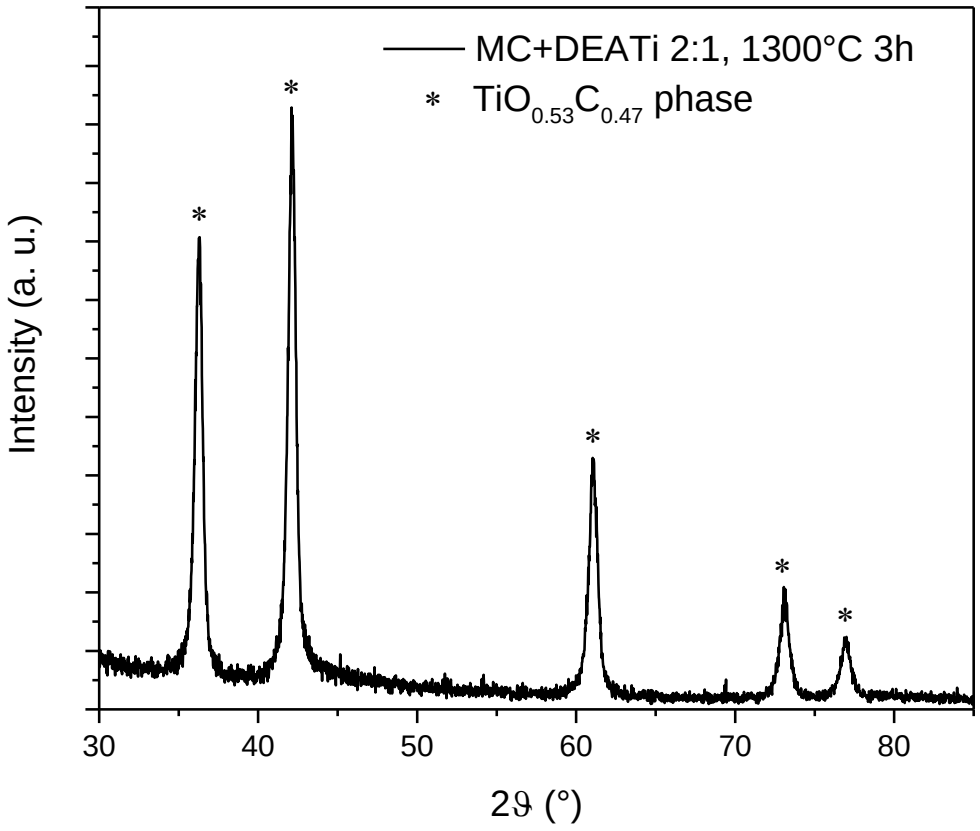

Figure 67, XRD pattern of MC+DEATi 2:1 heat treated at 1300°C for 3 hours

The last sample, treated for 6 hours, was made with the same non-treated MC+DEATi in order to eliminate all the variables from the preparation. The XRD pattern is in Figure 68. In Table 15 all the principal parameters of the sample are resumed.

1st peak position (°)	***2nd peak position (°)***	***3rd peak position (°)***	***4th peak position (°)***	***5th peak position (°)***	***Cell parameter (Å)***	***Oxygen content (mol%)***
36.23	42.08	61.00	73.02	76.85	4.2908	49

Table 15, peak positions, cell parameter and oxygen content for MC+DEATi 2:1 heat treated at 1300°C for 6 hours

*

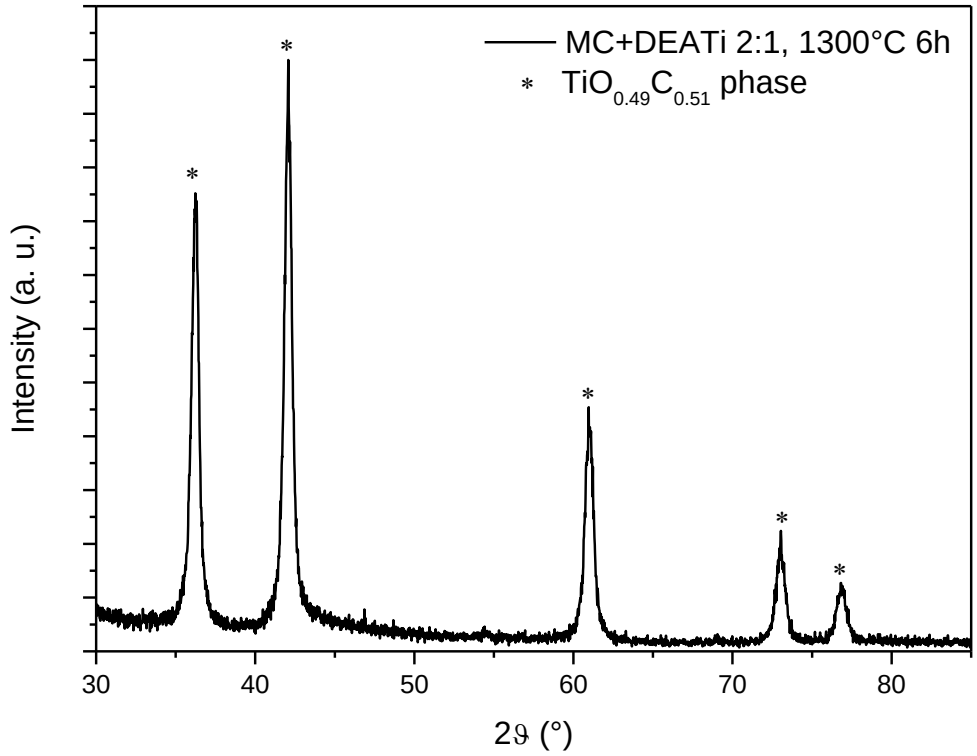

Figure 68, XRD pattern of MC+DEATi 2:1 heat treated at 1300°C for 6 hours

It is possible to observe a decrease of the cell parameter with the increase of the dwell time. The reduction of the cell parameter, and the subsequent increase of oxygen content, is not linear and seems to reach a plateau between 3 and 6 hours. We made another sample treated for 6 hours in order to understand if the value of the last one is already on the supposed plateau. The XRD pattern and peak positions, cell parameters, and oxygen content are reported in Figure 69 and Table 16, respectively.

1st peak position (°)	***2nd peak position (°)***	***3rd peak position (°)***	***4th peak position (°)***	***5th peak position (°)***	***Cell parameter (Å)***	***Oxygen content (mol%)***
36.24	42.09	61.02	73.05	76.86	4.2898	50

Table 16, peak positions, cell parameter and oxygen content for MC+DEATi 2:1 heat treated at 1300°C for 6 hours, sample #2

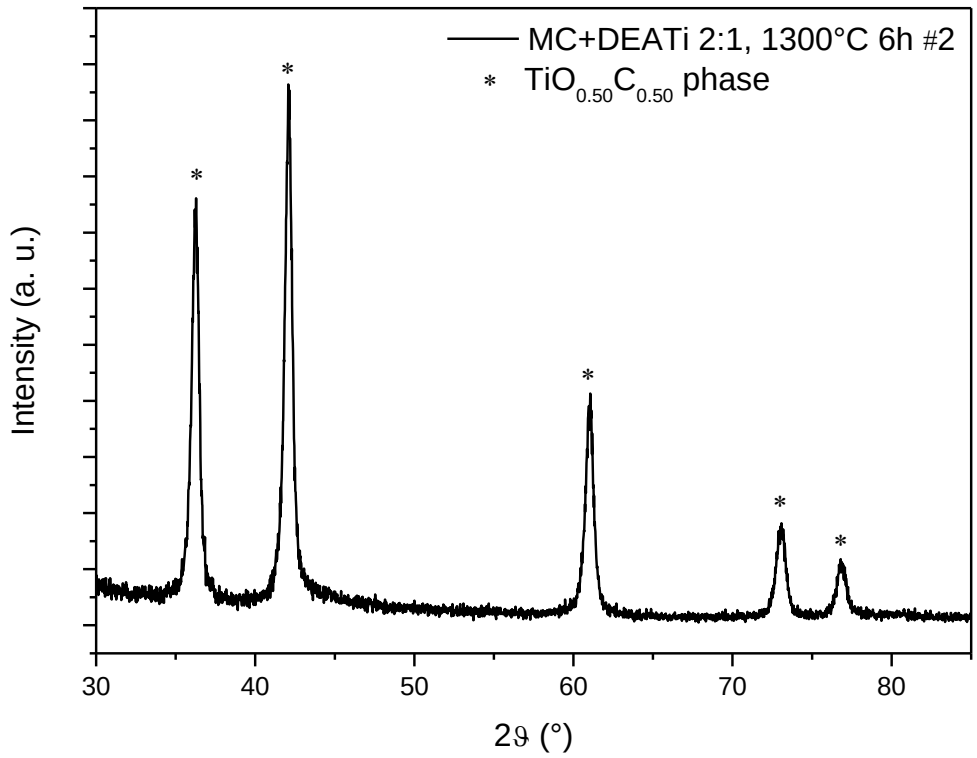

Figure 69, XRD pattern of MC+DEATi 2:1 heat treated at 1300°C for 6 hours, sample #2

The value of the cell parameter and oxygen content is very similar to what obtained with the previous sample, suggesting that we reached a plateau in correspondence of the expected values. In Figure 70 the oxygen content for each sample is plotted for a visual understanding and in Table 17 all the parameters for the different samples are reported.

Hours of treatment	***1st peak position (°)***	***2nd peak position (°)***	***3rd peak position (°)***	***4th peak position (°)***	***5th peak position (°)***	***Cell parameter (Å)***	***Oxygen content (mol%)***
1	36.31	42.18	61.14	73.21	77.05	4.2815	58
3	36.26	42.13	61.07	73.11	76.95	4.2864	53
6	36.23	42.08	61.00	73.02	76.85	4.2908	49
6	36.24	42.09	61.02	73.05	76.86	4.2898	50

Table 17, peak positions, cell parameters and oxygen contents for different time of treatment

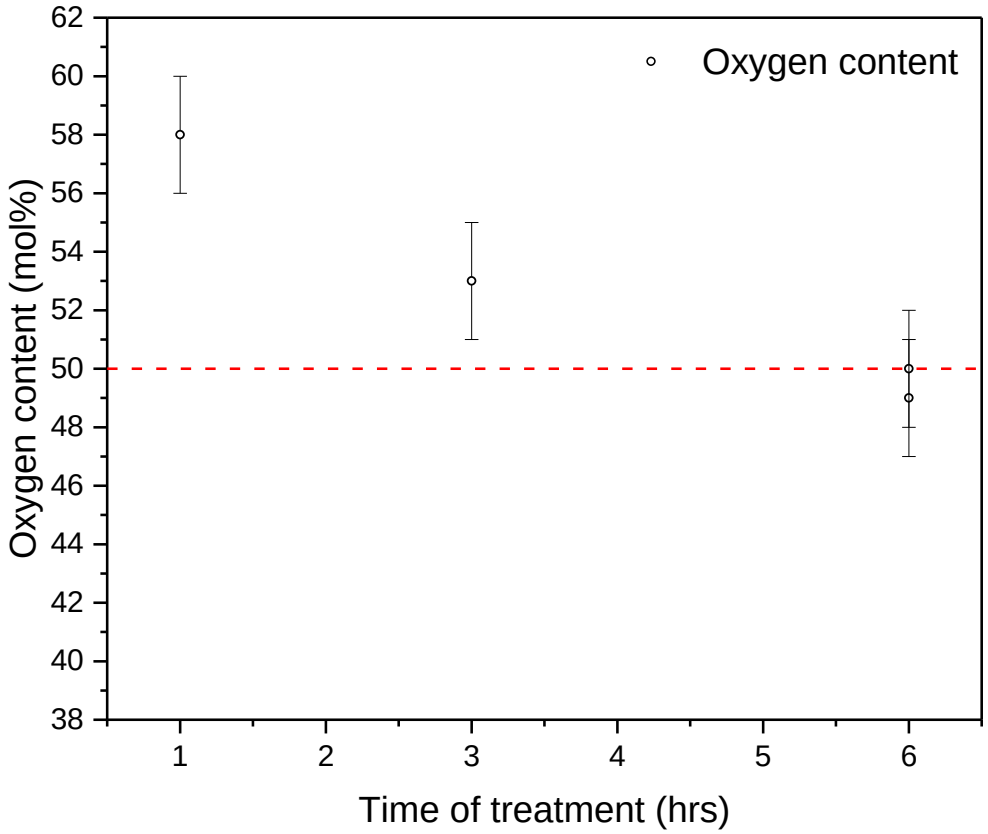

Figure 70, plot of oxygen content for MC+DEATi treated for various times. The expected value is highlighted in red.

We conducted more tests but with shorter heat treatment times, just to be sure that the right stoichiometry can be achieved faster, assuring a higher throughput for an eventual industrial production. We focused on three hours, carburizing different samples.

The first of the series gave us similar results, because it has a stoichiometry of $TiO_{0.56}C_{0.44}$, very close to the stoichiometry of the last sample treated for the same time, $TiO_{0.53}C_{0.47}$. Its XRD pattern is reported in Figure 71.

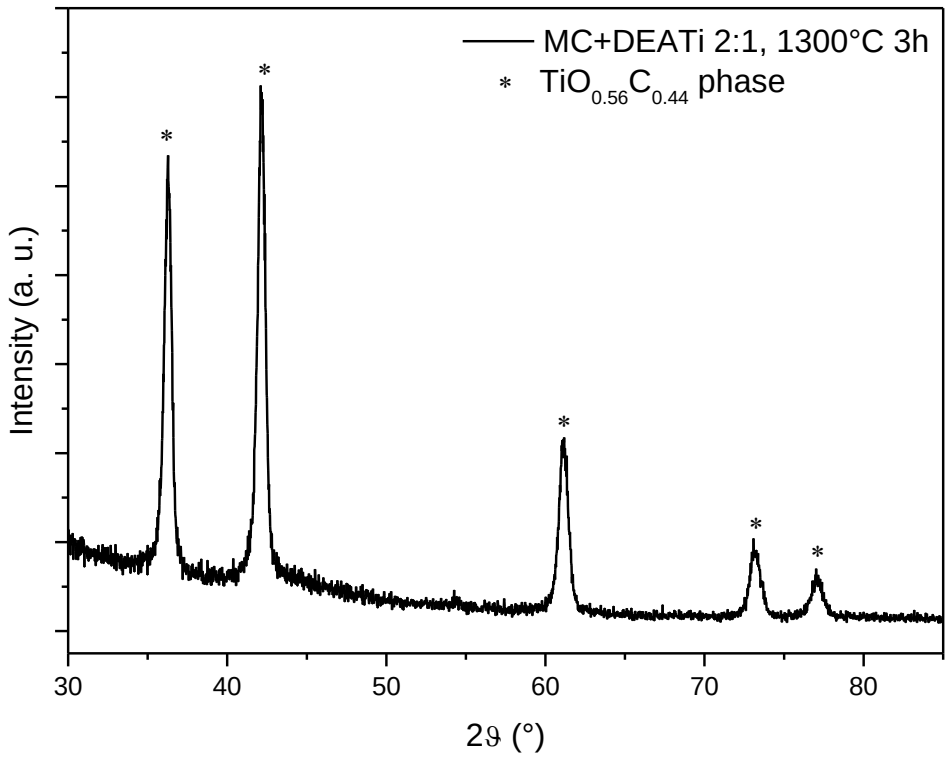

Figure 71, XRD pattern of MC+DEATi 2:1 heat treated at 1300°C for 3 hours, sample #2

We took also SEM images for this sample, in order to investigate the morphology of the powder. The grains look very different from the images of cabon black-based oxycarbides: in Figure 72, Figure 73 and Figure 74 , big chunks with a fine decoration of small particles can be seen.

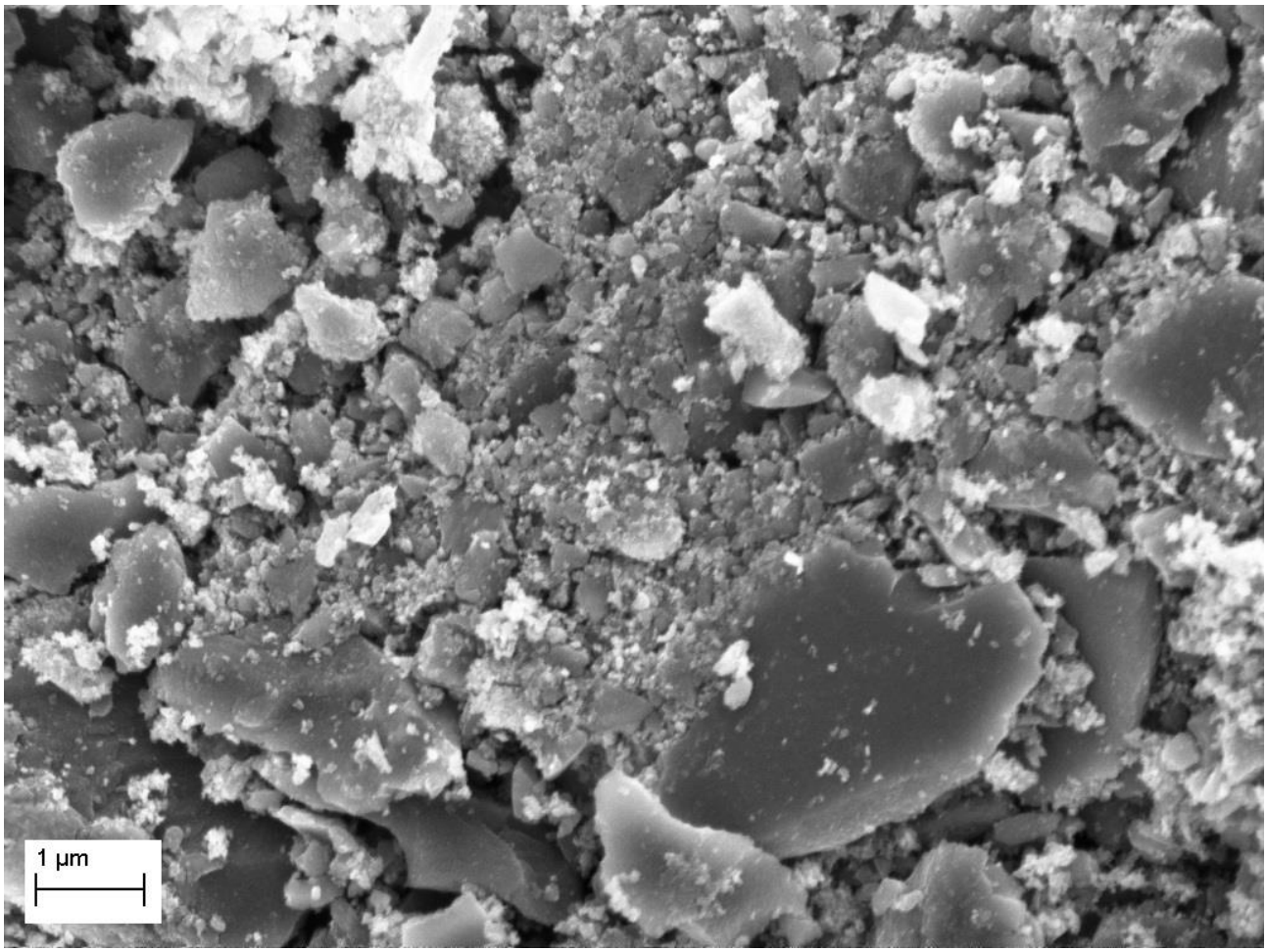

Figure 72, SEM image of MC+DEATi 2:1 heat treated at 1300°C for 3 hours, sample #2

In Figure 72, the morphology of the TiO_xC_{1-x} powder is clearly visible. There are large areas with only big uniform pieces, meanwhile elsewhere there is a fine and sponge-like powder. The big chunks are often bigger than one µm, while the small particles are in the range of hundreds of nanometers.

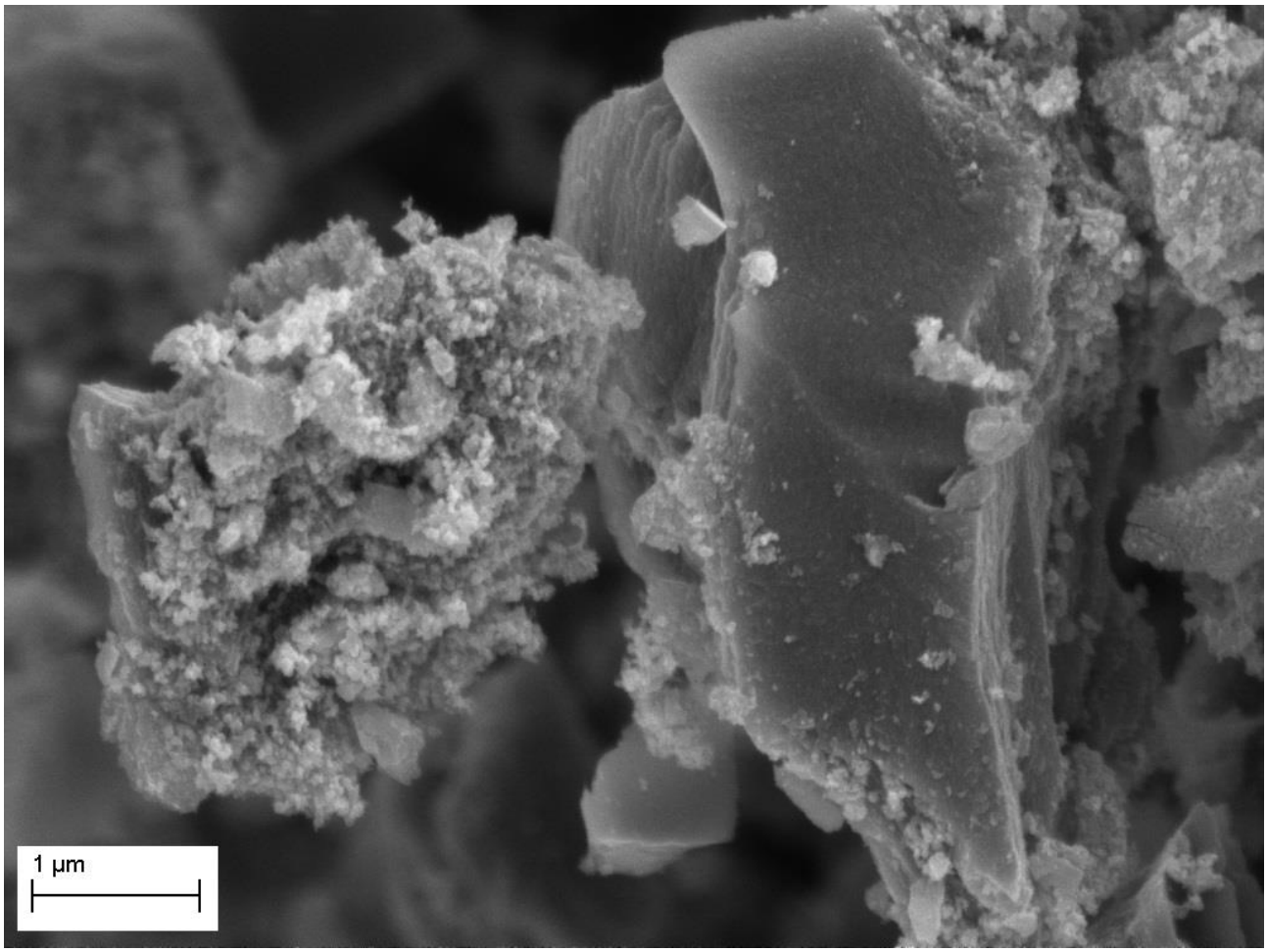

Figure 73, SEM image of MC+DEATi 2:1 heat treated at 1300°C for 3 hours, sample #2

In Figure 73, it is more evident the morphology of the larger pieces. Apparently, with lower magnifications, they appear to be smooth, but with a more detailed view they reveal a very irregular surface, with several ridges on the sides and uneven surfaces. It is also present a conglomerate of particles on the left, that are very small and not clearly distinguishable.

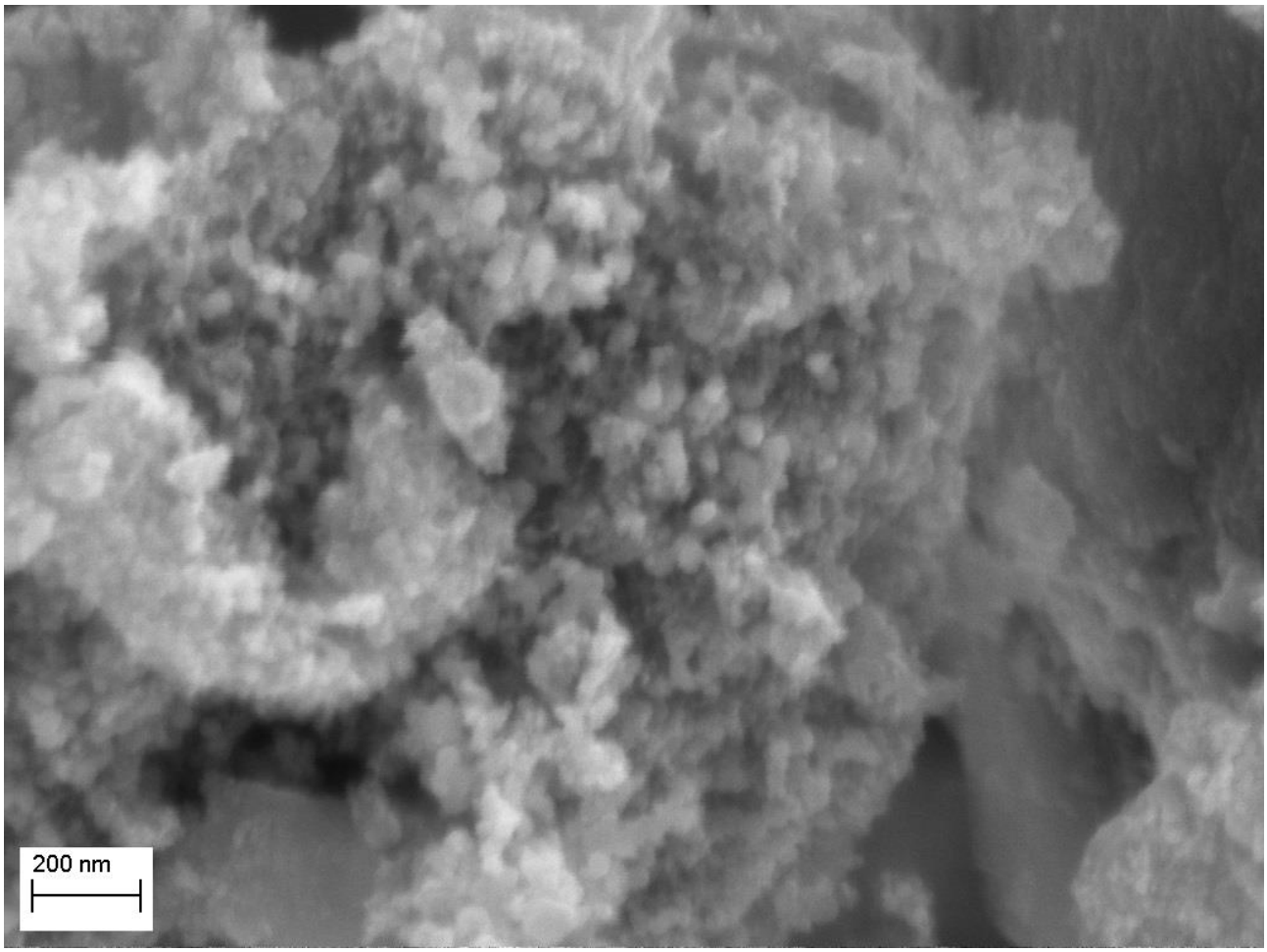

Figure 74, SEM image of MC+DEATi 2:1 heat treated at 1300°C for 3 hours, sample #2

In Figure 74 a more focused view on the particles is reported. The round nanoparticles have a diameter smaller than 50 nm, even if a complete analysis is not possible due to the low quality that blurs the profiles.

We studied also the stability of the MC+DEATi at room temperature for several days. The peak positions, cell parameter and oxygen contentare reported in Table 18.

Day	*1st peak position (°)*	*2nd peak position (°)*	*3rd peak position (°)*	*4th peak position (°)*	*5th peak position (°)*	*Cell parameter (Å)*	*Oxygen content (mol%)*
0	36.33	42.22	61.25	73.34	77.21	4.2761	62
1	36.27	42.14	61.14	73.19	77.07	4.2832	56
2	36.27	42.16	61.17	73.24	77.09	4.2817	58
3	36.22	42.11	61.10	73.16	77.00	4.2864	53
7	36.21	42.11	61.11	73.16	77.03	4.2862	53
8	36.25	42.14	61.15	73.22	73.07	4.2832	56
10	36.13	42.01	60.96	73.00	76.83	4.2954	44

Table 18, peak positions, cell parameters and oxygen content for MC+DEATi, all treated at 1300°C for 3 hours in different days

It is possible to note that the stoichiometry during the first 9 days does not change a lot, but has a rapid decrease at the 11th. This can be easily explained looking at the XRD patterns, which are reported in Figure 75.

In the graph there are two zones highlighted in grey where two peaks grow as the storage time increases. They are attributable to rutile, a high temperature phase of titanium dioxide.

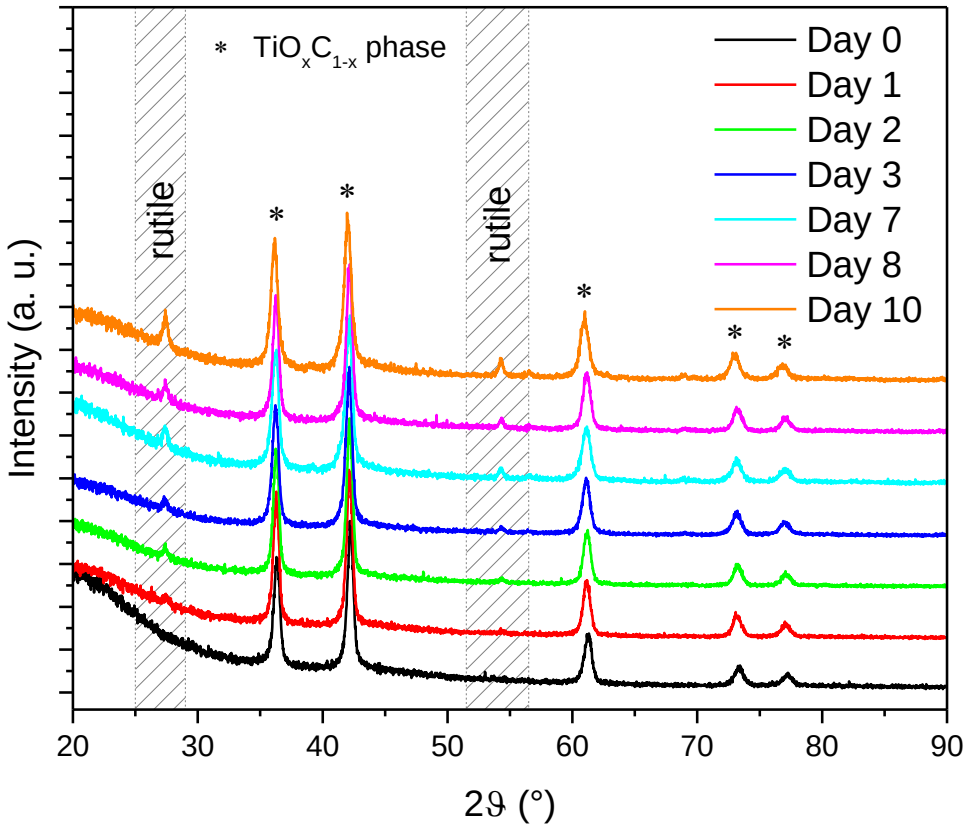

Figure 75, comparison of MC+DEATi 2:1, treated at 1300°C for 3 hours during different days

As said before, the compound of MC+DEATi tends to exude the titanium complex after some days. In this way, the methylcellulose does not encapsulate all the DEATi inside the polymeric network but becomes clad by the titanium dioxide precursor. During the heat treatment the external shell becomes rutile, meanwhile the methylcellulose reacts with a less content of titania, leading to a poorer content of oxygen.

We made a new batch of MC+DEATi and treated it as soon as possible. The XRD pattern did not show rutile peaks, as seen in Figure 76. This confirm that the useful lifetime of the MC+DEATi is limited to few days.

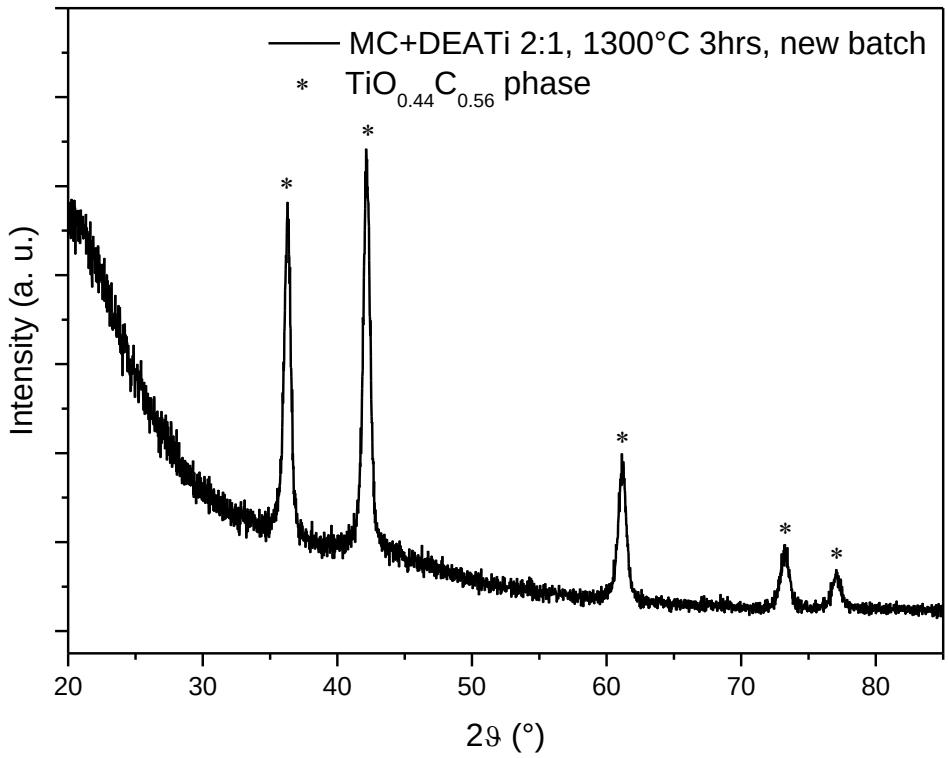

Figure 76, XRD pattern of MC+DEATi 2:1, treated at 1300°C for 3 hours as soon as possible after drying

After these experiments, we tried to understand if the synthesis is scalable or not. We made MC+DEATi with the same procedure, but multiplying the quantities by 5. Bigger quantities are not manageable with our laboratory equipment. We made four new batches, called "5x #1" to "5x #4" in order to have different samples and mitigate the little deviations that can occur during the preparation stages.

The samples of MC+DEATi 5x were treated like the previous ones, at 1300°C for 3 hours. The XRD patterns taken after the carburization of the four samples are reported in Figure 77. The patterns are very similar, as confirmed by Table 19, where the peak positions, cell parameter and oxygen content for each sample are listed.

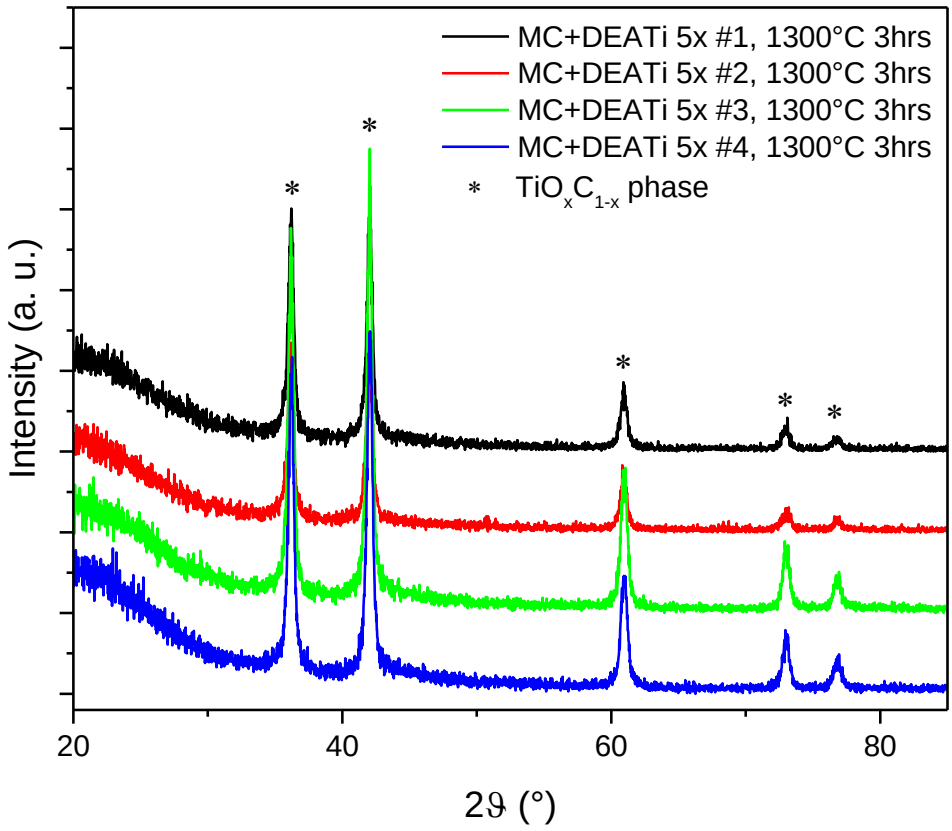

Figure 77, XRD pattern of MC+DEATi 5x #1. treated at 1300°C for 3 hours

Sample #	***1st peak position (°)***	***2nd peak position (°)***	***3rd peak position (°)***	***4th peak position (°)***	***5th peak position (°)***	***Cell parameter (Å)***	***Oxygen content (mol%)***
1	36.18	42.03	60.93	72.96	76.77	4.2952	44
2	36.16	42.01	60.92	73.00	76.85	4.2954	44
3	36.18	42.03	60.96	73.00	76.82	4.2940	45
4	36.19	42.04	60.96	73.00	76.81	4.2936	46

Table 19, peak positions, cell parameter and oxygen content for MC+DEATi 5x, after the treatment at 1300°C for 3 hours

The four samples shown a stoichiometry very similar amongst them and with a lower content of oxygen.

The only difference between the two sets of samples is the quantity of material used and carburized. Our hypothesis is that, given the geometry of the oven tube and the vessel inside, the quantity of starting material can influence the carburization process. The rectangular vessel was the same for the two sets with the only difference that it was fully loaded with precursors for the 5x batches meanwhile the quantity of MC+DEATi with the small batches was smaller, just enough to cover the bottom of the vessel. In this way inside the vessel during the degradation of the MC different atmospheres started to grow: in one hand, with less material the argon is free to circulate and remove the carbon byproducts, in the other, with more material that obstruct the flow of the gas, it is formed a carbon richer ambient that promote the carburization, leaning the oxygen content.

In order to validate this hypothesis, we made other two samples 5x, but this time the vessel was half loaded. The results are in line with our hypothesis, as can be seen in Table 20.

Sample #	***1st peak position (°)***	***2nd peak position (°)***	***3rd peak position (°)***	***4th peak position (°)***	***5th peak position (°)***	***Cell parameter (Å)***	***Oxygen content (mol%)***
1	36.25	42.10	61.01	73.04	76.85	4.2897	50
2	36.21	42.07	60.98	73.02	76.85	4.2917	48

Table 20, peak positions, cell parameter and oxygen content for MC+DEATi 5x, half loaded, treated at 1300°C for 3 hours

In Figure 78 the XRD patterns for the two samples are reported.

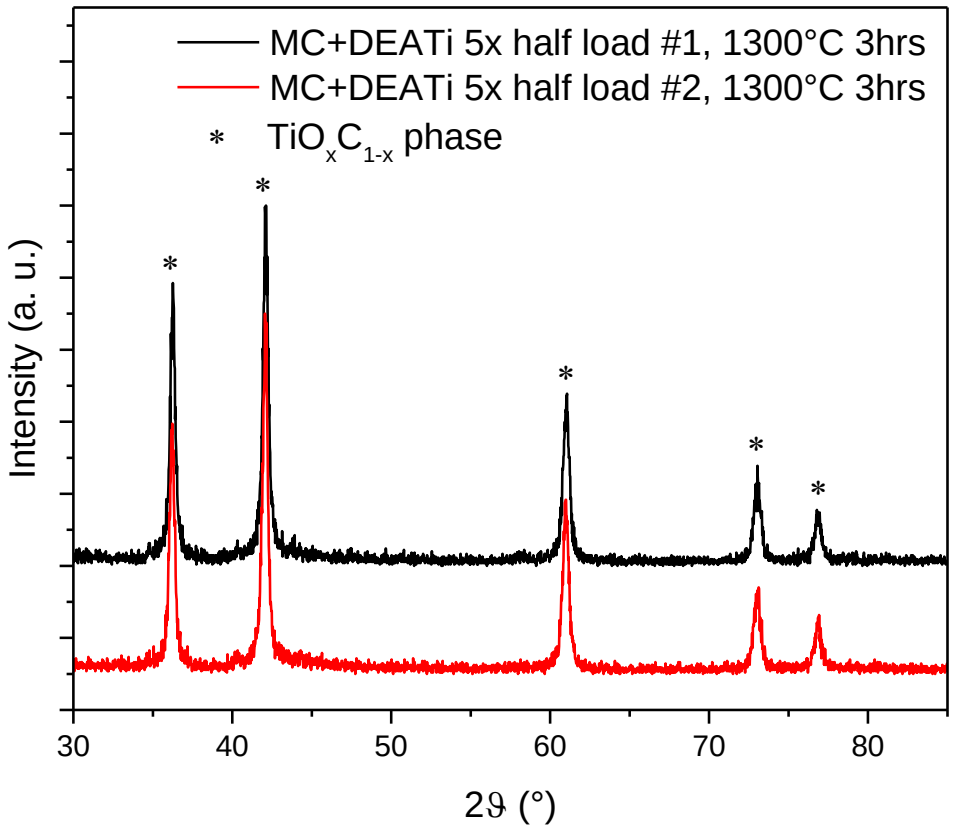

Figure 78, XRD pattern of MC+DEATi 5x, half-loaded and treated at 1300°C for 3 hours, #1

The oxygen content for the two samples is within the calculated error (2 mol%) and can be considered identical and with the expected stoichiometry, so the half-loaded samples represent a perfect result, validating the previous hypothesis and representing a viable path to synthetize $TiO_{0.5}C_{0.5}$.

After this discovery, we made other 6 samples in the same way to further validate the results. The respective XRD patterns are all shown together in Figure 79, meanwhile the peak positions, cell parameter and oxygen content are listed in Table 21.

Sample #	*1st peak position (°)*	*2nd peak position (°)*	*3rd peak position (°)*	*4th peak position (°)*	*5th peak position (°)*	*Cell parameter (Å)*	*Oxygen content (mol%)*
1	36.24	42.12	61.10	73.17	77.00	4.2856	54
2	36.17	42.03	60.94	72.96	76.80	4.2917	44
3	36.27	42.13	61.07	73.12	76.96	4.2860	54
4	36.20	42.09	61.02	73.05	76.85	4.2908	49
5	36.20	42.06	61.02	73.05	76.90	4.2909	49
6	36.24	42.11	61.07	73.10	76.95	4.2874	52

Table 21, peak positions, cell parameter and oxygen content for MC+DEATi new samples, half loaded and heat treated at 1300°C for 3 hours

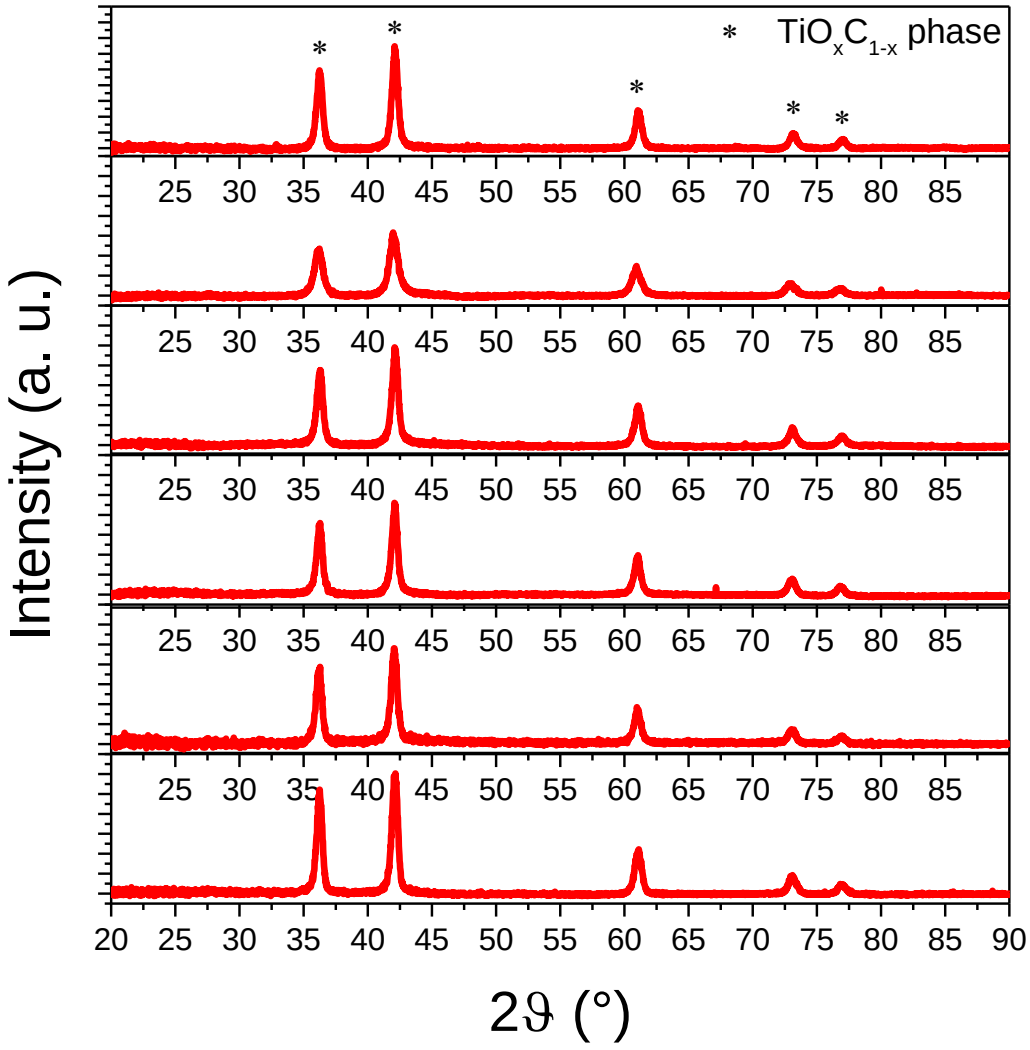

Figure 79, XRD patterns of MC+DEATi 2:1, half loaded, treated at 1300°C for 3 hours. The top pattern corresponds to sample #1, the bottom to sample #6

Even if the oxygen contents for the six samples are not all identical nor within the relative error (±2 mol%), on average the stoichiometry is $TiO_{0.50}C_{0.50}$.

We took SEM images for the sample #3, reported below.

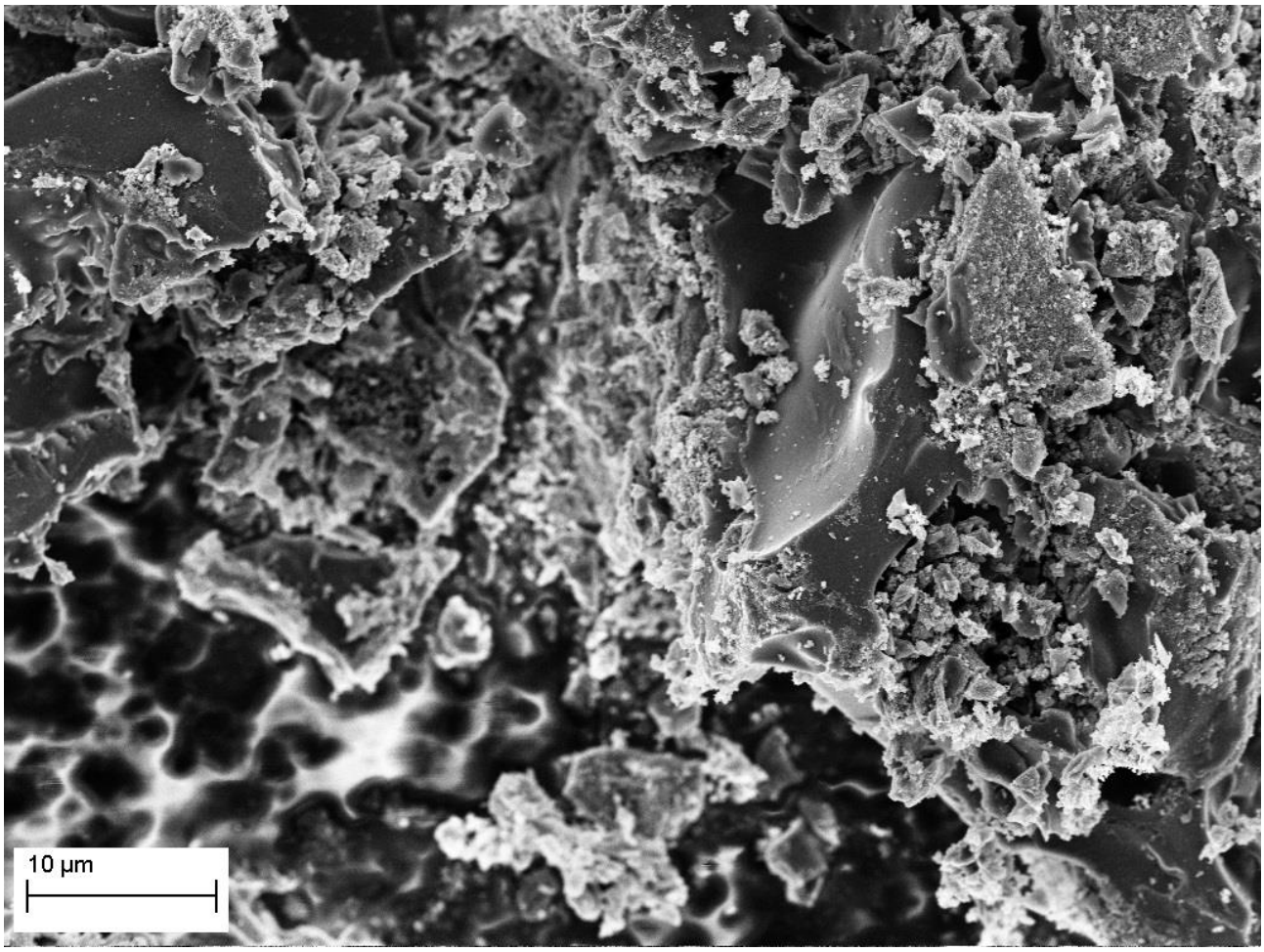

Figure 80, SEM image of MC+DEATi 5x heat treated at 1300°C for 3 hours, sample #3

In the first image, Figure 80, there are clearly visible the big pieces decorated with small particles, like the previous sample, albeit here the big chunks are bigger, probably due to a grosser grinding.

In Figure 81 and Figure 82 , the surface is scanned with higher magnifications, revealing the uneven surface of the chunks and the dimensions of the particles.

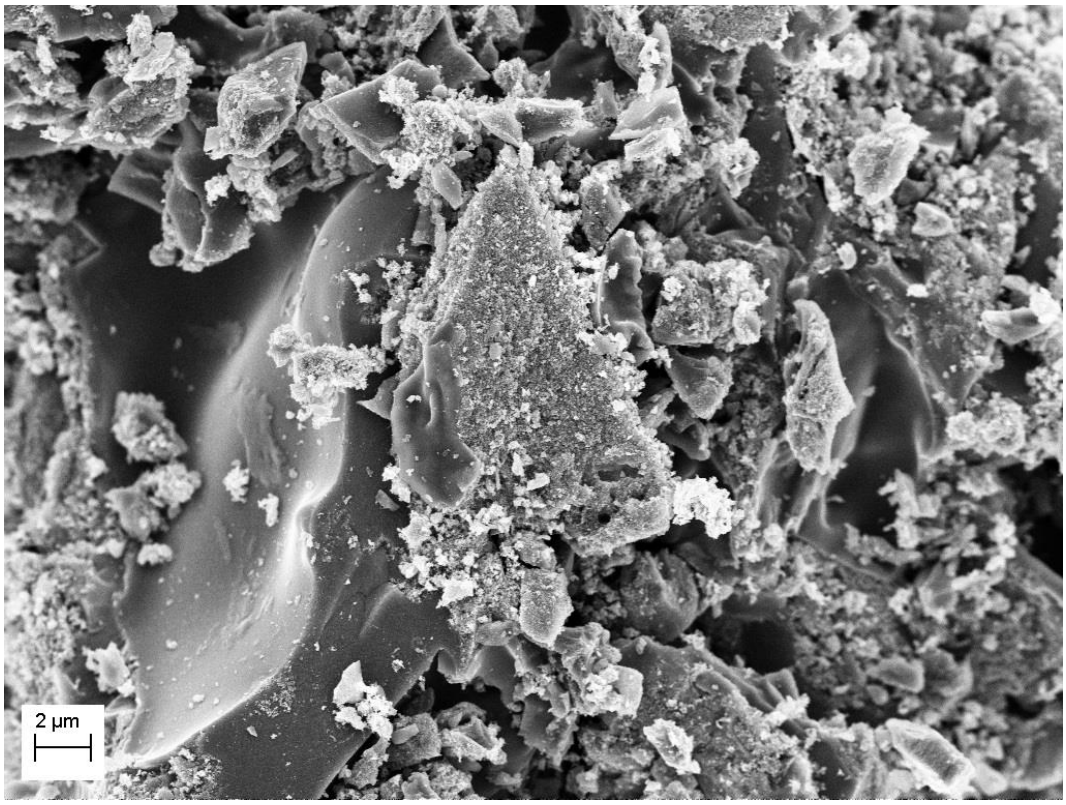

Figure 81, SEM image of MC+DEATi 5x heat treated at 1300°C for 3 hours, sample #3

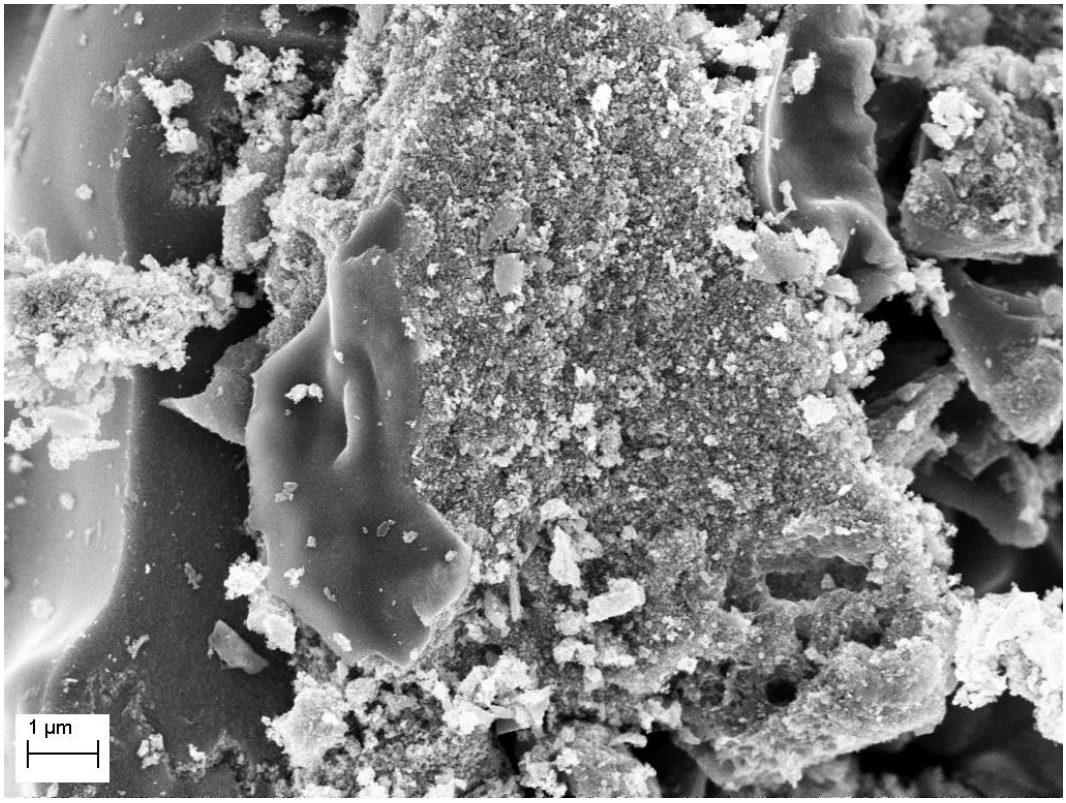

Figure 82, SEM image of MC+DEATi 5x heat treated at 1300°C for 3 hours, sample #3

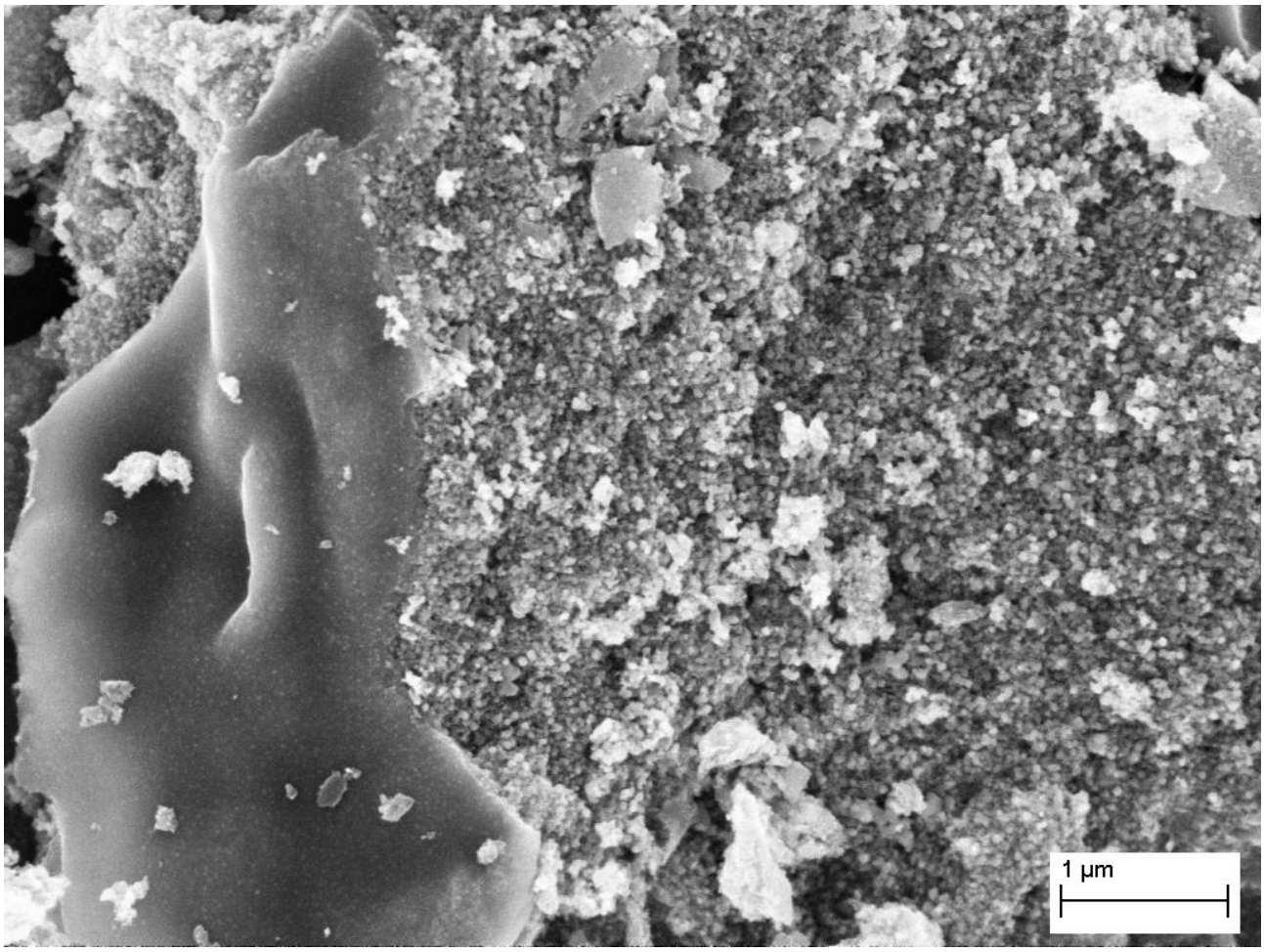

Figure 83, SEM image of MC+DEATi 5x heat treated at 1300°C for 3 hours, sample #3

In Figure 83 the surface of the chunk on the left starts to reveal a porous structure, that can be seen with higher resolution in Figure 84.

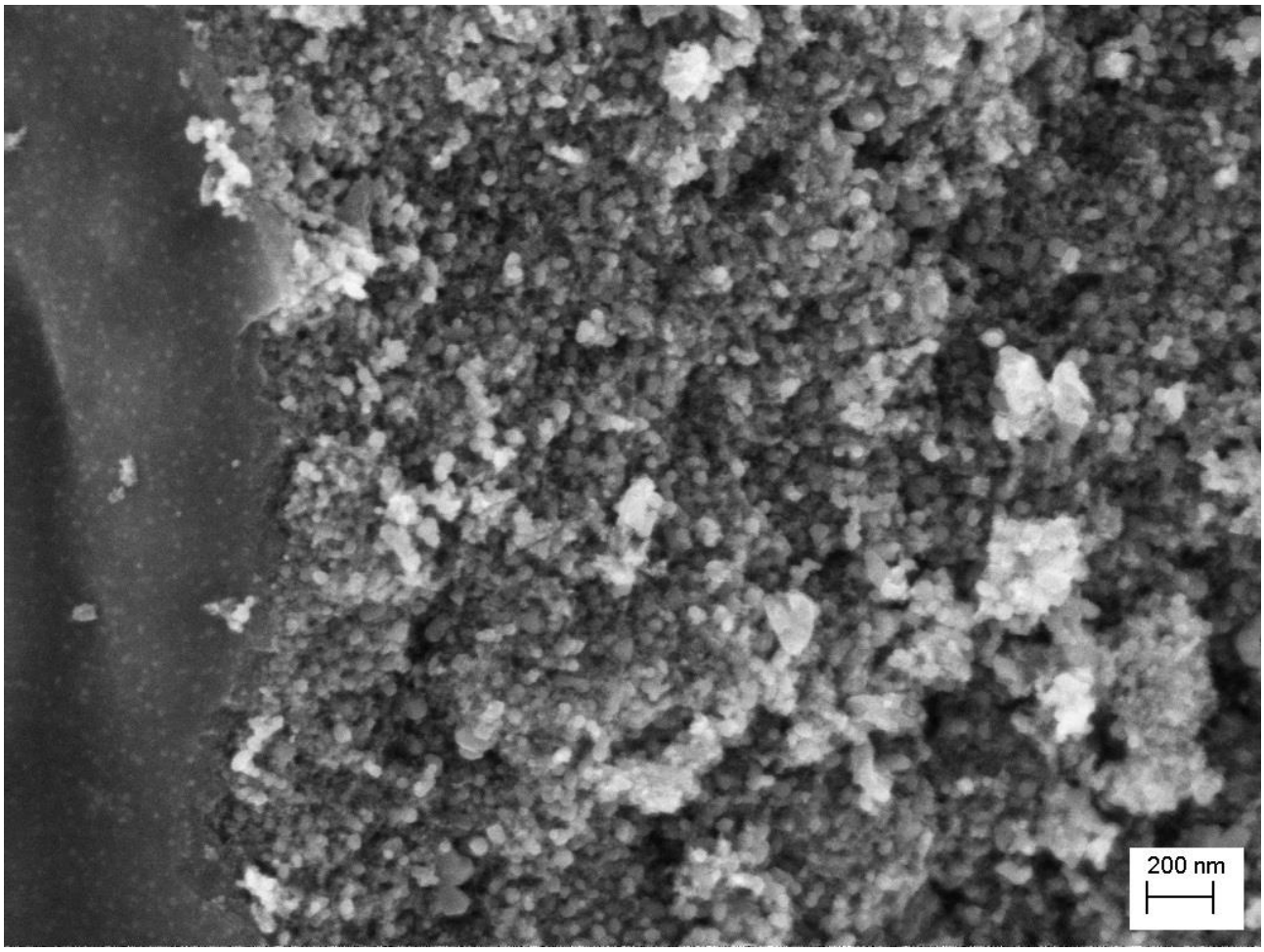

Figure 84, SEM image of MC+DEATi 5x heat treated at 1300°C for 3 hours, sample #3

On the left side of the image in Figure 84 there are small bright dots on a darker surface: these are very small nanopores on the surface of the big chunk. The remaining part of the image represents the small particles that decorate the surface, which can be better appreciated in the next image, Figure 85.

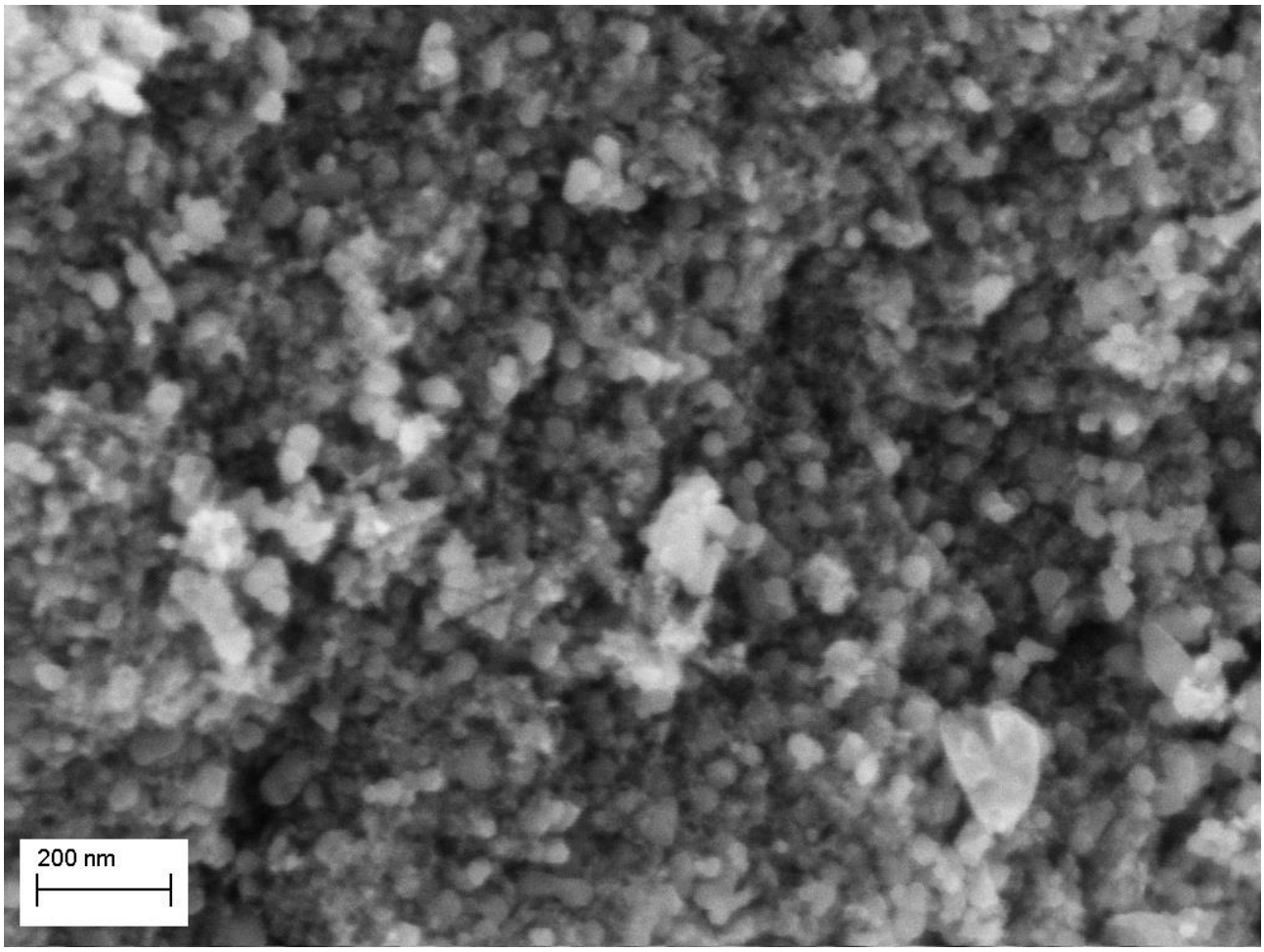

Figure 85, SEM image of MC+DEATi 5x heat treated at 1300°C for 3 hours, sample #3

Albeit not very sharp, in Figure 85 it is possible to see only the small particles on the surface of the big chucks. They are in the range of 20-40 nm in diameter with a round shape.

We investigated also the stoichiometric control over a broad range of the solid solution: we tried to prepare TiC (pure titanium carbide), $TiO_{0.25}C_{0.75}$ and $TiO_{0.75}C_{0.25}$. Obviously we didn't expected to reach these perfect compositions because the temperature and time of treatment are too low and short to have a complete reaction of the carbon with the titanium oxide and vice versa. We studied the limits for our carburization treatment. For pure titanium carbide higher temperatures and longer annealing time are required, in order to have a complete reaction of the carbon with the titanium oxide. However, for intermediate compositions, as $TiO_{0.25}C_{0.75}$ and $TiO_{0.75}C_{0.25}$, our conditions of carburization could be adequate. With these considerations in mind, we prepared three samples with an initial stoichiometry theorically appropriate to reach the extremity of the composition and the two intermediate points. We made a sample with a C:Ti ratio of 3:1 for TiC, one with a 2.5:1 ratio for $TiO_{0.25}C_{0.75}$ and the last with C:Ti equal to 1.5:1 for $TiC_{0.75}C_{0.25}$.

The XRD patterns, taken after the carburization treatment at 1300°C for 3 hours for each sample, are reported in Figure 86.

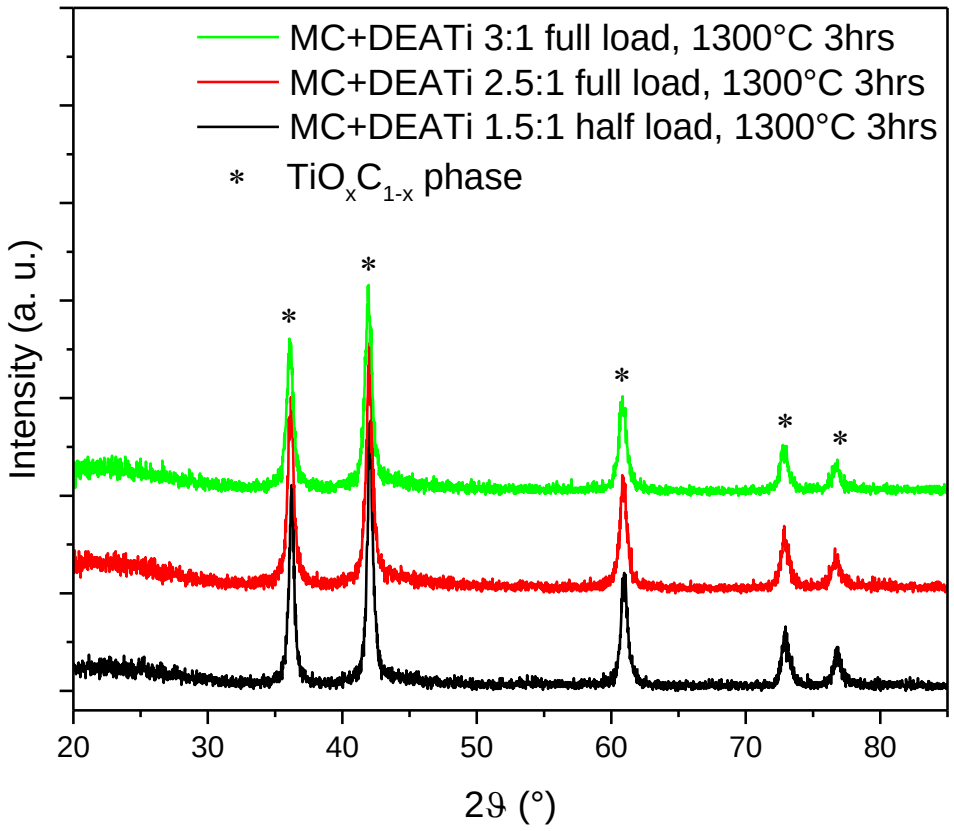

Figure 86, XRD pattern of MC+DEATi 3:1, treated at 1300°C for 3 hours

For these first two samples (with a C:Ti ratio of 3:1 and 2.5:1), as deducted before, we loaded as much as possible the vessel in order to create a reductive atmosphere inside the powder. For the last sample with a C:Ti ratio of 1.5:1, we made a first sample with a medium quantity of material.

The quantity used represented a mistake, because the obtained stoichiometry was $TiO_{0,47}C_{0,53}$, demonstrating that a major parameter for the stoichiometric control is represented by the loaded quantity or, to be more precise, the atmosphere around the sample. Since the quantity inside the vessel determines if argon can flow freely inside the powder or not, removing the carbon-rich gases that develops during the heat treatment, it can reconducted to the speed of the argon flow. Unluckily we haven't a proper setup to prove this theory.

After this consideration, we treated again the MC+DEATi 1.5:1, loading a very small quantity of powder avoiding the creation of more than one layer on the bottom of the vessel. In this way, we can indirectly verify the theory of the argon flow. The XRD pattern is reported in Figure 87.

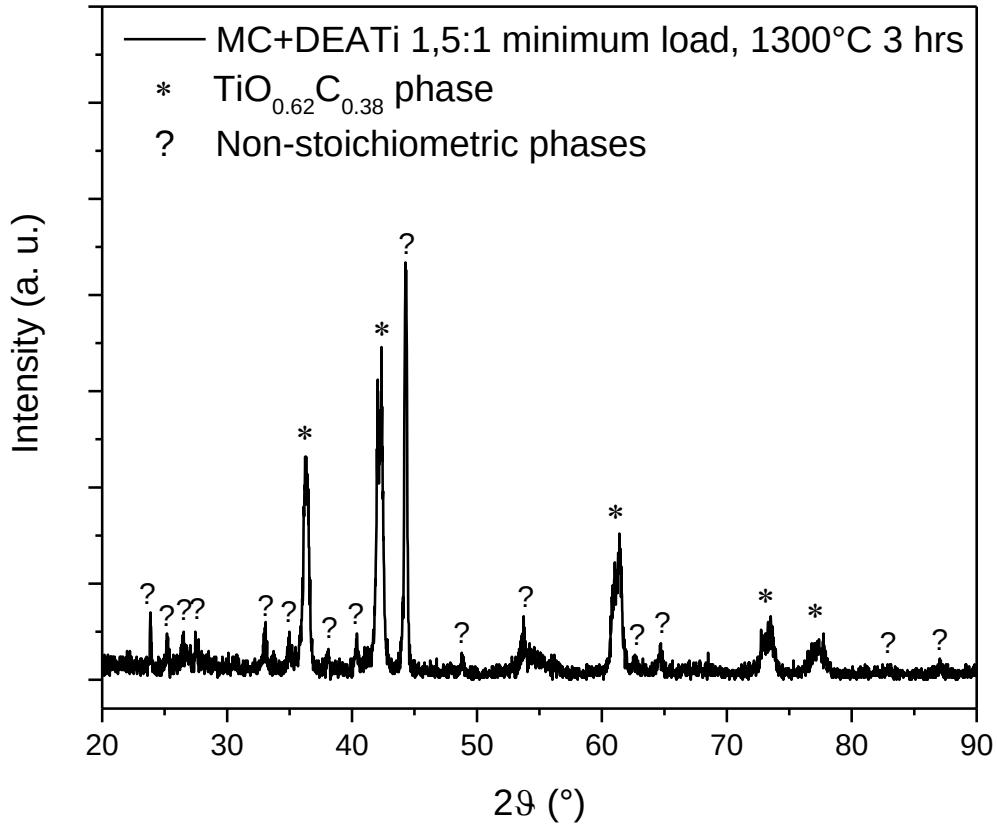

Figure 87, XRD pattern of MC+DEATi 1,5:1, low quantity loaded, treated at 1300°C for 3 hours

As can be seen in the previous image, along with the oxycarbide peaks there are also other peaks from non-stoichiometric phases, meaning that the quantity of titanium oxide is too high or the time of treatment is too short to allow a complete reaction.

In Table 22 the peak positions, cell parameters and oxygen content for the four samples are reported and in Figure 88 there is a comparison of three samples out of four, excluding the MC+DEATi 1.5:1, medium quantity loaded.

C:Ti ratio	*1st peak position (°)*	*2nd peak position (°)*	*3rd peak position (°)*	*4th peak position (°)*	*5th peak position (°)*	*Cell parameter (Å)*	*Expected oxygen content*	*Oxygen content (mol%)*
3	36.11	41.95	60.84	72.86	76.71	4.3011	0	37
2.5	36.17	42.01	60.90	72.91	76.73	4.2971	25	42
1.5	36.23	42.07	60.96	72.96	76.80	4.2926	75	47
1.5 low quantity	36.32	42.23	61.23	73.25	77.28	4.2766	75	62

Table 22, peak positions, cell parameter and oxygen content for MC:DEATi with different C:Ti ratios

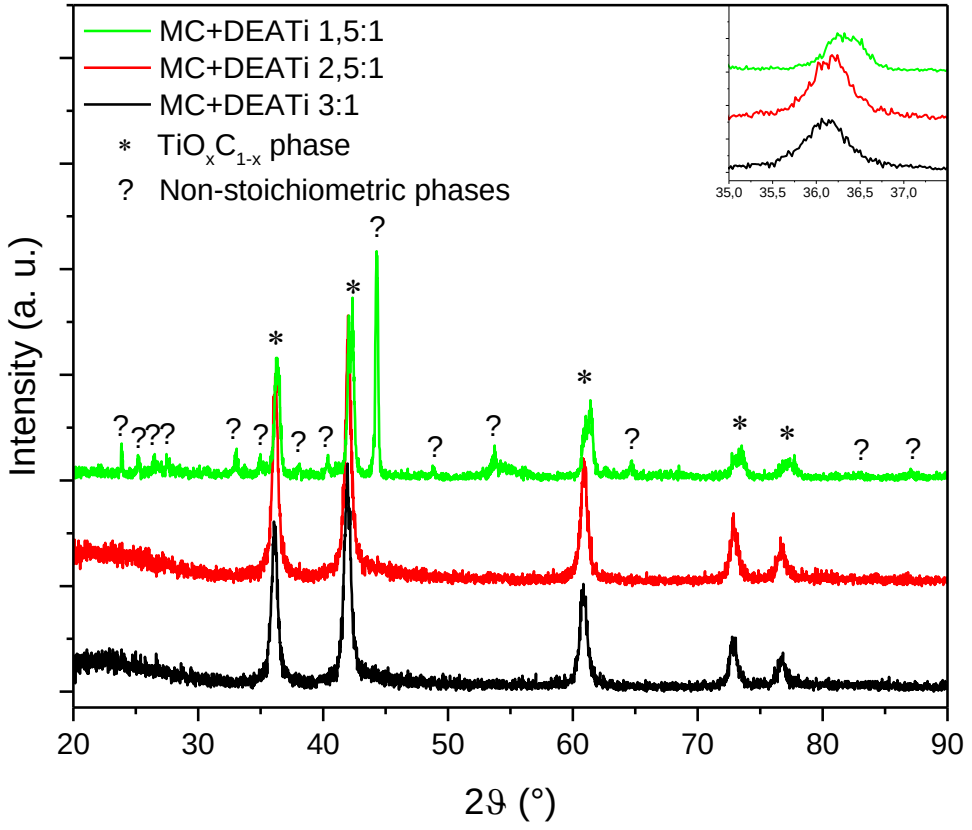

Figure 88, XRD patterns of MC+DEATi 1,5:1, 2,5:1 and 3:1, all treated at 1300°C for 3 hours. In the inset a zoom on the first peak position

The expected oxygen values were not reached, because the temperature and time were not high and/or long enough, as expected. This test however indicates the limits of stoichiometric control for the treatment at 1300°C for 3 hours.

After founding the best path to obtain the $TiO_{0.5}C_{0.5}$ composition in a controlled and replicable way, we focused on the surface area, another key parameter for a good electrocatalytic support.

The first sample we investigated was the one used for the studies about the length of the carburization treatment, specifically the one treated for 3 hours. Starting from the SEM images, we expect to have a pretty large specific surface area: indeed, from the BET analysis, it was determined to be 257 m^2g^{-1}, but the pore distribution analysis was not possible because an error encountered during the measure zeroed the first point, as can be seen in Figure 89, where the drop in the volume axis is highlighted by the logarithmic scale of the relative pressure.

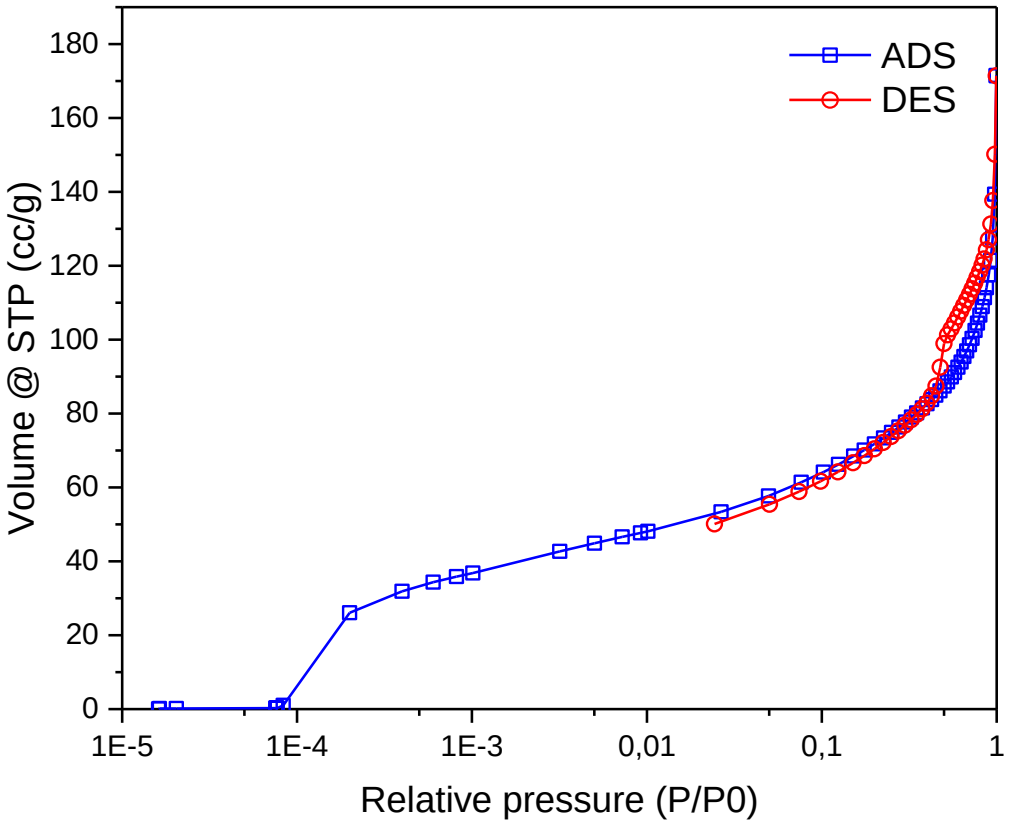

Figure 89, isotherm plot of MC+DEATi 2:1, treated at 1300°C for 3 hours during the tests for the treatment times

We tried with a sample obtained from the last batch of six samples treated at 1300°C for 3 hours, to be specific the number 3. The isotherm plot is reported in Figure 90. This time the DFT simulation was possible, as reported in Figure 91.

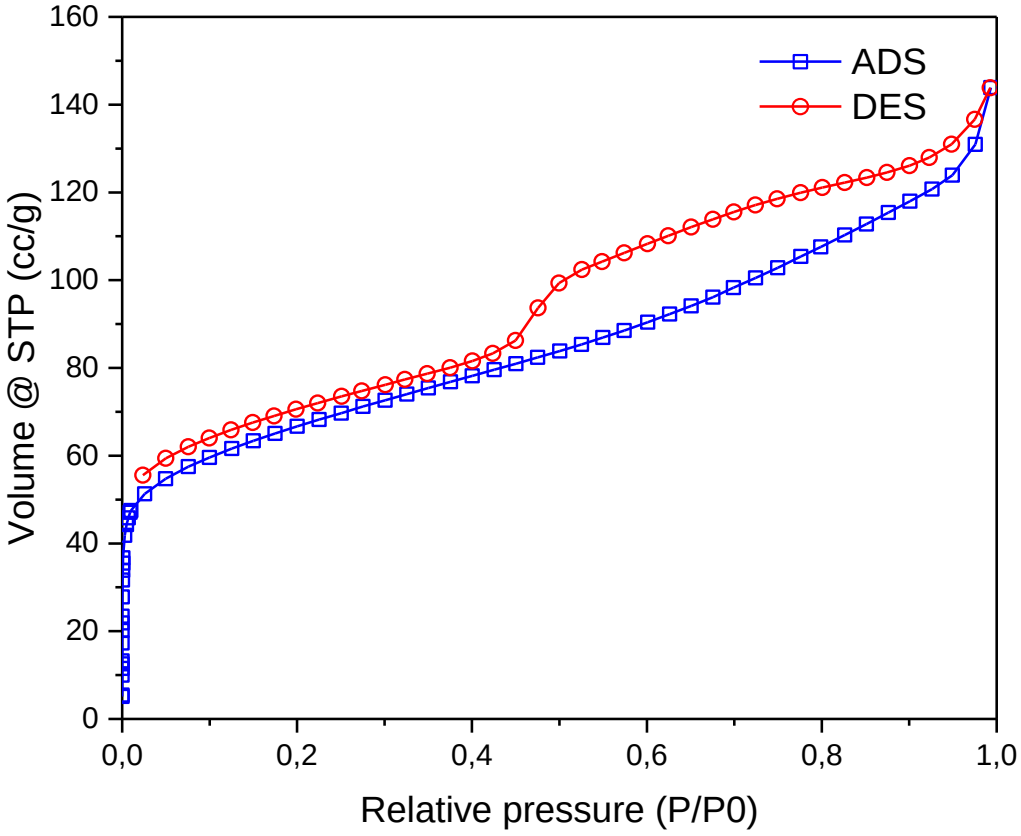

Figure 90, isotherm plot of MC+DEATi 5x #3, treated at 1300°C for 3 hours

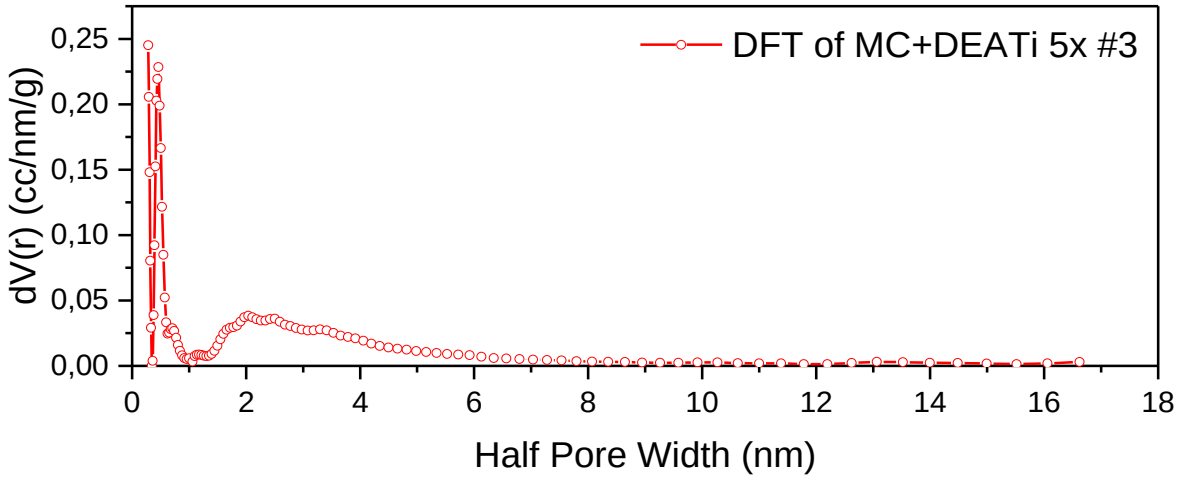

Figure 91, DFT analysis of MC+DEATi 5x #3, treated at 1300°C for 3 hours

Beside the first 4 points that are artifacts due to the extremely low pressures, the pore distribution is bimodal, with a first, very narrow peak at 0.4 nm and a second, broader, around 2 nm. This means that the main pore diameters are 0.8 and 4 nm, creating a microporous material. From the BET analysis the surface area value is 237 m^2g^{-1}, well over the minimum required value of 100 m^2g^{-1}, and very similar to what obtained from the previous sample. The pores that are visible from the SEM images (specifically in Figure 83 and Figure 84) probably are too big for a DFT analysis and represent only a small fraction of the total surface area.

As said before, for a good anodic support three objectives are requested: stoichiometry, purity and high specific surface area. For the stoichiometry, a control over the composition and a good reproducibility are achieved through the initial composition, quantity of treated powder and carburization parameters. The purity does not represent a problem, since all the samples treated within few days from the preparation have not spurious phases. The surface area minimum requirement was set to be 100 m^2g^{-1}, but with our samples we overdue this goal doubling the value.

Since the major requirements for a usable titanium oxycarbide are fully achieved, it can be tested in an electrochemical semicell to study the performances with standard and innovative catalysts. As starting catalyst, we used pure platinum, because it is the best solution for most electrocatalysis applications. Within the DECORE project, also different catalysts were proposed to lower the price, using platinum alloys, tungsten and molybdenum carbides or three-metal alloys. For my thesis we investigated only platinum alloy and tungsten carbide, meanwhile other research group studied other catalysts.

The first sample was decorated only with platinum in a very simple way, that can be defined “one-pot”. Indeed, the preparation steps for the MC+DEATi remain the same, but with the addition of hexachloroplatinic acid in the water-methylcellulose suspension. In this way, the platinum is added directly to the compound before the heat treatment without further steps [76]. Then the dried precursors can be carburized in the usual way, with an argon flow at 1300°C for 3 hours.

We prepared three different samples with this routine, changing the platinum loading. For the first sample we added 1 mol% of pure platinum (with respect to TiO_xC_{1-x}), for the second 3 mol% and for the last 5 mol%. They were heat treated as soon as possible after the drying step, to avoid titanium loss, as explained before.

The XRD pattern for the first sample with 1 mol% of platinum is reported below, in Figure 92.

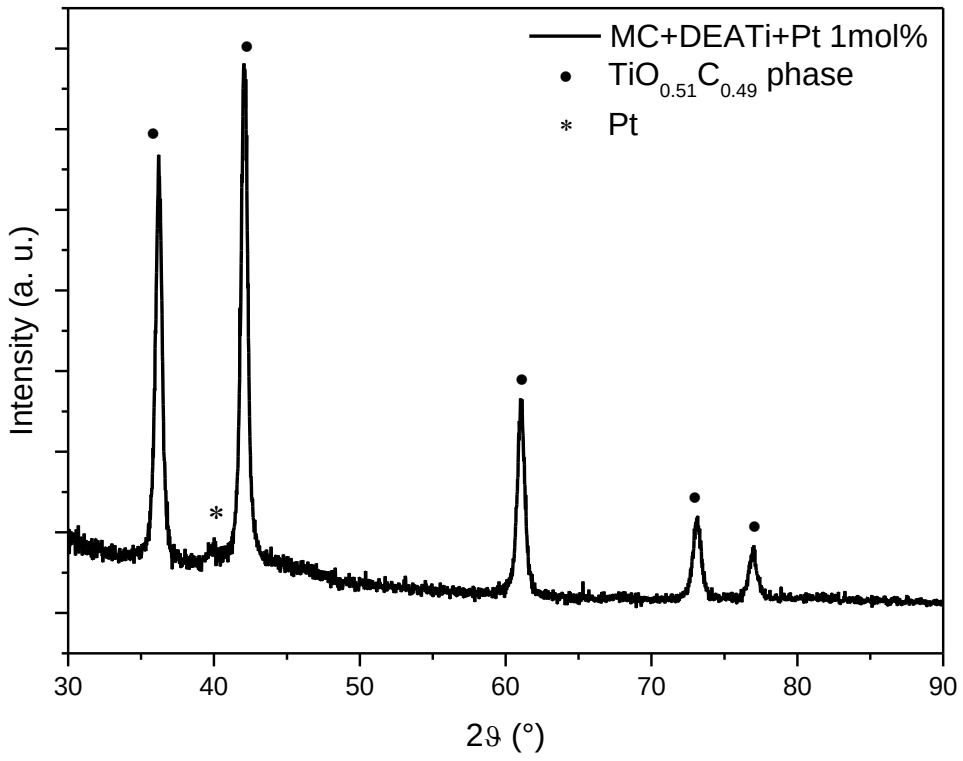

Figure 92, XRD pattern of MC+DEATi 2:1 with the addition of 1 mol% of Pt, heat treated at 1300°C for 3 hours

The peaks of the titanium oxycarbide are clearly visible meanwhile there is only a small peak that can be ascribed to the Pt phase at ~40°. This is the most intense peak for Pt, that corresponds to the [111]

direction. The stoichiometry for the TiO_xC_{1-x} results to be x=0.51, scoring a very good adhesion to the expected stoichiometry, as seen in the previous tests.

The next sample was made with 3 mol% of platinum and its XRD pattern is shown in Figure 93. There are more peaks visible in this sample: they are related mainly to metallic platinum but there are also small peaks derived from alloying platinum with titanium. The oxycarbide's peak positions, cell parameter and oxygen content are reported in Table 23.

1st peak position (°)	***2nd peak position (°)***	***3rd peak position (°)***	***4th peak position (°)***	***5th peak position (°)***	***Cell parameter (Å)***	***Oxygen content (mol%)***
36.23	42.07	61.00	73.01	76.86	4.2910	49

Table 23, peak positions, cell parameter and oxygen content of the TiO_xC_{1-x} phase for MC+DEATi added with 3 mol% of Pt

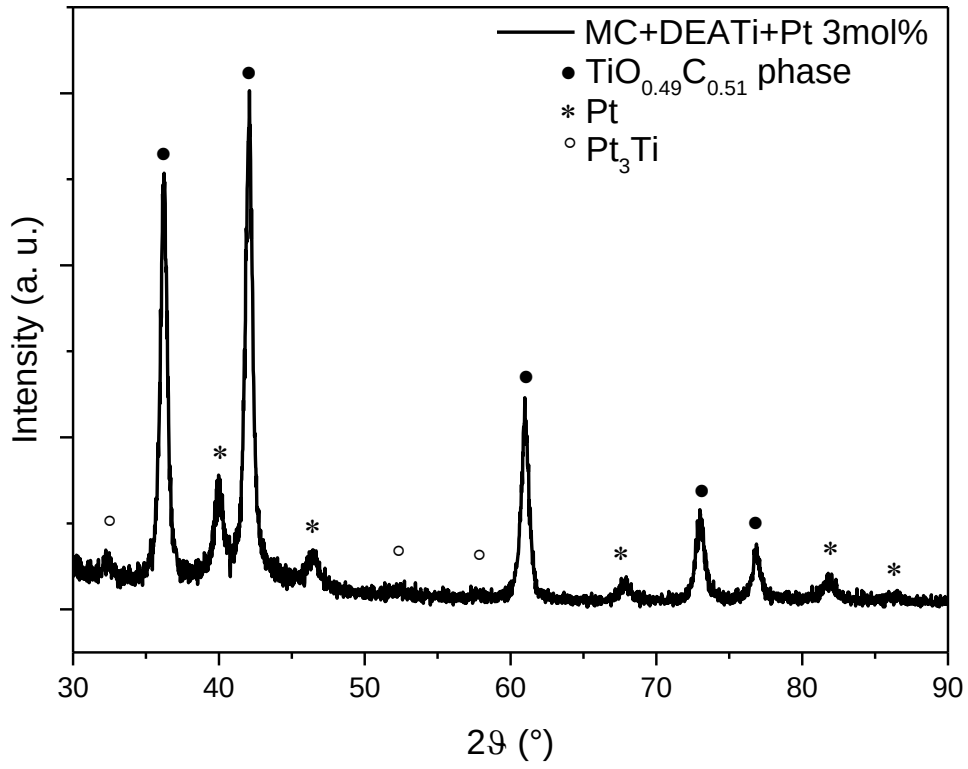

Figure 93, XRD pattern of MC+DEATi 2:1 with the addition of 3 mol% of Pt, treated at 1300°C for 3 hours

The last sample was made with an addition of 5 mol% of metallic platinum. This sample shown more intense peaks for the Pt_3Ti alloy, meaning that adding more platinum create more nanoparticles but tends

to create also a two-metal alloy. This can be seen in Figure 94. The peaks of the titanium oxycarbide phase are not changed, as can be noted in Table 24, where the peak positions, cell parameter and oxygen content are listed. The stoichiometry is nearly the same as the two previous samples, indicating that the introduction of the Pt precursor is not affecting too much the carburization process.

1st peak position (°)	***2nd peak position (°)***	***3rd peak position (°)***	***4th peak position (°)***	***5th peak position (°)***	***Cell parameter (Å)***	***Oxygen content (mol%)***
36.23	42.06	60.97	72.97	76.83	4.2923	47

Table 24, peak positions, cell parameter and oxygen content of the TiOC phase for MC+DEATi added with 5 mol% of Pt

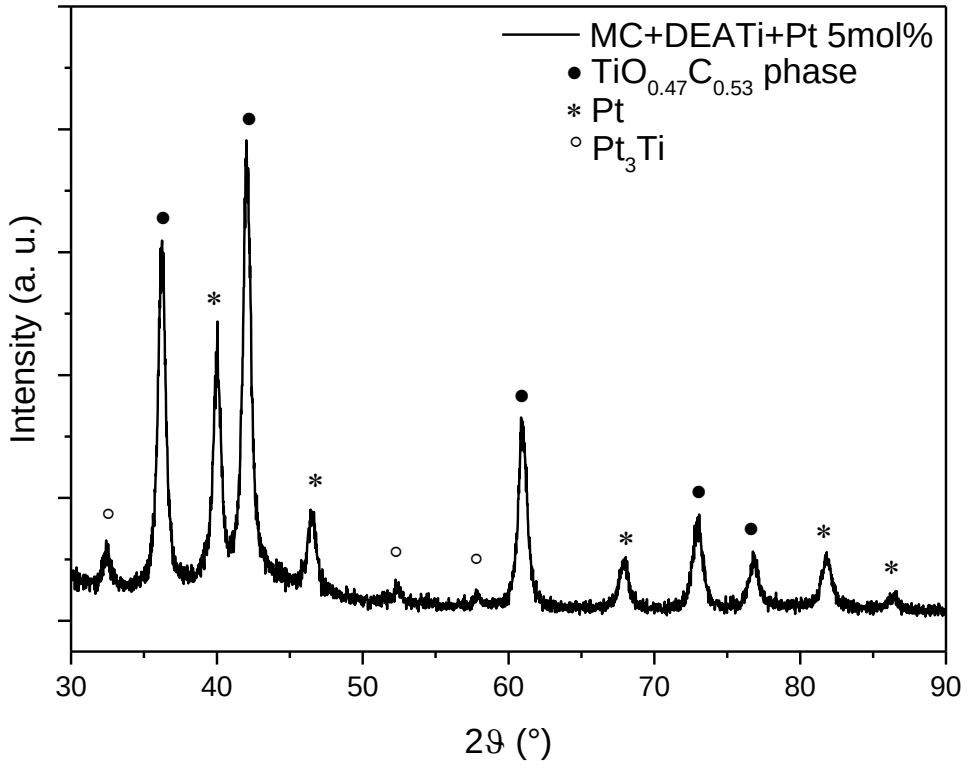

Figure 94, XRD pattern of MC+DEATi 2:1 with the addition of 5 mol% of Pt, treated at 1300°C for 3 hours

For a better visual comparison of the growth of the alloy and pure platinum peaks, the three XRD patterns are reported in the following image, Figure 95.

As can be seen, while the peaks of titanium oxycarbide have the same intensity, the peak related to metallic platinum increases with higher platinum loading, as expected, but also different peaks of the

titanium-platinum alloy appear. This means that the loading of the Pt nanoparticles is not the calculated value but a lower one, because a fraction of the platinum is lost in the alloy.

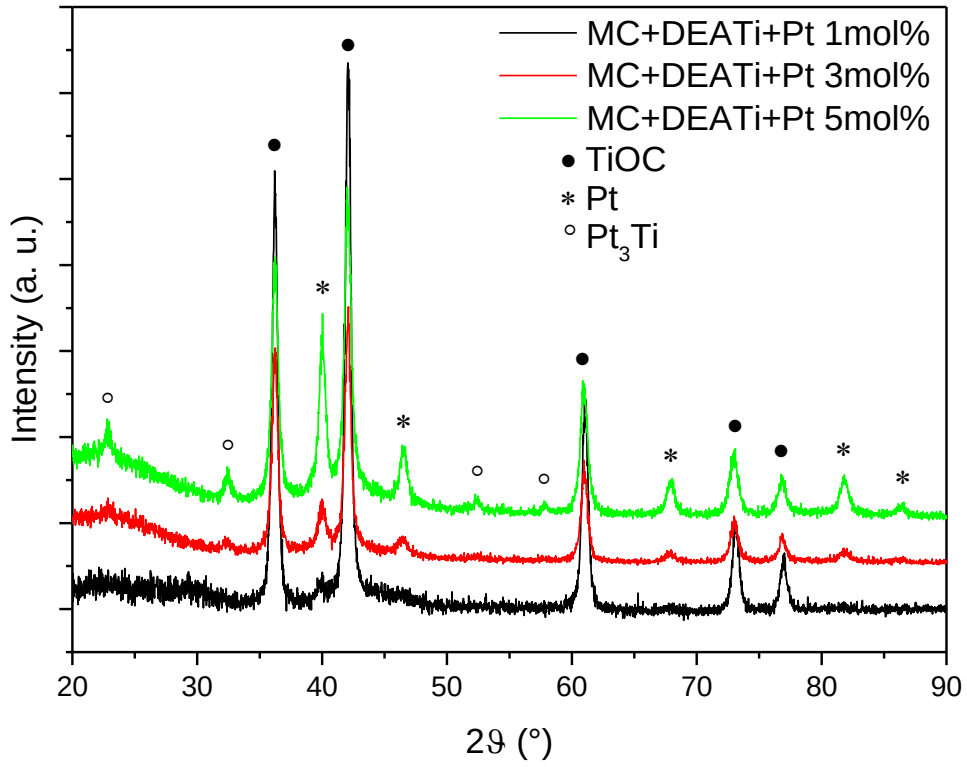

Figure 95, XRD patterns of MC+DEATi 2:1 with the addition of 1, 3 and 5 mol% of Pt, treated all at 1300°C for 3 hours

We investigated the surface of the two last sample (with 3 and 5 mol% of platinum) with the SEM and discovered similar structures to the titanium oxycarbide, but nanoparticles are clearly present on the surface, as can be seen in Figure 96, Figure 97 and Figure 98 for the sample with 3 mol% of Pt, and in Figure 99 and Figure 100 for the last sample.

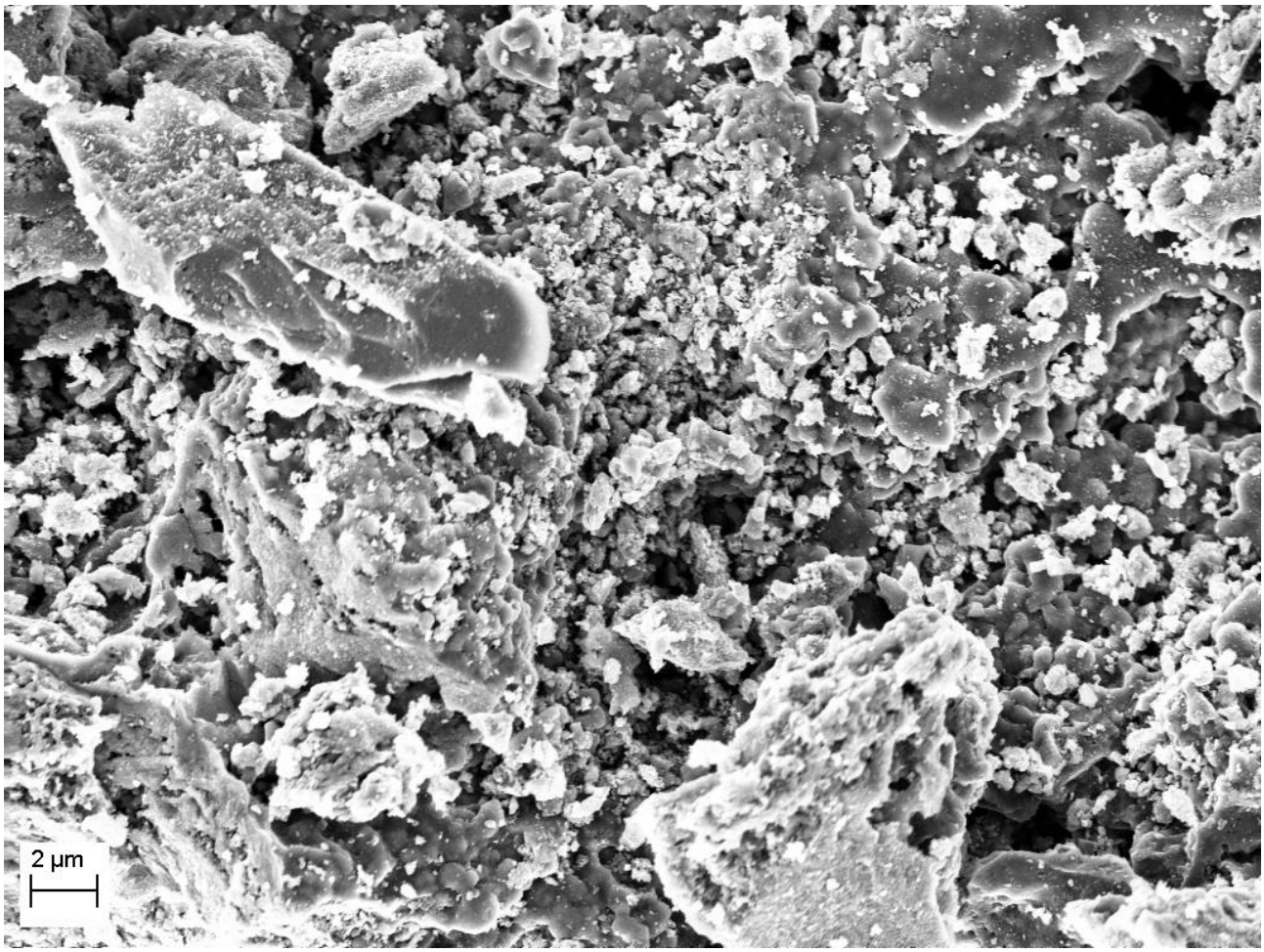

Figure 96, SEM image of MC+DEATi+Pt 3 mol%

As can be seen in the previous image, the surface still presents big chunks decorated with small particles, but this time the morphology of the large pieces appears to be more sponge-like, with minor depressions. It can be better noted in the following image, Figure 97.

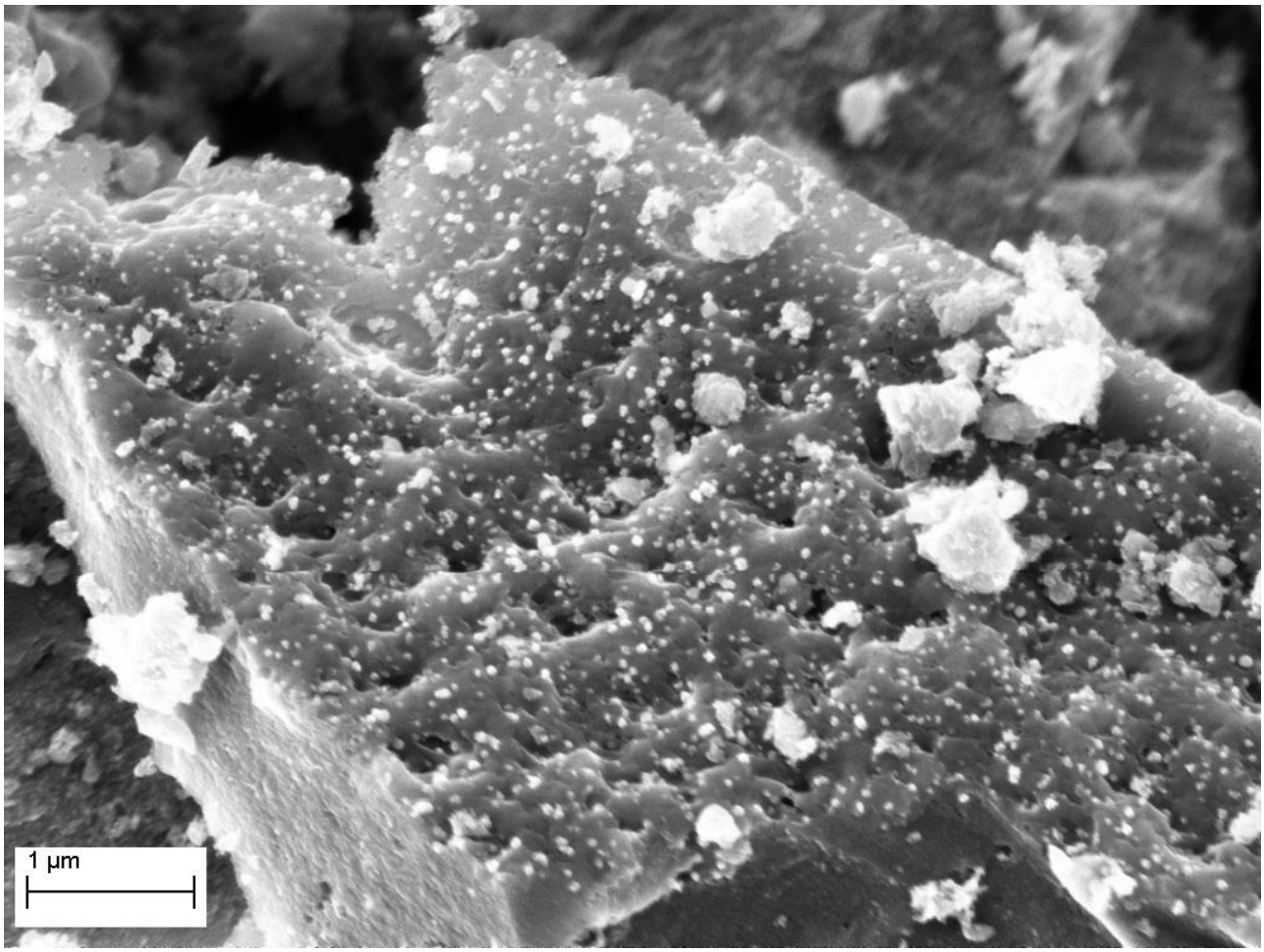

Figure 97, SEM image of MC+DEATi+Pt 3 mol%.

The surface morphology is not smooth but rough, with a lot of holes. Small bright dots of platinum nanoparticles can be also seen.

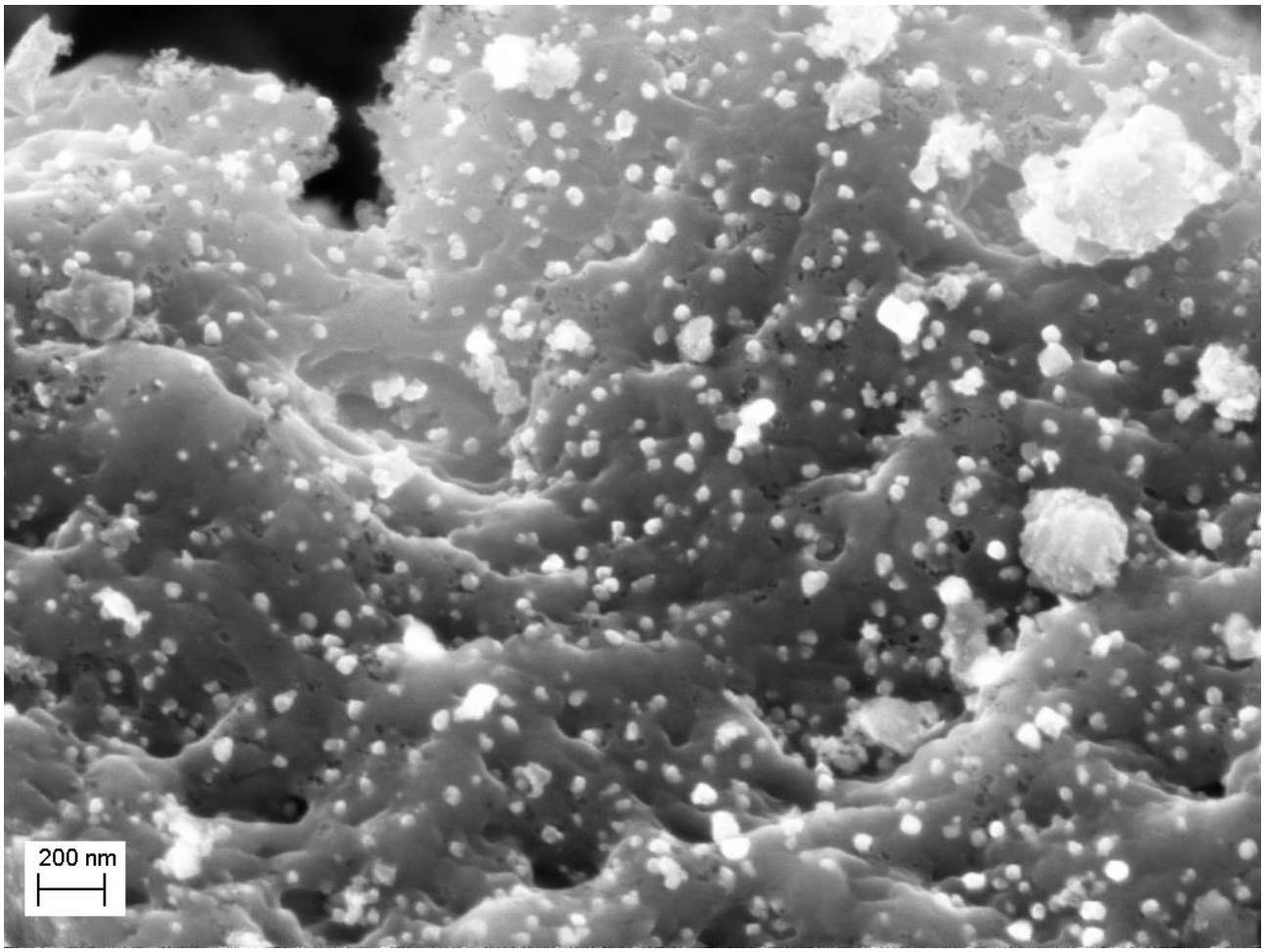

Figure 98, SEM image of MC+DEATi+Pt 3 mol%

In the image above, Figure 98, the platinum nanoparticles are clearly visible, showing a good dispersion on the uneven surface. We took also an EDX analysis to determine the elemental quantities of each component, but it wasn't very useful because the probe collected a very high signal for the elemental carbon, lowering all the other signal relatable to platinum and titanium.

For the sample with 5 mol% of platinum the titanium oxycarbide is very similar, but the distribution of the nanoparticles on the surface is very different, as can be seen in the following images taken with higher magnifications.

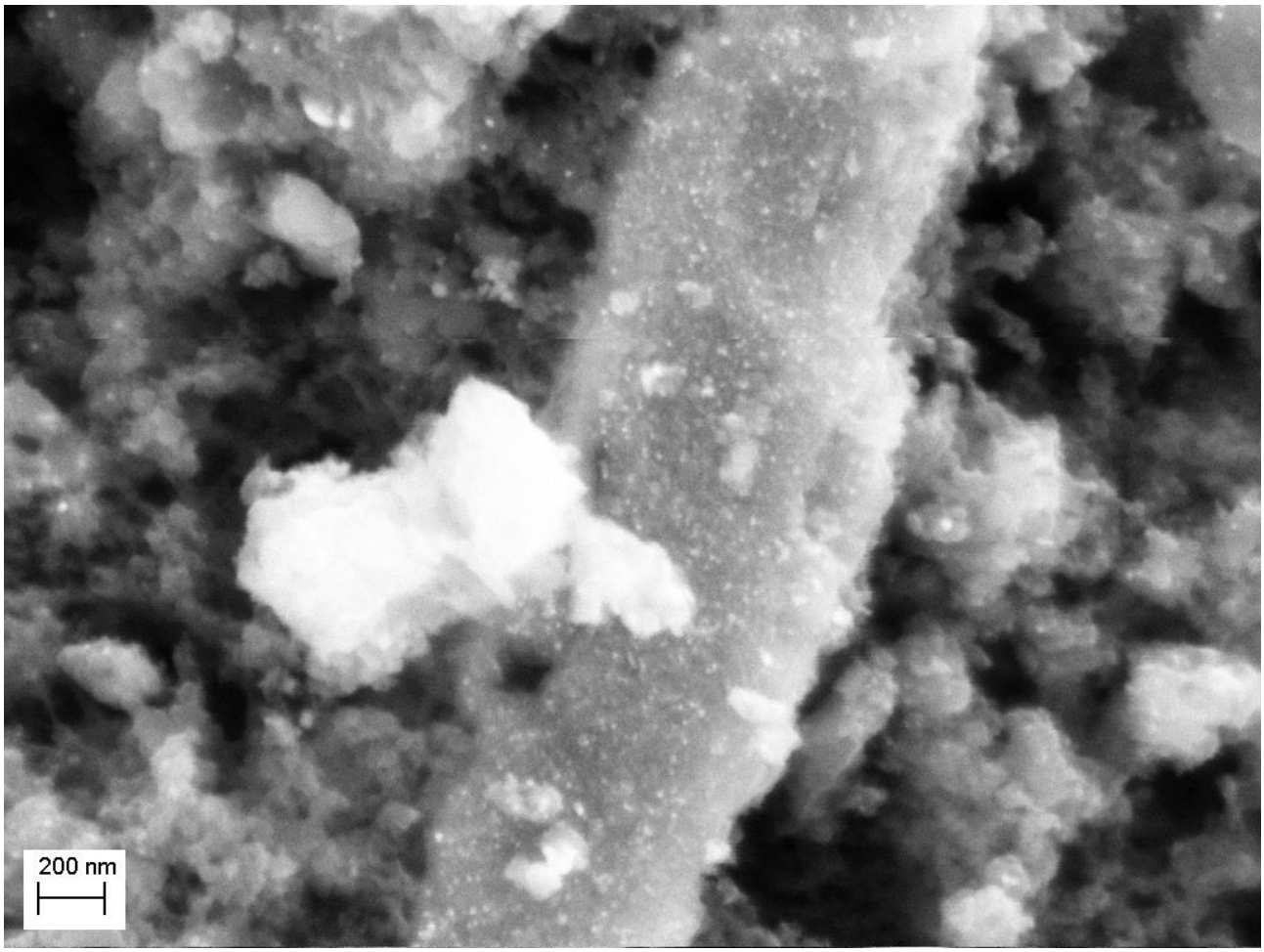

Figure 99, SEM image of MC+DEATi+Pt 5 mol%

In the image above, we can see that the Pt nanoparticles, represented by small white dots, are very small but evenly distributed.

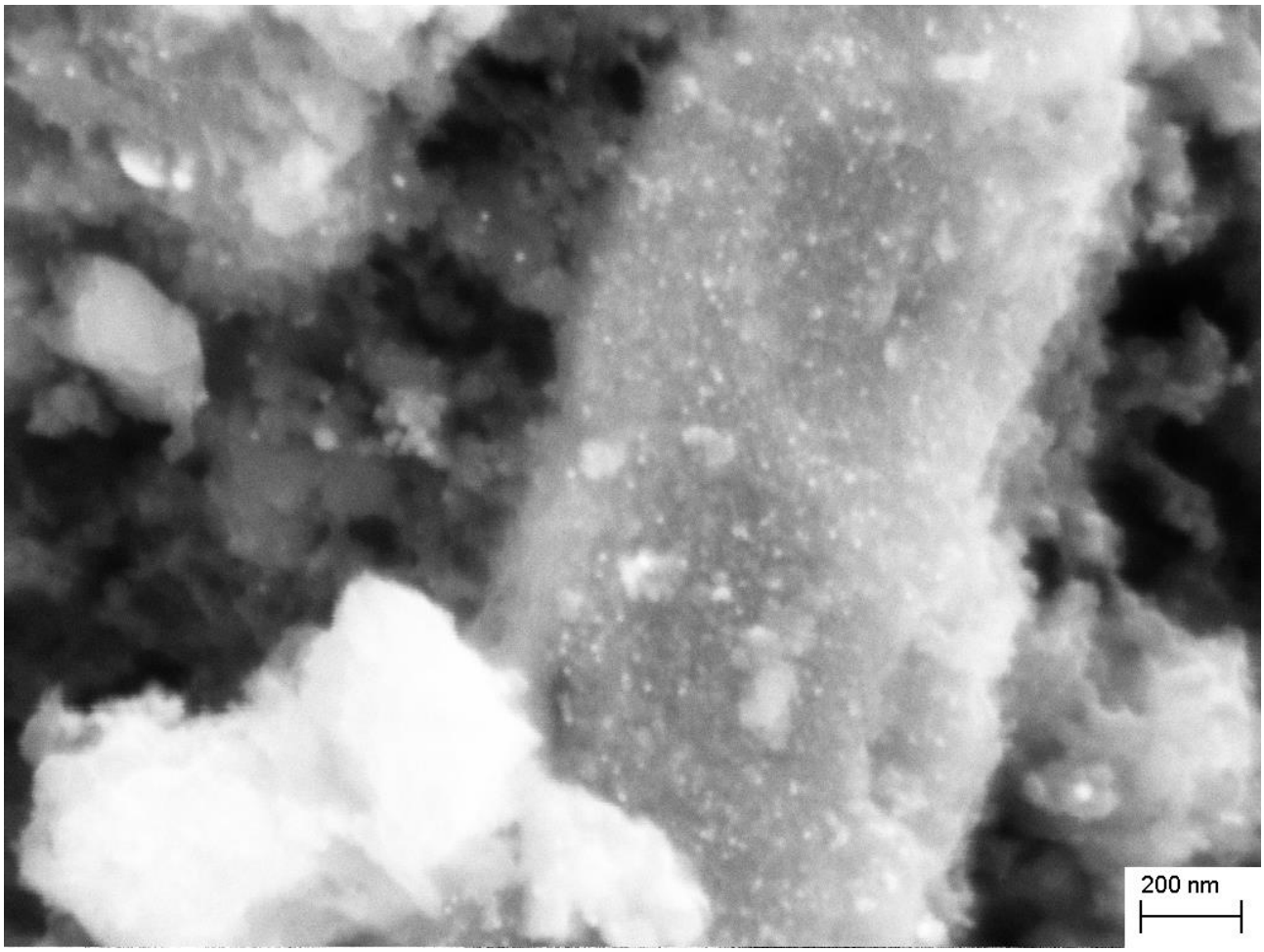

Figure 100, SEM image of MC+DEATi+Pt 5 mol%.

In Figure 100, that is a magnification of the previous image, the Pt nanoparticles are more recognizable, albeit their dimensions are very small.

From the EDX analysis we obtained that the ratio between titanium and platinum is ~10:1, comparable to the molar ratio used during the preparation of the sample.

After the SEM observations, we decided to make BET analyses in order to investigate if the rougher surface influences the total area. We compared these last results with ones obtained from MC+DEATi without nanoparticles decoration. They are very interesting because there is a clear trend. The isotherm plots are shown in Figure 101, meanwhile in Figure 102 there are the pores' distributions from the DFT simulations.

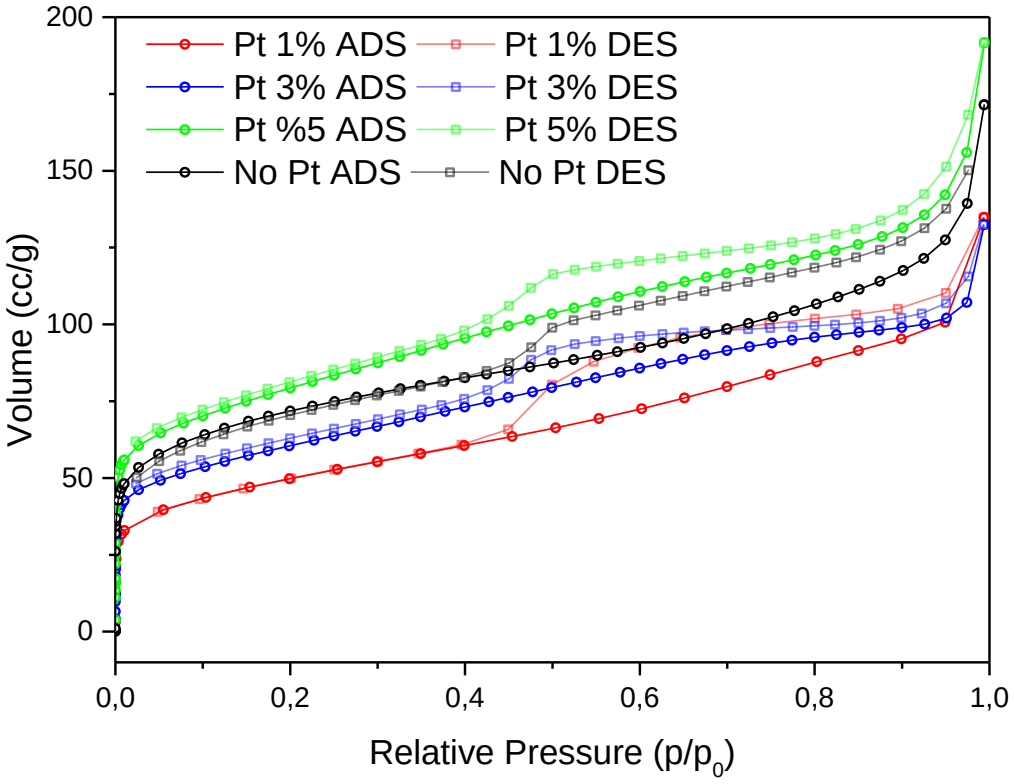

Figure 101, isotherm plot of MC+DEATi without Pt, with 1 mol%, 3 mol% and 5 mol% of platinum

The values of the specific surface areas are listed in Table 25:

Without Pt	***1 mol% Pt***	***3 mol% Pt***	***5 mol% Pt***
257 m^2g^{-1}	175 m^2g^{-1}	214 m^2g^{-1}	281 m^2g^{-1}

Table 25, surface area values for MC+DEATi without Pt, with 1 mol%, 3 mol% and 5 mol% of Pt

The values for the samples with 1 and 3 mol% of platinum are smaller than the reference one, obtained without the addition of hexachloroplatinic acid. Only in the richer sample, the surface area is larger. It is also interesting to note the pore distribution for the four samples, as reported in the following image.

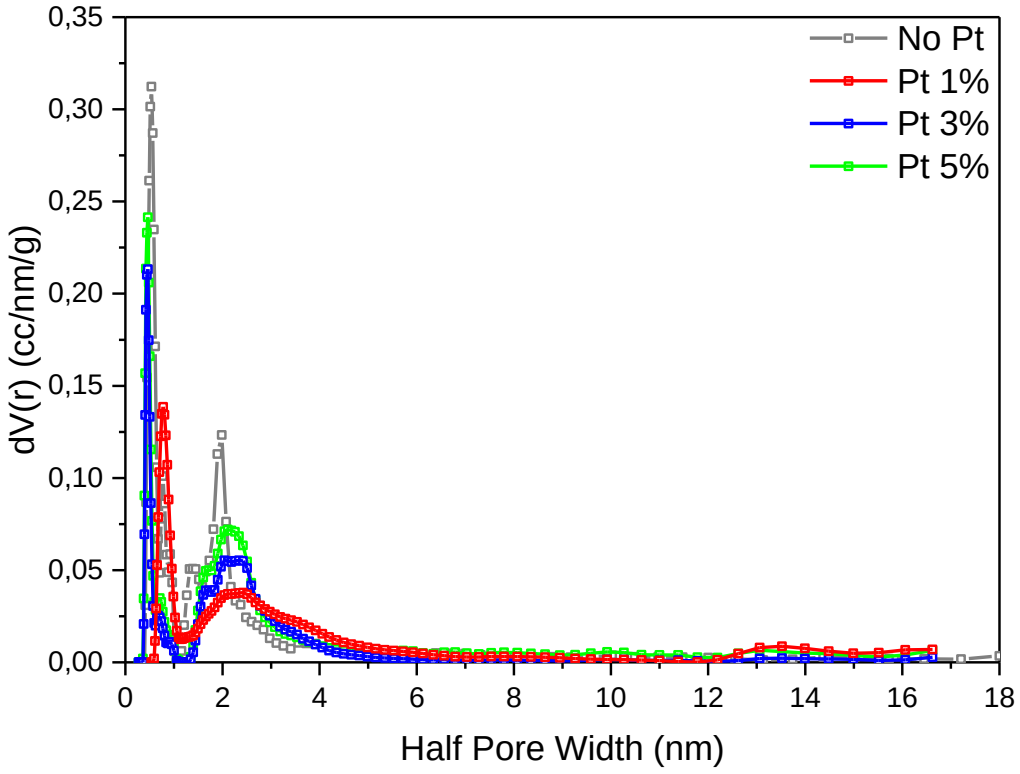

Figure 102, DFT analyses of MC+DEATi without Pt, with 1 mol%, 3 mol% and 5 mol% of platinum

The first peak for the non-decorated sample is always higher, meanwhile the other three increases with the platinum loading. The behavior of the second peak, around 2nm in radius, is more interesting. In this case there is a shift towards larger values and a broadening of the peak, meaning that the byproducts of the reduction of the platinum creates larger pores that helps to increase the surface area, only at heavier loading.

After testing the platinum we decided to try to synthetize a different type of nanoparticles that could act as catalysts in a direct ethanol fuel cell. In the DECORE project tungsten and molybdenum carbides are indicated as good substitutes to the more expensive platinum.

For our test we chose tungsten, because the synthesis of its carbides is similar to what we used for titanium. In order to add the tungsten carbide in the synthesis with MC and DEATi we tried to make a new complex using tungsten tetrachloride and triethanolamine (TEA), named TEAW. The synthesis of TEAW is pretty simple and very similar to DEATi but with small expedients due to the use of the halide.

In a closed flask purged with nitrogen a proper quantity of TEA and tungsten chloride are mixed, in proper quantity to reach a molar ratio of TEA:W equal to 4:1, letting the byproducts to develop. After the reaction is finished and a pale blue transparent solution is formed, heat is applied to evaporate all the byproducts. The solution retains its color and like the DEATi is stable for several days.

In the preparation of MC+DEATi with tungsten carbide nanoparticles, the TEAW is added to the water at the same time with the DEATi, and the solution is becoming bright blue. Then the MC is added normally and the carburization treatment is conducted as usual.

The treated MC+DEATi+TEAW powder looks very similar to the normal titanium oxycarbide powder. After grinding it in an agate mortar it is analyzed preliminary by XRD. The first sample had a 5 mol% of TEAW. Its pattern is reported below, in Figure 103.

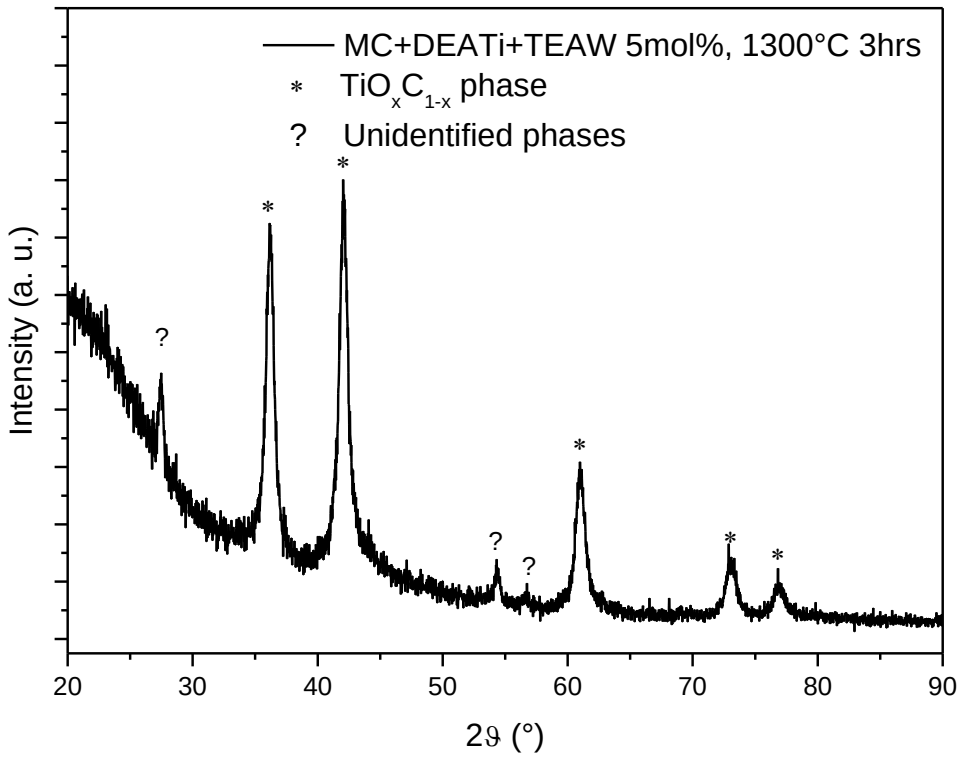

Figure 103, MC+DEATi with the addition of 5 mol% of TEAW, treated at 1300°C for 3 hours

Only eight peaks are recognizable. The five most intense are titanium oxycarbide phase, while the other three are unknown phases.

We made another sample in the same way, but the results were the same, as can be seen in Figure 104.

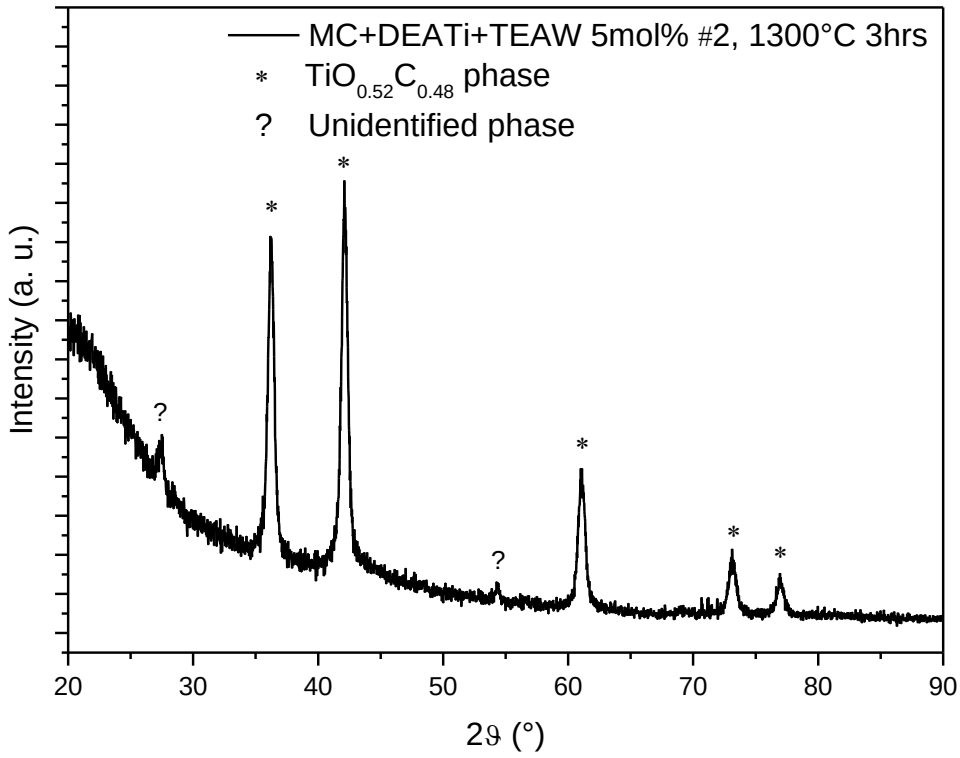

Figure 104, MC+DEATi with the addition of 5 mol% of TEAW #2, treated at 1300°C for 3 hours

Because peaks of the tungsten carbide were not visible, we tried to increase the molar quantity of tungsten carbide to 20%. The XRD from the treated sample is reported in Figure 105. A very small peak appears at ~40.30°, near the second peak for the titanium oxycarbide that strangely has a lower intensity than the first. This can be due to the presence of two different phases of the tungsten carbide: the first, with formula WC, has the strongest peak at 35.67°, very near to the first peak of $TiO_{0.52}C_{0.48}$; the second, with formula W_2C, has the strongest peak at 39.55°. The other peaks for both the phases are too weak to be detected.

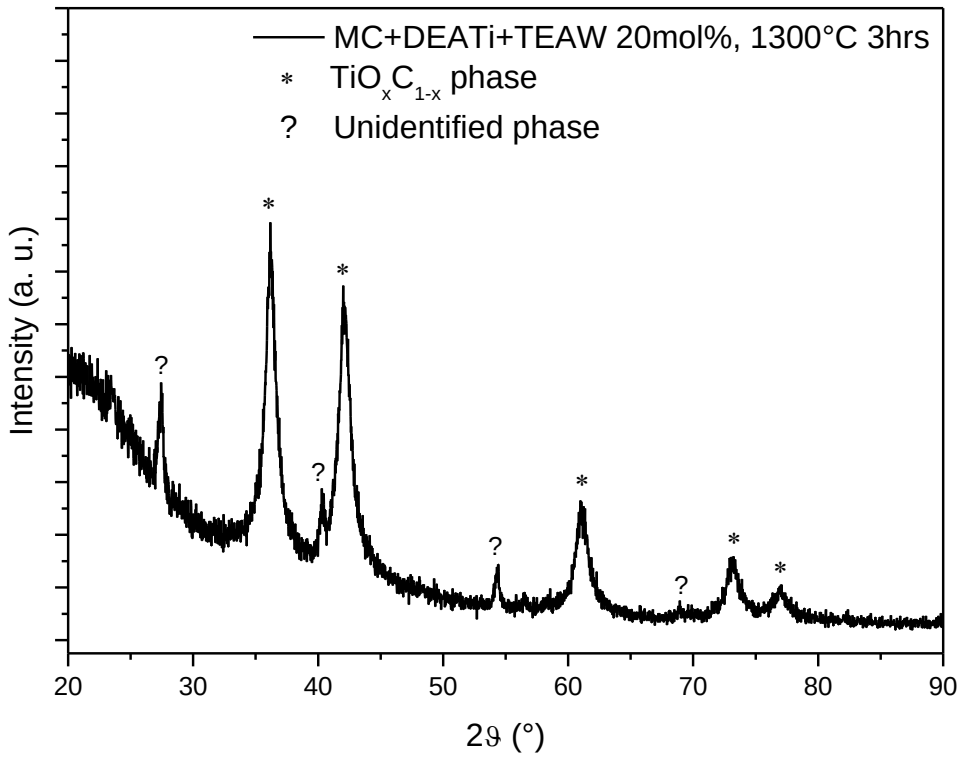

Figure 105, MC+DEATi with the addition of 20 mol% of TEAW, treated at 1300°C for 3 hours

We tried to treat the same sample at 1400°C, still for 3 hours. The results are even less satisfying, because none of the WC or W_2C peaks are visible, as can be seen in Figure 106, while the first peak of the titanium oxycarbide is still more intense than the second one. This can represent a hint of the presence of WC, but without other test and investigation it cannot be confirmed.

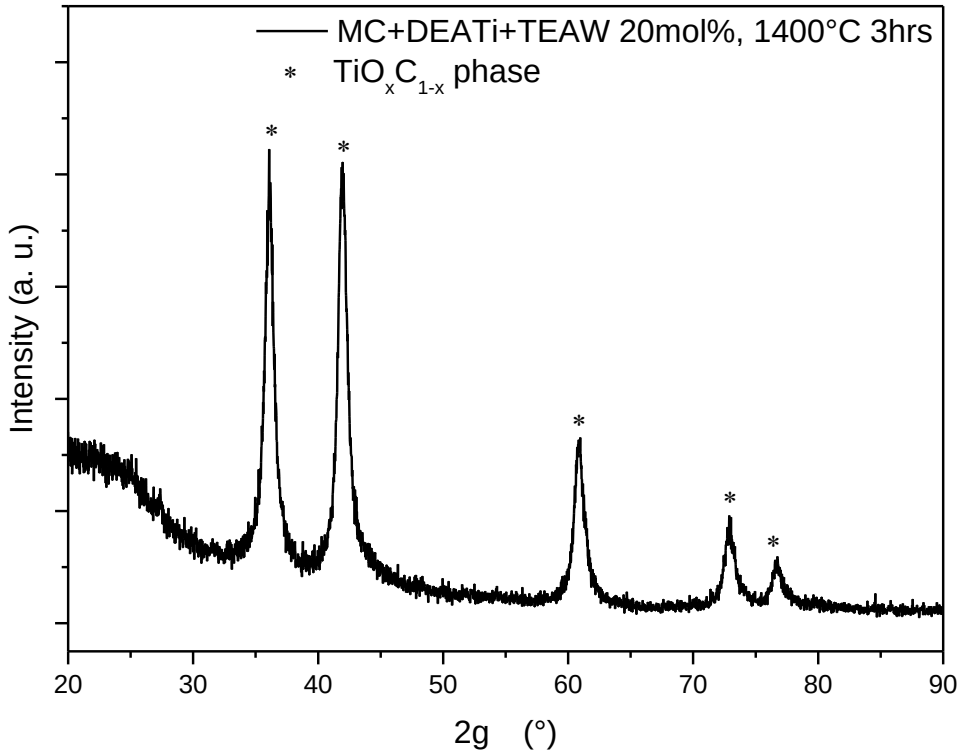

Figure 106, MC+DEATi with the addition of 20 mol% of TEAW, treated at 1400°C for 3 hours

The XRD patterns however do not show clear and intense peaks for the tungsten carbide, meaning that it is not crystalline or has made an alloy with the titanium oxycarbide. In either the cases, it is not suitable for electrochemical purposes.

These tested methods proved to have a major flaw that is represented by the intrinsic nature of the process: in fact, adding the hexachloroplatinic acid precursor or the TEAW before the carburization treatment, the nanoparticles don't grow all in the surface. The molar quantity of the platinum or tungsten carbide on the surface is then lower than the starting but, most important, the nanoparticles are coated with a very thin layer of carbon, as confirmed by an analysis with XPS conducted by the group of Prof. Julia Kunze in Innsbruck University. In this way, the nanoparticles don't react much in the electrochemical cell, because they behave like carbon, not as a catalyst.

As done with the TiOC from carbon black, we changed the path and adopted the polyol synthesis, concentrating our efforts on platinum and platinum-tin nanoparticles.

The first samples were made following the procedure used previously: for Pt and Pt_xSn nanoparticles, we mixed in a closed flask with nitrogen atmosphere the oxycarbide powder with the proper amount of precursors in a bath of ethylene glycol basified to a pH=13 with NaOH. Then, when the precursors are well mixed and dissolved, heat is applied up to 160°C and hold for 3 hours. Then the solution is let to dry naturally and when at room temperature it is washed and centrifuged three times with a HCl 1M solution in order to precipitate the powder. The final wash and centrifuge is conducted with acetone and then it is dried. For $Pt@SnO_2$ nanoparticles the reaction takes place in two different steps: the first involves only the tin precursor in non-basified EG. After 3 hours at 160°C NaOH and hexachloroplatinic acid are added in order to create the shell around the oxidic core. The reaction is conducted for 2 more hours, then it is stopped and let to dry naturally. The washing and centrifuge steps are the same.

The first sample was prepared with $TiO_{0.49}C_{0.51}$ made previously with MC+DEATi and Pt_3Sn. The molar content of nanoparticles is 5 mol%. Its XRD pattern is in Figure 107.

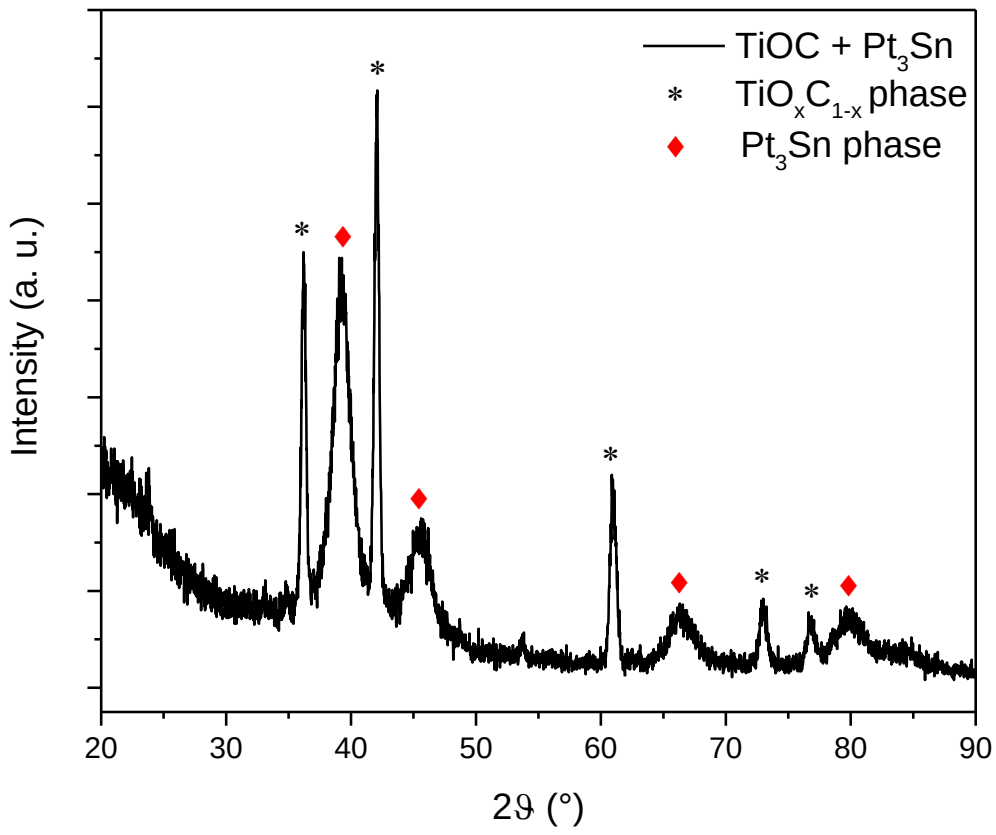

Figure 107, XRD pattern of TiOC from MC+DEATi decorated with Pt_3Sn NPs, made in ethylene glycol at 160°C for 3 hours

The peaks of the titanium oxycarbide and Pt_3Sn are visible. Analyzing the positions of the TiOC peaks we can say that the reaction of nucleation doesn't damage the stoichiometry of the support, because they are still in the same positions.

After this first test we prepared other samples in the same way, all with similar results, as can be seen in Figure 108 and Figure 109.

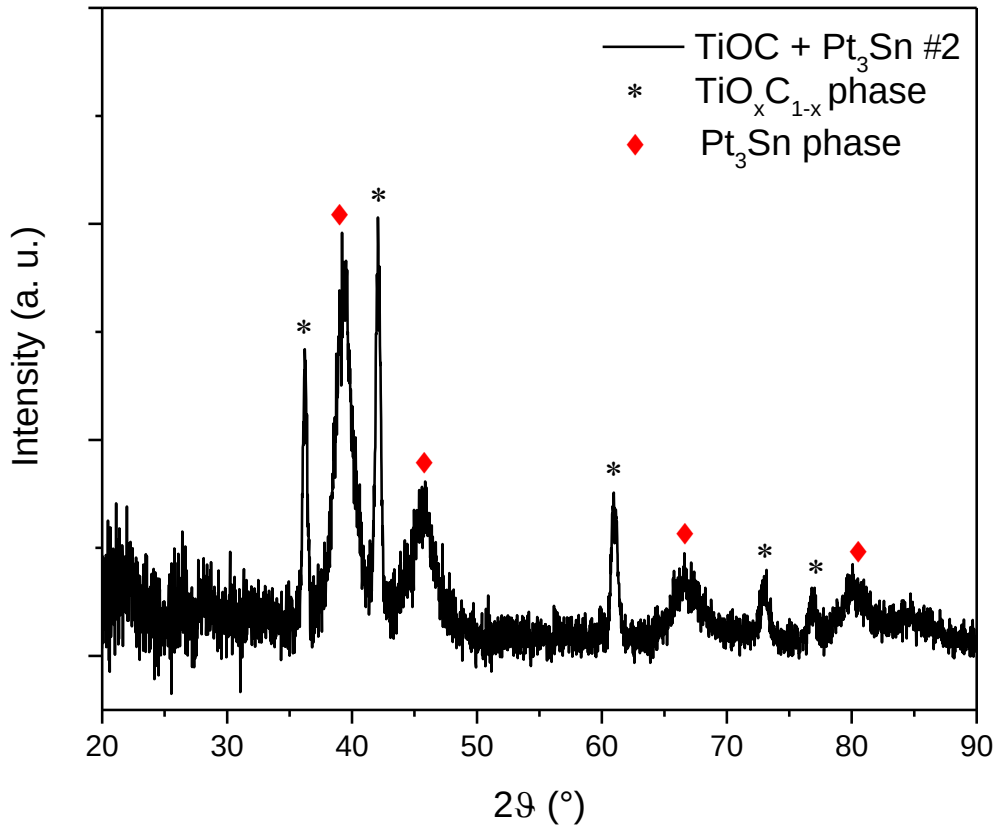

Figure 108, XRD pattern of TiOC from MC+DEATi decorated with Pt3Sn NPs, made in ethylene glycol at 160°C for 3 hours, #2

The XRD patterns are very similar, showing all the expected peaks. Also the heights of the peaks, that represent the quantity of each phase, are very similar among the three sample, determining that this is a good synthesis route to obtain reproducible samples.

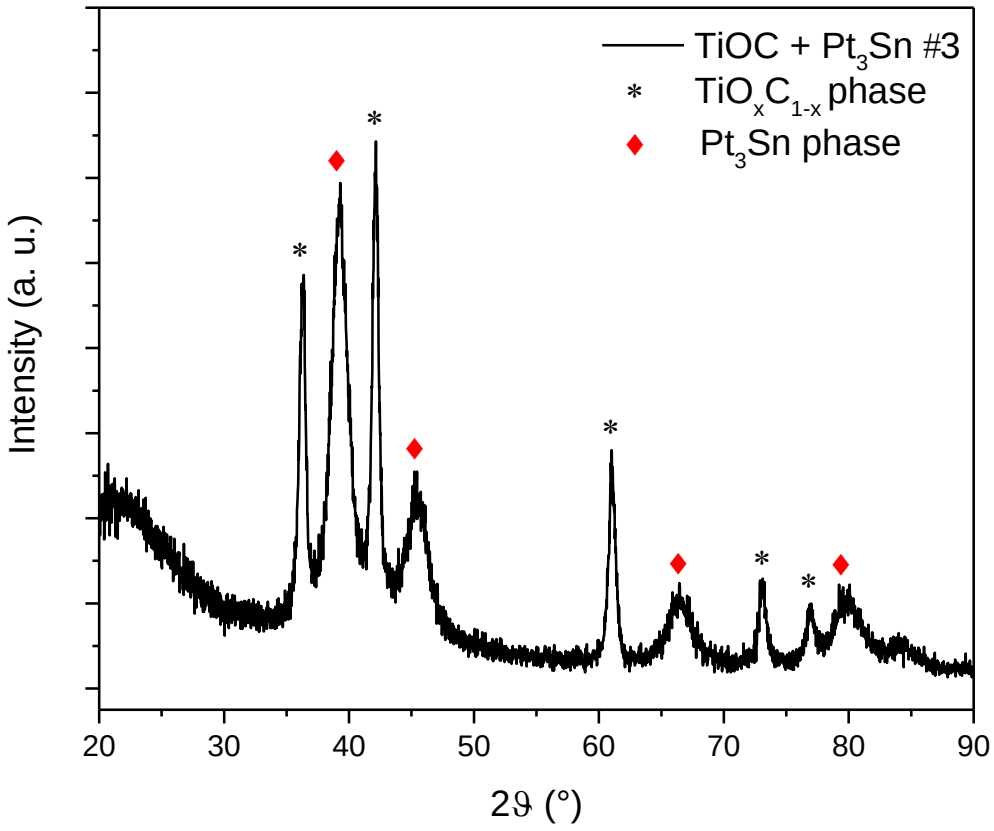

Figure 109, XRD pattern of TiOC from MC+DEATi decorated with Pt3Sn NPs, made in ethylene glycol at 160°C for 3 hours, #3

From this starting point we made also the Pt@SnO_2 nanoparticles, characterized by a core-shell structure made with the synthesis in two steps reassumed before. The used TiOC sample for this test is the same of the previous. Its XRD pattern is in Figure 110.

As can be clearly seen the pattern isn't very clean and clear, because the peaks of the core-shell nanoparticles are very strong and cover partially the other peaks. Moreover, there is also one peak at low angles, around ~22° that is presumably some form of tin oxide.

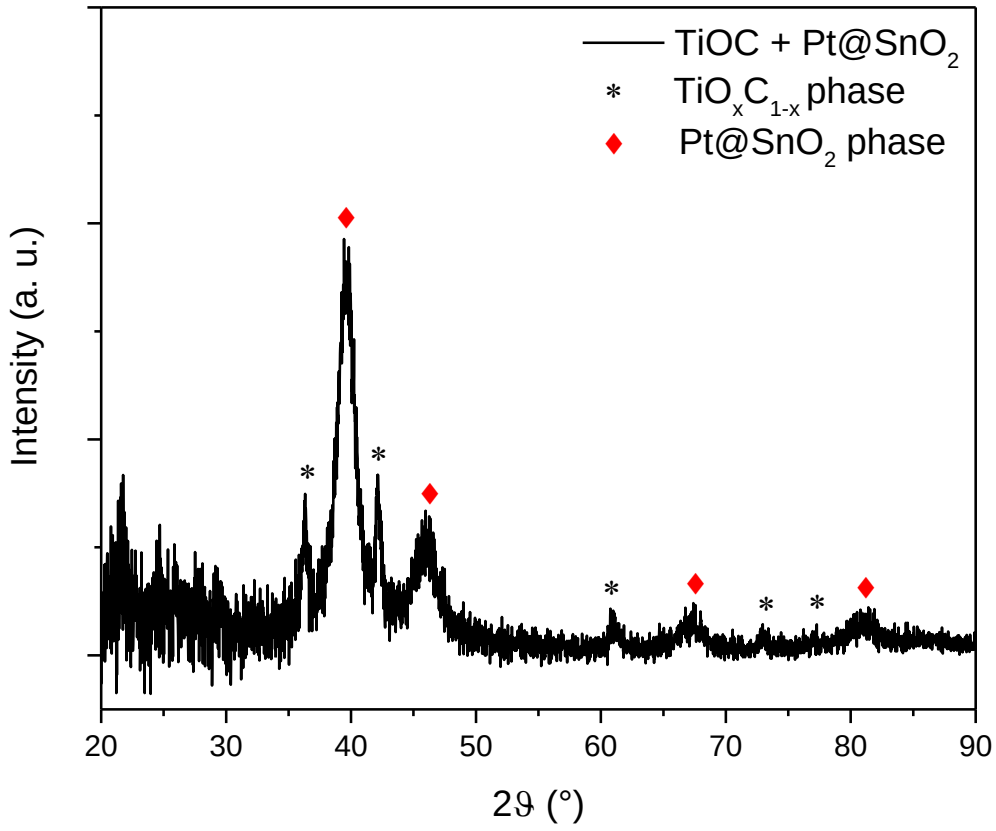

Figure 110, XRD pattern of TiOC from MC+DEATi decorated with Pt@SnO_2 NPs, made in ethylene glycol at 160°C for 3+2 hours

In collaboration with the University of Copenhagen we decided to increase the molar quantity of the nanoparticles to 20 weight%, that roughly correspond to 8 mol%. This change was deliberated in order to compare this sample with the commonly available carbon black/Pt catalysts.

The first sample with the higher loading was made with Pt_3Sn nanoparticles. Its XRD pattern is reported below, in Figure 111.

As can be seen the peaks of the NPs now are much higher and more intense than that of the titanium oxycarbide.

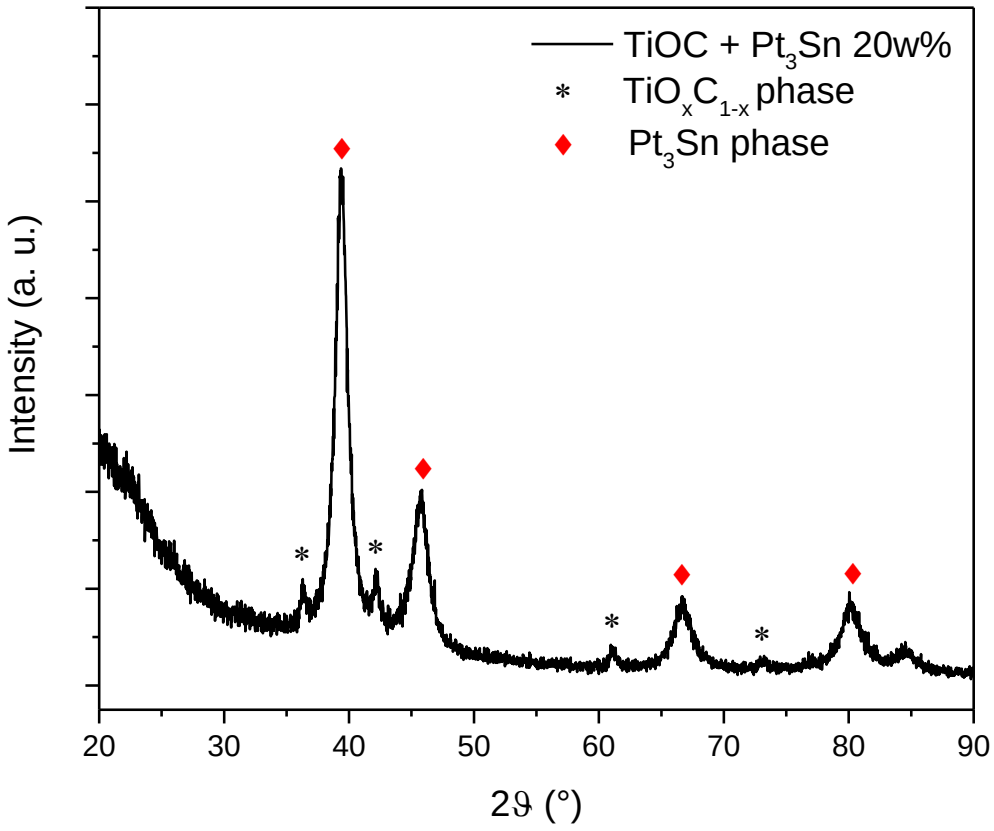

Figure 111, XRD pattern of TiOC from MC+DEATi decorated with 20 wt% of Pt3Sn NPs, made in ethylene glycol at 160°C for 3 hours

We prepared also a sample decorated with Pt@SnO_2 NPs, with the same loading of 20weigh%. The results are very similar, as can be seen in Figure 112.

The results are very similar, both as intensities both as peak positions. This can be due to the complete reaction of the platinum with the tin oxide core or a too thick platinum shell. Anyhow the nanoparticles act like platinum-tin alloy, making this core-shell reaction too long in order to obtain the same results.

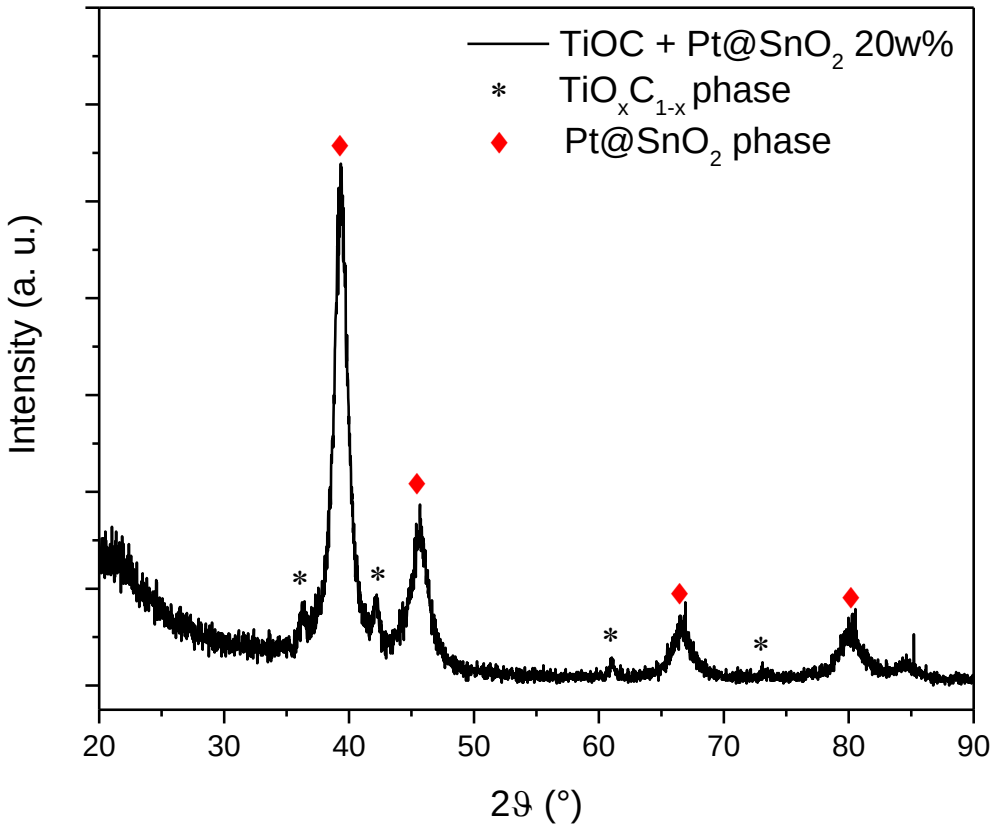

Figure 112, XRD pattern of TiOC from MC+DEATi decorated with 20 wt% of Pt@SnO2 NPs, made in ethylene glycol at 160°C for 3+2 hours

In Copenhagen we tried to accelerate further the reaction using a microwave (MW) reactor, a CEM Discover SP. The synthesis is a modification of one found in literature [63], where we substituted the carbon black with the titanium oxycarbide. The reaction parameters were set according to the previous synthesis, reaching a top temperature of 160°C as fast as possible in nitrogen atmosphere. The maximum temperature was hold with a forced air cooling in order to apply as much power as possible to the solution. After 3 minutes the microwaves are shut down and the vial cooled down. The solution with the precursors were mixed with a stirring bar during all the treatment, to avoid the sedimentation of the powder.

The MW route is faster but also more precise, because all the parameters used during the reaction are controlled by the reactor itself in a more accurate way. This leads to more reproducible samples that are made in a fraction of time: for the complete synthesis, from room temperature to room temperature, it needs only 10 minutes, while with the normal polyol route takes 3 hours only at the highest temperature.

In order to investigate the electrochemical properties of the Pt_xSn nanoparticles supported by the titanium oxycarbide we decided to vary the stoichiometry of the NPs, spacing from Pt_2Sn to Pt_4Sn, leaving obviously Pt_3Sn in the middle.

The XRD analyses of the samples with Pt_2Sn and Pt_4Sn were conducted in Padua, after the electrochemical tests. In the following pictures, Figure 113, Figure 114 and Figure 115, are visible the XRD patterns for the three samples.

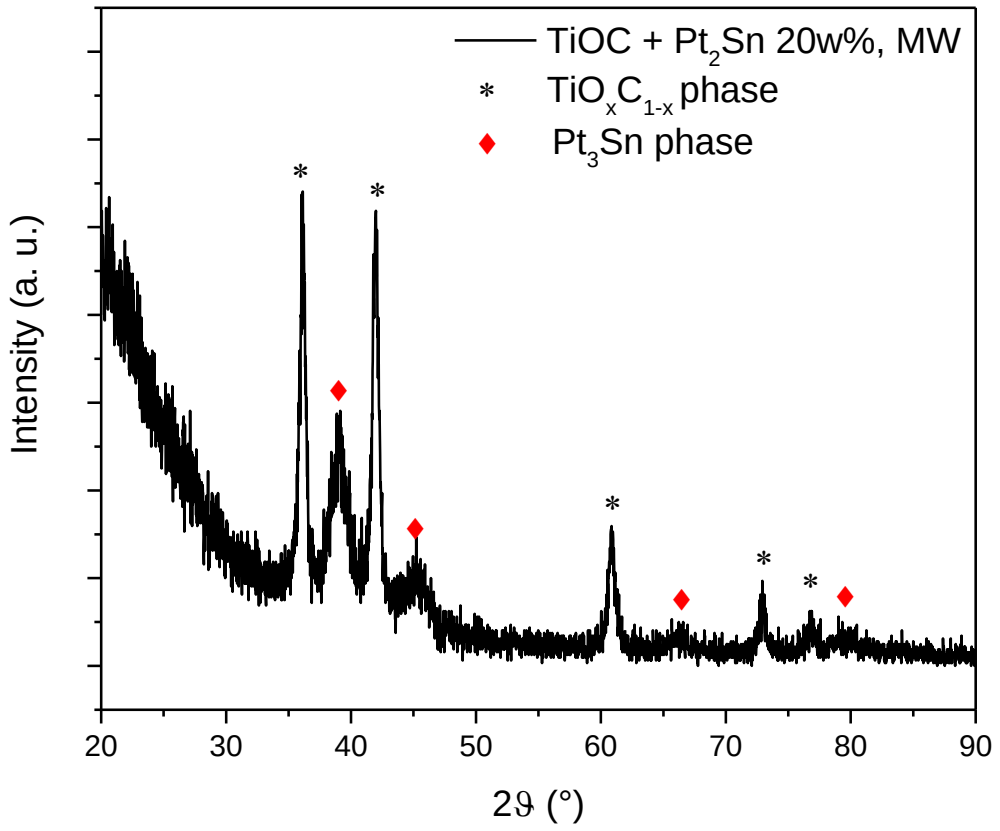

Figure 113, XRD pattern of TiOC from MC+DEATi decorated with 20 wt% of Pt_2Sn NPs, made with MW reactor

The change in intensity of the Pt_xSn peaks for the x=2 and x=4 samples are due to the electrochemical tests that was been done before the XRD analyses.

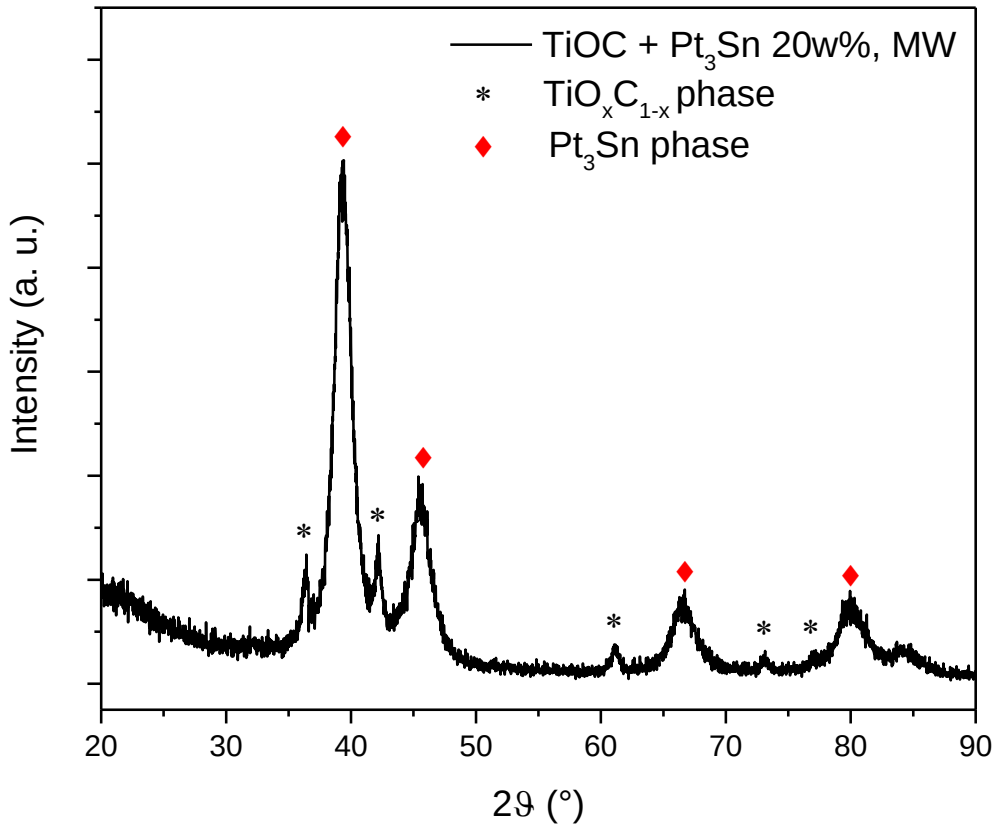

Figure 114, XRD pattern of TiOC from MC+DEATi decorated with 20 wt% of Pt_3Sn NPs, made with MW reactor

The sample above, with Pt_3Sn was analyzed before the tests, so the titanium oxycarbide and the NPs aren't affected by the harsh conditions encountered in the anodic semi-cell.

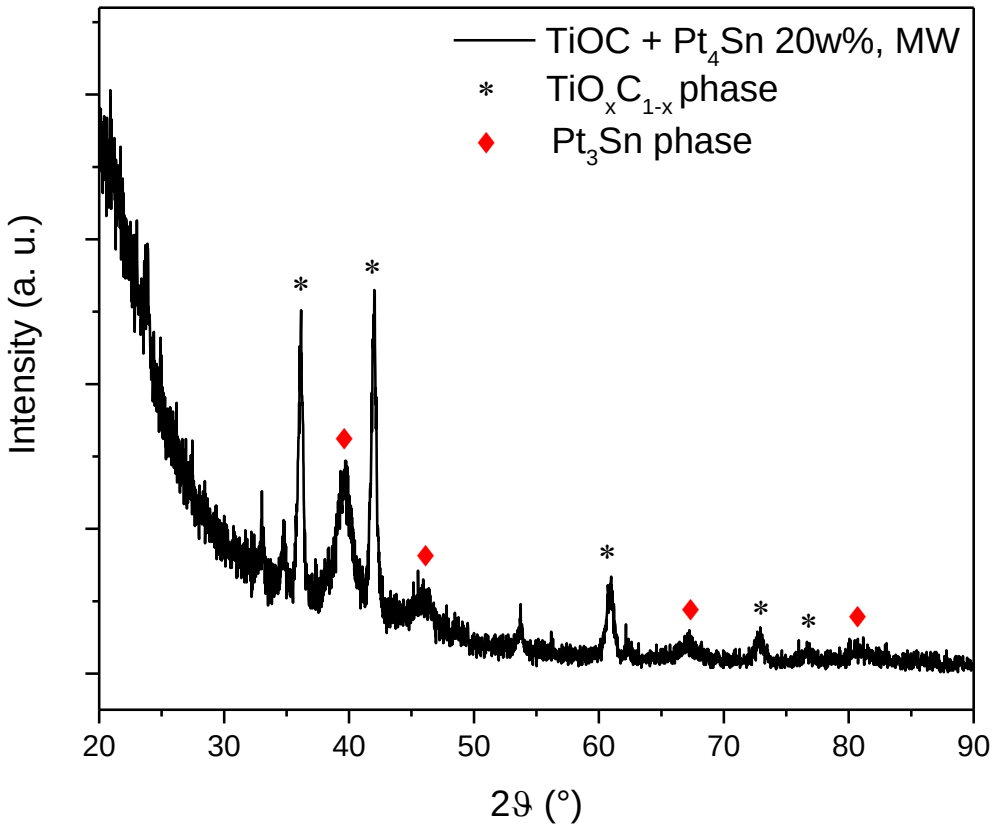

Figure 115, XRD pattern of TiOC from MC+DEATi decorated with 20 wt% of Pt_4Sn NPs, made with MW reactor

In the next image, Figure 116, all the three XRD patterns are compared, adding also the titanium oxycarbide used as substrate.

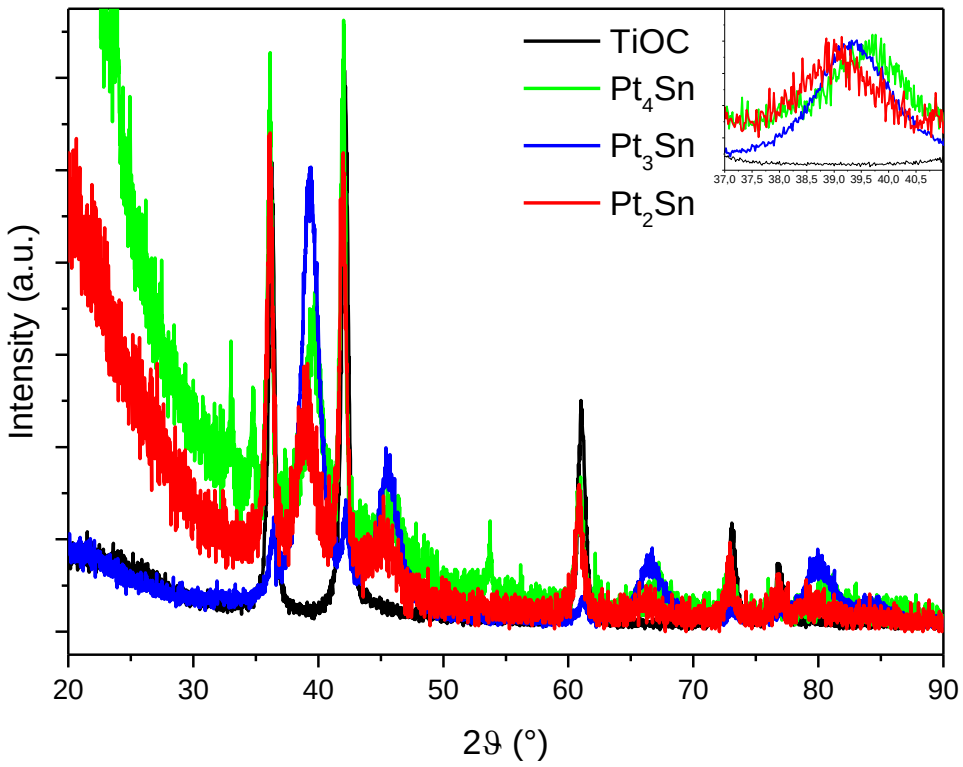

Figure 116, comparison of the XRD patterns of TiOC from MC+DEATi decorated with 20 wt% of Pt_4Sn, Pt_3Sn and Pt_2Sn NPs, made with MW reactor and using TiOC as substrate

In the offset on the top right corner, there are highlighted the first Pt peaks of the samples. It can be stated that the peaks for the different NPs shifts according to the stoichiometry, confirming the different compositions among the three samples.

We made also other three samples in a different way, because the nanoparticles were created alone in the MW heated ethylene glycol and then added to the titanium oxycarbide. The washed and centrifuged NPs were suspended in an ethanol/water 1:1 by volume solution and then the titanium oxycarbide was added in the same solution. The new suspension is put in an ultrasonic bath for 30 minutes and then used in the anodic semi-cell. Unluckily, as will be seen beyond, the adhesion of the nanoparticles on the surface of the TiOC was not so strong and after repeated cycles of cyclovoltammetry the NPs separated and XRD analyses weren't possible.

However the microwave assisted synthesis proved to be a very clever and smart way to create Pt_xSn nanoparticles with controlled stoichiometry on the surface of titanium oxycarbide. In this way, a good anodic compound is created and can be electrochemically tested properly.

3.3. Electrochemistry

The electrochemical tests that were conducted with the supervision of Prof. Mathias Arentz in Copenhagen. The principal aim of these tests was to determine the durability of the titanium oxycarbide on the working conditions of a direct ethanol fuel cell. They are pretty harsh, because the electrolyte used is concentrated phosphoric acid at 150°C. Carbon cannot resist in this environment, so TiO_xC_{1-x} phases was seen as suitable. We investigated the best stoichiometry for Pt_xSn nanoparticles for the ethanol oxidation, without using Pt NPs because they have worst performances [59, 61, 64, 68, 69], suffering also from CO poisoning [61]. We performed cyclovoltammetries in order to investigate the behavior of the support during several cycles. As reference we used a reference hydrogen electrode (RHE), while for counter-electrode we chose a platinum mesh. Firstly, argon was set to pass through a bubbler with ethanol or ethanol/water 1:1 by volume solution and then to bubble in concentrated phosphoric acid to degas the solution for 1 hour and the setup was brought to 150°C. After half an hour at 150°C, the electrodes were inserted in the solution and the tests were started. To switch between ethanol and ethanol/water solution the electrodes are removed and the phosphoric acid is maintained at 150°C with pure argon bubbling for 1 hour to remove all the traces of the previous reagent. Then, the argon is redirected to the chosen bubbler of ethanol or ethanol/water and then blown inside the electrolyte. After half an hour the electrodes are inserted again and the new measure is started.

In Figure 117 the various compositions and paths are compared. The second row of images refers to the samples decorated with Pt_xSn NPs made previously in the MW heated ethylene glycol, while in the first row the results from the NPs growth directly on the surface of TiO_xC_{1-x}.

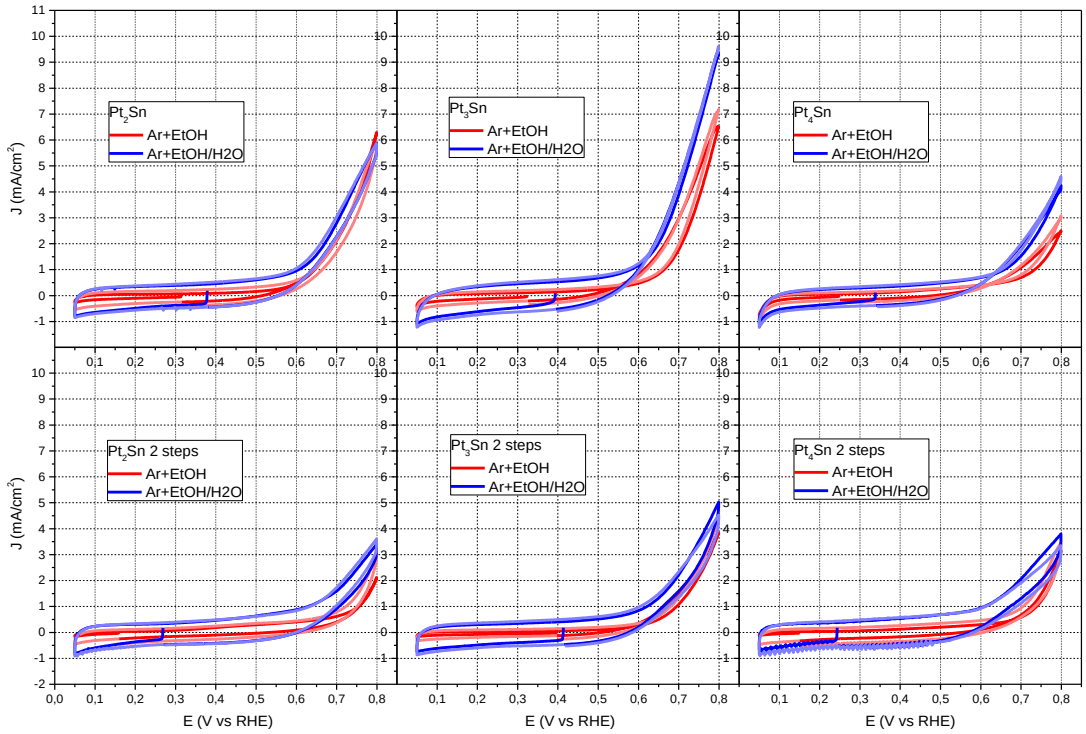

Figure 117, RDE cyclovoltammetries for Pt_2Sn, Pt_3Sn and Pt_4Sn growth (first row) and deposited (second row) on TiOC surface, tested in concentrated phosphoric acid at 150°C with bubbling argon

The sweep rate was set to 10 mV/sec between 0.05 V and 0.8 V (both vs RHE). For every sample we tested the oxidation firstly of pure ethanol and in a second time of ethanol/water. This explain the thicker section of the plateau for every sample, because they weren't completely fresh but underwent to cycles before, degrading slightly the sample.

It is easy to see that Pt_3Sn NPs have the best performances compared to Pt_2Sn and Pt_4Sn, while the 2 steps preparation, that involves the synthesis of the NPs alone and the deposition of them on the TiOC in a second time, has worst results. The Pt_3Sn NPs growth directly on the surface of TiO_xC_{1-x} shows the best results, with a top current density of 9.60 mA/cm^2. The oxidation of ethanol for every sample is aided by the presence of water in the solution, as expected, and it starts at ~0.6 V (vs RHE). This value seems to be independent from the composition of the Pt alloy.

4. MAX phases

4.1. Introduction

The MAX phases are a wide class of ternary carbides and nitrides with unique properties. The name "MAX" comes from their general formula $M_{n+1}AX_n$, where n = 1–3, M is an early transition metal, A is an A-group element (mostly IIIA and IVA), and X is C and/or N [77-79]. All the MAX phases share a common hexagonal structure. The unit cell consists of M_6X octahedra interleaved with A layers. The difference between the three structures is the number of M layers separating the A layers, as drawn in Figure 118 [80].These phases are layered hexagonal compound, classified according to the value of n: 211 for M_2AX, 312 for M_3AX_2 and 413 for M_4AX_3. They have extraordinary properties due to their layered structure, with $M_{n+1}X_n$ slabs intercalated with pure A-element layers that lend to this ceramic class characteristic from metals and pure ceramics. They conduct heat and electricity [81], are machinable [82] and resist thermal shocks and mechanical damages like metals, but at the same time, they are strong, brittle, heat-tolerant and resist in oxidative and corrosive atmosphere like ceramics. With a wide selection of elements for the M and A layer, 60 different combinations are known that are summarized in Figure 119 [83].

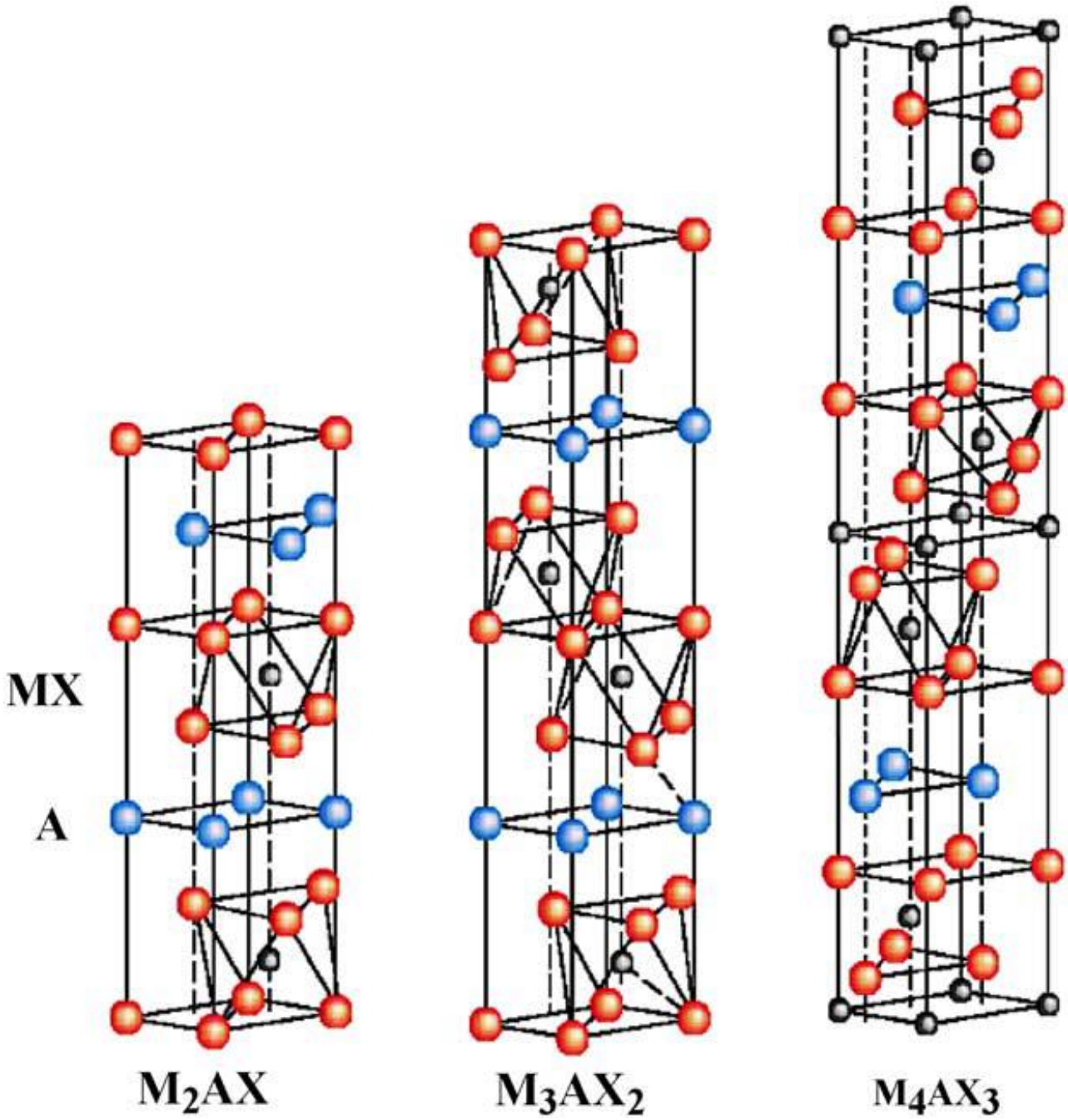

Figure 118, hexagonal crystal structures for the MAX phases

M element	A-group element				
	s^2 (group 12)	$s^2 p^1$ (group 13)	$s^2 p^2$ (group 14)	$s^2 p^3$ (group 15)	$s^2 p^4$ (group 16)
211 Phases					
3*d*	Ti_2CdC	Sc_2InC Ti_2AlC Ti_2GaC Ti_2InC Ti_2TlC V_2AlC V_2GaC Cr_2GaC Ti_2AlN Ti_2GaN Ti_2InN V_2GaN Cr_2GaN	Ti_2GeC Ti_2SnC Ti_2PbC V_2GeC Cr_2AlC Cr_2GeC	V_2PC V_2AsC	Ti_2SC
4*d*		Zr_2InC Zr_2TlC Nb_2AlC Nb_2GaC Nb_2InC Mo_2GaC Zr_2InN Zr_2TlN	Zr_2SnC Zr_2PbC Nb_2SnC	Nb_2PC Nb_2AsC	Zr_2SC Nb_2SC
5*d*		Hf_2InC Hf_2TlC Ta_2AlC Ta_2GaC	Hf_2SnC Hf_2PbC Hf_2SnN		Hf_2SC
312 Phases					
3*d*		Ti_3AlC_2 V_3AlC_2	Ti_3SiC_2 Ti_3GeC_2 Ti_3SnC_2		
5*d*		Ta_3AlC_2			
413 Phases					
3*d*		Ti_4AlN_3 V_4AlC_3 Ti_4GaC_3	Ti_4SiC_3 Ti_4GeC_3		
4*d*		Nb_4AlC_3			
5*d*		Ta_4AlC_3			

Figure 119, the 60 known MAX phases

For our purposes the MAX phases represent very good candidates, because they, as said before, have a good electrical conductivity and can resist in acidic atmosphere, as could do an anodic support that would work in concentrated phosphoric acid at 150°C carrying out the electrons produced by the oxidation of ethanol on the surface of the catalysts.

We concentrated our efforts on three different phases, that are nowadays the most studied and known: Ti_3SiC_2, Ti_2AlC and Ti_3AlC_2. The first two are also commercially available, under the commercial name of Maxthal [84].

Usually the MAX phases are made with solid-state reaction synthesis, by mixing fine powders of raw elements and treating then at high temperatures [85, 86], with the optional aid of high pressure [87-89], to create an ordered structure. Other techniques are available, consisting in pulse discharge sintering [90-92], thin-film growth [80, 93, 94], magnetron sputtering [80] and others [95-101].

The simplest way for us was the solid-state reaction synthesis because it does not require specific equipment that are not present in our laboratories.

4.2. Ti_3SiC_2

Before starting with the raw materials, we tried to obtain Ti_3SiC_2 through modifications of the MC+DEATi route. Methylcellulose can be used as a good carbon precursor, leaving after the heat treatment 10 weight % of carbon. It is water-soluble and this allows us to use soluble precursors achieving perfect mixing. Obviously, the problems arise for the solubility of metallic precursors. For titanium we realized a very good amine-complex, DEATi, that is perfectly soluble and stable for weeks. As precursor of silicon we used a variation of DEATi, called DEASi because it involves diethanolammine and tetraethoxysilane (TEOS). The synthesis of DEASi is pretty simple: proper quantity of DEA is put in a closed flask purged with nitrogen and stirred with a magnetic bar. TEOS is added slowly in a molar ratio of 1:4 respect the DEA and stirred for 3 hours. The viscous solution is then heated at 100°C for 1 hour to eliminate all the byproducts of the reaction.

The new synthesis will involve MC and DEATiSi, changing the stoichiometric ratios between the species in order to eliminate all the oxygen present. To obtain Ti_3SiC_2 the reaction with TiO_2 and SiO_2 will be the following:

$$3TiO_2 + 1SiO_2 + 10C \rightarrow Ti_3SiC_2 + 8CO_2$$

Adjusting the quantities for DEATi, DEASi and MC, considering for the last the remaining carbon residue and the molar weight, the reaction should follow the path below:

$$3DEATi + 1DEASi + 15MC \rightarrow Ti_3SiC_2 + 8CO_2 + other\ byproducts$$

The other byproducts are mainly due to the degradation of DEA and MC, consisting in alcohols and nitrogen and carbon oxides.

With these considerations we tried to make DEATiSi, combining the synthesis of DEATi and of DEASi. In a usual synthesis, 9,58mL of DEA is put in closed flask purged with nitrogen. Then 5,92mL of titanium isopropoxide and 1,09mL of TEOS are added slowly and stirred for 3 hours. A transparent and pale yellow solution is obtained. It is heated for 1 hour at 100°C in order to evaporate all the byproducts and then it is ready for the use. It is completely soluble in water, leaving no precipitates.

After the preparation, DEATiSi is diluted to 4 times the initial volume with doubly distilled water and heated to 60°C in order to add methylcellulose under heavy stirring. When an even suspension is made, it is made to cool down still applying stirring in order to obtain a highly viscous fluid with a pale yellow color and a translucent appearance. It is then dried at 50°C for 48 hours to obtain a polymer with a yellow soft, non-sticky plastic appearance that can easily be ground to a finer powder with the aid of a mechanical grinder, in a similar way as used for MC+DEATi.

The first sample was treated with the same parameters of MC+DEATi, i.e. a heating ramp of 10°C/min, a top temperature of 1300°C hold for 3 hours and then the oven is let to cool down naturally. The samples after the heat treatment had a dark grey color. The XRD pattern is shown in Figure 120.

There are 6 recognizable peaks: the first is very broad and centered around 21° and it is related to amorphous silicon dioxide; the others are from TiO_xC_{1-x} phase with a stoichiometry close to pure TiC. The results are far from the expected, because there were not peaks from the expected phase, Ti_3SiC_2.

The amorphous silicon dioxide did not react with TiO_xC_{1-x} and in the solid solution, there is still a lot of oxygen that prevents the formation of the layered structure. This can be due to the low temperature and short time of treatment.

For the next experiment, we changed only the duration of the heat treatment, leaving the temperature the same, 1300°C.

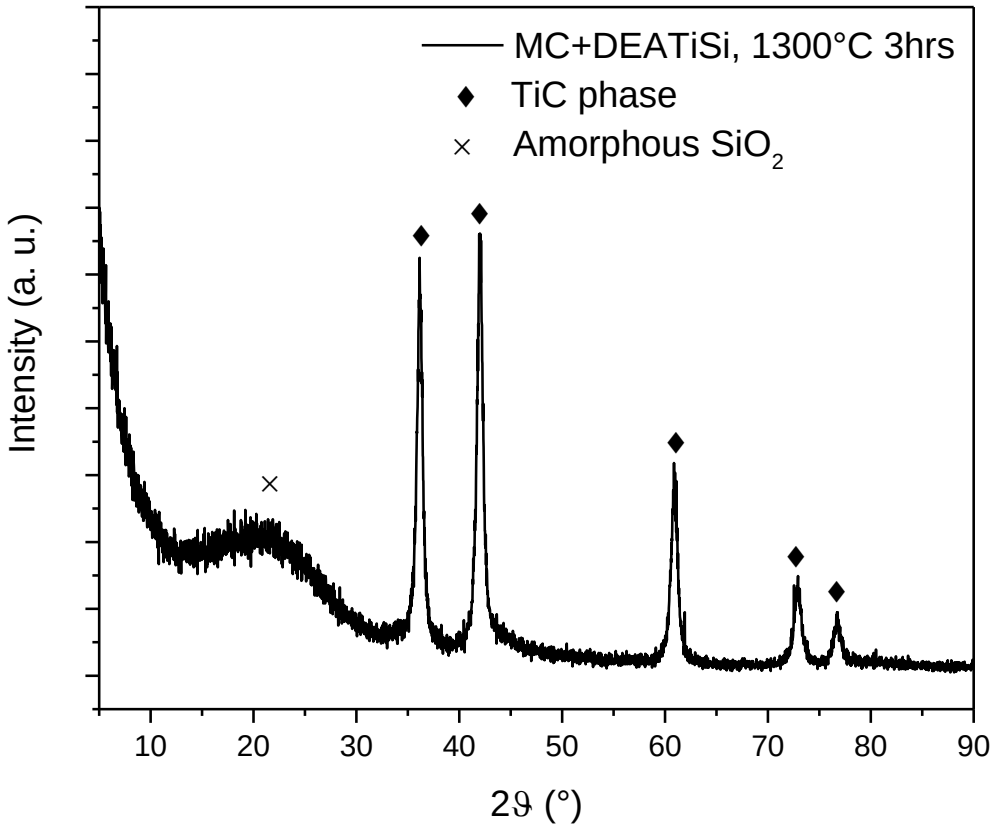

Figure 120, XRD pattern of MC+DEATiSi, treated at 1300°C for 3 hours

The results in this case are very similar to the previous sample, as can be seen in the following XRD pattern, in Figure 121.

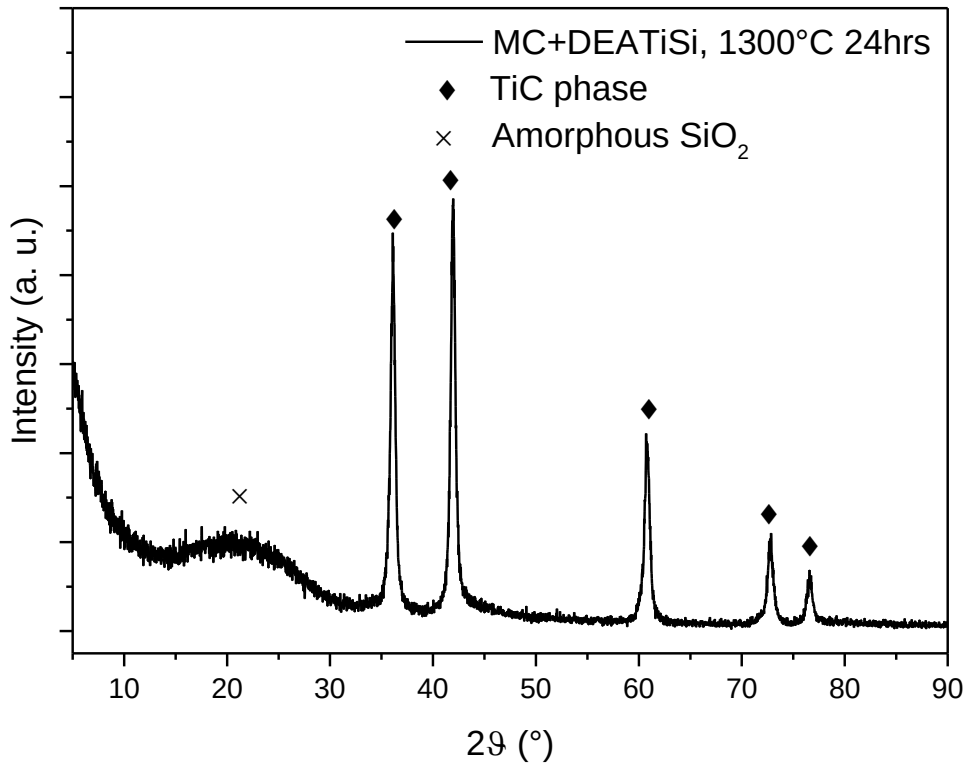

Figure 121, XRD pattern of MC+DEATiSi, treated at 1300°C for 24 hours

There are present the same peaks of the amorphous silica and titanium oxycarbide, because the diffusion coefficients are not high enough to allow the perfect mixture of the different phases. This means that the temperature is too low for a reaction between the two species and the complete depletion of oxygen. We tried to investigate if higher temperatures could resolve the problem, rising the heat treatment temperature up to 1500°C for 3 hours. We decided to abstain from prolonging the time of treatment in order to preserve the oven, which in this condition works at the maximum specifications. In Figure 122 there is reported the XRD pattern obtained from this sample. As can be seen, it is not very different from the previous one, with the broad peak of amorphous silica at ~21° and the five peaks of TiO_xC_{1-x}. Probably also at 1500°C the temperature does not increase in a considerable manner the values of the diffusion coefficients, not allowing the depletion of oxygen while reducing the metals with carbon.

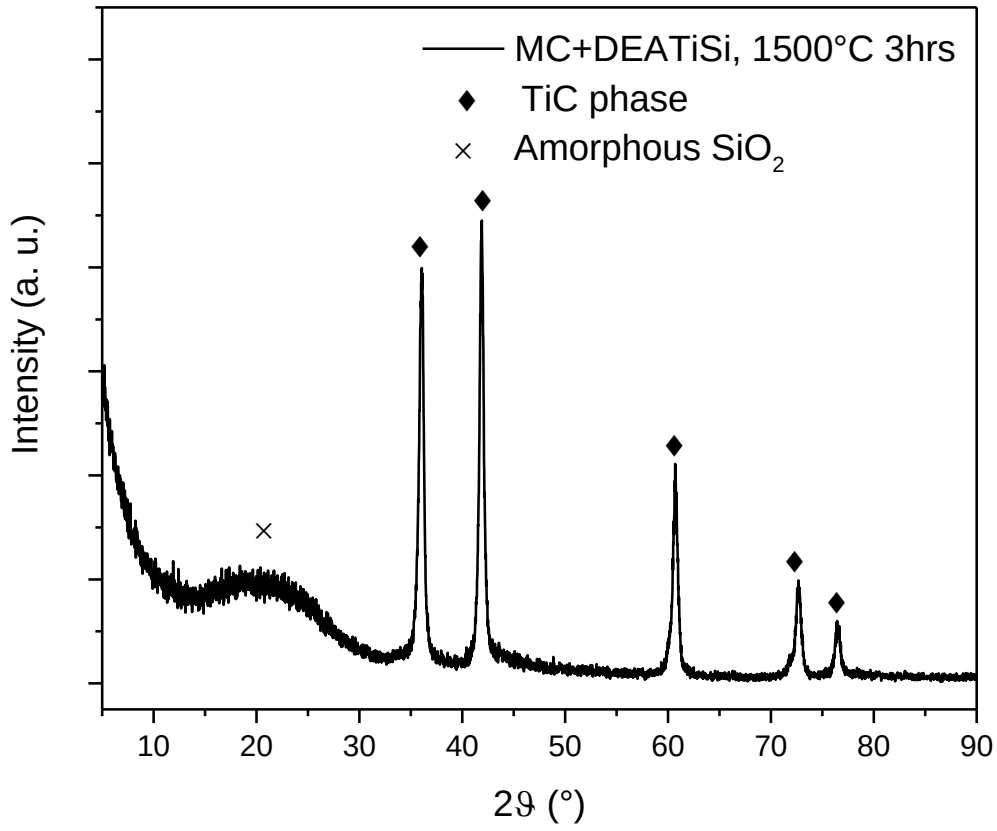

Figure 122, XRD pattern of MC+DEATiSi, treated at 1500°C for 3 hours

In Figure 122, the three XRD patterns are compared. The peaks are in the same positions, confirming that the tried combinations of time and temperature are not the right ones to allow a carburization of the silica and titania. Probably to achieve the reaction of the two phases longer times at the higher temperature are required, but with our setup, this was not possible.

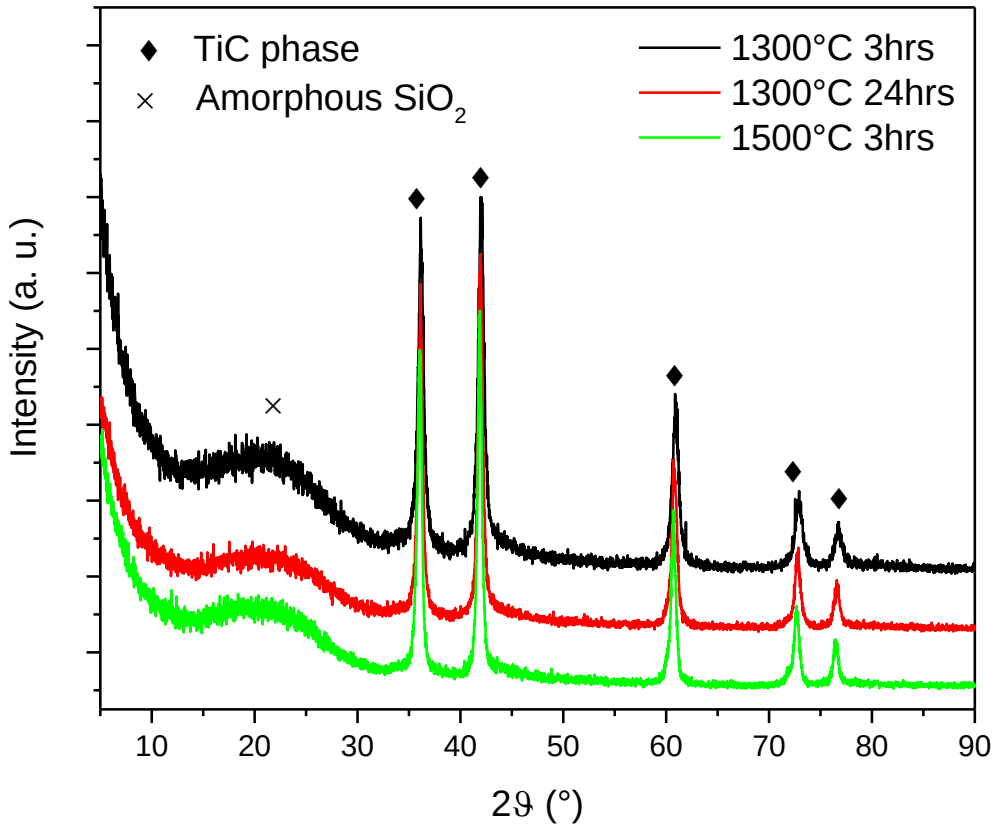

Figure 123, XRD patterns comparison of MC+DEATiSi treated at 1300°C for 3 hours, 1300°C for 24 hours and 1500°C for 3 hours

In all the three samples there is always amorphous silica that did not reacted with titania and carbon. We investigated if MC+DEASi, treated at 1300°C for 6 hours, can provide at least traces of silicon carbide or it is thermodynamically impeded. We prepared a sample with MC and DEASi in a ratio of 4,5:1 to have theoretically silicon carbide. The XRD pattern taken after the heat treatment is reported in Figure 124.

There are small peaks at 36°, 60° and 72° that are the three most intense peaks of the silicon carbide. There is also a peak at 22°, due to a polymorphic phase of silicon dioxide, cristobalite, which arises from the big and broad peak of the amorphous silica. That means the DEASi can form silicon carbide with this combination of temperature and time, albeit in small traces.

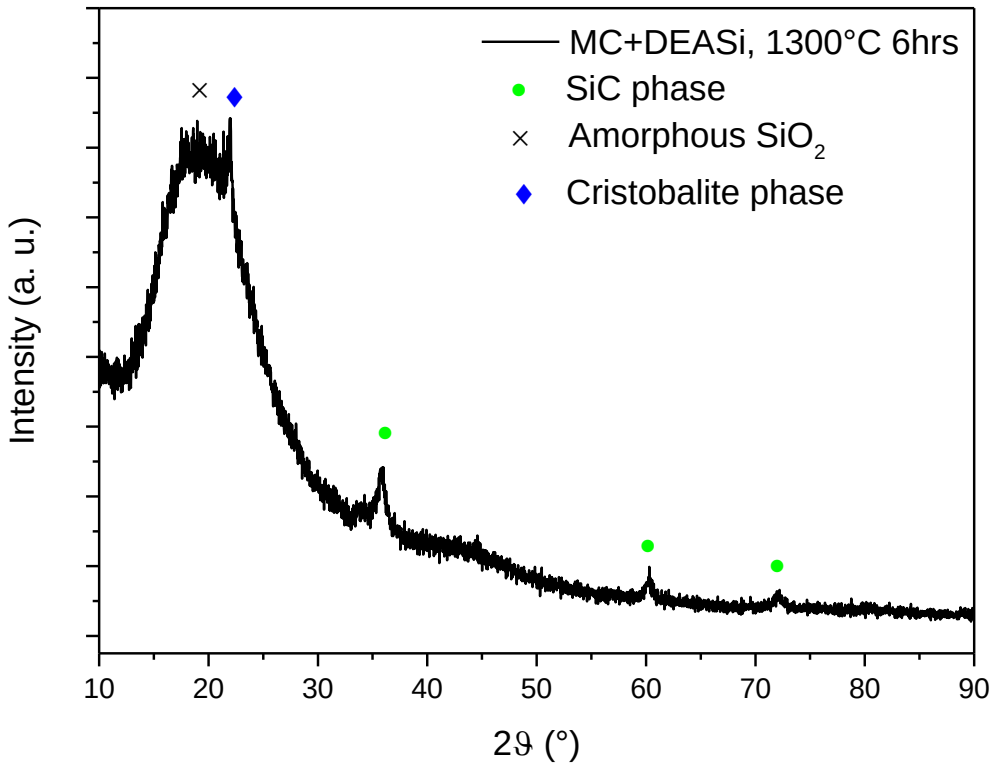

Figure 124, MC+DEASi 4,5:1, treated at 1300°C for 6 hours

With these considerations in mind, we tried to circumnavigate the limitations creating a more reducing environment. Two ways are possible: the first is to increase the quantity of carbon, changing the ratio between MC and DEATiSi; the second is to flow a reactive gas during the heat treatment.

Covering the first way, the decided to change the molar quantities of each component as follow:

$$3DEATi + 1DEASi + 20MC \rightarrow Ti_3SiC_2 + 8CO_2 + 1{,}3C + other\ byproducts$$

Obviously, an excess of unreacted carbon will be present at the end of the reaction, but it can be removed easily at low temperatures in a second moment. The new sample made with the excess of carbon was treated at 1300°C for 6 hours. In Figure 125 the XRD pattern is reported.

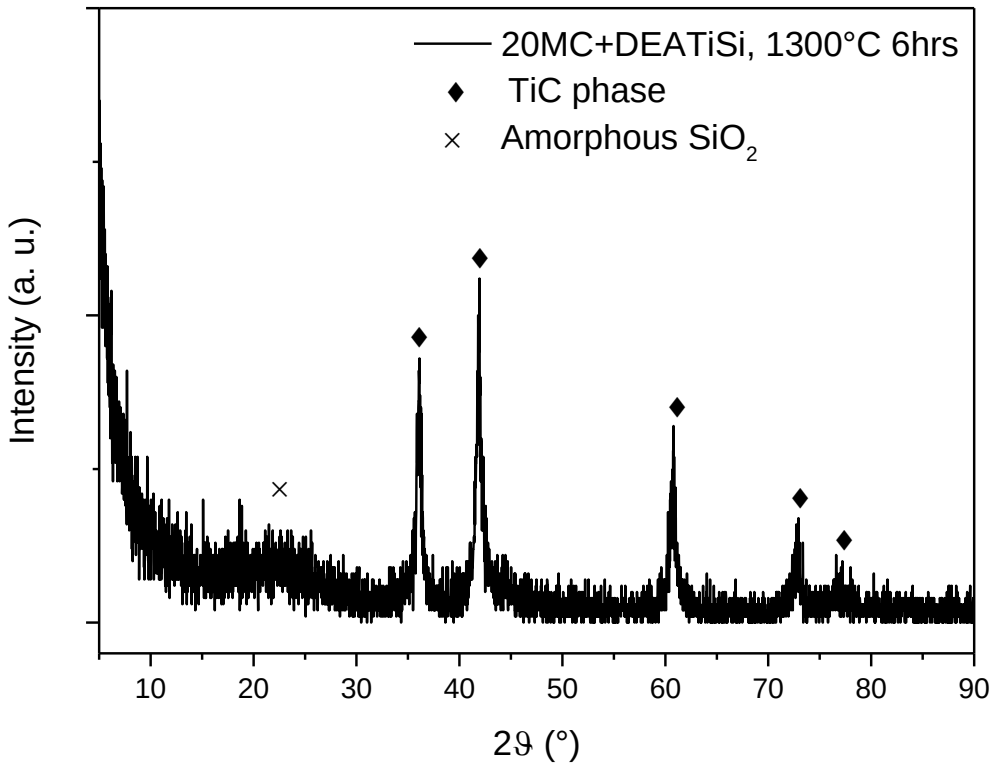

Figure 125, XRD pattern of MC+DEATiSi with an excess of MC, treated at 1300°C for 6 hours

The results are not different from the previous test, because, albeit a slight excess of carbon that promotes the reduction of titania and silica, the temperature and time are still too low and short to start the carburization and probably the quantity of silicon carbide is too low to interact with titanium carbide and to form significant quantities of Ti_3SiC_2.

After these unsatisfactory results, we tried the second way, the use of a reductive atmosphere during the heat treatment. We used a mixture of gases consisting in argon and hydrogen with a concentration of 5 vol%. The addition of H_2 promotes the reduction of the oxide favoring the creation of H_2O. Before further tests, we tried this path with MC+DEATi in order to check if the reactive gas can shift the composition from TiO_xC_{1-x} (as seen before in the previous chapter) to TiC. So we prepared a sample with a ratio between MC and DEATi of 4.5:1 and treated it at 1300°C for 3 hours with the argon and hydrogen gas flow. The XRD pattern is shown in Figure 126.

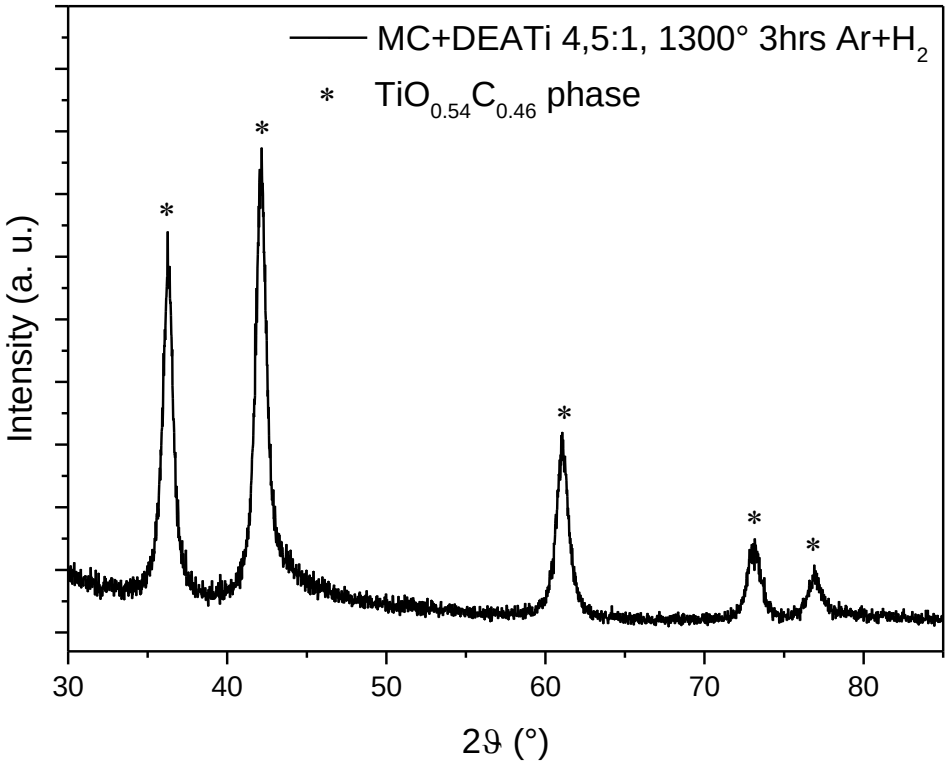

Figure 126, MC+DEATi 4.5:1, treated in Ar+H_2 at 1300°C for 3 hours

The positions of the peaks, the cell parameter and oxygen content for this sample are reassumed in Table 26.

1st peak position (°)	***2nd peak position (°)***	***3rd peak position (°)***	***4th peak position (°)***	***5th peak position (°)***	***Cell parameter (Å)***	***Oxygen content (mol%)***
36.27	42.14	61.07	73.12	76.95	4.2859	54

Table 26, peak positions, cell parameter and oxygen content for MC+DEATi 4.5:1, treated in Ar+H_2 at 1300°C for 3 hours

The oxygen content is very high considering the initial molar ratio and the presence of H_2 in the gas flow. This can be explained with the capacity of the hydrogen to form simple alkanes with carbon at these temperatures, like CH_4 and C_2H_6. This can reduce the total amount of available carbon during the carburization, leading to a higher than expected quantity of oxygen. We tried to treat another sample with the same ratio of MC and DEATi of 4.5:1 at higher temperatures, to see if hydrogen at higher

temperatures reacts not only with carbon but also with oxygen. The XRD pattern after the heat treatment at 1450°C for 3 hours is in Figure 127.

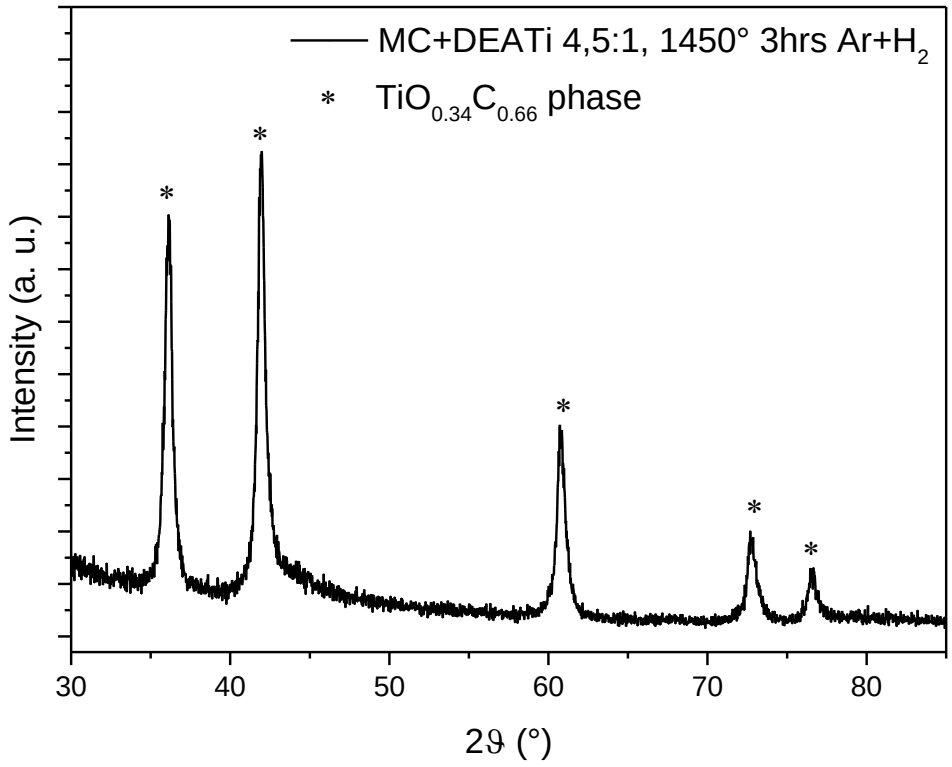

Figure 127, MC+DEATi 4.5:1, treated in Ar+H2 at 1450°C for 3 hours

The peak positions, cell parameter and oxygen content are listed below, in Table 27.

1st peak position (°)	***2nd peak position (°)***	***3rd peak position (°)***	***4th peak position (°)***	***5th peak position (°)***	***Cell parameter (Å)***	***Oxygen content (mol%)***
36.12	41.96	60.80	72.78	76.60	4.3031	34

Table 27, peak positions, cell parameter and oxygen content for MC+DEATi 4,5:1, treated in Ar+H2 at 1450°C for 3 hours

For this sample, the results are more satisfactory because the quantity of oxygen is decreased in a significant way, albeit the final stoichiometry is far from the expected one. In order to check if the addition of hydrogen in the gas flow gives some benefits to our synthesis or this result is only due to kinetic factors we prepared another sample with the same MC:DEATi ratio and treated it at the same conditions without hydrogen.

The XRD pattern is reported in Figure 128, while in Table 28 there are listed its major parameters.

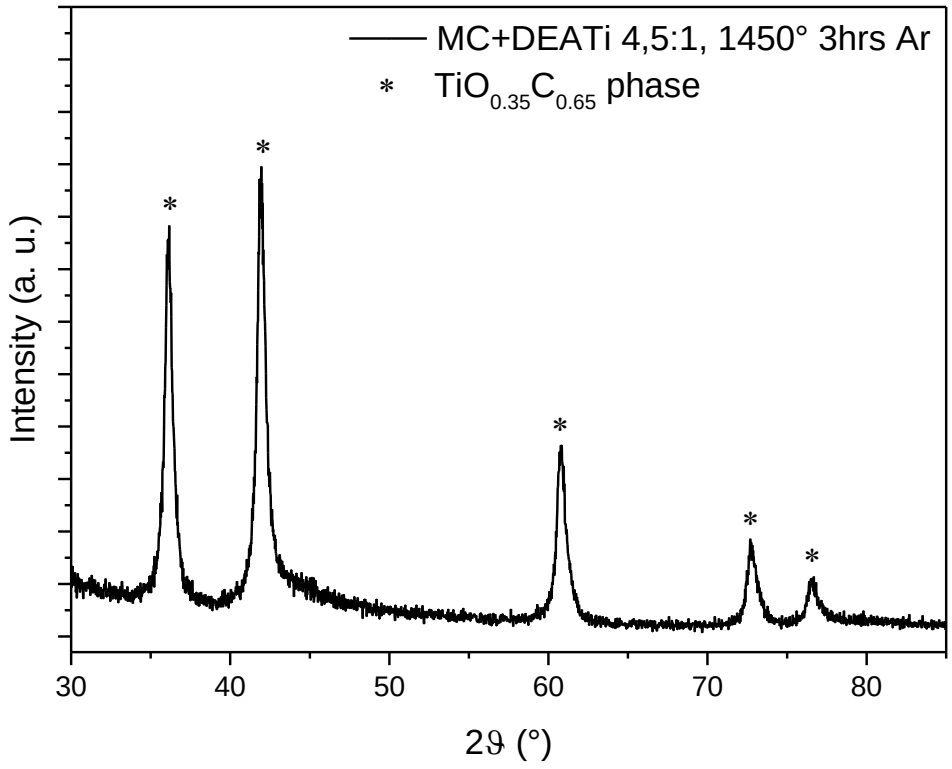

Figure 128, MC+DEATi 4.5:1, treated in Ar at 1450°C for 3 hours

1st peak position (°)	***2nd peak position (°)***	***3rd peak position (°)***	***4th peak position (°)***	***5th peak position (°)***	***Cell parameter (Å)***	***Oxygen content (mol%)***
36.13	41.96	60.81	72.81	76.61	4.3023	35

Table 28, peak positions, cell parameter and oxygen content for MC+DEATi 4,5:1, treated in Ar at 1450°C for 3 hours

The oxygen content is very similar to the sample treated with hydrogen. This means that the hydrogen at this temperature reacts with both oxygen and carbon, lowering their amount, but cannot influence the stoichiometry of the titanium oxycarbide ceramic. In Figure 129 there is the comparison of the three samples, while in Table 29 the parameters for each sample are listed.

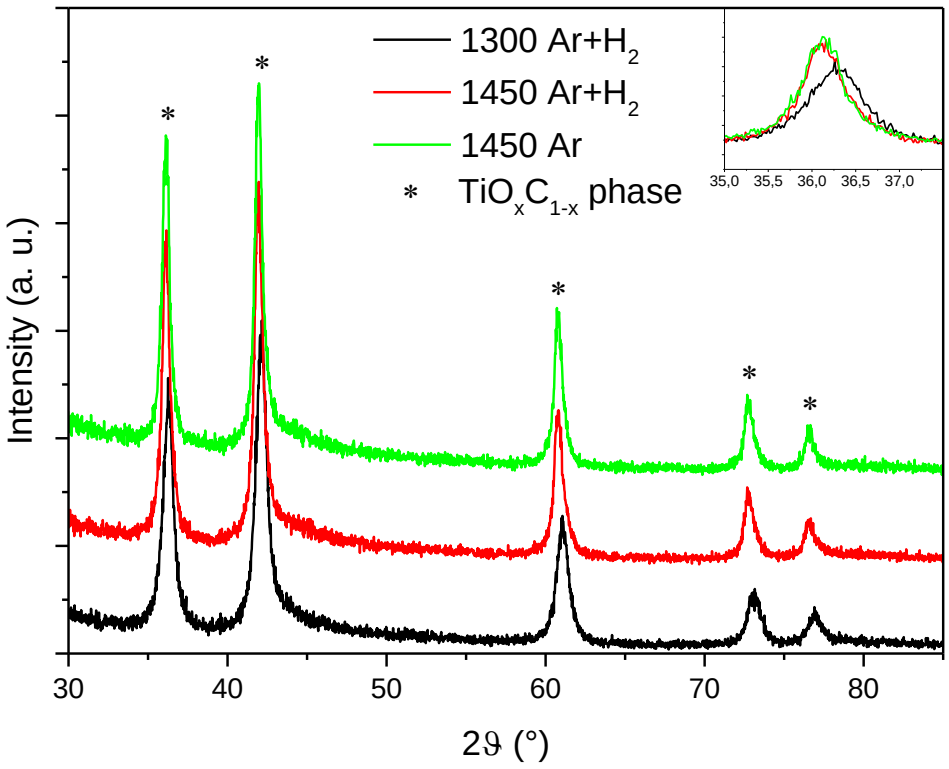

Figure 129, XRD patterns comparison of MC+DEATi 4,5:1 treated at 1300°C with Ar+H₂, 1450°C for 3 hours with Ar+H₂ and 1450°C for 3 hours with Ar

Heat treatment	***1st peak position (°)***	***2nd peak position (°)***	***3rd peak position (°)***	***4th peak position (°)***	***5th peak position (°)***	***Cell parameter (Å)***	***Oxygen content (%)***
1300°C Ar+H_2	36.27	42.14	61.07	73.12	76.95	4.2859	54
1350°C Ar+H_2	36.12	41.96	60.80	72.78	76.60	4.3031	34
1450°C Ar	36.13	41.96	60.81	72.81	76.61	4.3023	35

Table 29, peak positions, cell parameters and oxygen contents for MC+DEATi 4,5:1 treated at 1300°C in Ar+H₂, 1450°C in Ar+H₂ and 1450°C in Ar

The treatment with hydrogen did not gave the expected results, leading at an impasse. Starting from the conclusions that can be taken from these tests, two paths can be traced: the first arises from the consideration that higher temperatures and longer times of treatment are required in order to remove all the oxygen from the stoichiometry, leading to change the oven; the second evaluates the possibilities to use precursors that don't contain oxygen.

We decided to try the easiest way, changing the precursors, because it was cheaper than buying a new oven and faster to accomplish. Several types of precursors were valuated both for silicon and titanium, like diphenilsilane, triphenilsilane, triethylsilane or silicon carbide. The common feature of them is that they are organometallic precursor soluble in some organic solvent without oxygen in the composition, in order to work in reductive environment.

Unluckily most of the considered precursors where not easily available or too pricy, so we had to simplify the reaction starting from the raw elemental materials. We decided also to change the MAX phases, choosing Ti_2AlC and Ti_3AlC_2 instead of Ti_3SiC_2 because they have lower temperature of sintering and can be made at atmospheric pressure [86], not requiring special tools [87, 90, 95, 102, 103].

4.3. Ti_2AlC and Ti_3AlC_2

The first experiment aimed to prepare Ti_3AlC_2 using aluminum from ACROS Organics (99% purity, 200 mesh particle size), titanium (99,98% purity, particle size <45 μm) and graphite (99,99% purity, particle size ≤150 μm, sifted with a 325 mesh sieve) both from Sigma-Aldrich. The metals are stored under argon in glove box, in order to reduce the oxidation and minimize the variation of the precursors over the time. Three moles of titanium and one of aluminum were weighted in glove box and put in a zirconia jar. The jar is then sealed with parafilm in order to minimize the air contamination before the addition of two moles of graphite. After all the powders are inside the jar, a proper number of zirconia spheres is added with a weight ratio between them and the powders of 3:1. The jar is sealed again and put in the ball mill machine to sustain the grinding at 250 rpm for 18 hours.

As the grinding is finished, all the zirconia spheres are removed and the powder is put in an alumina vessel and put in the furnace oven for the sintering. An argon flow of 0.5 L/min is started 1 hour before the heat treatment for a complete evacuation of air inside the tube. Then the heat is applied with a ramp of 10°C/min up to 1360°C. The top temperature is hold for 2 hours before the natural cooling.

The sample after the sintering appeared as a compact bulk, with brittle consistence and grey matte color. It was ground by hand in an agate mortar and XRD analysis was done.

We also made XRD on a sample of Ti_3AlC_2, kindly sent to us by the research group of Prof. Barsoum from Drexel University, to set the benchmark. The pattern is reported below, in Figure 130.

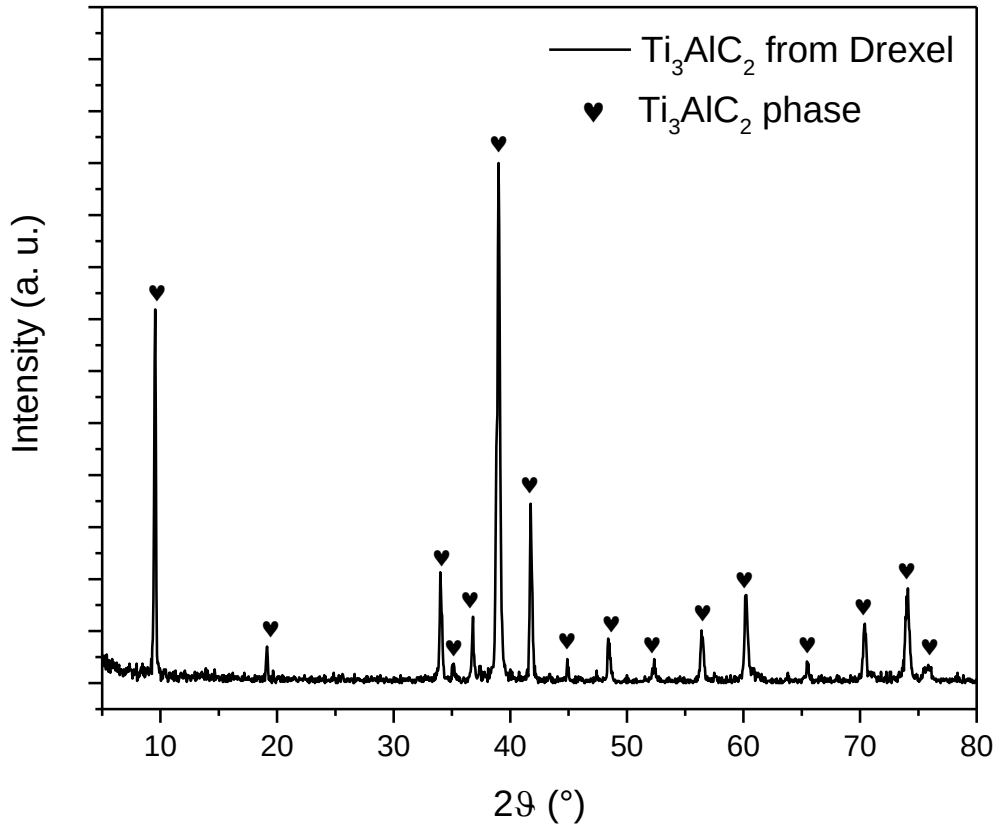

Figure 130, XRD pattern of Ti_3AlC_2 received from Drexel University

In Figure 131 there is the pattern from our sample, while in Figure 132 there is a comparison of the two samples.

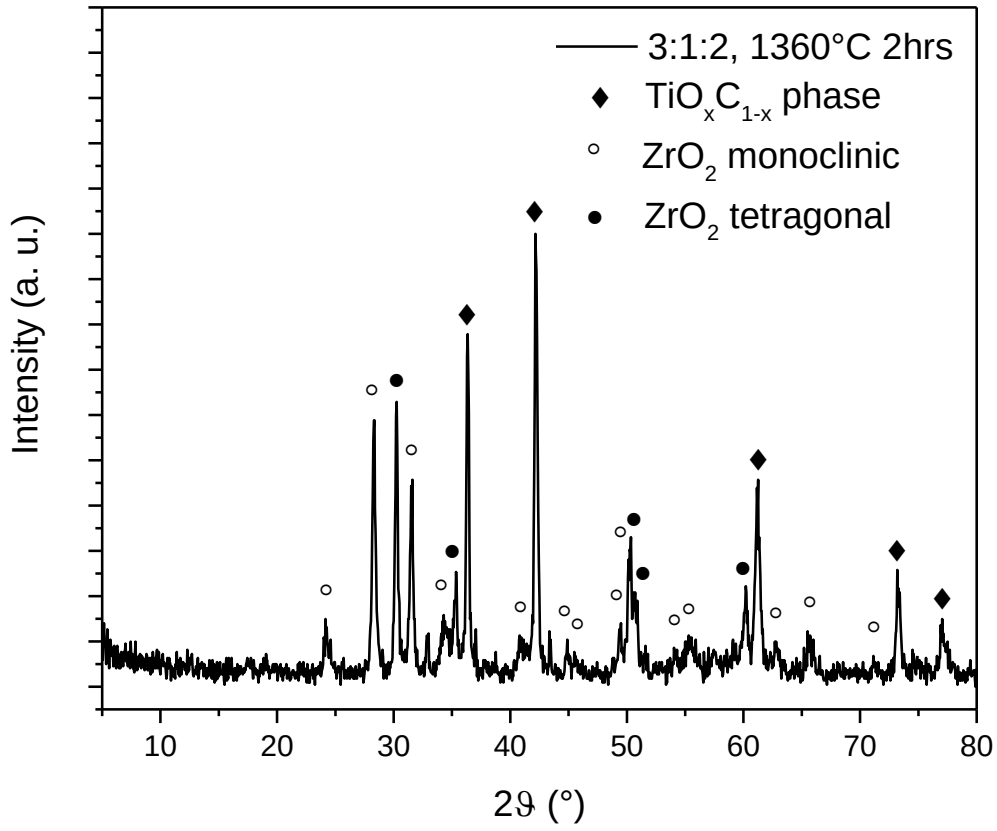

Figure 131, XRD pattern of Ti, Al and C powders with molar ratio of 3:1:2, after sintering at 1360°C for 2 hours

As can be clearly seen, the pattern from our sample is completely different. The MAX phase's peaks are not present. There are peaks ascribable to two different phases of ZrO_2, the monoclinic and tetragonal, while the most intense peaks are from TiO_xC_{x-1} phase.

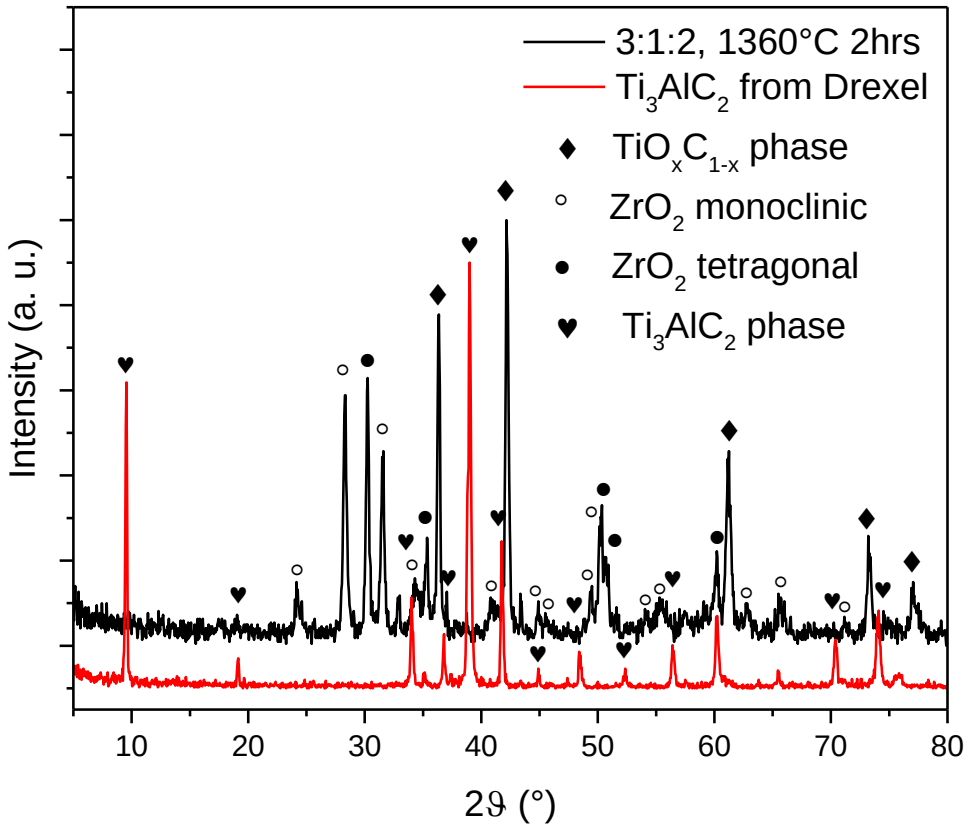

Figure 132, XRD patterns comparison of Ti, Al, C powders with molar ratio of 3:1:2, treated at 1360°C for 2 hours and Ti_3AlC_2 from Drexel University

Because the peaks from the zirconia are related only to the milling process, we ground another batch of raw powders and made an XRD in order to investigate the composition before the sintering. The pattern is reported in Figure 133.

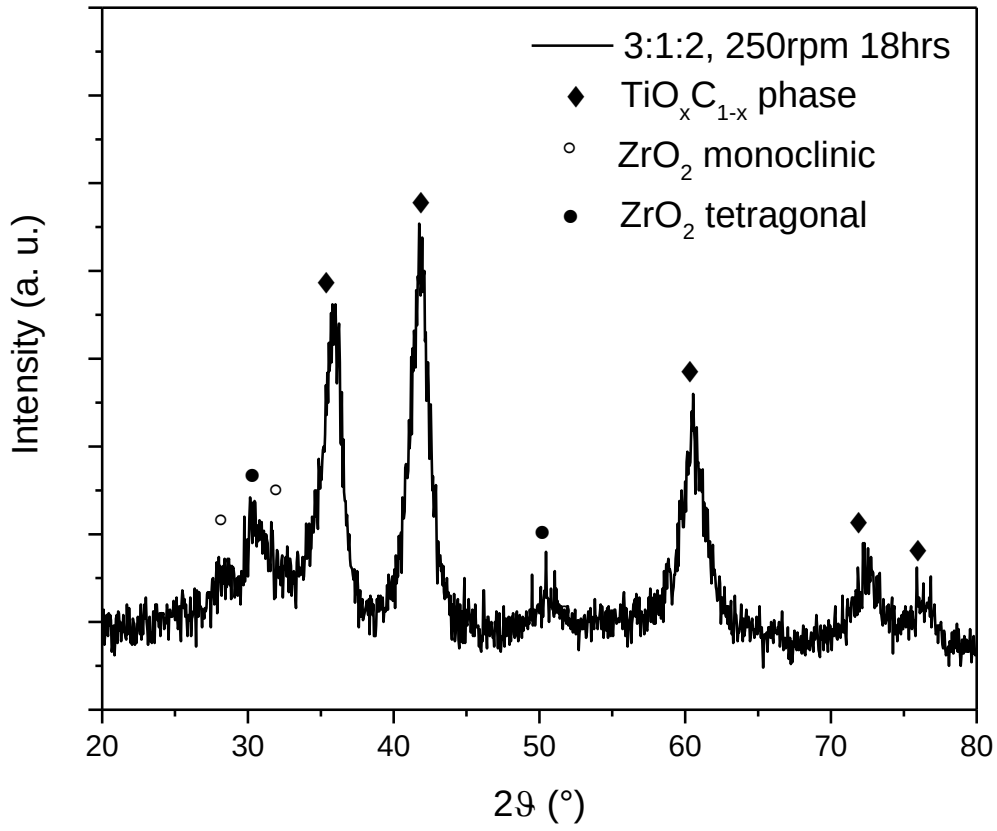

Figure 133, XRD pattern of Ti, Al and C powders with molar ratio of 3:1:2, after ball milling for 3 hours at 250rpm

Before the sintering, the zirconia balls contaminate the powders with two different phases and promote the formation of TiC with traces of oxygen. Aluminum phases are not visible, probably because they were amorphous due to the energetic grinding.

After this discovery, we changed the initial molar ratio between the elements and the ball milling parameters. We lowered the amount of carbon and increased that of aluminum, because at the temperature of sintering aluminum is in liquid phase and the vapor pressure is not negligible, leading to a depletion of it. The new molar ratio for Ti, Al and C are respectively 3:1.2:1.8. The ball milling was reduced to 1 hour, in order to minimize the contamination of zirconia from the jar and the balls but we increased at the same time the speed of rotation to 350 rpm to be sure that an efficient grinding took place.

Two parts of the new sample were pressed into circular shape with the aid of a hydraulic press exerting 100 MPa and 200 MPa for 5 minutes. The pressed samples were sintered together at 1350°C for 4 hours, with a heating ramp of 10°C/min and then natural cooling. The XRD patterns of the two samples are superimposed to that from Drexel University for better comparison in Figure 134.

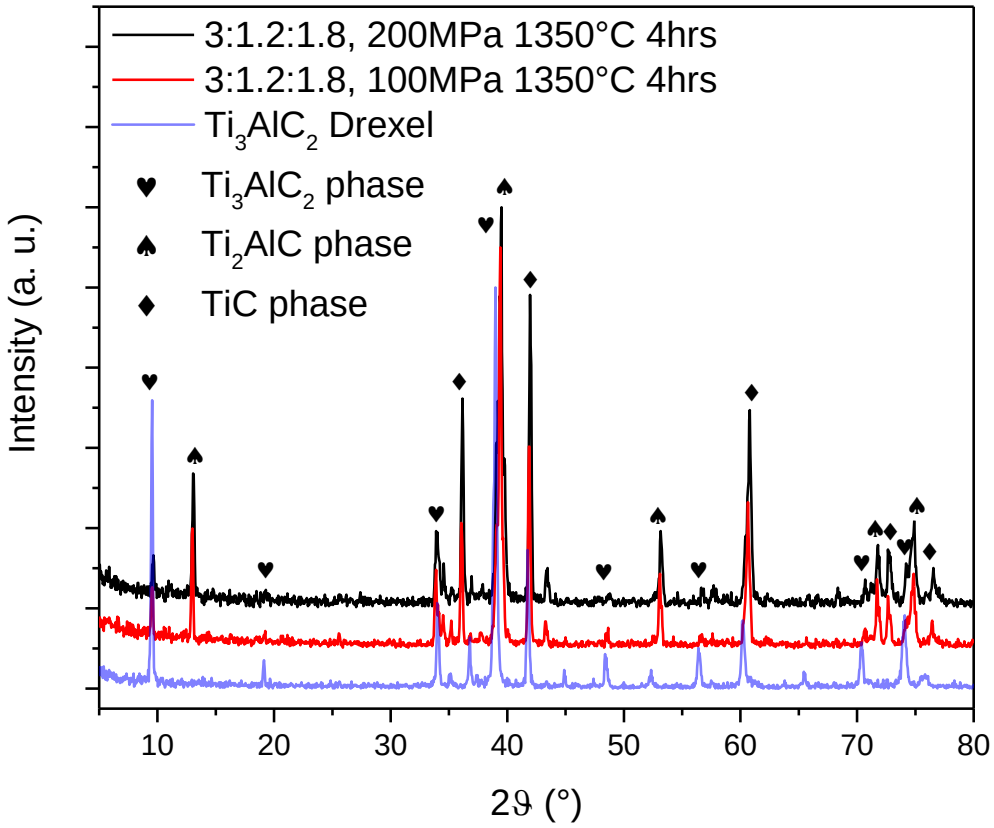

Figure 134, XRD patterns for two samples with Ti, Al and C powders with molar ratio 3:1.2:1.8, pressed at 200MPa and 100MPa for 5 minutes and sintered at 1350°C for 4 hours. In blue the XRD pattern of Ti_3AlC_2 from Drexel University

The results with the two different samples are very similar and a small fraction of Ti_3AlC_2 is visible in both, with slightly more intense peaks from the sample pressed at 200 MPa. Unluckily there is present also the 211 phase and TiC in bigger quantities than Ti_3AlC_2. This is probably due to the time of sintering, because at this temperature TiC is more favored than Ti_3AlC_2 and probably the latter decomposes is the two simpler phases. We investigated the morphology of these two samples by SEM. The images are reported below in Figure 135, Figure 136 and Figure 137 for the sample pressed with 100 MPa and in Figure 138, Figure 139 and Figure 140 for the other sample.

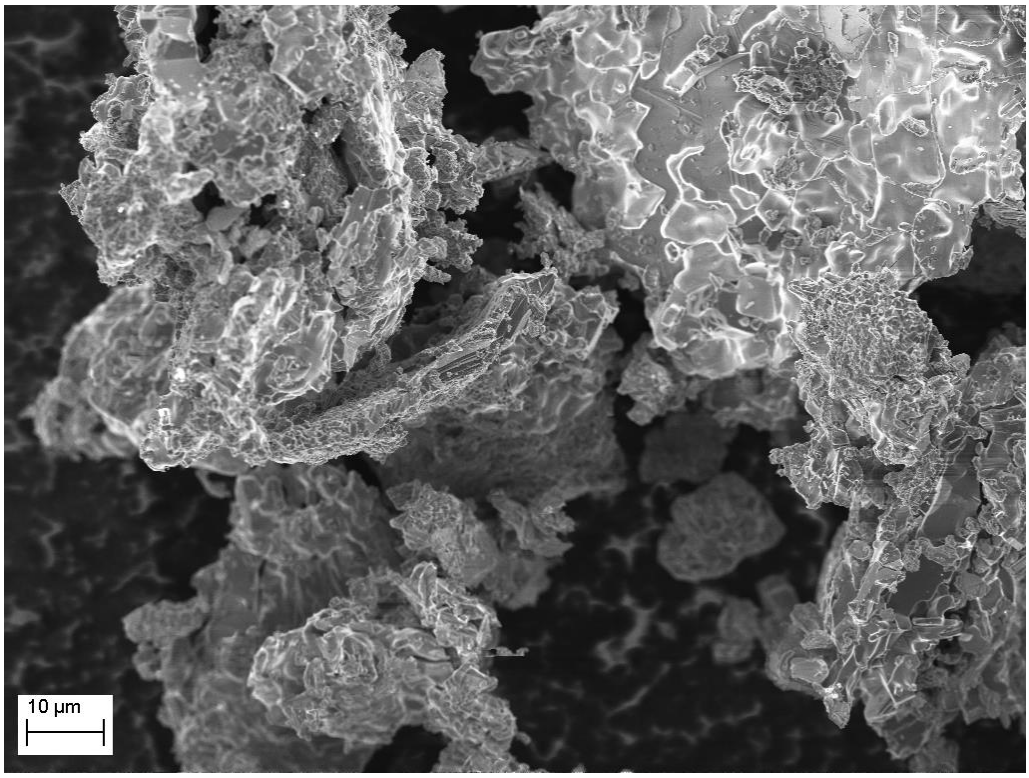

Figure 135, SEM image of Ti, Al and C powders with molar ratio 3:1.2:1.8, pressed at 100 MPa for 5 minutes and sintered at 1350°C for 4 hours

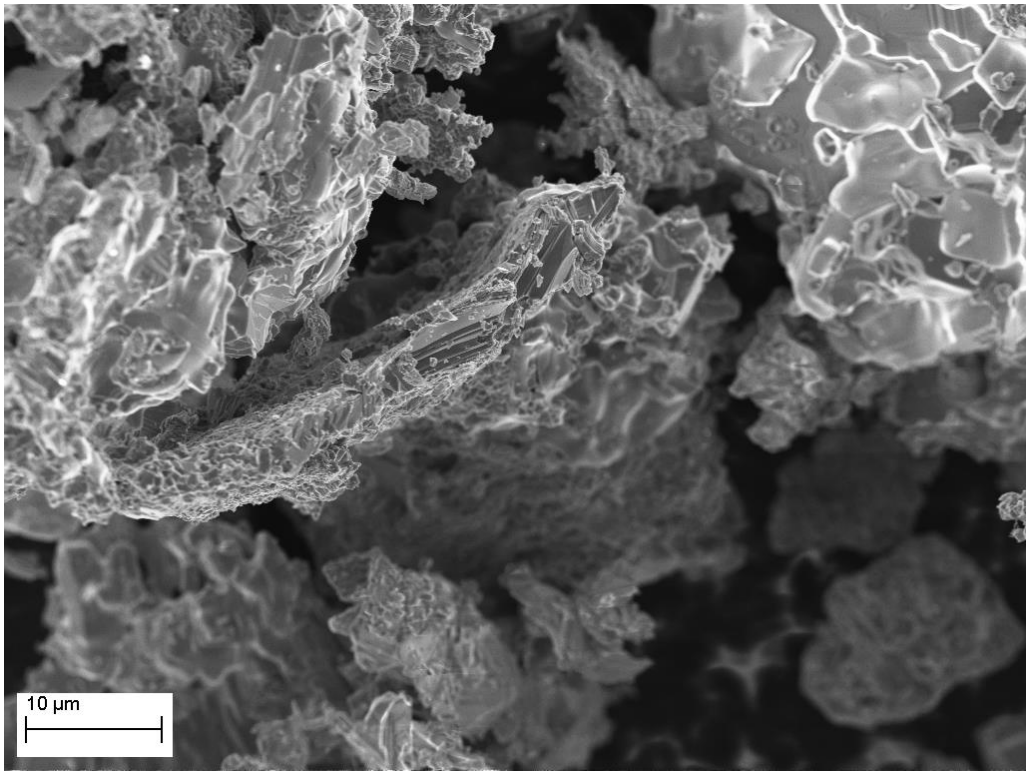

Figure 136, SEM image of Ti, Al and C powders with molar ratio 3:1.2:1.8, pressed at 100 MPa for 5 minutes and sintered at 1350°C for 4 hours

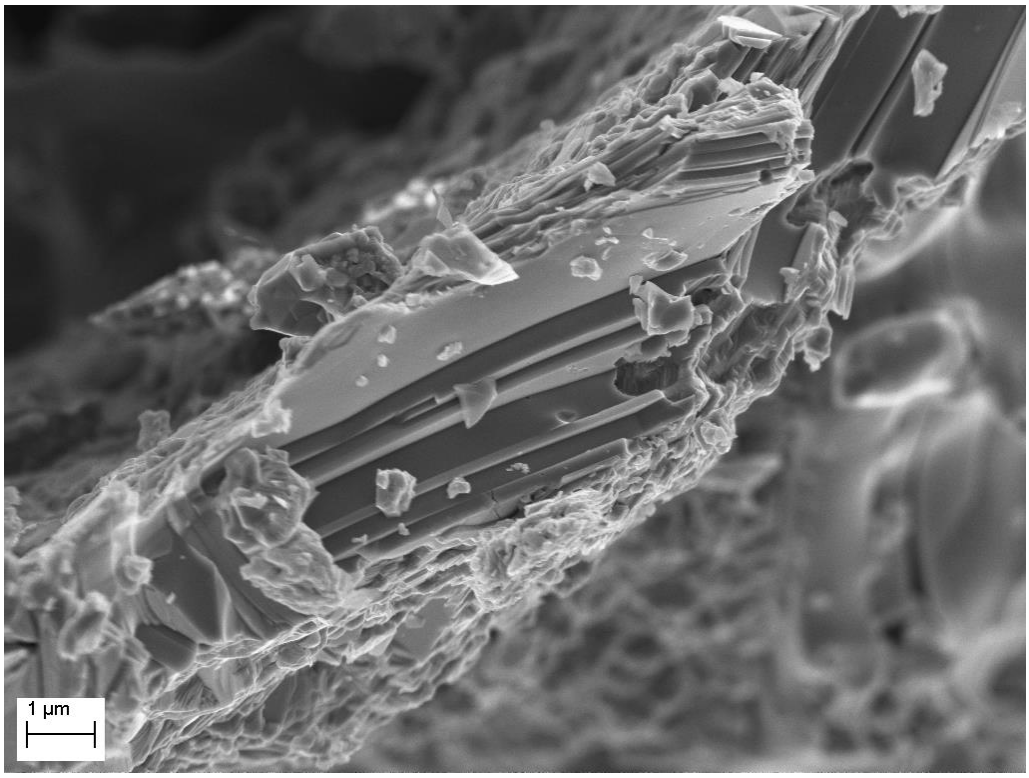

Figure 137, SEM image of Ti, Al and C powders with molar ratio 3:1.2:1.8, pressed at 100 MPa for 5 minutes and sintered at 1350°C for 4 hours

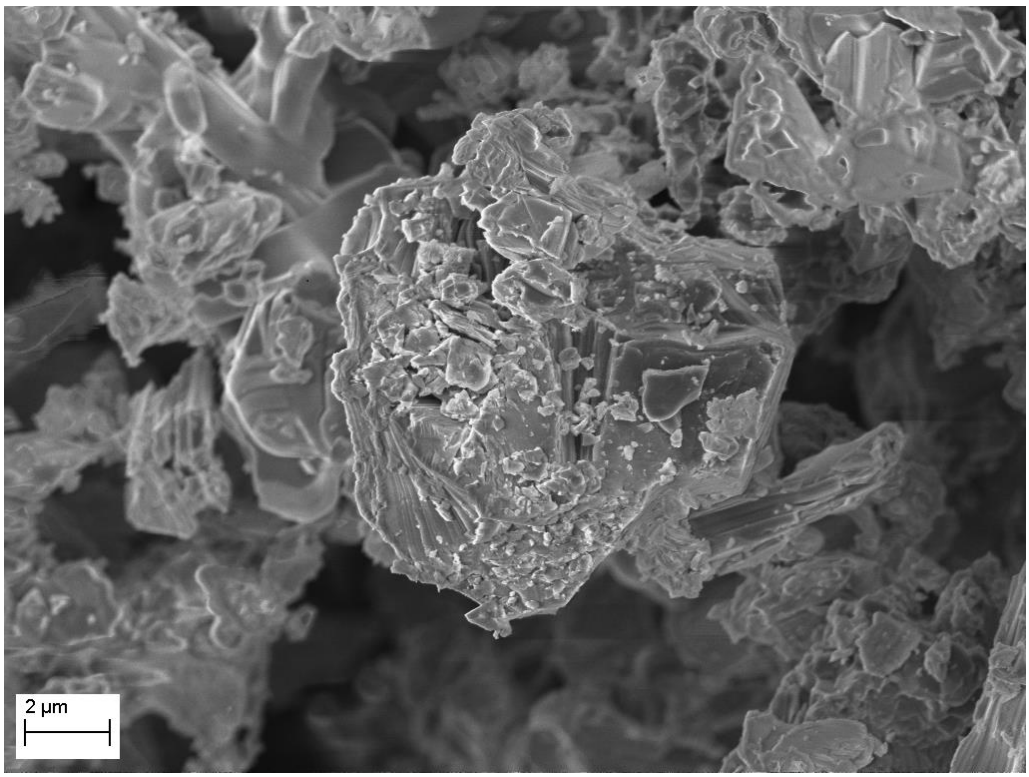

Figure 138, SEM image of Ti, Al and C powders with molar ratio 3:1.2:1.8, pressed at 200 MPa for 5 minutes and sintered at 1350°C for 4 hours

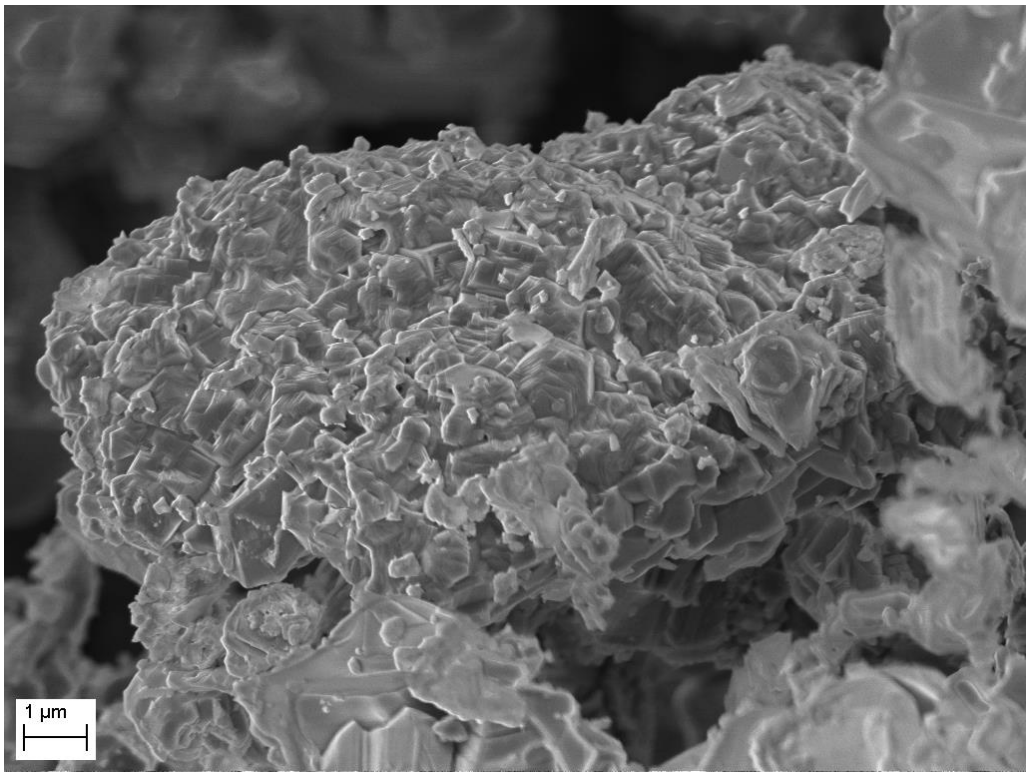

Figure 139, SEM image of Ti, Al and C powders with molar ratio 3:1.2:1.8, pressed at 200 MPa for 5 minutes and sintered at 1350°C for 4 hours

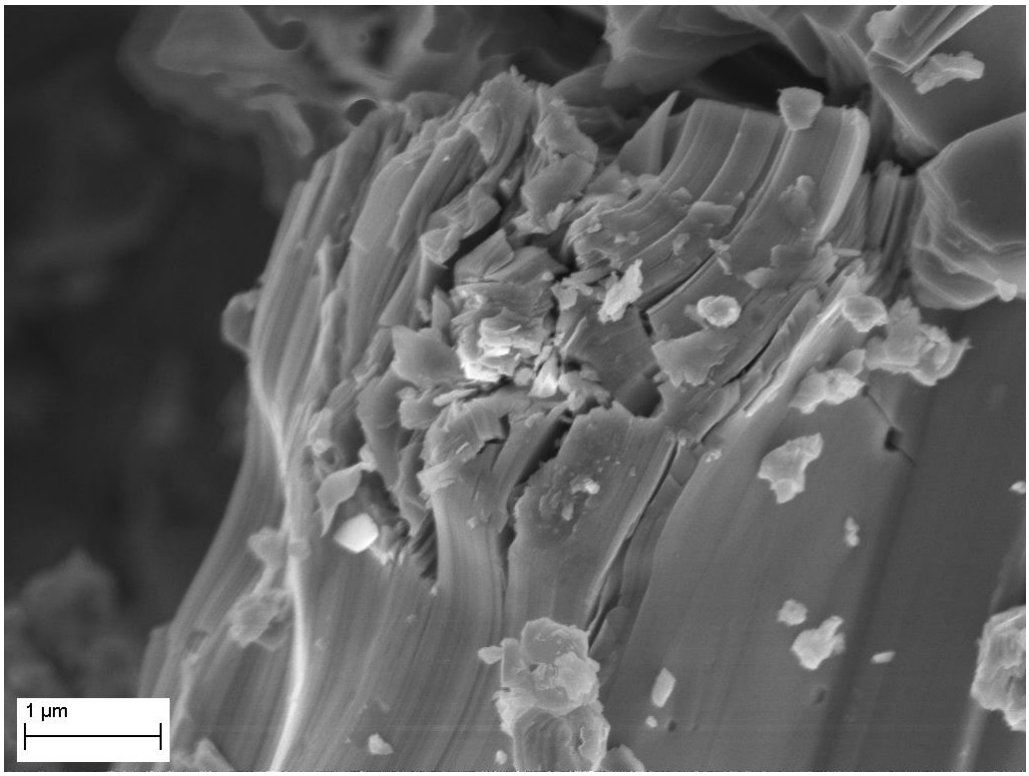

Figure 140, SEM image of Ti, Al and C powders with molar ratio 3:1.2:1.8, pressed at 200 MPa for 5 minutes and sintered at 1350°C for 4 hours

Both the samples show clearly crystalline zone with the characteristic layered structures but also amorphous agglomerates. In Figure 139 there are the layered structures that are covered by a thin layer that blurs all the edges. The exact nature of this layer is not clear. One hypothesis is that the aluminum, being in liquid phase at that temperature, covers for the surface tension all the small grains without penetrating inside. During the cooling, the aluminum does not crystalize in a regular form and remain amorphous, so it is not visible by XRD and the content of Al inside the crystalline phases is lower. In order to find a confirmation of this hypothesis, we decided to shorten the time of sintering to 2 hours, still using the same molar ratio, ball milling parameters and the higher pressure of 200MPa for pressing. The XRD pattern is reported below, in Figure 141.

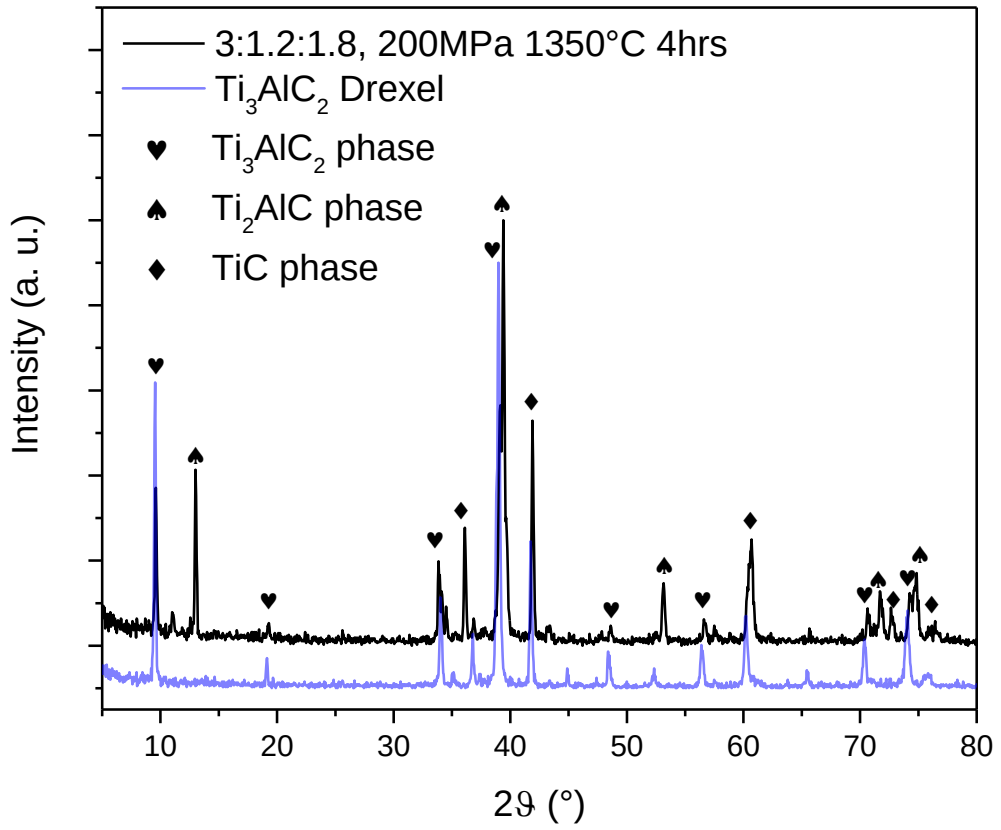

Figure 141, XRD pattern for Ti, Al and C powders with molar ratio 3:1.2:1.8, pressed at 200 MPa for 5 minutes and sintered at 1350°C for 2 hours. In blue the XRD pattern of Ti3AlC2 from Drexel University

For this sample, the peaks related to the 312 phase are more intense, albeit there are still present peaks from 211 phase an TiC.

Following the suggestions received from Prof. Barsoum, we changed the path for the preparation of the samples using two steps. The first step was to synthetize Ti_2AlC and use it as precursor for Ti_3AlC_2 according to the following reaction path:

$$2Ti + 1Al + 1C \rightarrow 1Ti_2AlC$$

$$1Ti_2AlC + 1TiC \rightarrow 1Ti_3AlC_2$$

For the synthesis of the 211 phase, the recipe is very similar to that one already used, but with relevant modifications: the starting elements in the right molar ratios firstly have to be ball milled with alumina spheres in a polyethylene jar for 18 hours at 300 rpm. The obtained powder undergoes a heat treatment at 1400°C for 4 hours under argon flow, with a heating ramp of 10°C/min and natural cooling.

For the 312 phase, the obtained Ti_2AlC has to be ground to have a particle size smaller than 45μm, and then it can be mixed with titanium carbide in the right molar ratio and milled for 18 hours in a polyethylene jar with alumina balls at 300 rpm. The new powder can be treated at 1350°C for 2 hours under argon flow, with the same heating ramp and cooling of the previous treatment.

The first test was done following the given instruction but with a slight addition of 10% of aluminum to compensate the loss during the sintering, giving a starting ration between Ti, Al and C of 2:1,1:1. After the milling process and the sintering, the powder was ground by hand prior to XRD analysis. Its pattern is reported in the following Figure 142.

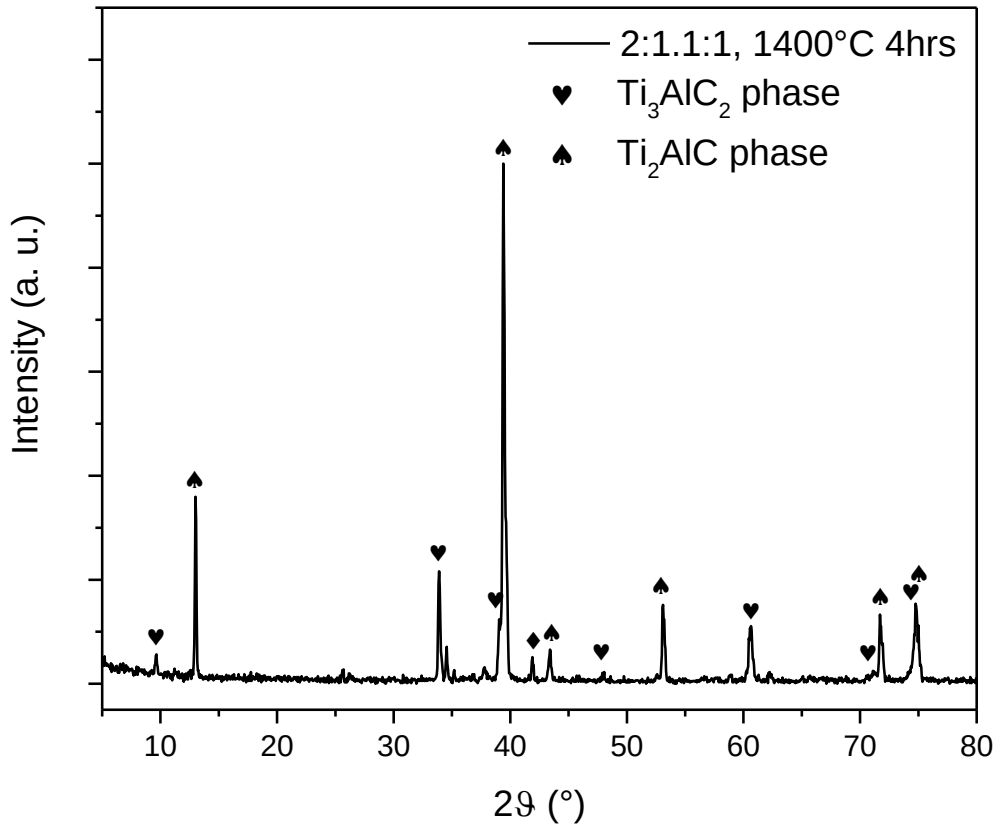

Figure 142, XRD pattern of Ti, Al and C powders with molar ratio 2:1.1:1, sintered at 1400°C for 4 hours

Only the peaks only of 211 and 312 phases are present. The ratio between the two different phases can be calculated comparing the intensities of the peaks and it was estimated that there is 87% of 211 and 13% of 312. This is a promising start because there are no traces of TiC or oxides.

The next step is to add to this powder TiC in proper quantity to transform the 211 in 312. Because we had not pure TiC at that time, we added the equivalent molar quantity of titanium and carbon; in this case the molar ration between 211, Ti and C were 1:0.87:0.87. The three powders were milled together in the polyethylene jar at 300 rpm for 18 hours. When ready, they were sintered at 1350°C for 2 hours.

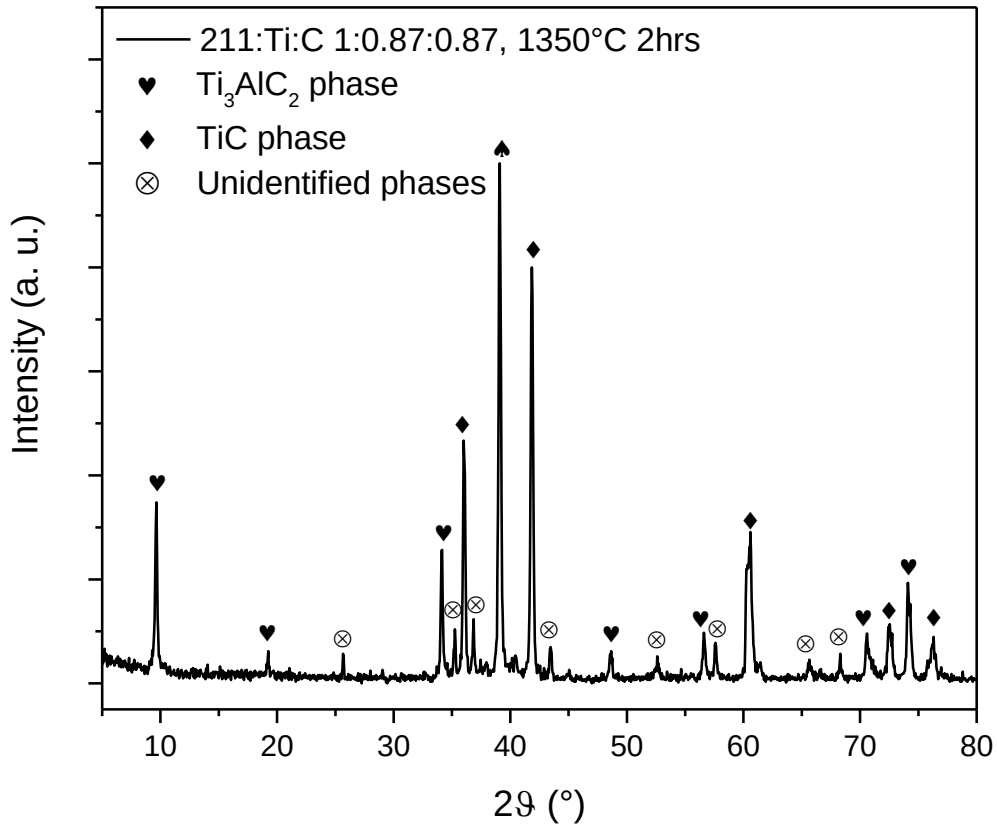

Figure 143, XRD pattern of 211, Ti and C powders with molar ratio of 1:0.87:0.87, sintered at 1350°C for 2 hours

The 211 phase completely reacted with titanium and carbon but, aside the 312 phase, there is TiC in high quantity and also unidentified phases with undefined stoichiometry.

For the next sample we sifted the graphite with a 325 mesh sieve in order to use powders all with the same particle size. The molar ratio between Ti, Al and C are still retained 2:1.1:1 and the milling and sintering followed the previous parameters.

The XRD analysis, as can be seen in Figure 144, shows the peaks ascribable to the 211 phase but there are also few peaks from the 312, while the most intense are absent. Furthermore, the last two peaks, at 55.15° and 60.55°, sit between the ones relatable to the 211 and 312 phases with a broadening of the width.

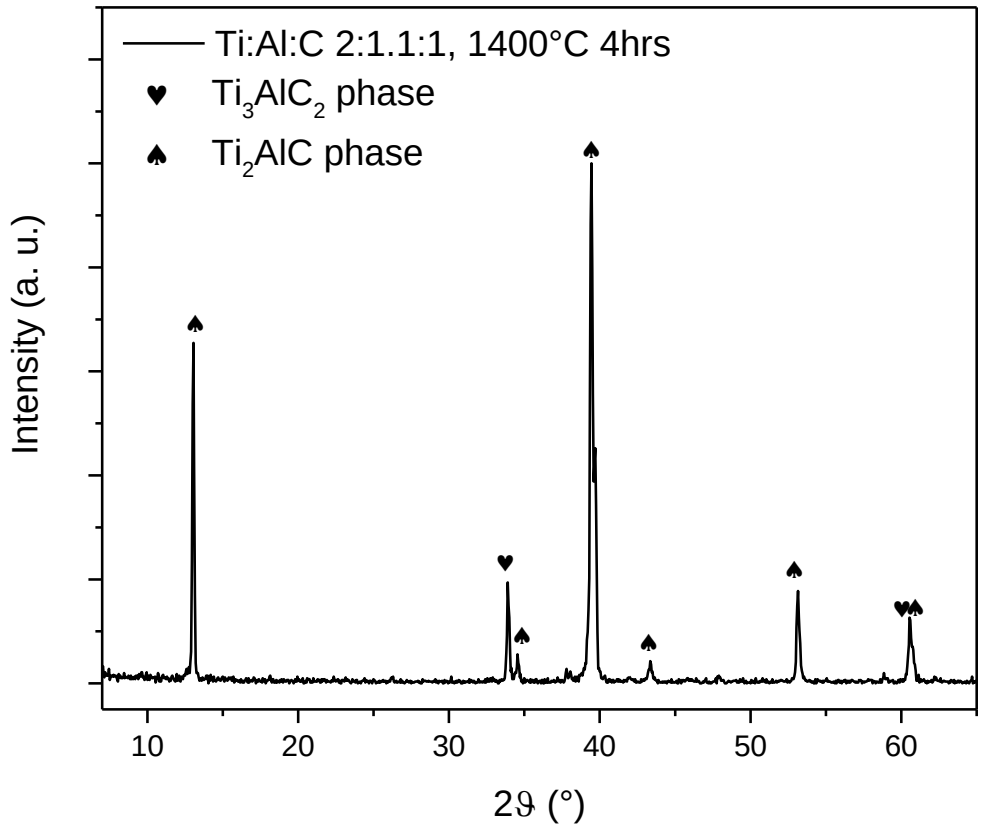

Figure 144, XRD pattern of Ti, Al and C powders with molar ratio of 2:1.1:1, sintered at 1400°C for 4 hours

The exact reason behind this strange phenomenon is still not clear. With this sample, we decided to add titanium carbide to the powder in order to sinter Ti_3AlC_2. Since it was not possible to calculate the exact quantity of the already formed 312 phase, we added TiC with a molar ratio of 1 respect to the 211 phase. We used the same milling and sintering parameters, i.e. 300 rpm for 18 hours in a polyethylene jar with alumina spheres and 1350°C for 2 hours, with a heating ramp of 10°C/min, respectively.

The obtained sample was harder than the previous ones with a darker color, symptoms of a relevant presence of titanium carbide. This was confirmed by the XRD analysis, as can be seen in Figure 145.

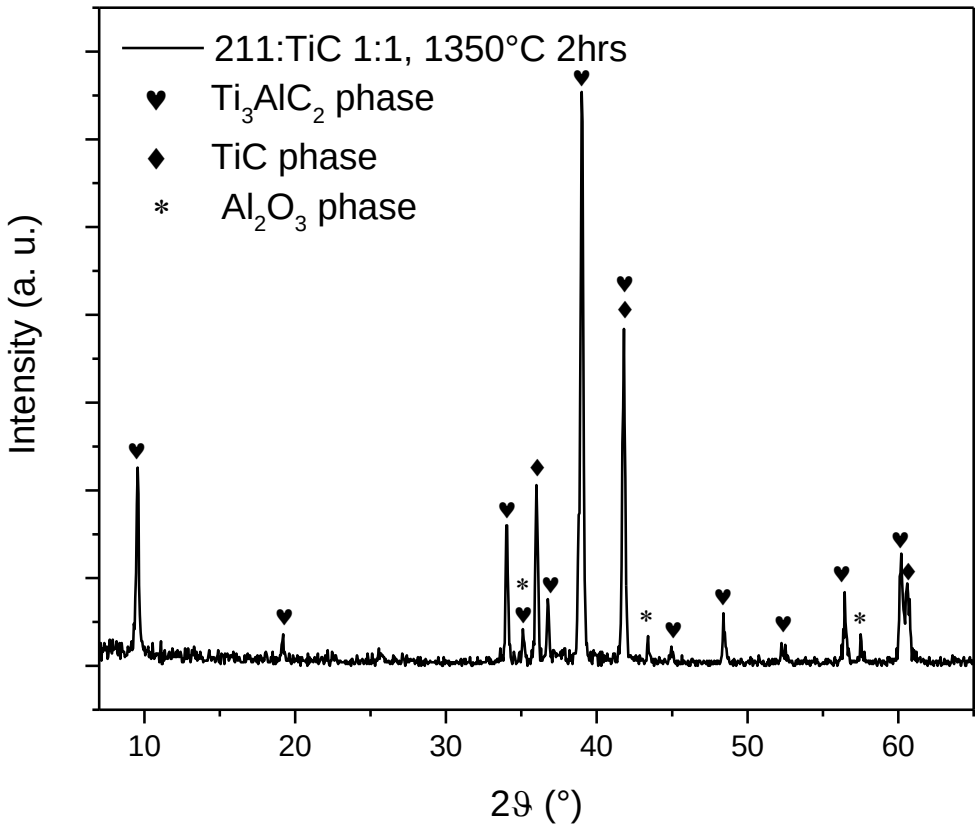

Figure 145, XRD pattern of 211 and TiC powders with molar ratio of 1:1, sintered at 1350°C for 2 hours

The quantity of unreacted TiC is not very large as in the previous sample of 312, but three peaks from Al_2O_3 are present that is probably due to the surface contact with the alumina vessel during the sintering. We took also SEM images of these samples, to see the morphology and check if there are amorphous phases like for the previous samples. The images are below, in Figure 146, Figure 147 and Figure 148.

Apparently, there are large areas covered with amorphous material, but at higher magnifications, they appear to be layered structures plastically bent, as can be seen with more clarity in the last image (Figure 148). It is probably due to the fact that sintering happened in the presence of a liquid pahse. Especially on the right side, there is a layered structure with curvy etches, because we caught a cross section where not all the layer growth in the same way. There are also other small particles that are probably TiC or Al_2O_3. With an EDX analysis the atomic ratio between Ti, Al and C were measured to be 5.40:1:1.27, with an additional 2.08:1 of O:Al.

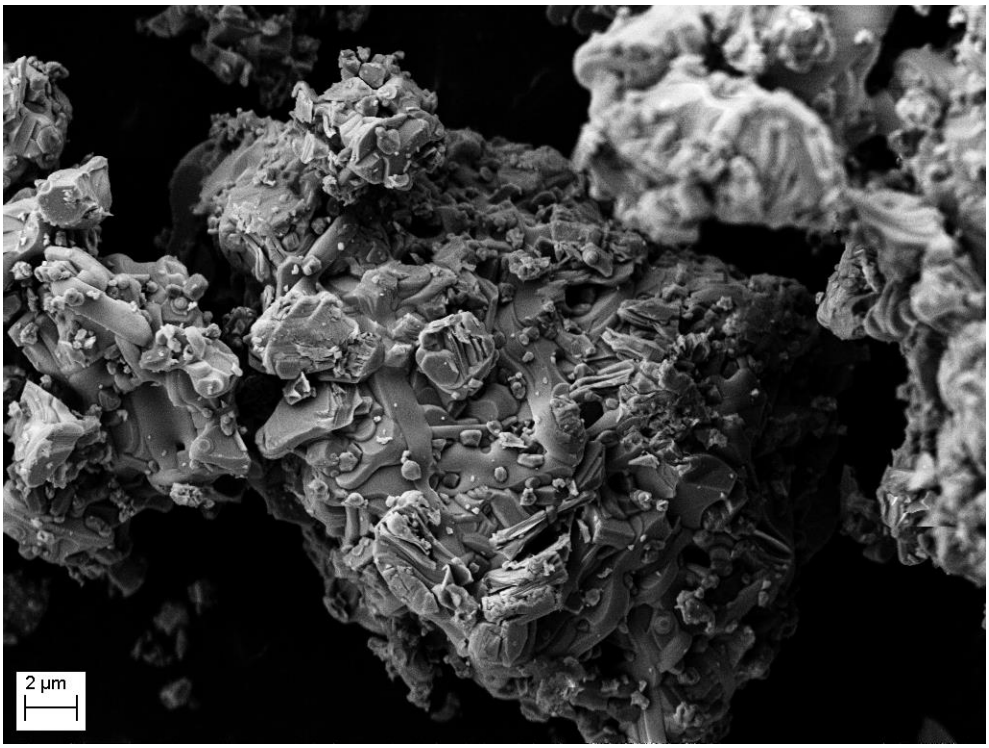

Figure 146, SEM image of 211 and TiC powders with molar ratio of 1:1, sintered at 1350°C for 2 hours

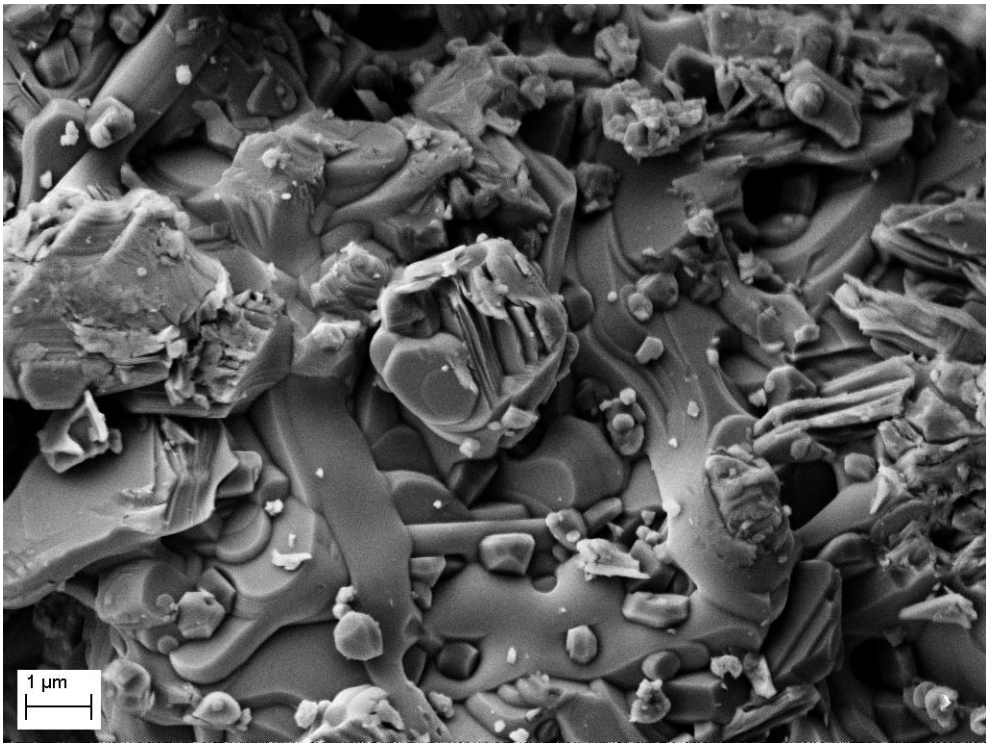

Figure 147, SEM image of 211 and TiC powders with molar ratio of 1:1, sintered at 1350°C for 2 hours

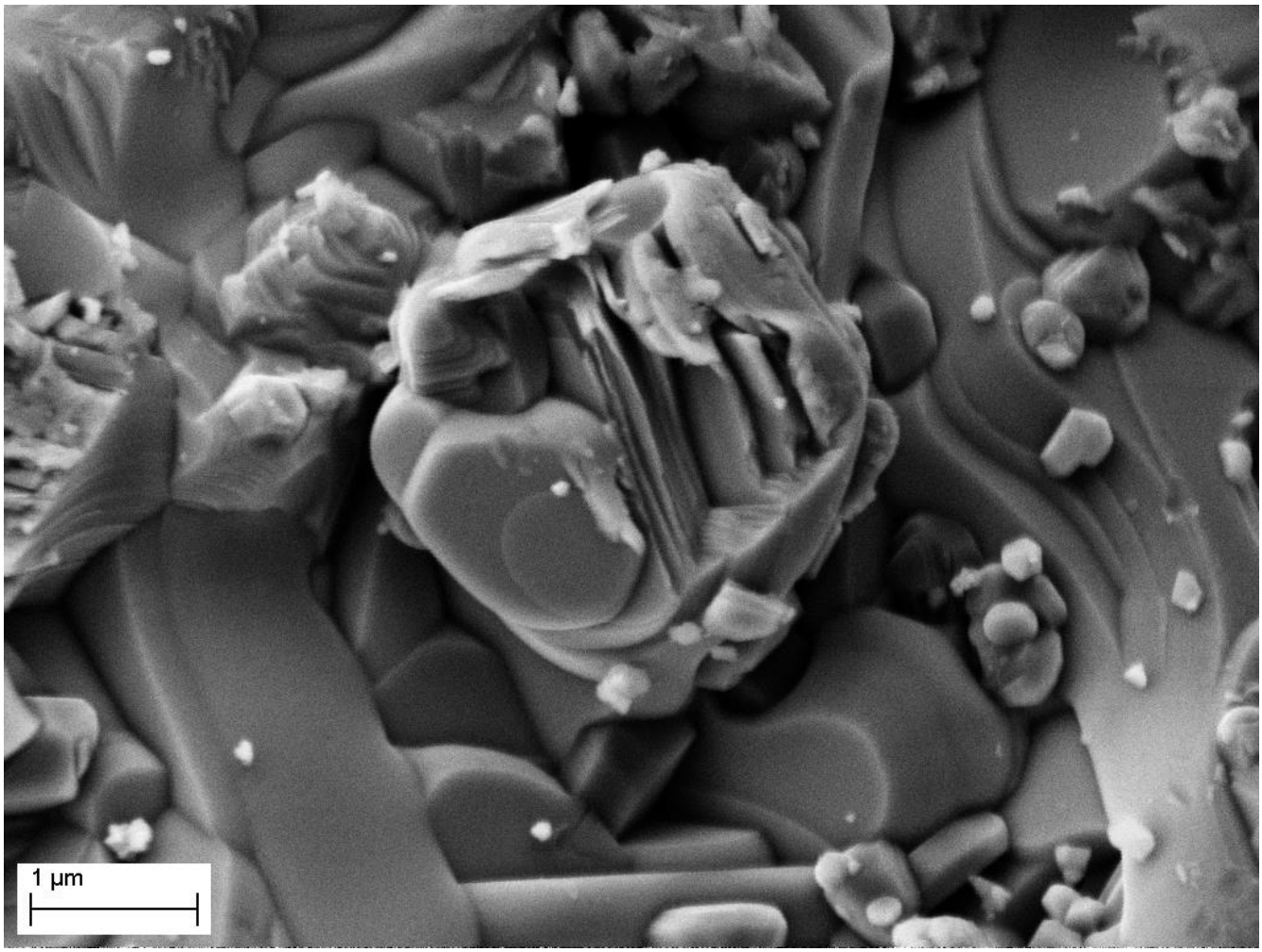

Figure 148, SEM image of 211 and TiC powders with molar ratio of 1:1, sintered at 1350°C for 2 hours

The next steps were all focused toward the improvement of the starting stoichiometry, ball milling and sintering condition to obtain a 211 phase as pure as possible, reducing the traces of Ti_3AlC_2. In the next tests, we tried to understand how the single factors (stoichiometry, ball milling and sintering condition) could affect the final composition.

For the next samples, we changed only the initial quantity of aluminum to avoid the loss due to evaporation and obtain only Ti_2AlC. The 312 phase indeed needs less aluminum because of its stoichiometry. Locally there could be areas with a lower concentration of Al during the sintering that leads to the formation of Ti_3AlC_2 or, from the already sintered Ti_2AlC some aluminum evaporates changing the ratios between the elements. To avoid the reduction of the quantity of aluminum we changed the starting Ti:Al:C molar ratio, trying firstly a big excess of Al with 2:1.25:1.

For the next samples, the ball milling and sintering conditions were the same that means 300 rpm for 3 hours and 1400°C for 4 hours. The XRD pattern of the first sample is presented in Figure 149.

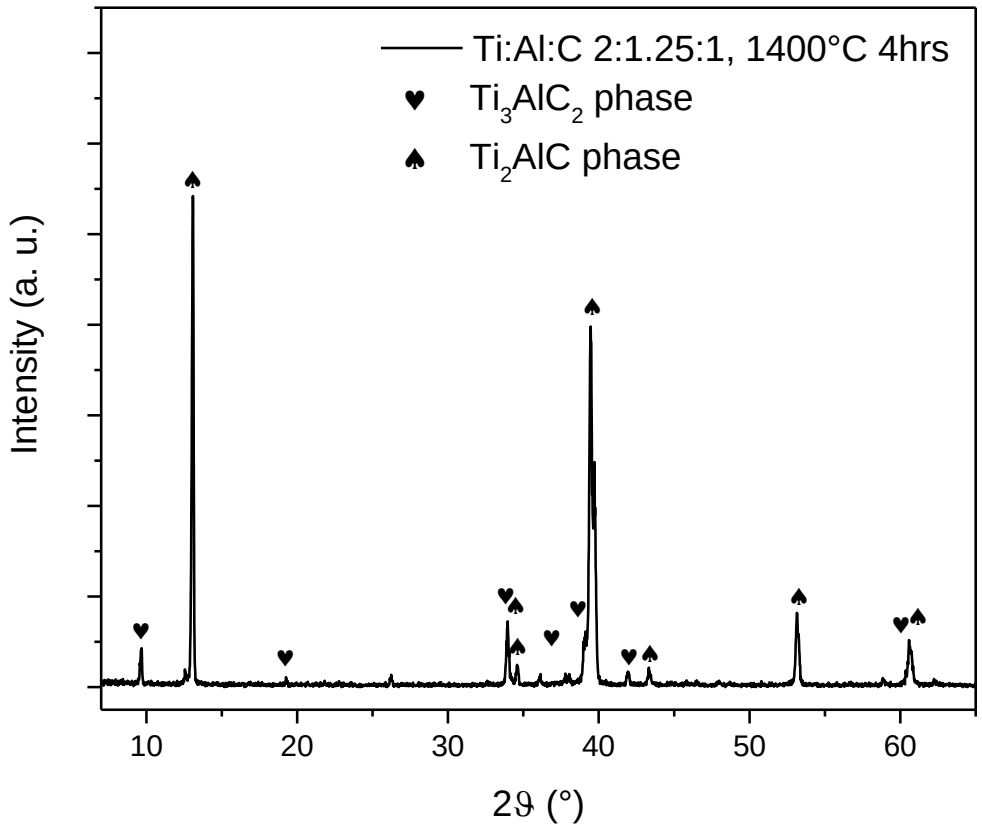

Figure 149, XRD pattern of Ti, Al and C powders with molar ratio of 2:1.25:1, sintered at 1400°C for 4 hours

This result is very strange, because of the first peak of Ti_2AlC is more intense than the theoretically most intense one, which is at 40°. Moreover, this peak is very complex in shape, showing 3 sub peaks that aren't relatable exactly to the 211 phase. Our hypothesis is that there is too much aluminum, that does not form a crystalline phase but it forms defects in the structure.

From the SEM images we were not able to confirm this hypothesis, because there are visible only layered structures (visible in Figure 150, Figure 151 and Figure 152) with a small amount of particles that cannot be identified because of their small dimensions (Figure 153, circled).

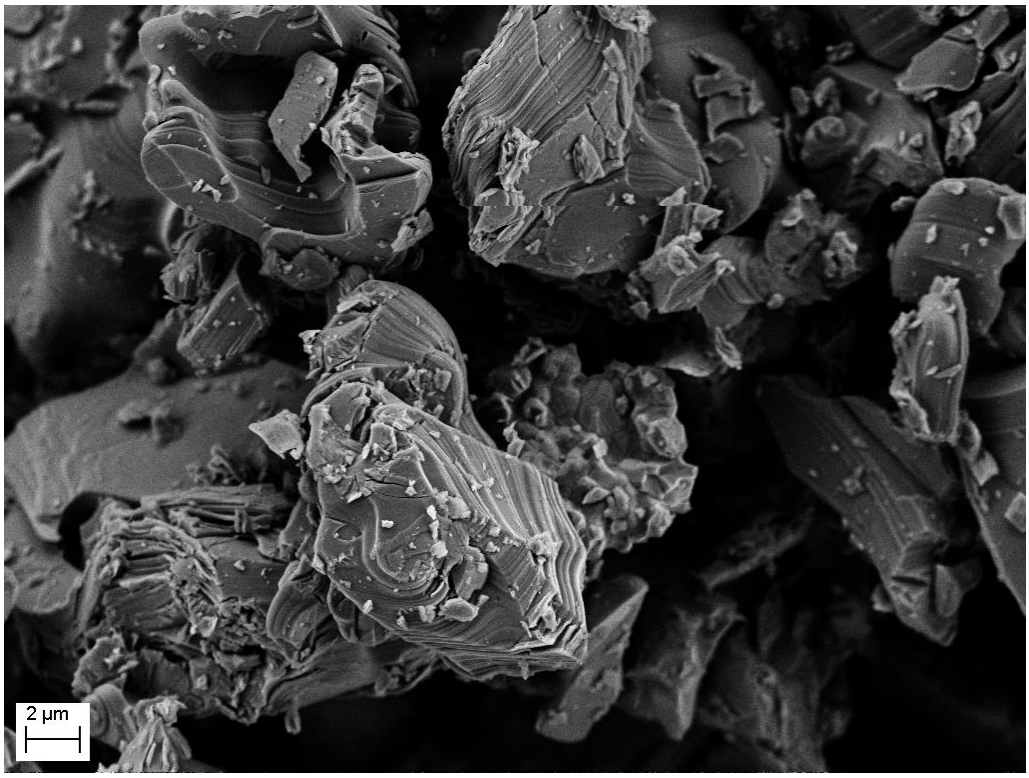

Figure 150, SEM image of of Ti, Al and C powders with molar ratio of 2:1.25:1, sintered at 1400°C for 4 hours

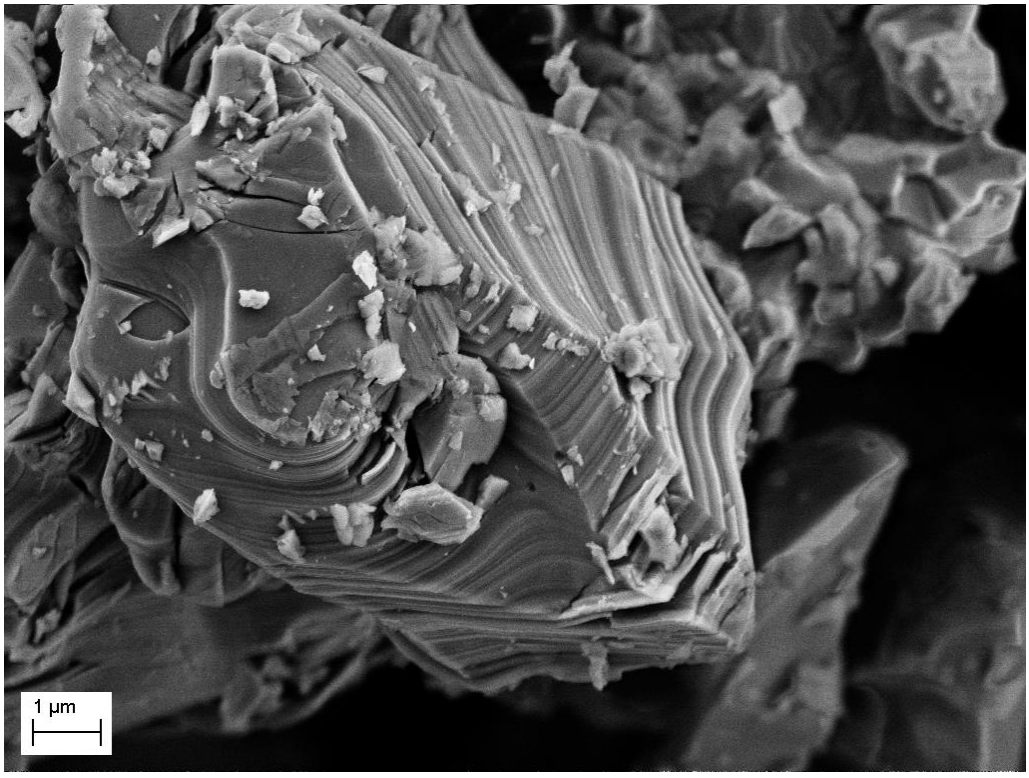

Figure 151, SEM image of of Ti, Al and C powders with molar ratio of 2:1.25:1, sintered at 1400°C for 4 hours

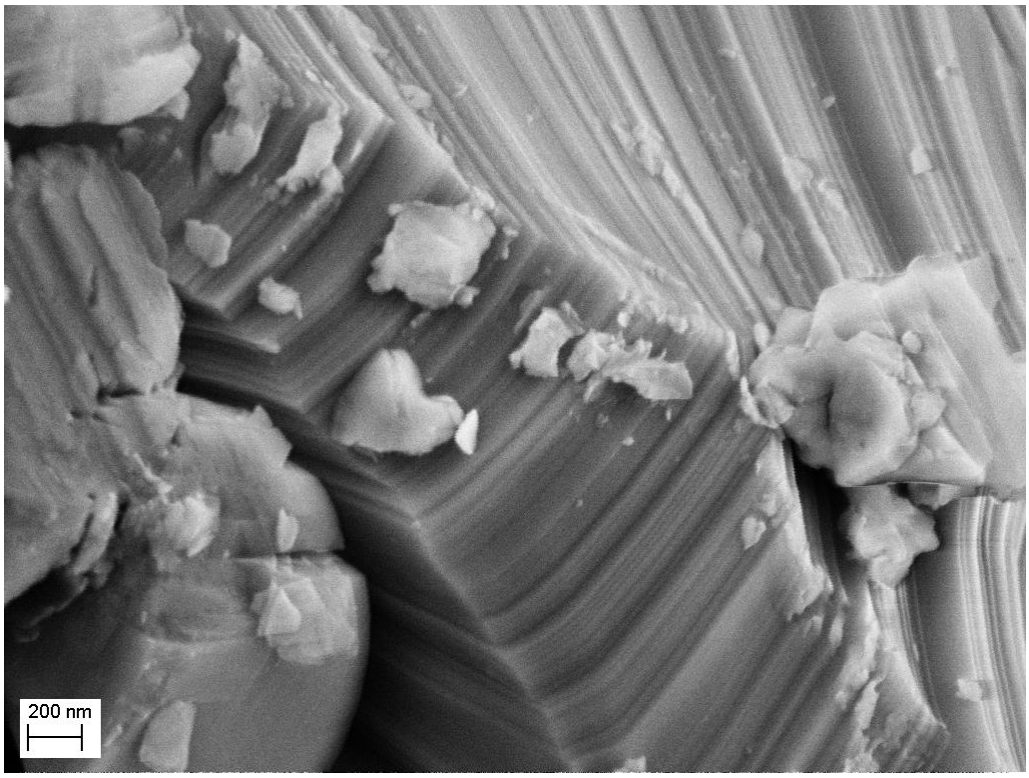

Figure 152, SEM image of of Ti, Al and C powders with molar ratio of 2:1.25:1, sintered at 1400°C for 4 hours

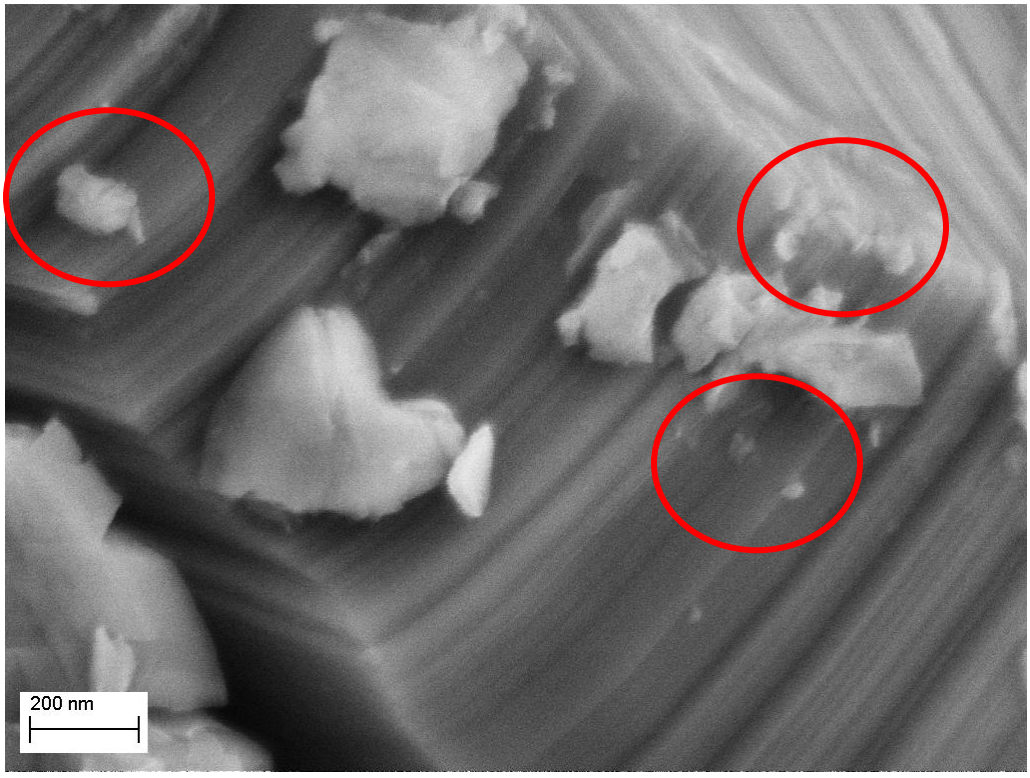

Figure 153, SEM image of of Ti, Al and C powders with molar ratio of 2:1.25:1, sintered at 1400°C for 4 hours

From the EDX analysis, we obtained a ratio between Ti, Al and C of 4.55:1.25:0.84. This is very strange because the amount of carbon is very low meanwhile the titanium is too high.

To adjust the quantity of carbon we lowered the starting aluminum quantity to 1.15 respect to the other elements, reaching a ratio between Ti, Al and C of 2:1.15:1. The powders were milled and sintered with the same procedures and the XRD analysis is shown below, in Figure 154.

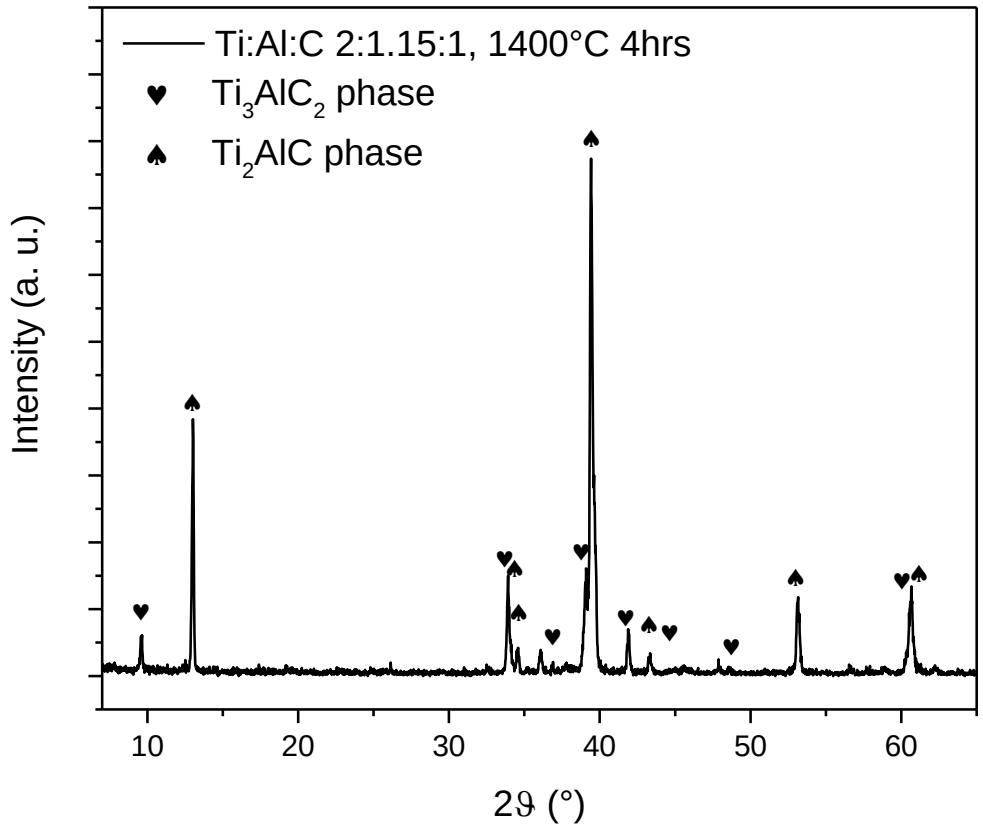

Figure 154, XRD pattern of Ti, Al and C powders with molar ratio of 2:1.15:1, sintered at 1400°C for 4 hours

With this initial composition the peaks of the 211 phase shows the correct intensities, but a small fraction of Ti_3AlC_2 is still present, meaning that the aluminum content is too low.

The SEM images we took from these samples, in Figure 155, Figure 156 and Figure 157, show always the layered structures and small particles (circled) with uncertain forms because they are too small to obtain sharp images of them.

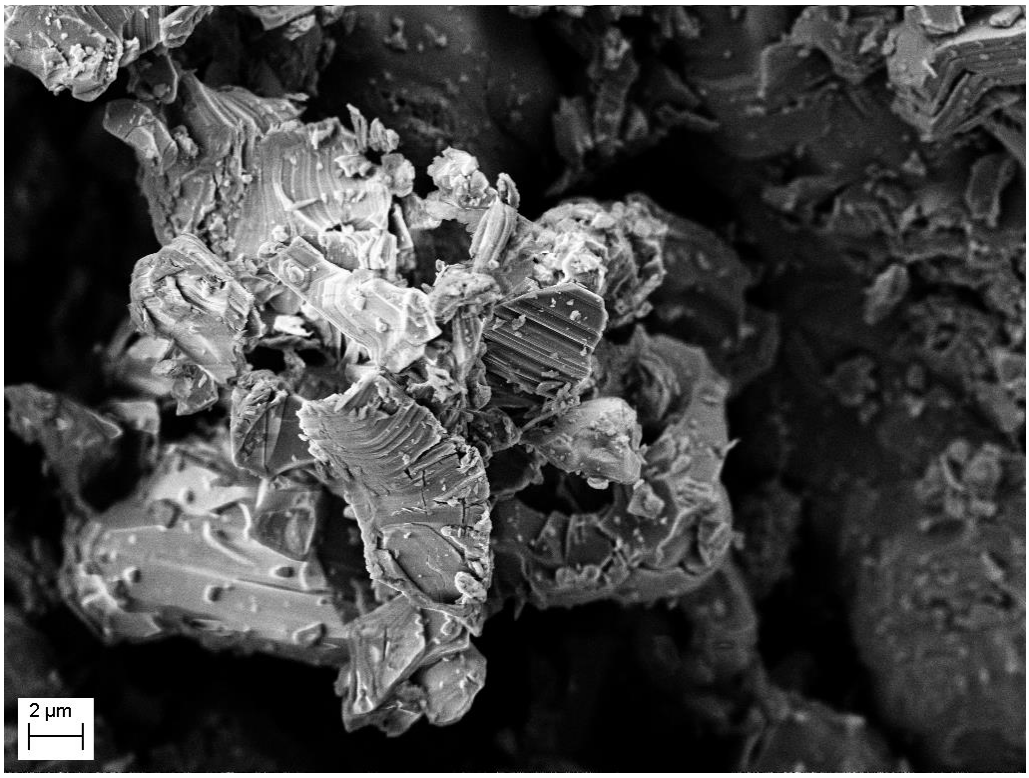

Figure 155, SEM image of of Ti, Al and C powders with molar ratio of 2:1.15:1, sintered at 1400°C for 4 hours

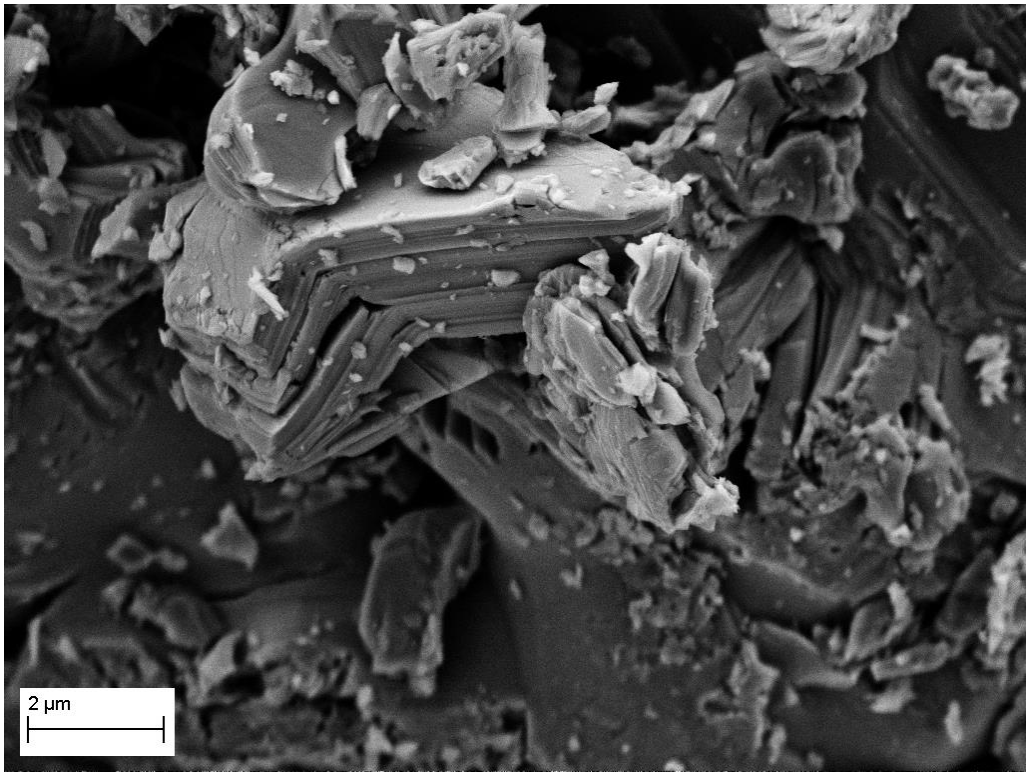

Figure 156, SEM image of of Ti, Al and C powders with molar ratio of 2:1.15:1, sintered at 1400°C for 4 hours

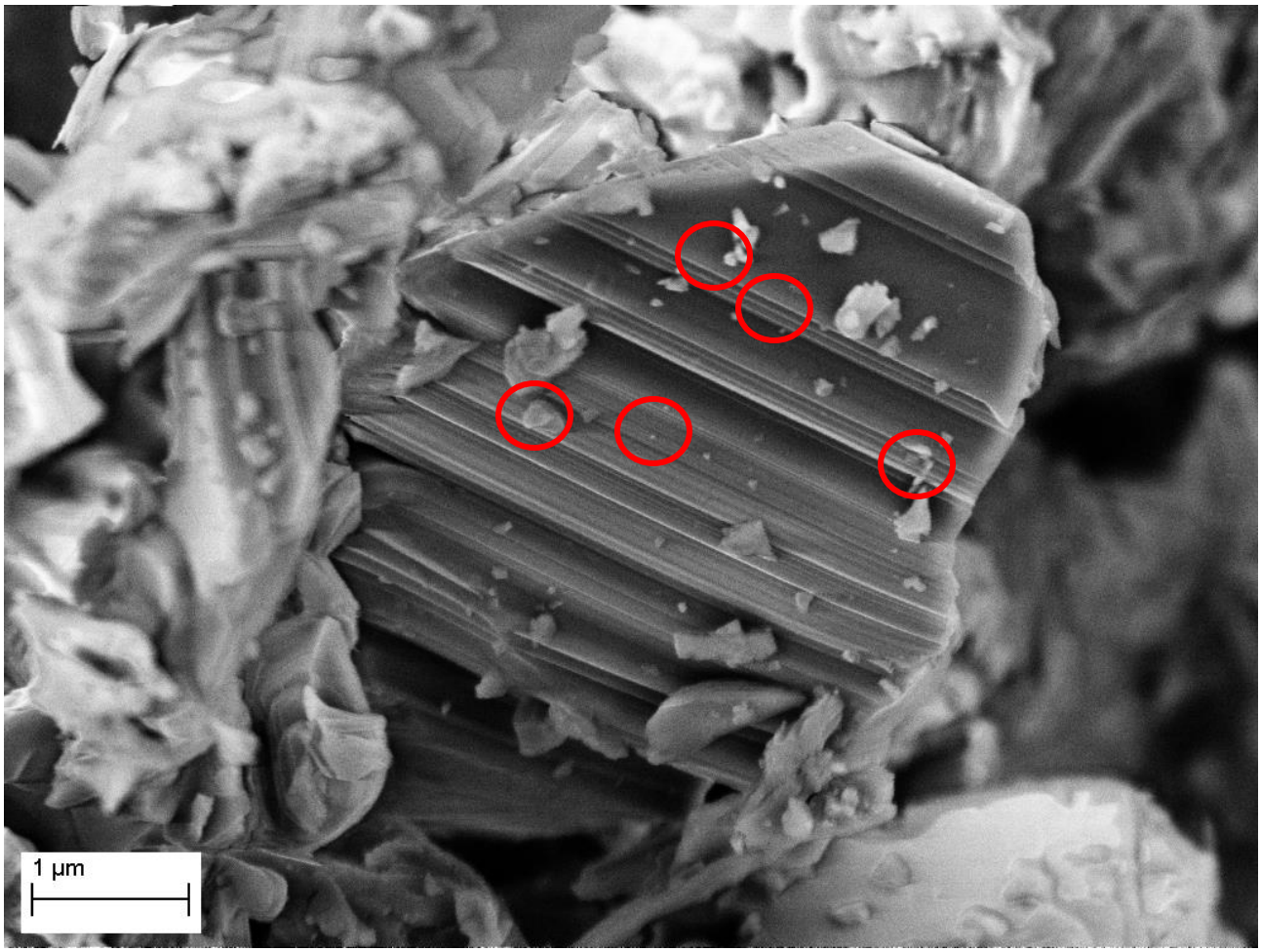

Figure 157, SEM image of of Ti, Al and C powders with molar ratio of 2:1.15:1, sintered at 1400°C for 4 hours

From EDX the atomic ratio between Ti, Al and C is 3.97:1.15:0.89. The quantity of carbon is still lower with respect to the carbon present before the sintering, even if the obtained stoichiometry is slightly better than the previous result. Titanium instead is too high.

From the XRD results, for the next sample we used a molar quantity of Al in-between the previous two, 1.20. Also for these powders, the milling and sintering were conducted in the same conditions. The XRD pattern of these last samples can be seen in Figure 158.

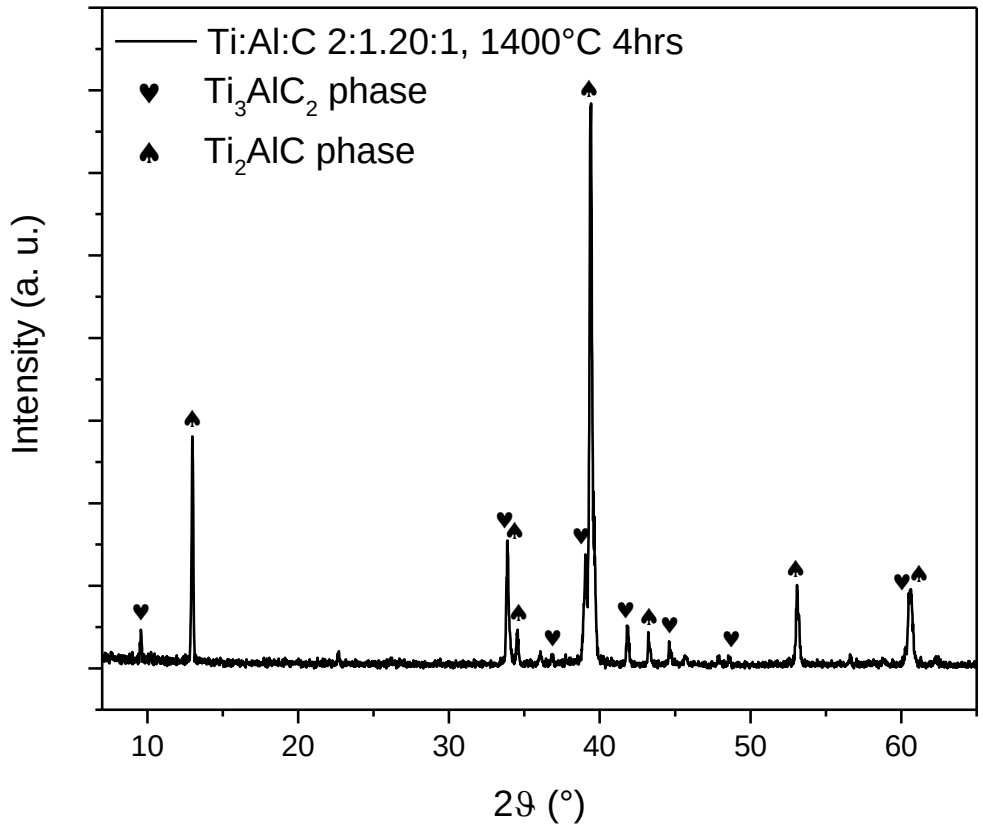

Figure 158, XRD pattern of Ti, Al and C powders with molar ratio of 2:1.20:1, sintered at 1400°C for 4 hours

With a molar ratio between Ti, Al and C of 2:1,20:1 we obtained the best results, because the peaks from Ti_3AlC_2 are the lowest obtained so far. This means that the right amount of aluminum to obtain the purest possible powder of 211 phase is near to this ratio. We took also SEM images from this sample, shown below in Figure 159, Figure 160 and Figure 161. The morphology is very similar to the previous two samples, with the layered structures and small particles. In the last image a kink can be seen clearly in the laminate structure, confirming the ductility of the material.

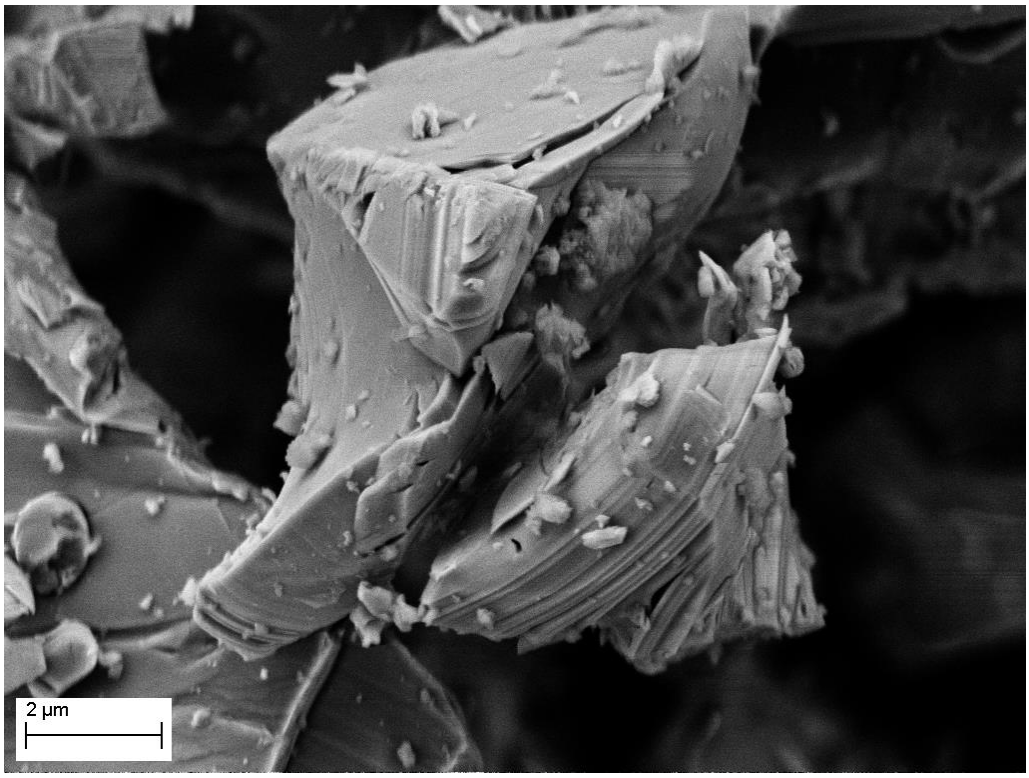

Figure 159, SEM image of of Ti, Al and C powders with molar ratio of 2:1.20:1, sintered at 1400°C for 4 hours

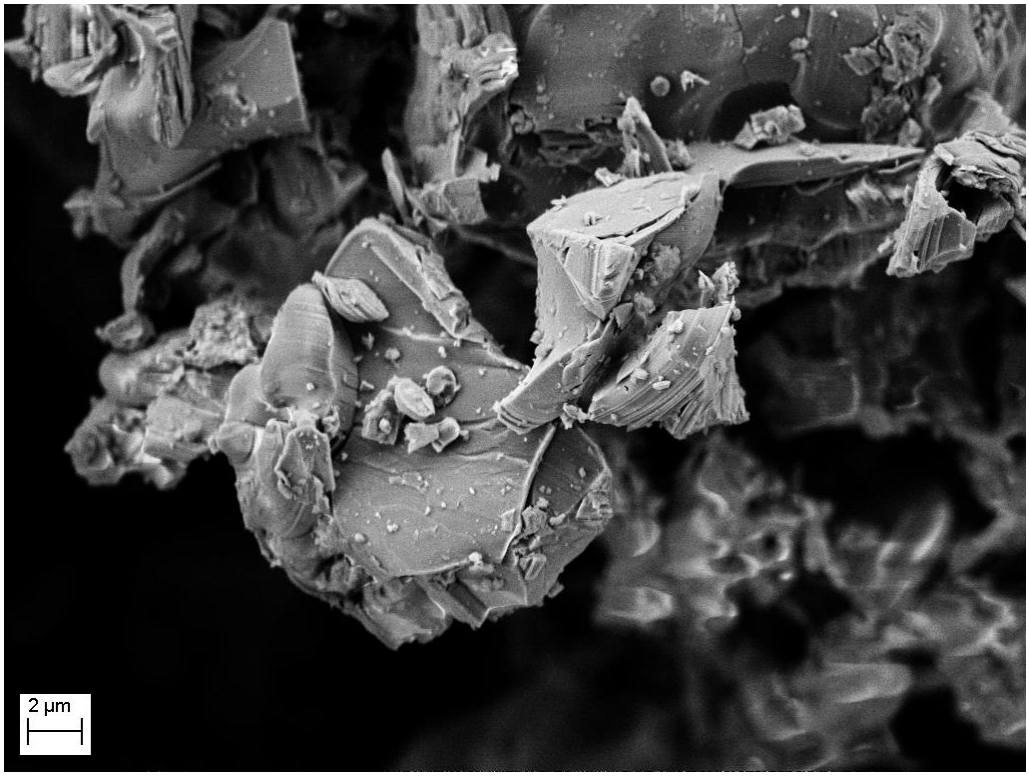

Figure 160, SEM image of of Ti, Al and C powders with molar ratio of 2:1.20:1, sintered at 1400°C for 4 hours

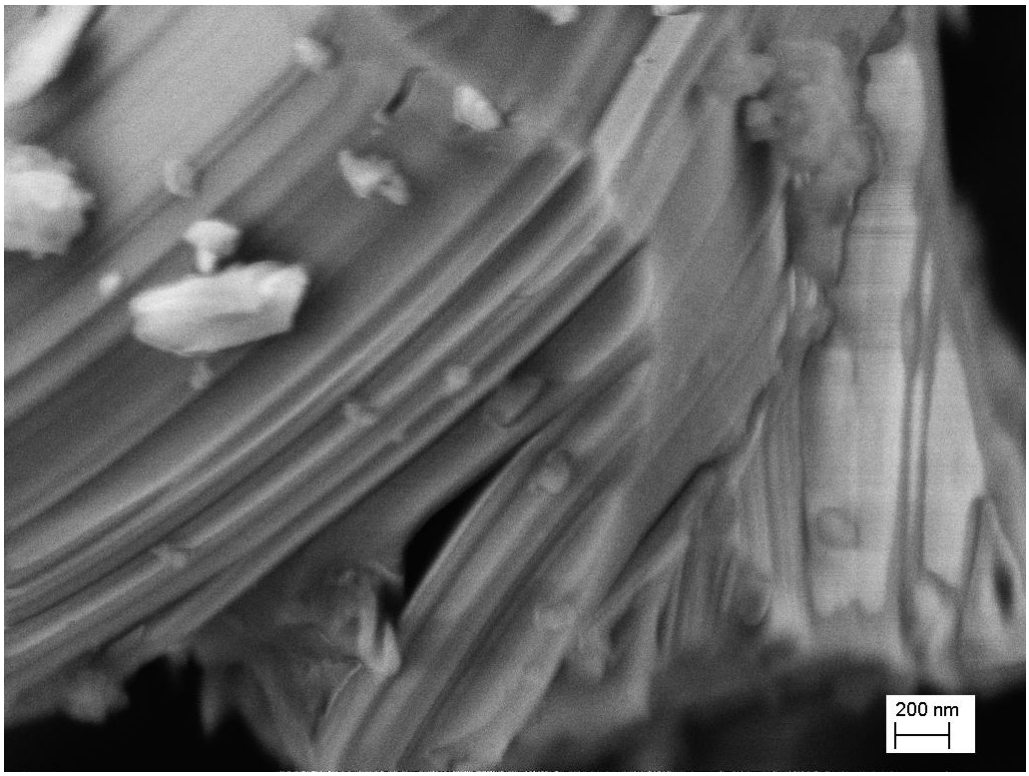

Figure 161, SEM image of of Ti, Al and C powders with molar ratio of 2:1.20:1, sintered at 1400°C for 4 hours

From the EDX, also with this sample the atomic values of each element are not equal to the starting one. In this case, we have a ratio between Ti, Al and C of 4.45:1.20:0.87. The values for each element are between the two previous samples, albeit with a consistent drift for Ti and a minor one for C. It is worth to note that the EDX measurements could be affected by the sensitivity of the detector and the obtained values could be not very accurate.

After these samples, we decided to sieve the aluminum powder in order to have, for the three elements, similar particle sized. We replicated the last synthesis, both as molar ratio and as milling and sintering conditions. From XRD the result is similar to the previous one, meaning that the particle size reduction did not help so much in the formation of pure Ti_2AlC albeit a theoretically more homogeneous mixture of the precursors, as can be seen in Figure 162. Some less intense peaks related to Ti_3AlC_2 however disappeared, while the remaining peaks have a lower height compared to those from Ti_2AlC. The first peak at 13.02° for the 211 phase, that is the reflection of the [002] direction, has a larger intensity than the expected one, meaning that perhaps there is a preferred growth direction.

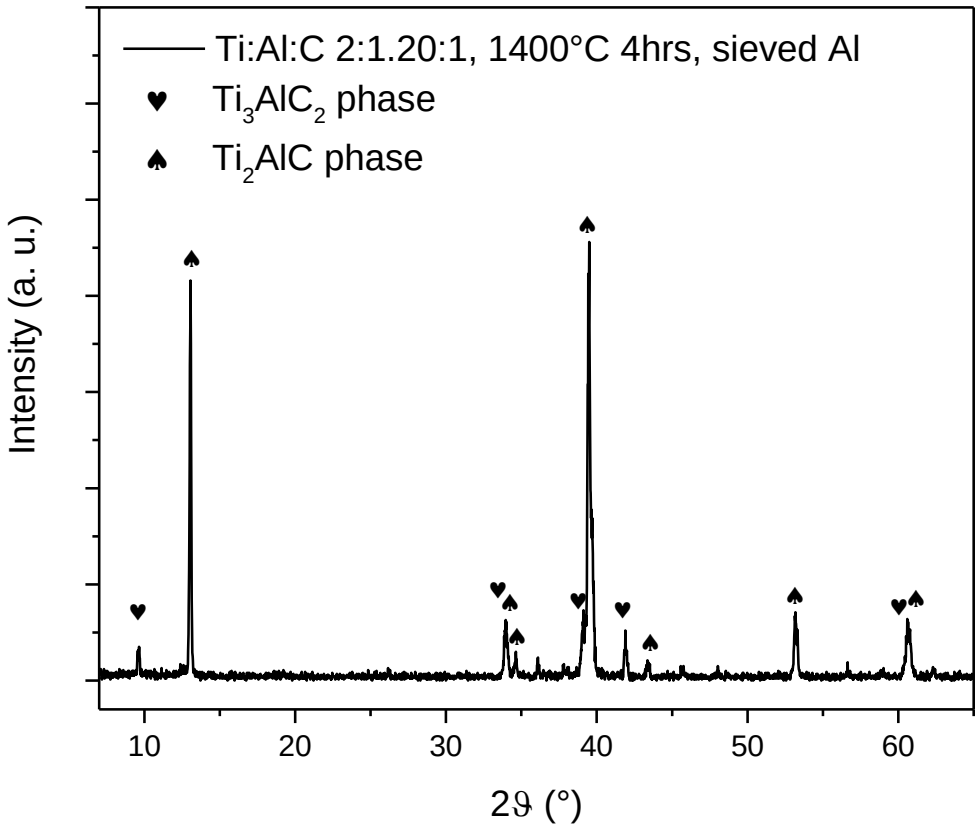

Figure 162, XRD pattern of Ti, Al and C powders with molar ratio of 2:1.20:1, sintered at 1400°C for 4 hours

We tried to understand if the observed behavior could be related to the milling process, varying the parameters of rotational speed and time in order to obtain a better mixing of the powders. The first trial was conducted increasing the revolutions per minute of the polyethylene jar, going from 300 rpm to 370 rpm for 18 hours. The initial molar ratio was maintained constant, mixing 2 moles of Ti, 1.20 of Al and 1 of C. After the milling process we made an XRD characterization to control if anomalous phases (mainly relatable to alumina) were formed during this step. In Figure 163 it is possible to see the XRD pattern. The only crystalline phases are ascribable to titanium, aluminum and graphite, while there are not evidences of the presence of Al_2O_3 or some combination of the three precursors, like TiC or aluminum alloys.

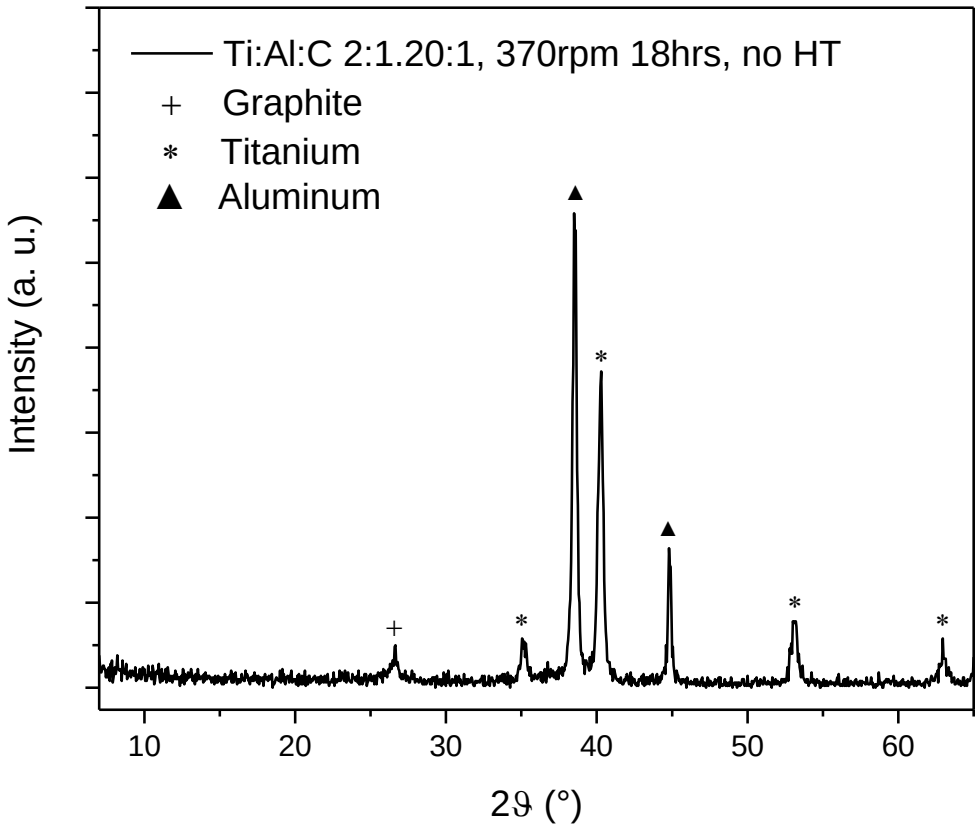

Figure 163, XRD pattern of Ti, Al and C powders with molar ratio of 2:1.20:1, ball milled at 370 rpm for 18 hours

We sintered this sample with the standard sintering procedure, i.e. at 1400°C for 4 hours. The bulk material after the treatment was ground by hand and analyzed again by XRD to evaluate if the new milling has sorted some effect. The pattern is reported below, in Figure 164.

As can be noted the intensities of the peaks from Ti_3AlC_2 are greatly reduced and the estimated quantity of the 312 phase is slightly over 10 mol%.

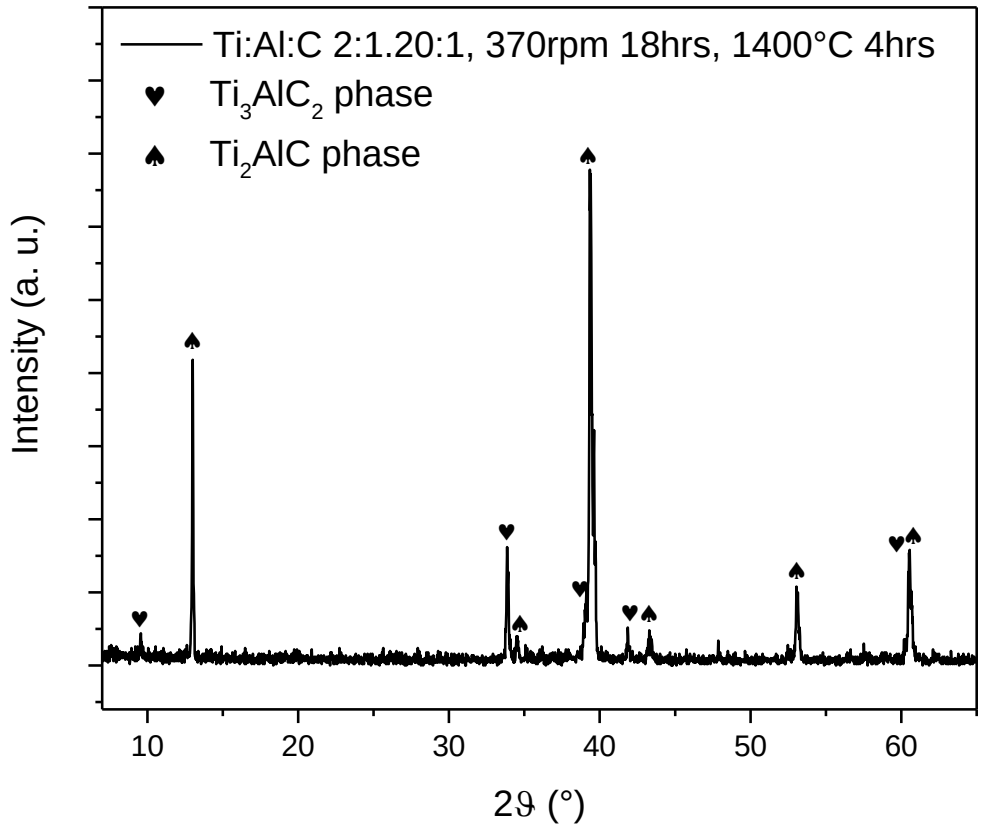

Figure 164, XRD pattern of Ti, Al and C powders with molar ratio of 2:1.20:1, ball milled at 370 rpm for 18 hours and sintered at 1400°C for 4 hours

In order to further reduce the quantity of the 312 phase, we decided to increase the time of milling, not the speed, because at higher rpm the polyethylene jar would be damaged. We extended the time from 18 to 24 hours, with a rotational speed of 370 rpm.

Unluckily, after 24 hours, we discovered that these milling parameters are too harsh for the powder. The particle size of the metal powders was so small that a simple electrostatic sparkle between the jar and the glove of the operator during the opening caused the complete burning of the sample, due to the very low ignition energy of the metal powders. We investigated what remained from this sample with XRD, looking for unexpected results or phases. As can be seen below, in Figure 165, there are peaks from TiC and graphite, but also from small amount of Ti_2AlC and Ti_3AlC_2. There are also three unidentified peaks that probably are related to the byproducts of the combustion of the metal powders with polyethylene.

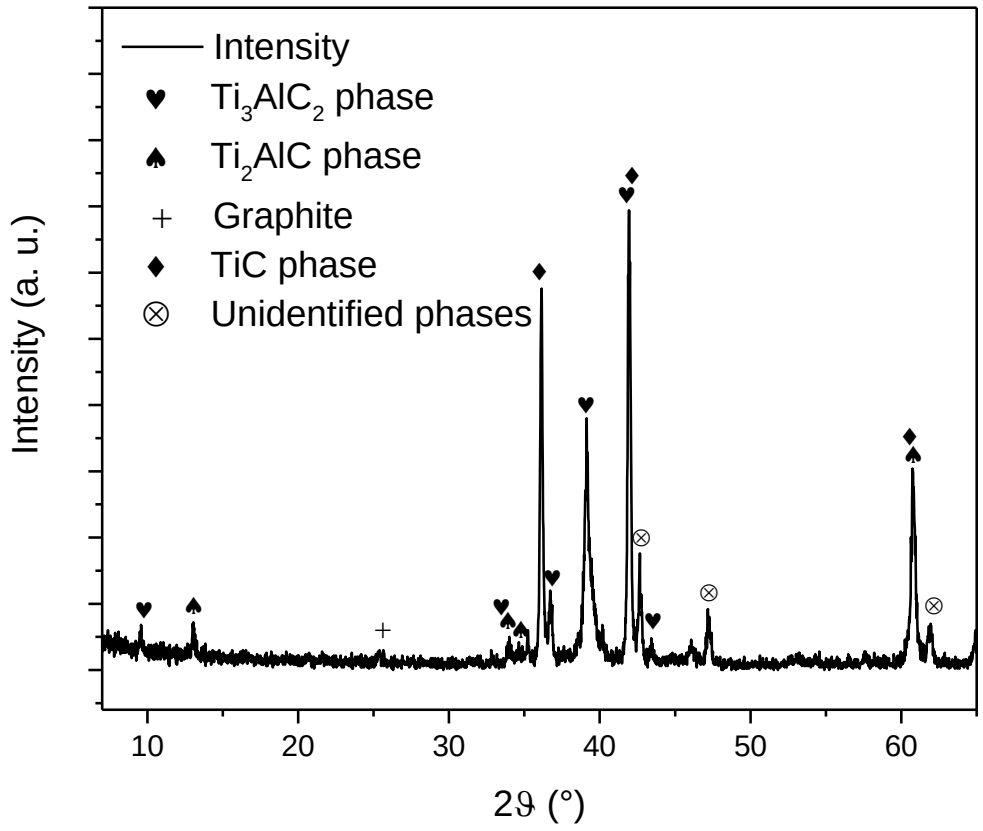

Figure 165, XRD pattern of Ti, Al and C powders with molar ratio of 2:1.20:1, burned after milling at 370rpm for 24 hours

After the destruction of the sample due to the prolonged time of milling we decided to revert back to 300 rpm for 18 hours to avoid metallic flames. We instead concentrated on the research of the best conditions for the sintering. At first during the sintering, we cover the vessel containing the powders because at 1400°C the volatility of aluminum is not negligible. In this way, inside the vessel there should be a less turbulent and slower flow of argon, and the evaporation of Al should be reduced. The first sintered sample was analyzed by XRD (see Figure 166). The intensity of the peaks related to Ti_3AlC_2 is very small, confirming that with the flow of argon some aluminum is removed at high temperature and the cover could represent a good way to minimize the loss.

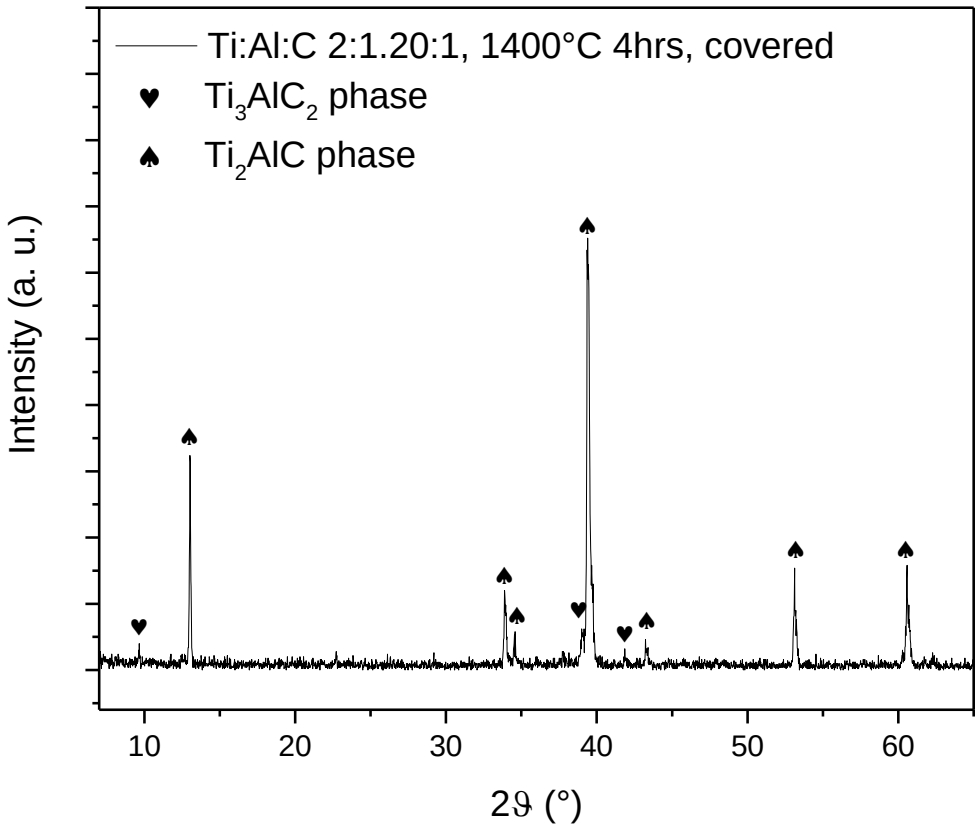

Figure 166, XRD pattern of Ti, Al and C powder with molar ratio of 2:1.20:1, sintered in covered vessel at 1400°C for 4 hours

With this consideration in mind, we slightly increased the quantity of aluminum, using a molar ratio between Ti, Al and C of 2:1.22:1. The sample with the higher content of aluminum was milled at 300 rpm for 18 hours and sintered again at 1400°C for 4 hours but inside the covered vessel. The results from the XRD analysis are reported below, in Figure 167. There are only two residual peaks from the 312 phase, meaning that the quantity of it is very low. After these encouraging results, we made another sample with the same parameters, in order to check if there were some small error during the preparation, e.g. weight tolerances.

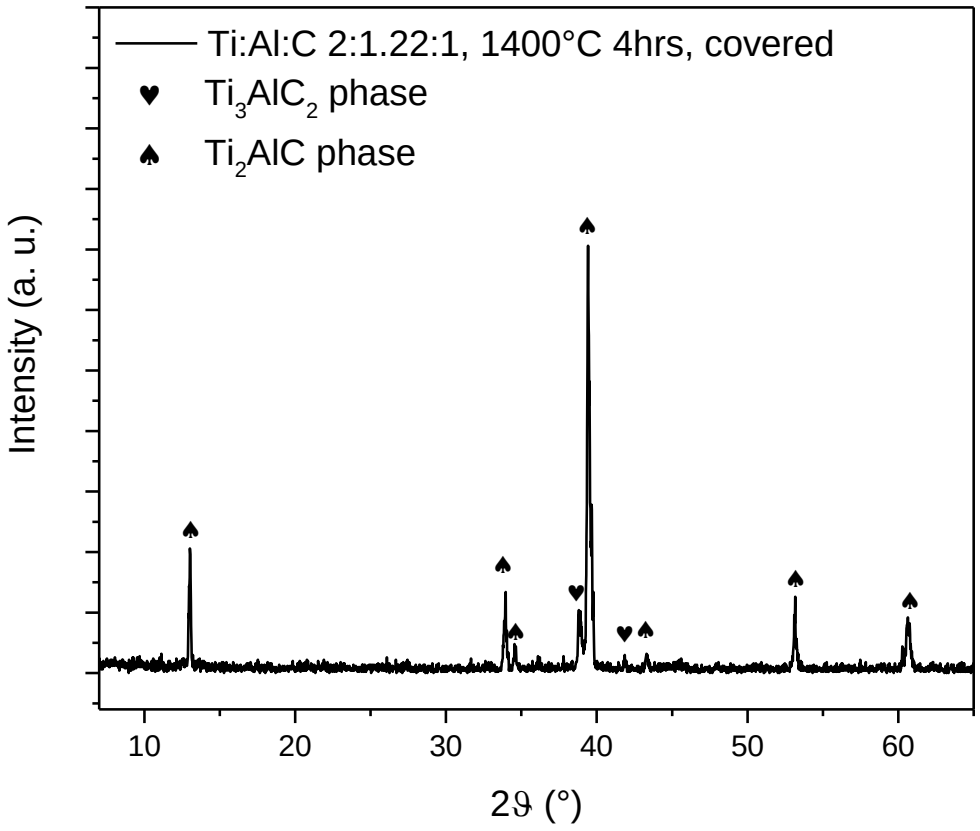

Figure 167, XRD pattern of Ti, Al and C powder with molar ratio of 2:1.22:1, sintered in covered vessel at 1400°C for 4 hours

The next sample was prepared in the same way, paying more attention on the preparation stages. It was milled at 300 rpm for 18 hours and sintered at 1400°C for 4 hours.

The results were very good, as can be seen below, in Figure 168. There is only one remaining peak from the 312 phase and its quantity can be considered marginal.

To test the repeatability of these results we made other two samples in the same way. The XRD patterns are reported in Figure 169 and Figure 170.

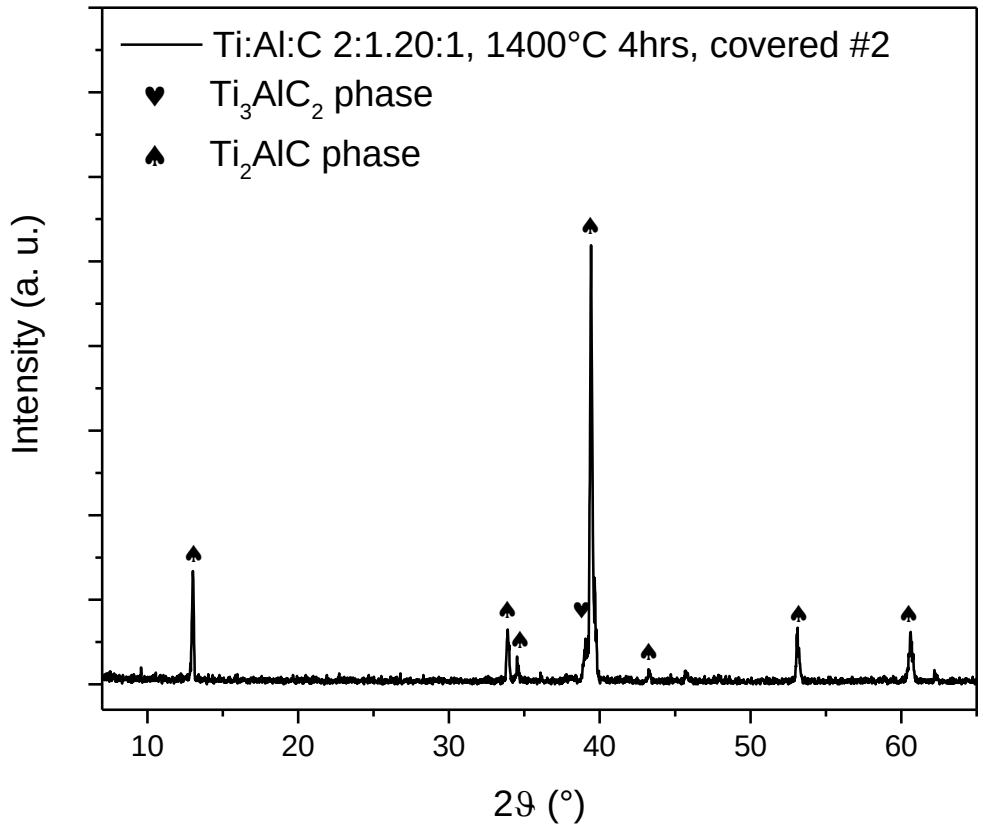

Figure 168, XRD pattern of Ti, Al and C powder with molar ratio of 2:1.22:1, sintered in covered vessel at 1400°C for 4 hours, sample #2

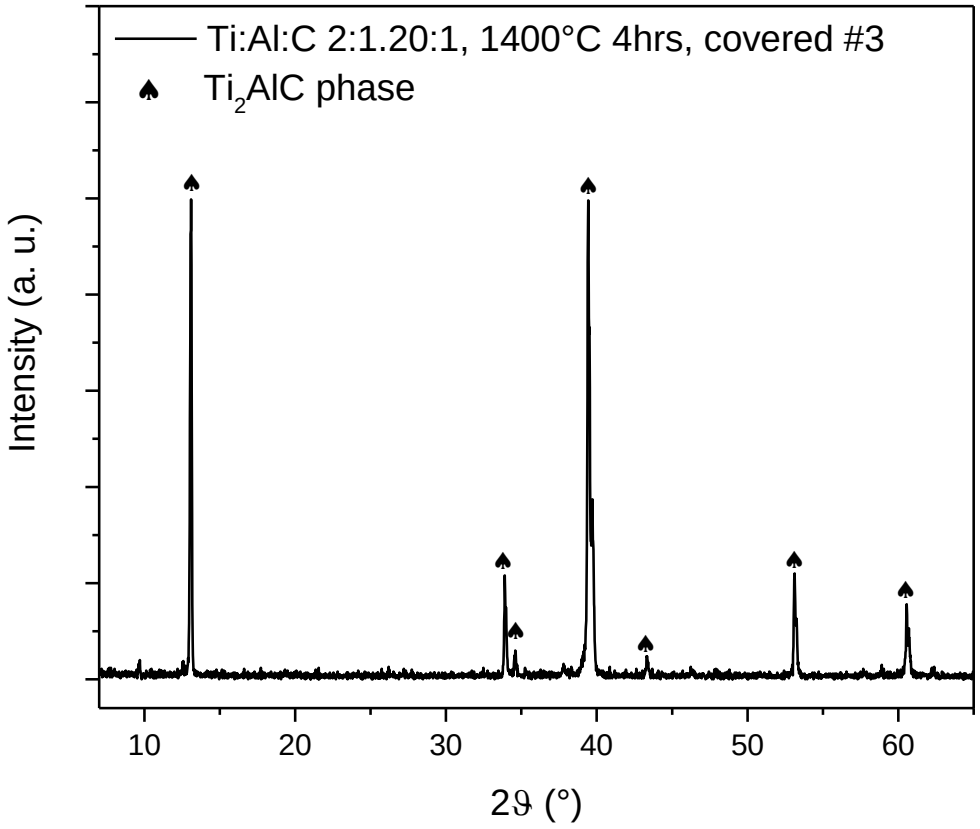

Figure 169, XRD pattern of Ti, Al and C powder with molar ratio of 2:1.22:1, sintered in covered vessel at 1400°C for 4 hours, sample #3

The sample presented in Figure 169, the #3, does not show peaks from Ti_3AlC_2, albeit the first peak is particularly intense in comparison to the others. This does not happen with the sample #4, that shows a XRD pattern with only Ti_2AlC with the right intensities (see Figure 170).

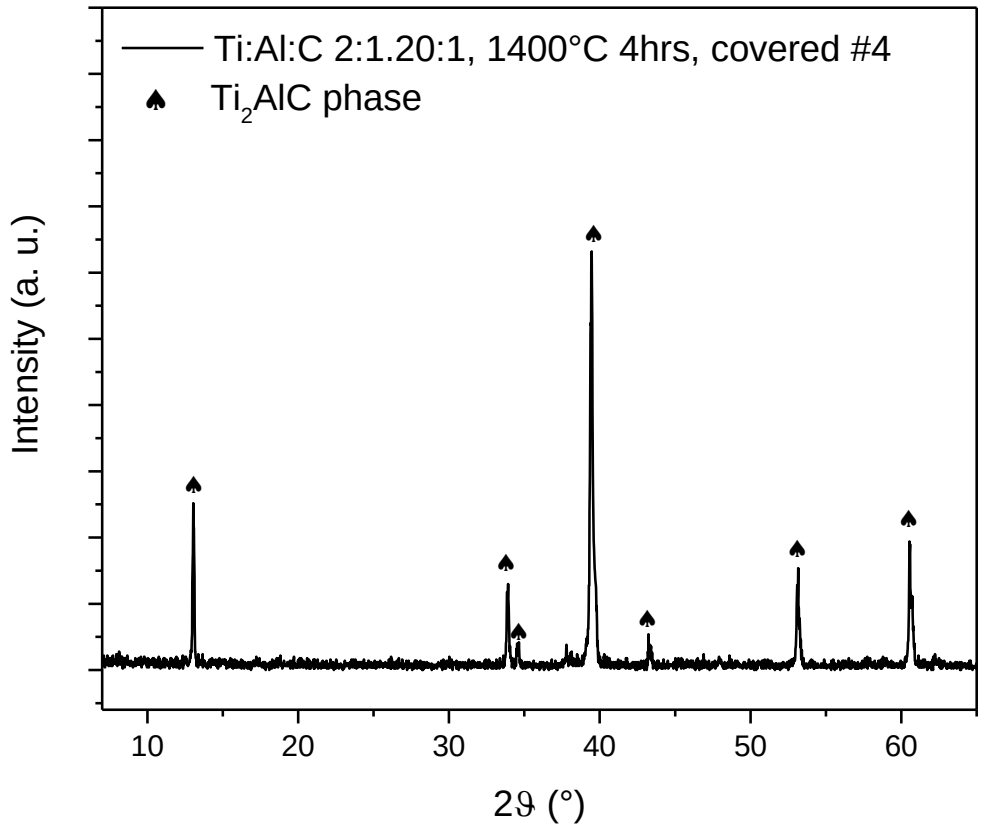

Figure 170, XRD pattern of Ti, Al and C powder with molar ratio of 2:1.22:1, sintered in covered vessel at 1400°C for 4 hours, sample #4

For a better visual comparison, we grouped the XRD patterns of the four last samples in one graph, in Figure 171. It is possible to see, from the top to the bottom, that there is a decrease of the small peak at the feet of the most intense one at 39.40°. This means that the quantity of Ti_3AlC_2 is decreased, giving a nearly perfect sample without impurities.

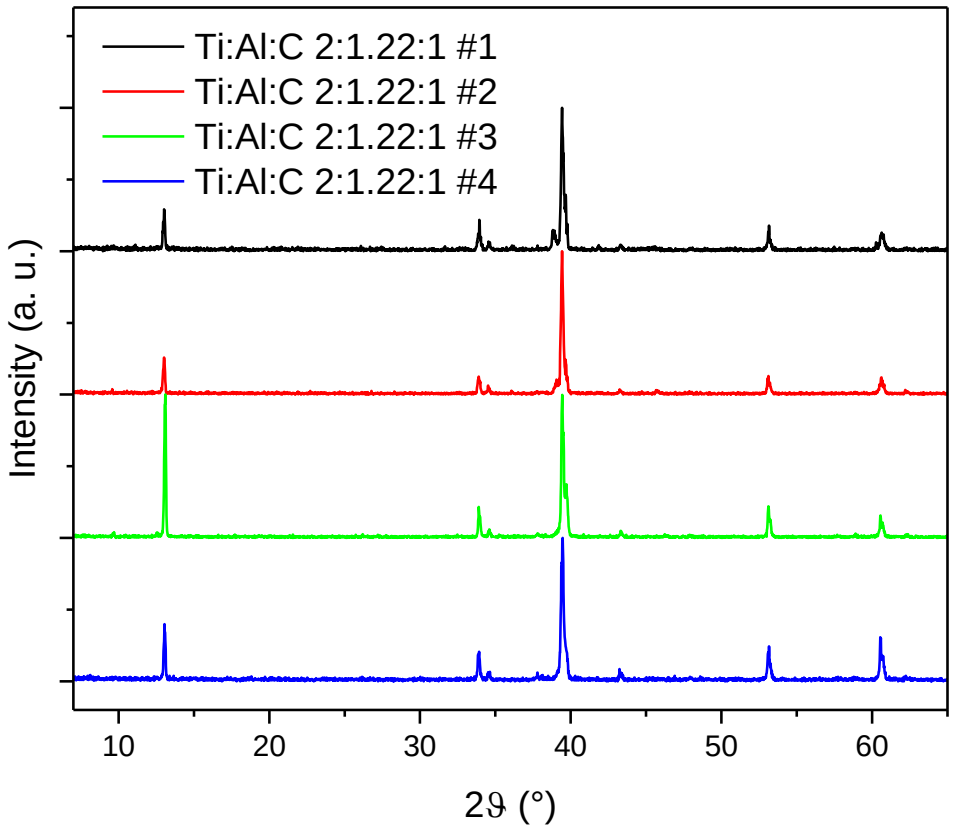

Figure 171, XRD patterns comparison of 4 samples of Ti, Al and C powder with molar ratio of 2:1.22:1, sintered in covered vessel at 1400°C for 4 hours

The best parameters for the sintering of Ti_2AlC with negligible traces of Ti_3AlC_2 can be reassumed as follow:

1. Starting stoichiometry: 2 moles of Ti + 1.22 moles of Al + 1 mole of C
2. Milling: ball milling in polyethylene jar with 5 mm alumina sphere at 300 rpm for 18 hours, weight ratio between powders and sphere of 1:50
3. Sintering: Ar flow of 0.5 L/min, sample in a covered vessel, ramp of 10°C/min up to 1400°C, dwell time of 4 hours and natural cooling.

With these parameters, we were able to prepare suitable powder for the next step that is the addition of TiC for the sintering of Ti_3AlC_2.

We started using a commercial 211 phase powder, the Maxthal 211 from Kanthal, as base for the addition of TiC because our quantities of Ti_2AlC were too low for an extensive use. The new samples have not to be stored and managed in glove box with inert atmosphere because they do not react with oxygen or nitrogen at room temperature. The sintering process has to be conducted with argon because the high temperatures favor the reactivity toward these gases.

The very first test was done following the recipe obtained from prof. Barsoum: Ti_2AlC and TiC are mixed with a molar ratio of 1:1 and then ball milled for 18 hours at 300 rpm in polyethylene jar with alumina spheres. The sintering parameters, as stated in the recipe, are slightly changed compared to those used for the previous sintering of the 211 phase, because the top temperature is lowered to 1350°C and the dwell time shortened to 2 hours, but the heating ramp, cooling and closed vessel are retained.

After the heat treatment, the sample is ground by hand in an agate mortar and analyzed by XRD. The relative pattern is reported below, in Figure 172.

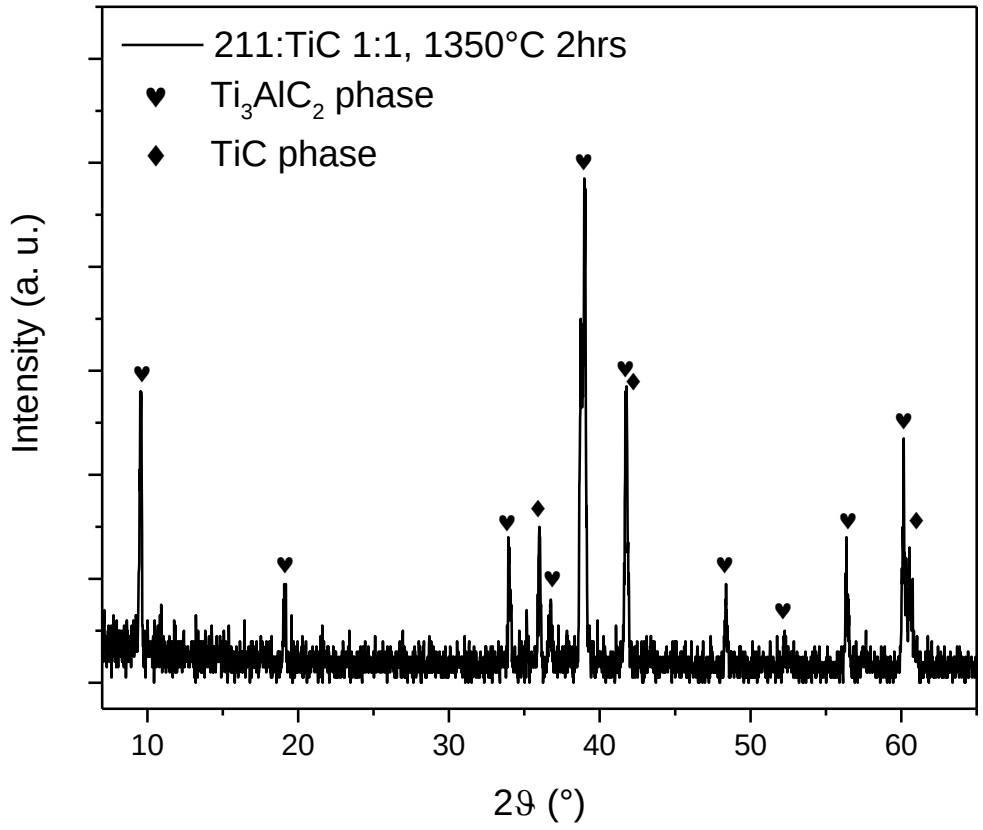

Figure 172, XRD pattern of 211 and TiC powder with molar ratio of 1:1, sintered at 1350°C for 2 hours

There are not traces of unreacted Ti_2AlC, but, aside the Ti_3AlC_2 peaks, there are two peaks ascribable to TiC that did not react during the sintering. This can be due to the high starting loading of TiC or a too short sintering time that did not allow the complete diffusion of the species.

For the next samples, we decided to change the dwell time, lengthening it to 4 hours, and decreasing the TiC molar ratio. In this way we prepared three samples with 211:TiC ratios of 1:1, 1:0.9 and 1:0.8. All of them were sintered with the same treatment at 1350°C for 4 hours in a closed vessel. The XRD patterns for each sample are shown below, in Figure 173, Figure 174 and Figure 175. For a better comparison, all the three patterns are presented together in Figure 176, where two dashed rectangles highlight the peaks of TiC.

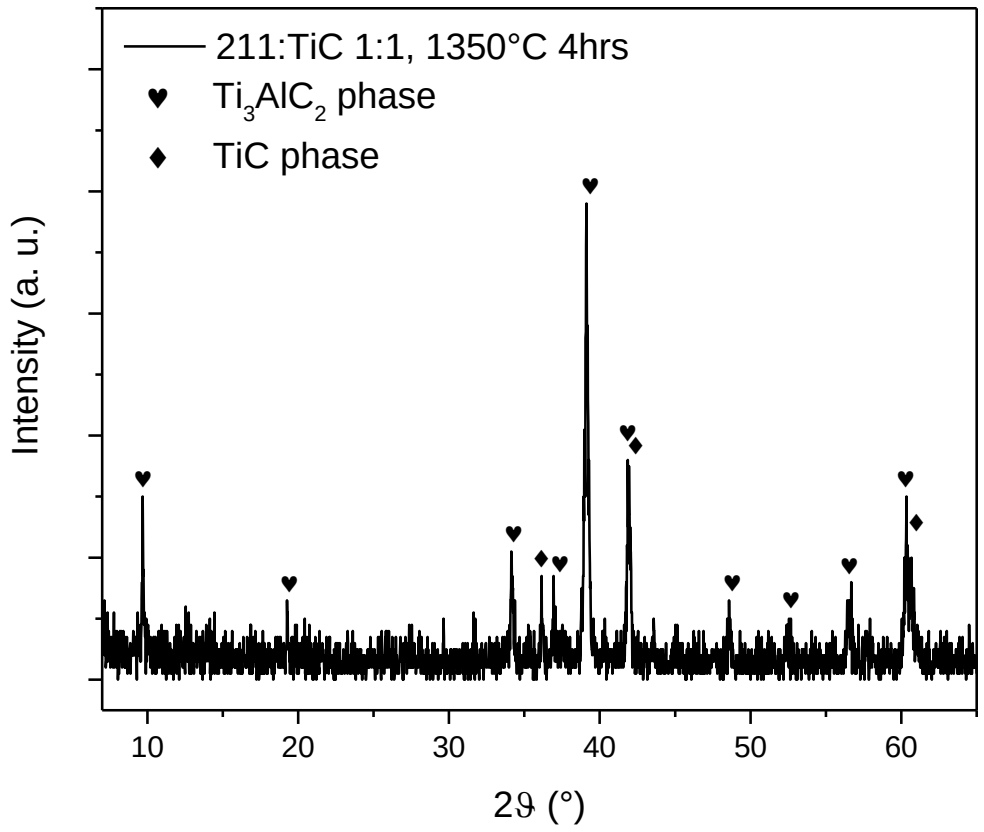

Figure 173, XRD pattern of 211 and TiC powder with molar ratio of 1:1, sintered at 1350°C for 4 hours

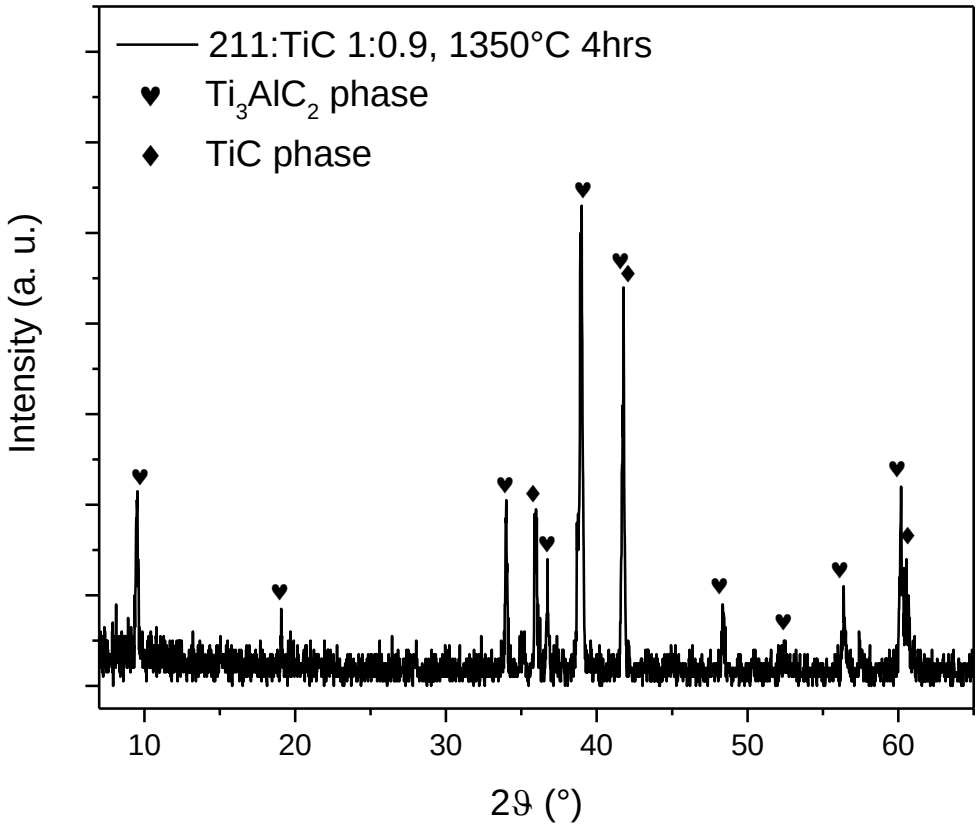

Figure 174, XRD pattern of 211 and TiC powder with molar ratio of 1:0.9, sintered at 1350°C for 2 hours

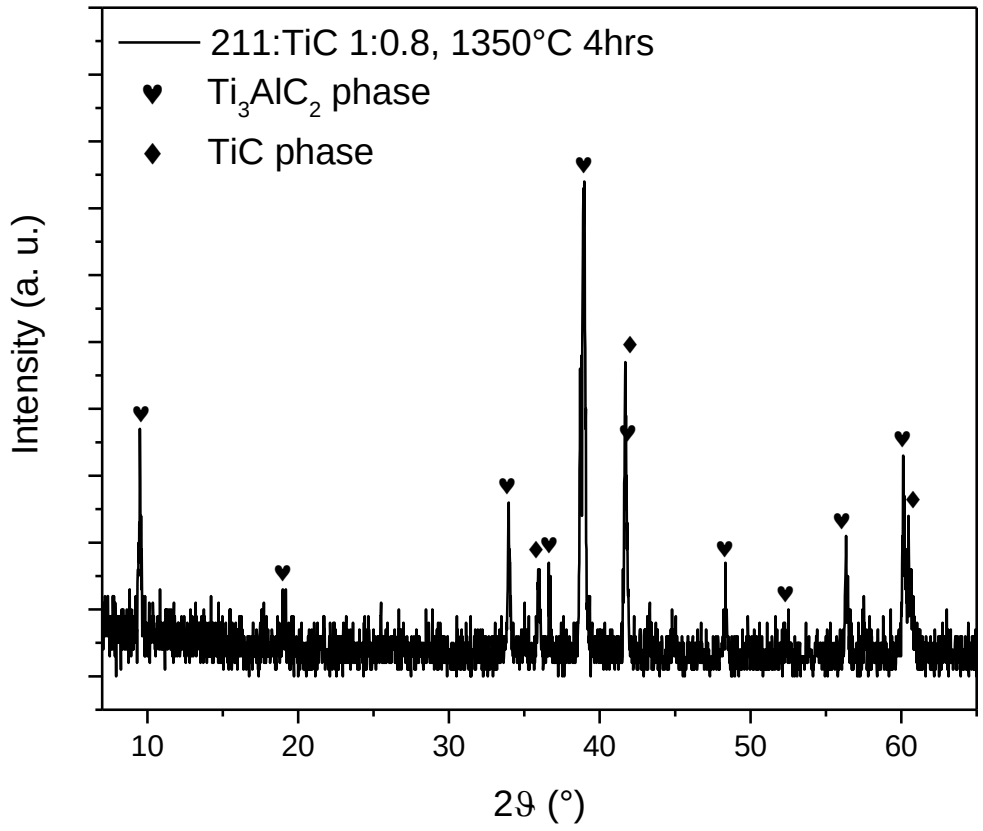

Figure 175, XRD pattern of 211 and TiC powder with molar ratio of 1:0.8, sintered at 1350°C for 2 hours

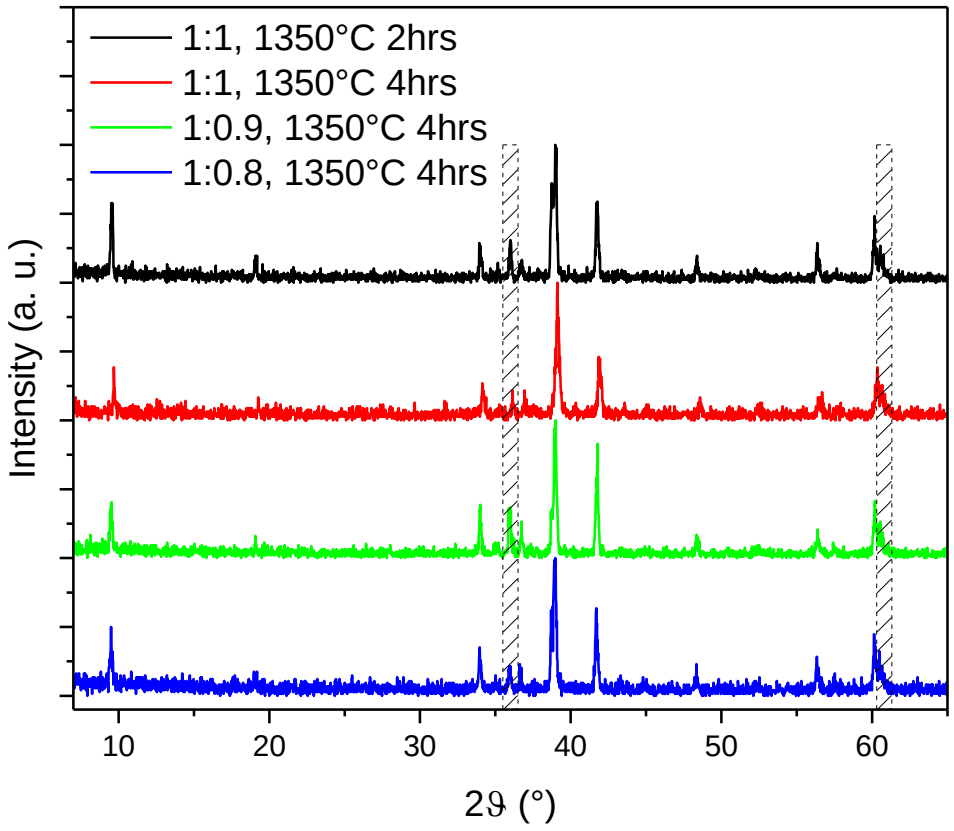

Figure 176, XRD patterns comparison of 211 and TiC powders with molar ratio of 1:1, 1:0.9 and 1:0.8, sintered at 1350°C for 2 hours or 4 hours. The dashed rectangles highlight the TiC peaks

As can be noted there is not a clear correlation between the starting and the unreacted quantity of TiC. The reason behind the remaining quantities of titanium carbide are caused by other mechanism, so we started to study each of them, grouping them under the milling and sintering processes.

The first thing we analyzed was the ball milling influence. The first four samples were milled with the parameters already used for the synthesis of Ti_2AlC, i.e. 300 rpm for 18 hours but probably such conditions are not appropriated for considering the different hardness of the powders. For the next tests, we did not change the rotational speed but the time of milling. Three samples with the same 211: TiC=1:1 molar ratio were treated for 6, 12 and 18 hours and each one was analyzed by XRD before and after the sintering, conducted at 1350°C for 4 hours.

The first sample, milled for 6 hours, shownthe peaks relatable only to TiC and Ti_2AlC (Figure 177), meaning that the process was too short to start an alloying between the species.

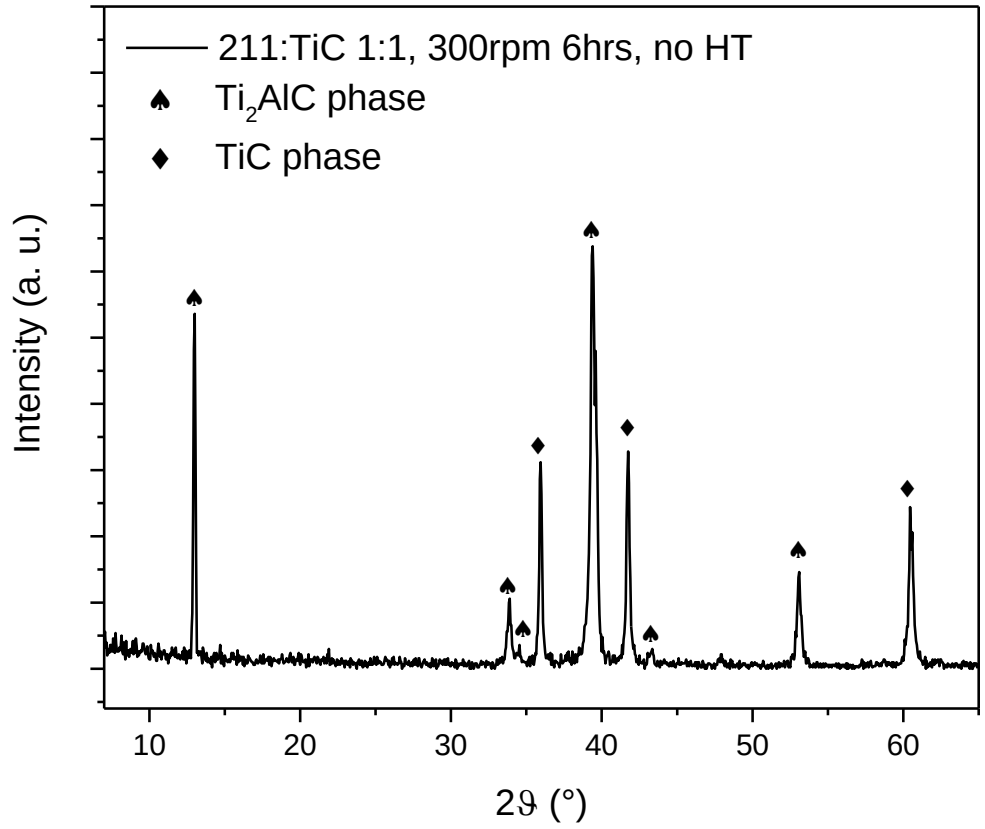

Figure 177, XRD pattern of TiC and Ti_2AlC powders with molar ratio of 1:1, ball milled at 300 rpm for 6 hours

After the sintering, the Ti_3AlC_2 phase is formed, but there are also traces of TiC and Ti_2AlC, as can be seen below, in Figure 178. This means that the milling process is not long enough to ensure a good mixing of the two species and longer times are required. We prepared the next sample with a longer milling, doubling the time to 12 hours.

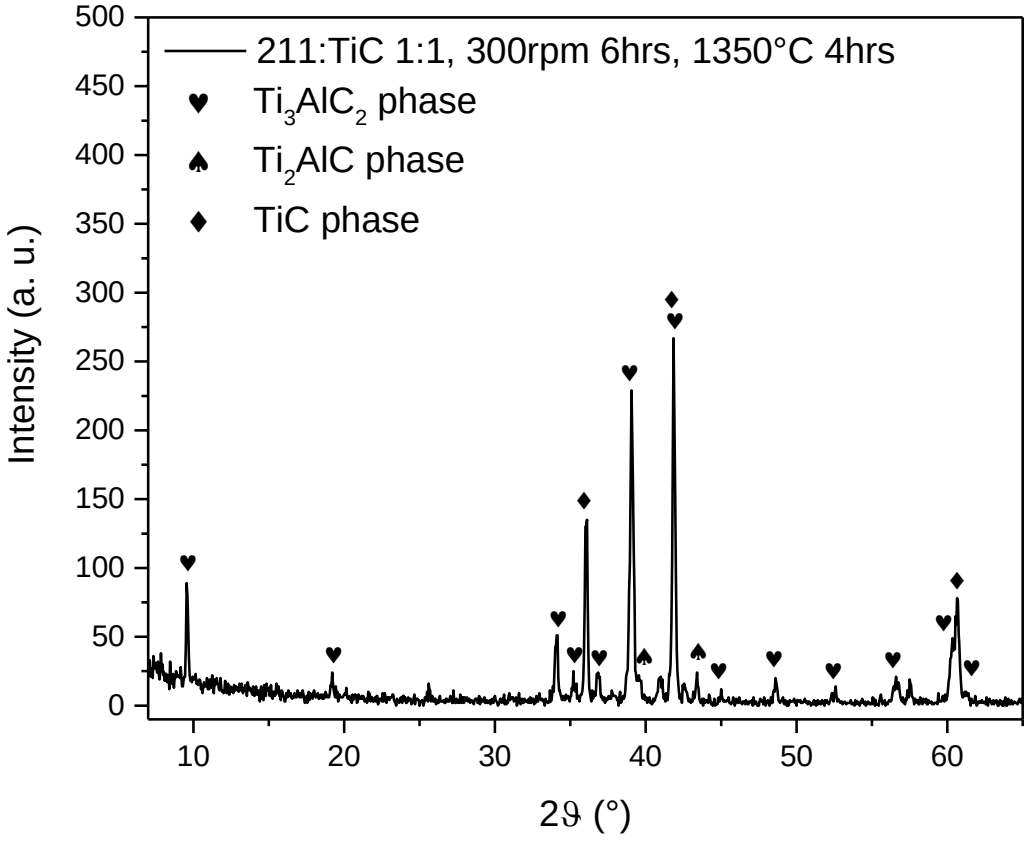

Figure 178, XRD pattern of TiC and Ti2AlC powders with molar ratio of 1:1, ball milled at 300 rpm for 6 hours and sintered at 1350°C for 4 hours

Also for this sample we made XRD analysis after the sintering and its pattern is shown in Figure 179. In this case, with a longer milling time, there are still unreacted TiC and Ti_2AlC, but the peak at 39.50° shown also a weak contribute from another peak at 39.07°, that is ascribable to Ti_3AlC_2. Doubling the time of mixing, the powders of TiC and Ti_2AlC started to react due to the continuous forces that the alumina spheres apply to the grains. We treated also this sample at 1350°C for 4 hours, still in a covered vessel to minimize the loss of aluminum.

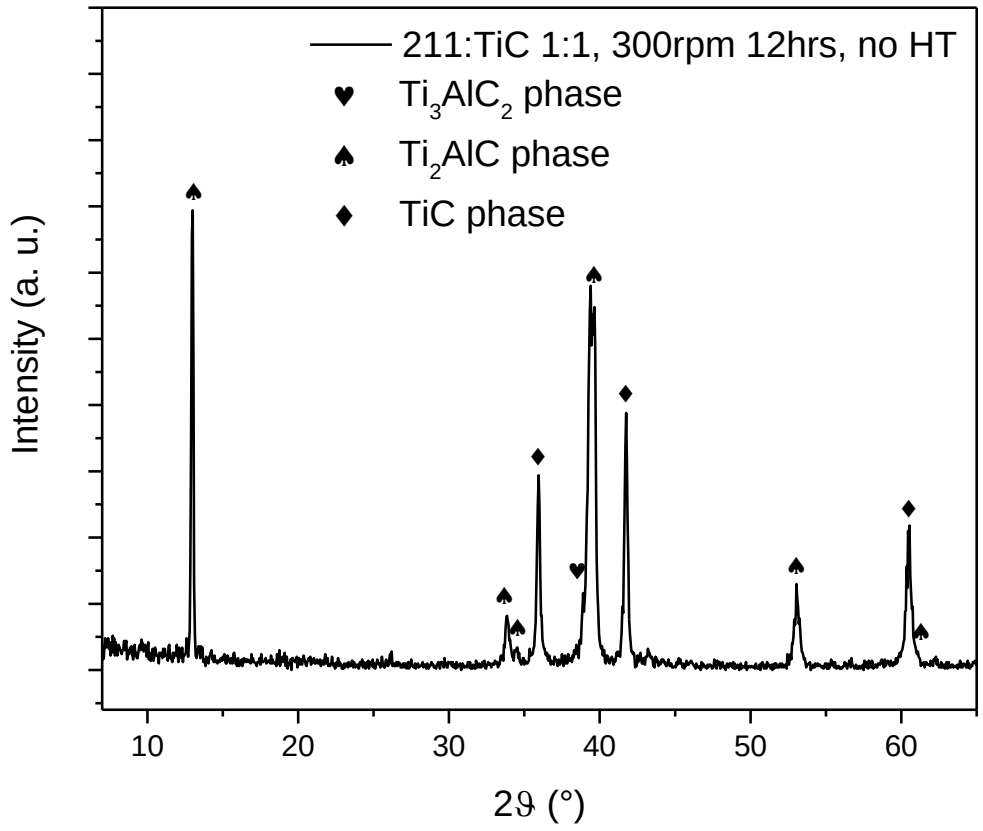

Figure 179, XRD pattern of TiC and Ti2AlC powders with molar ratio of 1:1, ball milled at 300 rpm for 12 hours

After the sintering, the results were better than before because, as can be seen in Figure 180, the intensity of the peak related to the 211 phase at 39.07° is lower and the peak itself is barely visible. The excess of TiC remains constant, meaning that probably the problem cannot be resolved only optimizing the ball milling parameters.

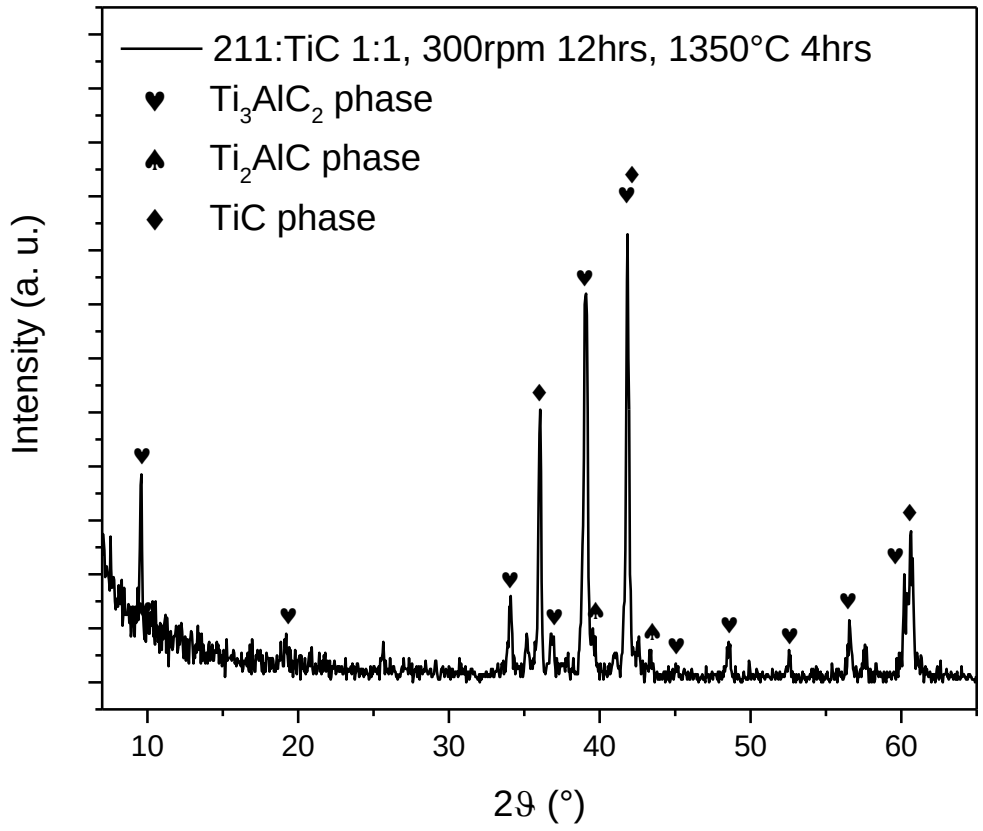

Figure 180, XRD pattern of TiC and Ti2AlC powders with molar ratio of 1:1, ball milled at 300 rpm for 12 hours and sintered at 1350°C for 4 hours

We prepared another sample with the same stoichiometry and milled it for 18 hours, as the initial method, to investigate the crystalline phases that are present after this process. The XRD pattern after the milling and before the sintering can be seen in Figure 181. With the longer milling time, the most intense peak at 39.40° is slightly larger than before because of the contribution of Ti_3AlC_2 that broadens the base. It is related to the two previous samples because the contribution of the 312 phase is for each sample more important, confirming that the action of the alumina sphere is energetic enough to promote the alloying of the more complex phase. However, the quantity of the 312 phase is still very low, for a complete conversion of 211 to 312 probably several days or weeks should be requested, but for such prolonged milling the polyethylene jar probably could contaminate the powders for the excessive stress and heat.

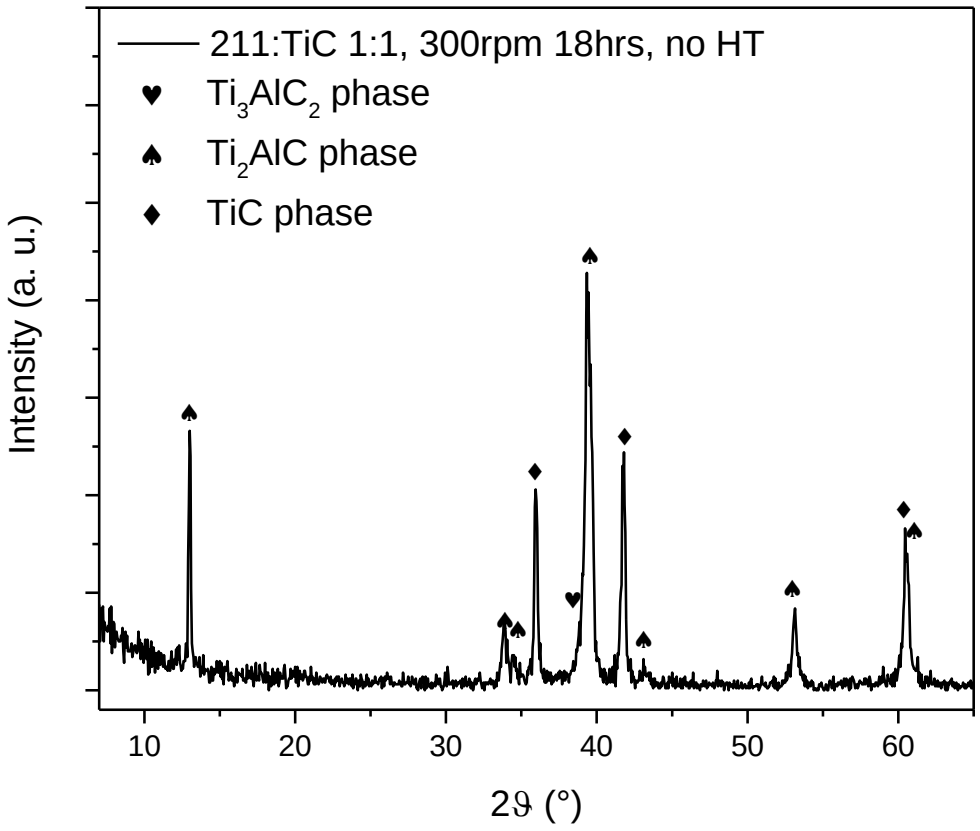

Figure 181, XRD pattern of TiC and Ti2AlC powders with molar ratio of 1:1, ball milled at 300 rpm for 18 hours

We sintered this sample at 1350°C for 4 hours, as made previously to confirm the already obtained results. The XRD pattern is shown in Figure 182. The results are similar to those obtained before, with traces of TiC and smaller amount of Ti_2AlC. This means that the longer ball milling time can reduce the quantity of unreacted Ti_2AlC, but does not significantly reduce the presence of unreacted TiC.

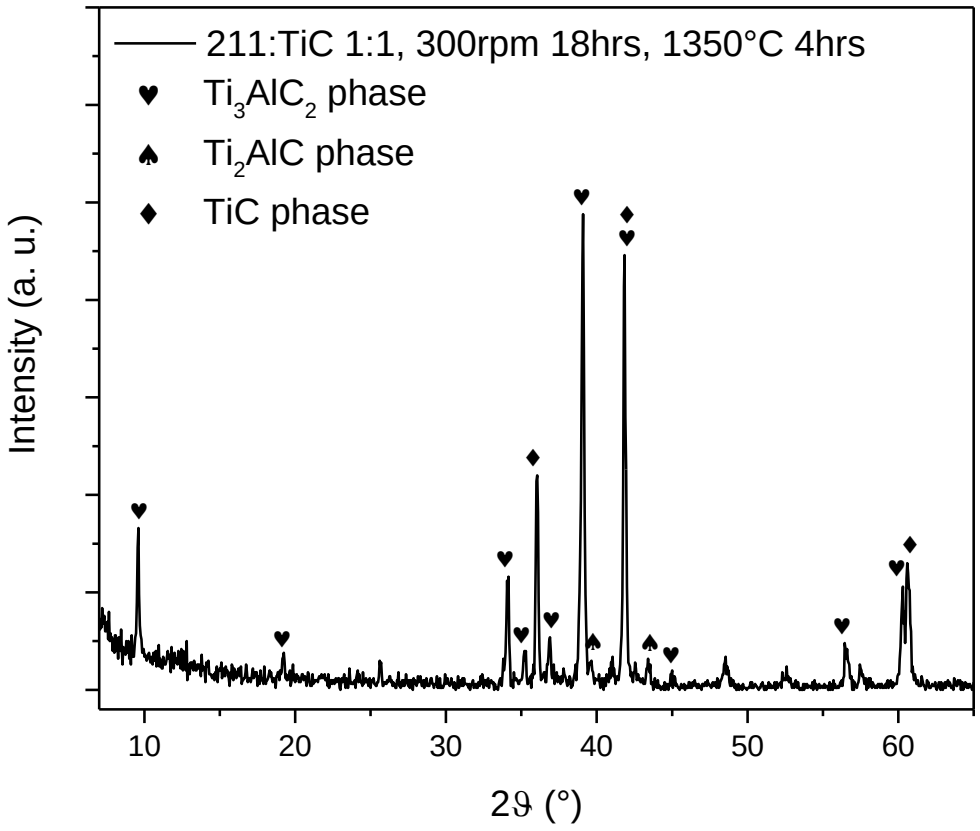

Figure 182, XRD pattern of TiC and Ti2AlC powders with molar ratio of 1:1, ball milled at 300 rpm for 18 hours and sintered at 1350°C for 4 hours

After these considerations, we decided to lower the starting ratio between Ti_2AlC and TiC. Previously we tested from 1:1 to 1:0.8, but in every case there were traces of titanium carbide. We decided to try to lower the ratio to 1:0.7, milling the powders with the last parameters (300 rpm for 18 hours) to ensure the reduction of unreacted 211. The XRD analysis before the sintering revealed a slightly different pattern, as can be seen in Figure 183. The peaks are broader and less defined, probably because of the smaller grain sizes of Ti_2AlC that was broken during the milling, being a softer material than TiC.

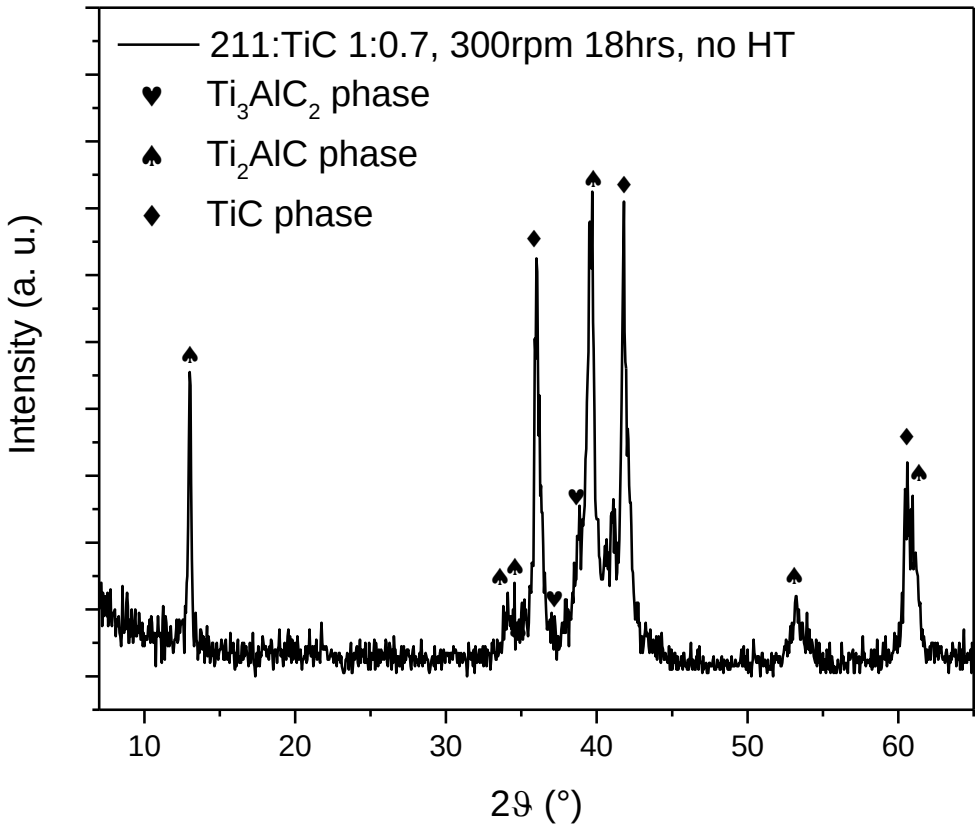

Figure 183, XRD pattern of TiC and Ti2AlC powders with molar ratio of 1:0.7, ball milled at 300 rpm for 18 hours

We treated the sample for sintering at 1350°C for 4 hours, but in order to reduce as possible the loss of aluminum we covered completely the vessel to ensure smaller turbulences inside. This gimmick was a double-edged sword, because the flow inside the vessel was so low that the evacuation of air wasn't completed during the sintering step. It can be deducted from the XRD pattern, in Figure 184. There aren't traces of Ti_3AlC_2 but, instead, there is unreacted Ti_2AlC in significant quantity beside TiC. The more shocking discover was the presence of unexpected phases, i.e. from Al_2O_3, Ti_3AlN_2 and other unidentified compounds, that can be related only to the presence of air inside the vessel when the sintering took place. Subsequently we treated this sample again with the same sintering conditions hoping that a longer time (4 hours from the last sintering plus 4 hours of the second treatment) could let the various phases react and give better results.

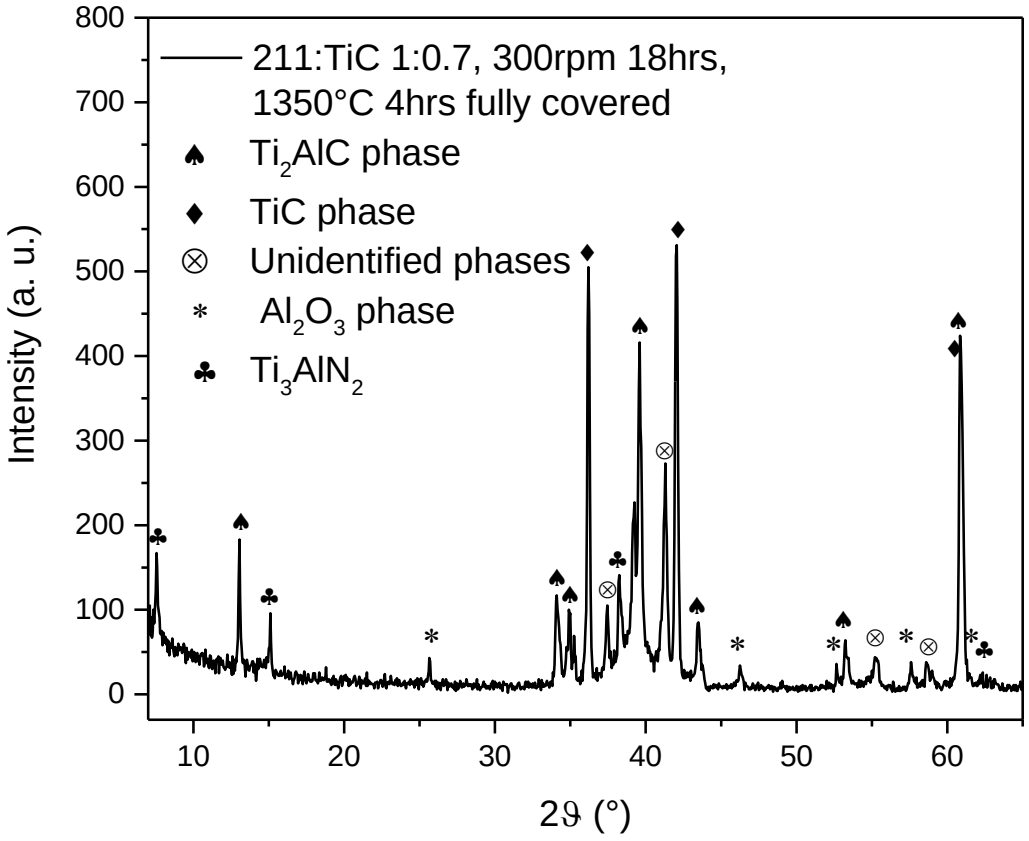

Figure 184, XRD pattern of TiC and Ti2AlC powders with molar ratio of 1:0.7, ball milled at 300 rpm for 18 hours and sintered at 1350°C for 4 hours fully covered

Neither this treatment gave us better results, as can be seen in Figure 185. Ti_2AlC reduced its quantity, but now there are more unidentified phases that are probably the results of the sintering of various phases containing nitrogen and oxygen. Ti_3AlC_2 is still not present, while there is a bigger amount of alumina.

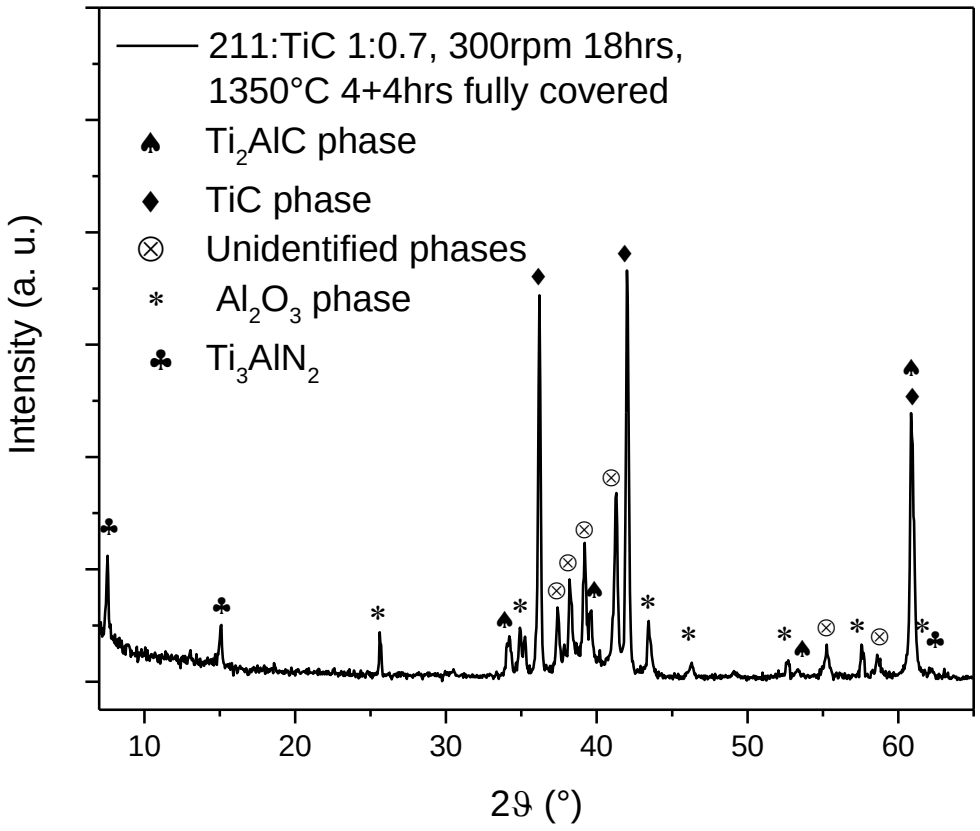

Figure 185, XRD pattern of TiC and Ti2AlC powders with molar ratio of 1:0.7, ball milled at 300 rpm for 18 hours and sintered at 1350°C for 4+4 hours fully covered

After these strange results we prepared a new sample with the same molar ratio and milling procedure, but this time the vessel inside the tube will be partially covered in order to allow a constant flow of argon but at reduced speed, in the hope to decrease the alumina loss due to the high temperature. The sintering was done with the same parameters, 1350°C for 4 hours.

After the heat treatment the sample was covered by a white thin layer, clue to an air leak during the sintering. We separated the top layer from the base and made XRD analyses for each. Their pattern, from the top layer and from the base, are compared in Figure 186. The two patterns aren't very different, there are still present peaks from Ti_3AlN_2 and Al_2O_3, confirming the presence of air during the sintering. This can due to a non-perfect seal of the o-rings put at the extremities of the tube or to fissure of it.

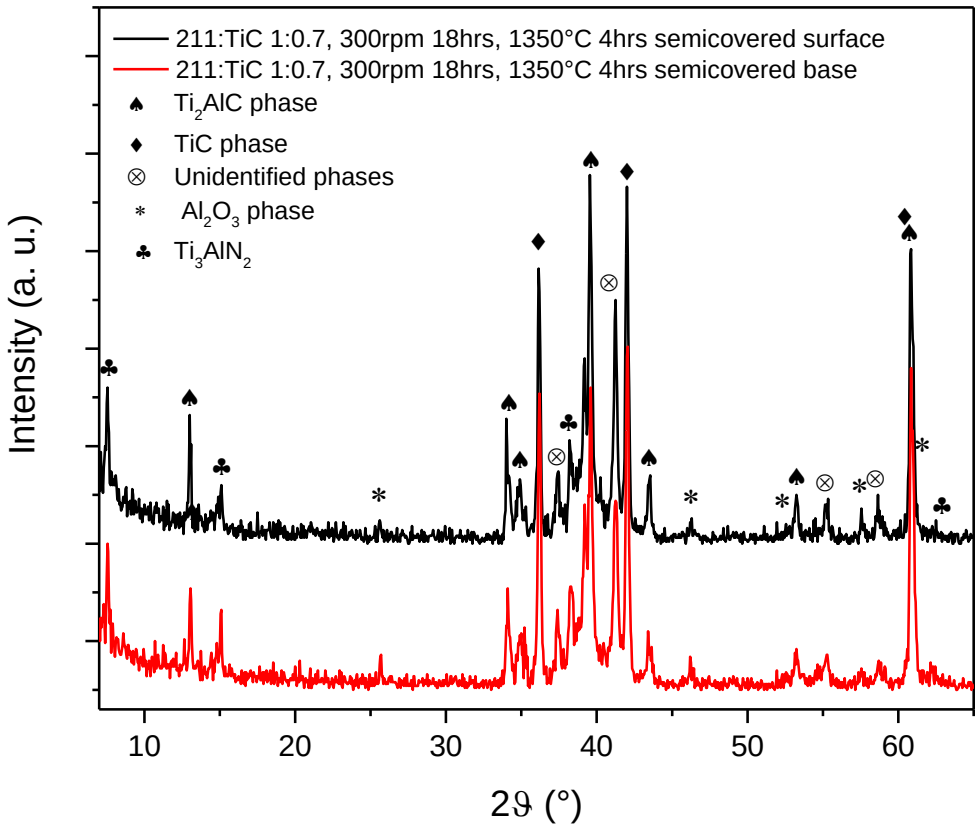

Figure 186, XRD patterns comparison of TiC and Ti_2AlC powders with molar ratio of 1:0.7, ball milled at 300 rpm for 18 hours and sintered at 1350°C for 4+4 hours semi covered, on top the surface, bottom the base

We checked the integrity of the tube, washed and lubed all the seals in order to avoid every leak during the sintering. After that, we put the same sample inside and treated again, both to check the airtight seal and to check if, in absence of oxygen and nitrogen, the faulted sample can be somehow recovered. The XRD pattern after the sintering is not very dissimilar to that from the fully covered sample treated for 8 hours, as can be seen below, in Figure 187.

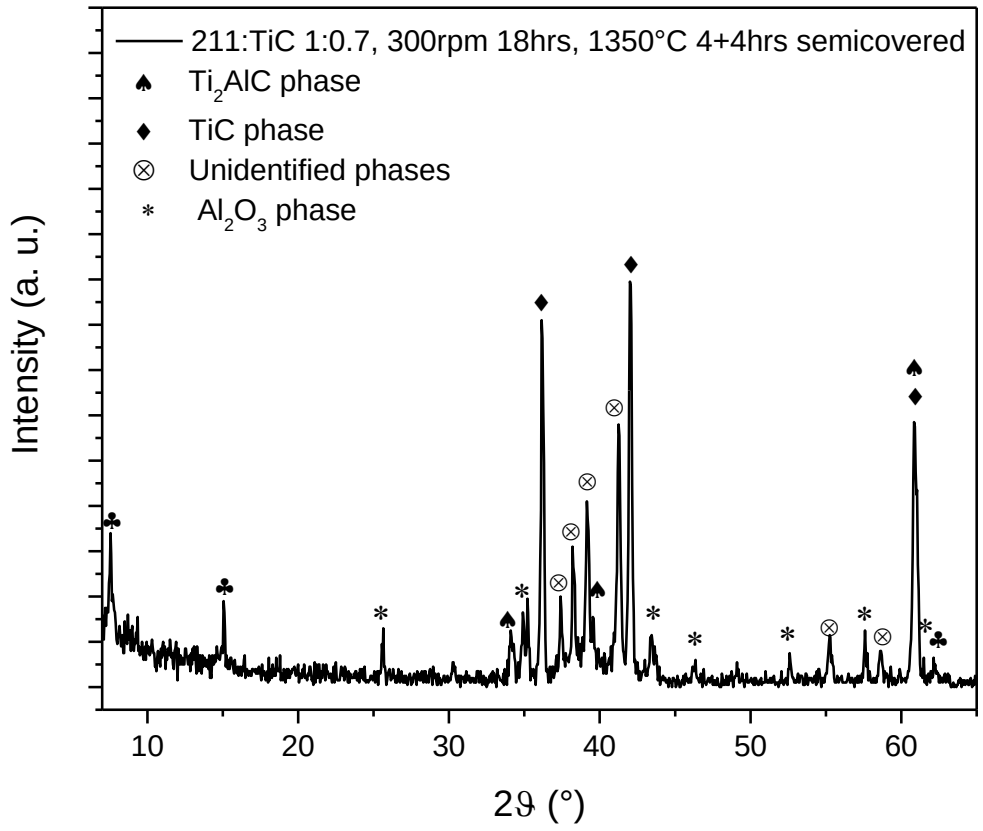

Figure 187, XRD pattern of TiC and Ti_2AlC powders with molar ratio of 1:0.7, ball milled at 300 rpm for 18 hours and sintered at 1350°C for 4+4 hours semicovered

After this sample, we believed that also the polyethylene jar could have contaminated the sample, losing small pieces of plastic. We changed the jar with a new one and, after the milling, we performed an XRD analyses to check if the pattern is changed.

In Figure 188 there is a comparison of the XRD patterns obtained from the new and old jar. It is possible to note that with the new jar there are more peaks ascribable to Ti_3AlC_2. This confirm that the jar reached its end of life and probably it lost some traces in the previous samples.

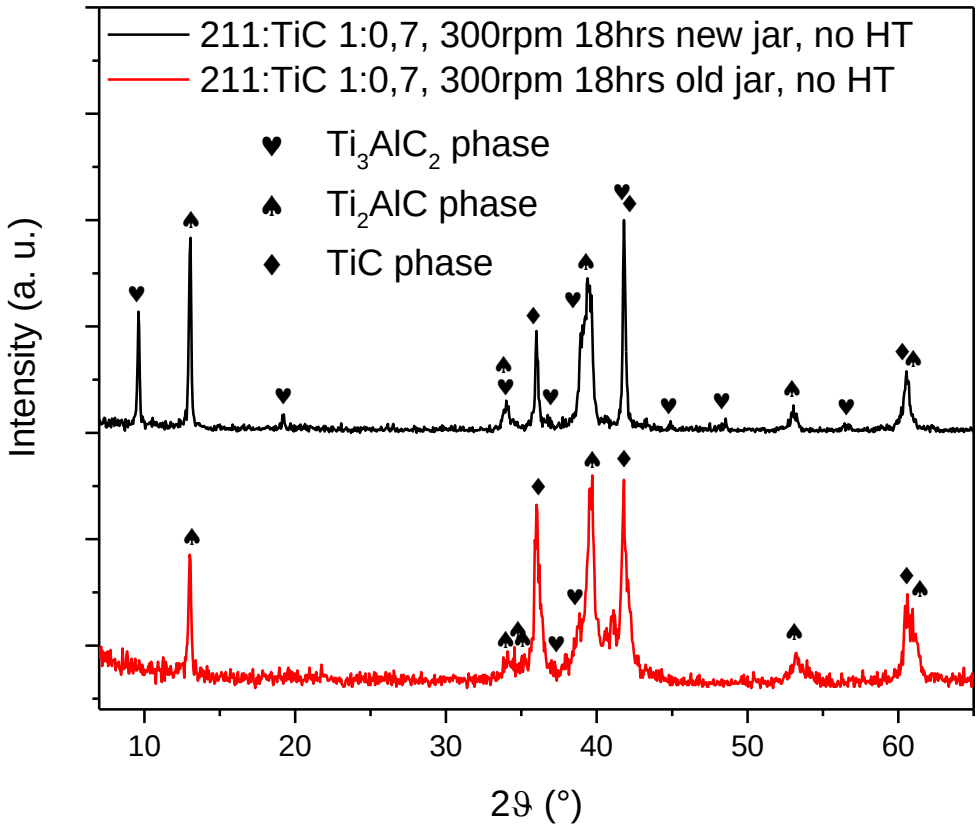

Figure 188, XRD patterns comparison of TiC and Ti_2AlC powders with molar ratio of 1:0.7, ball milled at 300 rpm for 18 hours with new and old polyethylene jar

The new sample was sintered still at 1350°C for 4 hours but without cover, to eliminate all the possibilities that some air could be trapped inside the vessel.

The sintered powder shown again a thin white layer on the surface and from the XRD pattern, in Figure 189, the peaks of Al_2O_3 are evident. The phase with nitrogen is not present, meaning that during the sintering an air leak didn't take place but, instead, some oxygen could be present before the heat treatment in form of moisture probably.

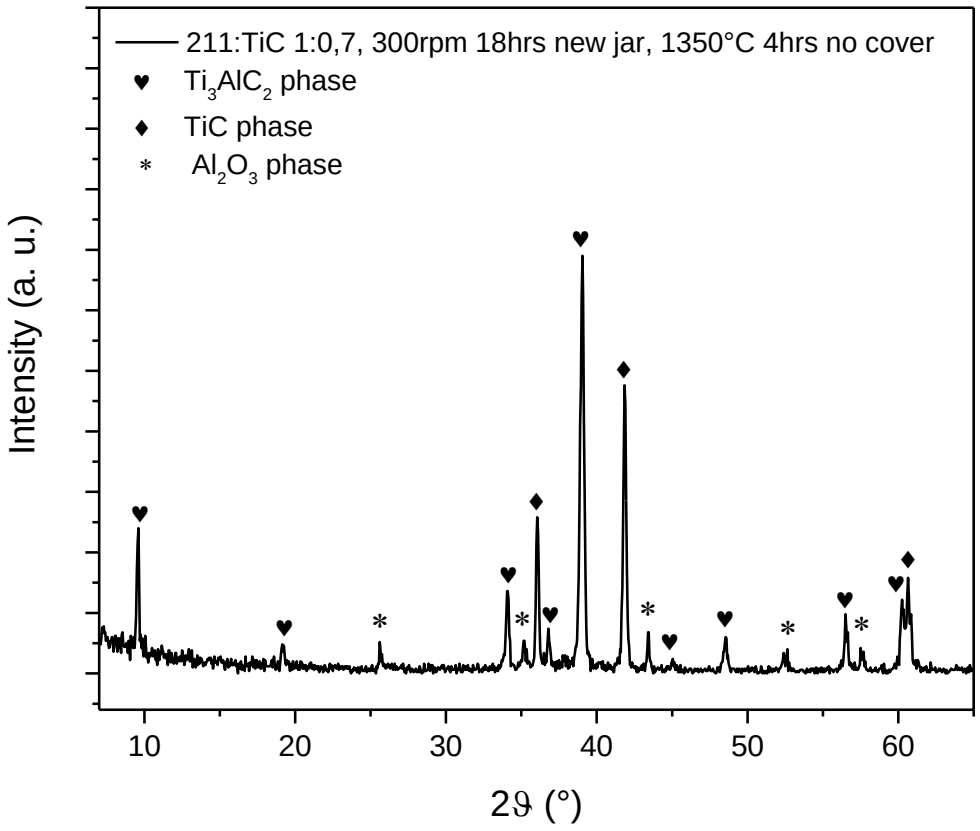

Figure 189, XRD pattern of TiC and Ti2AlC powders with molar ratio of 1:0.7, ball milled at 300 rpm for 18 hours and sintered at 1350°C for 4 hours without cover

In order to remove the moisture before the heat treatment, we decided to modify the seals at the extremities of the tube to be able to apply vacuum inside. In this way we are also capable to check the airtight seal and remove all the traces of residual air. For the next samples, before the heat treatment we reached pressures of 0.1 bar and applied the vacuum for one hour. After this interval, without possibilities to allow some air to enter, we flown argon at 0.5L/min, as before done.

The first sample sintered with the new vacuum stage was made as the last one, milled in the new polyethylene jar at 300 rpm for 18 hours. After applying the vacuum for one hour, the sintering took place with the usual parameters, i.e. at 1350°C for 4 hours. The XRD pattern of this sample is reported in Figure 190.

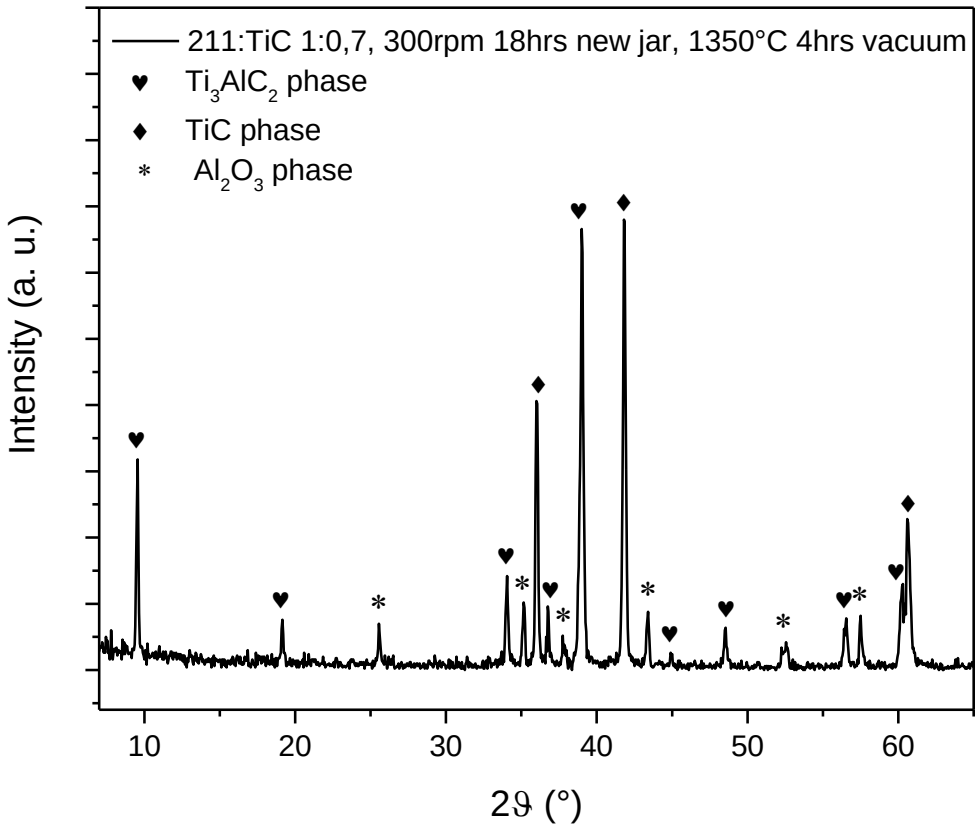

Figure 190, XRD pattern of TiC and Ti2AlC powders with molar ratio of 1:0.7, ball milled at 300 rpm for 18 hours and sintered at 1350°C for 4 hours with a vacuum stage

Again, we obtained a sample partially covered with a thin white layer of alumina, that can be found in XRD pattern. There is also unreacted TiC, but we didn't want to lower anymore the ratio between Ti_2AlC and TiC because it was already well below the theoretical one. Forgetting for a moment the issue of the alumina, we tried to make another sintering on the same sample to check if the unreacted titanium carbide can be dissolved and make the 312 phase. We applied again vacuum before the sintering and conducted it at 1350°C for 4 more hours.

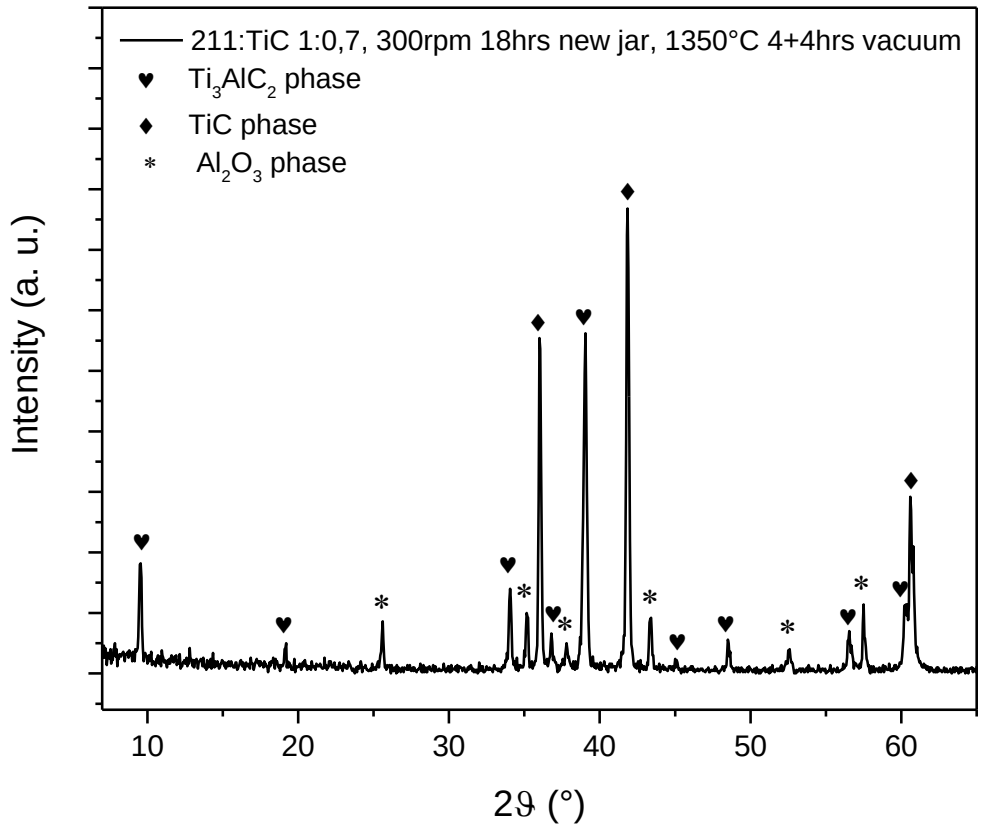

Figure 191, XRD pattern of TiC and Ti2AlC powders with molar ratio of 1:0.7, ball milled at 300 rpm for 18 hours and sintered at 1350°C for 4+4 hours with a vacuum stage

The obtained powder shown more intense peaks related to titanium carbide with a lowering of the ones from the 312 phase compared to the alumina peaks. This means that the formation of Ti_3AlC_2 is kinetically disadvantaged in favor of the creation of titanium carbide that is more stable. This consideration led us to consider that the right sintering time is below 4 hours, near the two hours that were recommended.

We prepared two new samples with the same parameters, only with the reduction of the duration of sintering to 1.5 hours and 2 hours. After the sintering, a smaller quantity of white powder was on the surface. This can be also observed in the two XRD patterns, in Figure 192 for the 1.5 hours long treatment and in Figure 193 for the 2 hours long one.

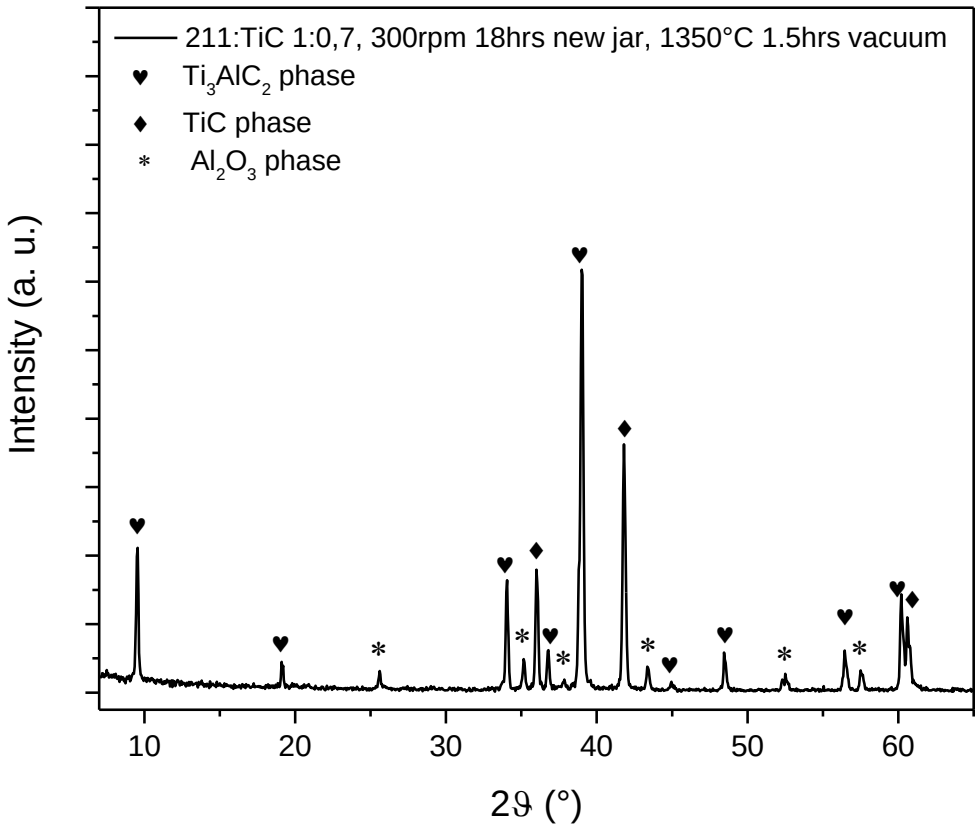

Figure 192, XRD pattern of TiC and Ti_2AlC powders with molar ratio of 1:0.7, ball milled at 300 rpm for 18 hours and sintered at 1350°C for 1.5 hours with a vacuum stage

The peaks related to alumina are very weak, meaning that the quantity of Al_2O_3 present in the powder is very low. Also the height of titanium carbide peaks is very low compared to Ti_3AlC_2. This proves the hypothesis formulated above. The height ratio of the main peaks for the two phases, Ti_3AlC_2 and TiC, can give a rough comparison of the quantities for each phase for the two samples, minding that it is not a very precise estimation but only a qualitative guideline. In this case, for the sample treated for 1.5 hours, the height ratio between the most intense peaks related to 312 (39.05°) and TiC (41.75°) is 1:0.59. Obviously, from this calculation we do not obtain the molar ratio between the two species, also because the peak of the titanium carbide has a contribution from a small peak of Ti_3AlC_2 that sits very narrow, at 41.85°. The height ratio has to be considered only for comparing two samples with the same phases and approximatively evaluate what is the best one.

The second sample shows a similar XRD pattern, with weak peaks from alumina. The heights of the peaks are pretty the same as the previous sample, but calculating the height ratio between the most intense peaks related to 312 and TiC, that is 1:0.51, we observed that this second sample has a lower quantity of titanium carbide.

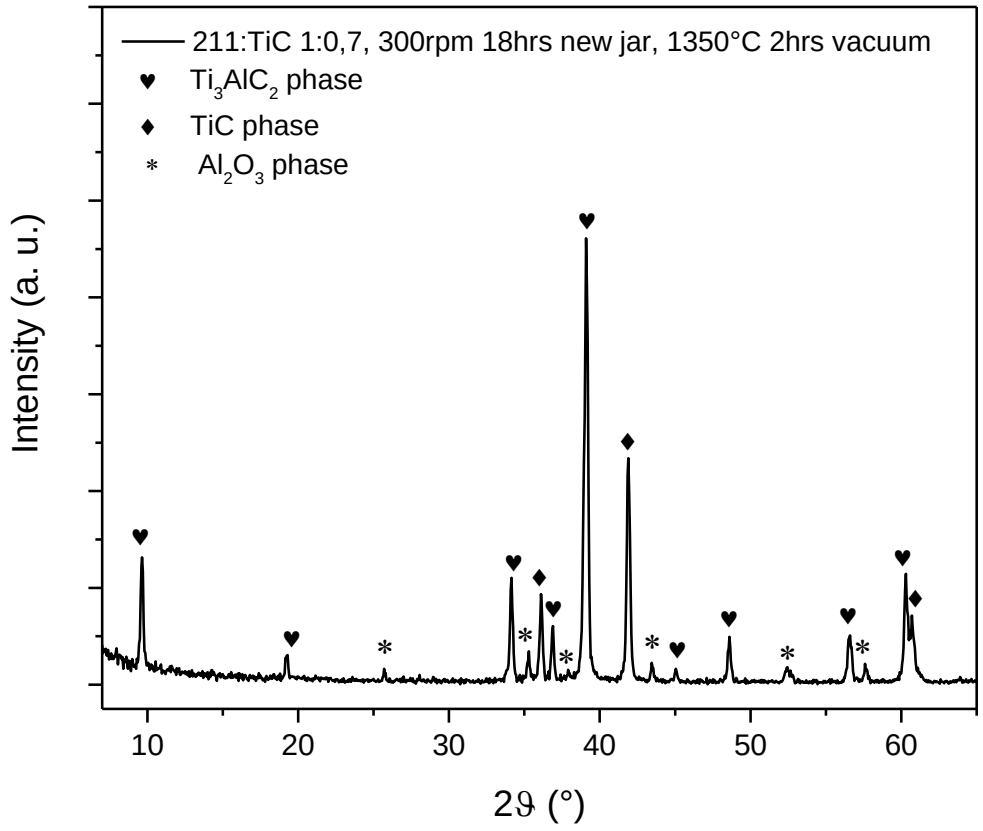

Figure 193, XRD pattern of TiC and Ti_2AlC powders with molar ratio of 1:0.7, ball milled at 300 rpm for 18 hours and sintered at 1350°C for 2 hours with a vacuum stage

This can be explained in a different way in respect to the enrichment of TiC phase with longer sintering times. While in the first case the titanium carbide is kinetically favored, in this second case we have the uncomplete reaction and sintering of TiC and Ti_2AlC. However the quantity of 211 is so low that it cannot be detected.

For these two samples we paid more attention on the exterior appearance of the powder. Both samples were associated by three different and visible layers, from the surface to the interior of the sintered material: the surface was covered with a thin white layer, relatable to alumina and ascribable to an

imperfect airtight seal; below there was a more compact and harder layer with a darker appearance than the core, that was grey and brittle. The middle layer, darker and harder, is probably a TiC-richer layer that is formed from the evaporation of aluminum during the sintering. The core instead is richer in 312, because the diffusion the aluminun takes longer. In order to prove this, we made two more samples from only one batch of powders with the same starting composition, with a 211:TiC ratio of 1:0.7, milled in the new polyethylene jar at 300 rpm for 18 hours and then sintered at 1350°C for 2 hours applying vacuum for 1 hour before the heating ramp. The only difference between the two samples is represented by the quantity of used powder. For the first one we used more powder in order to fill half the vessel, for the second we put less powder inside to have a thin layer of powder. In this way we can obtain a part that has a small influence from the superficial depletion of aluminum (the fulfilled half vessel), while the other part, being thinner, will be poorer in Al and confirm our supposition.

For each sample we separated the first few millimeters from the core with a steel spatula. In this way we have four different cases: the core and the surface for both the sample with a big volume and the one with small volume. Each XRD pattern is reported below, in Figure 194, Figure 195, Figure 196 and Figure 197. In three patterns there is a strong peak ascribable to the aluminum sample holder, because the powders didn't covered completely the surface of it.

It is interesting to note the height ratio between the main peaks of TiC and Ti_3AlC_2 for each sample. They are tabulated below, in Table 30.

Sample	Core from big volume	Surface from big volume	Core from small volume	Surface from small volume
312:TiC height ratio	1:0.51	1:1.28	1:0.61	1:1.91

Table 30, ratios between the most intenste peak of 312 (39.05°) and TiC (41.75°) from the different zone of the sample with big and small volume

It can be noted that for the results from the inner part of both the samples are better than that from the surface. This supports our supposition, confirming also that the quantity of Ti_3AlC_2 from the core of the sample with more powder (and thus bigger volume) is greater than that from the sample laid in thin layer (with a smaller volume compared to the surface area).

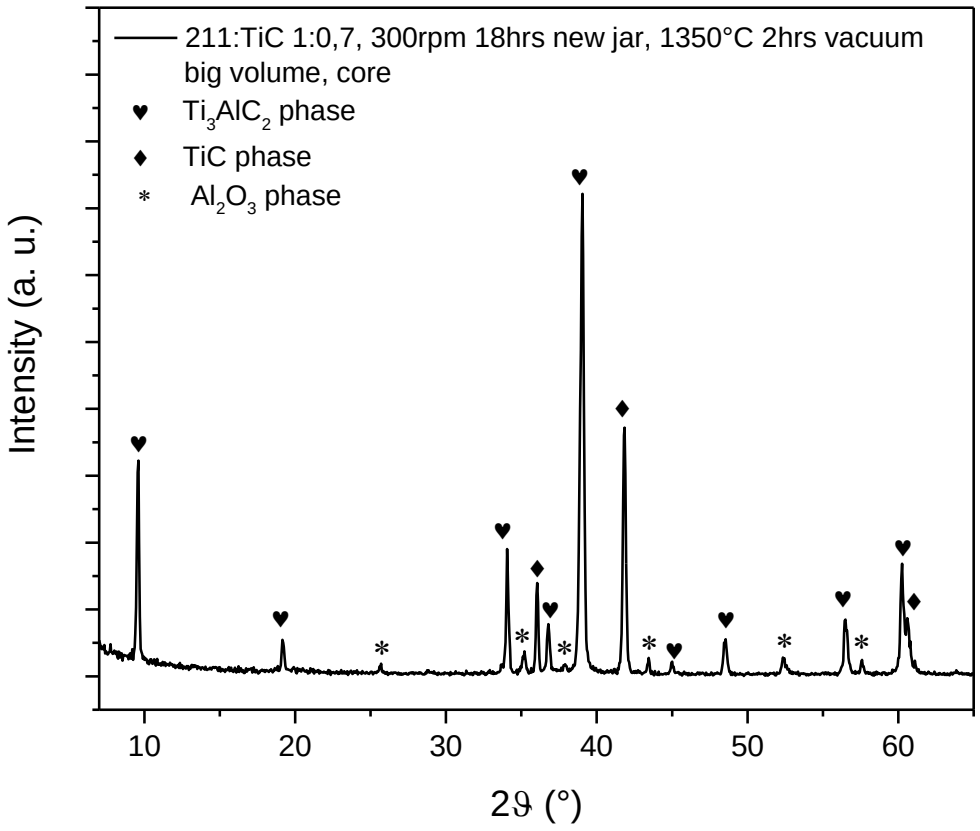

Figure 194, XRD pattern of TiC and Ti_2AlC powders with molar ratio of 1:0.7, ball milled at 300 rpm for 18 hours and sintered at 1350°C for 2 hours with a vacuum stage, core from big volume

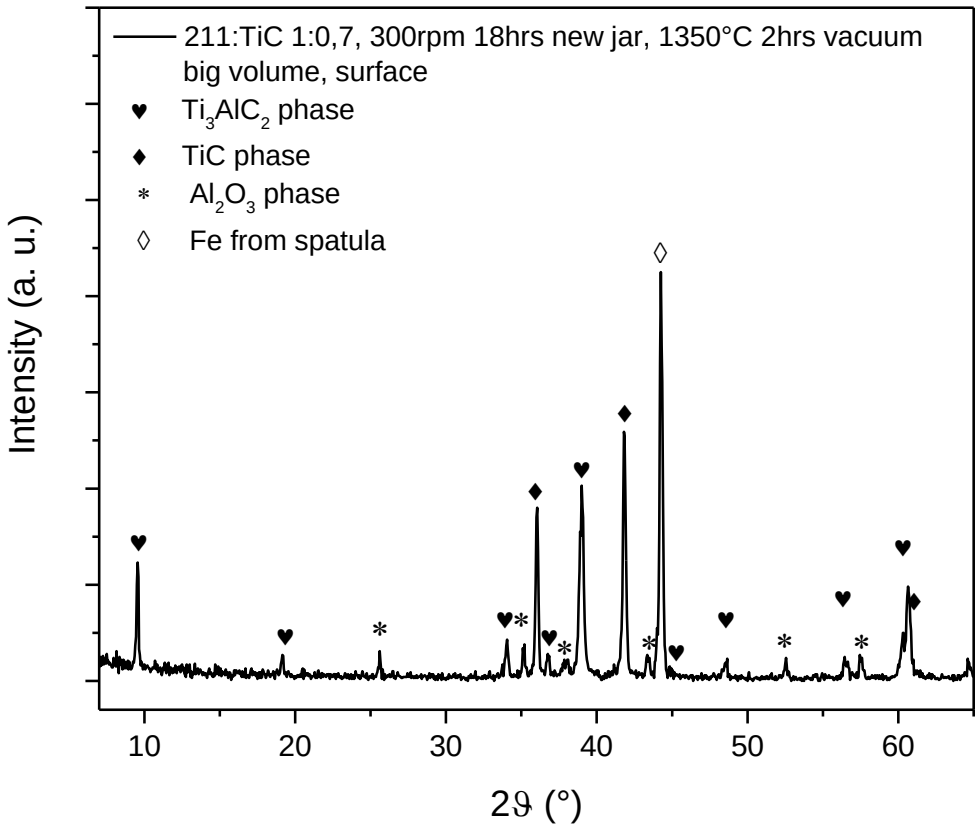

Figure 195, XRD pattern of TiC and Ti_2AlC powders with molar ratio of 1:0.7, ball milled at 300 rpm for 18 hours and sintered at 1350°C for 2 hours with a vacuum stage, surface from big volume

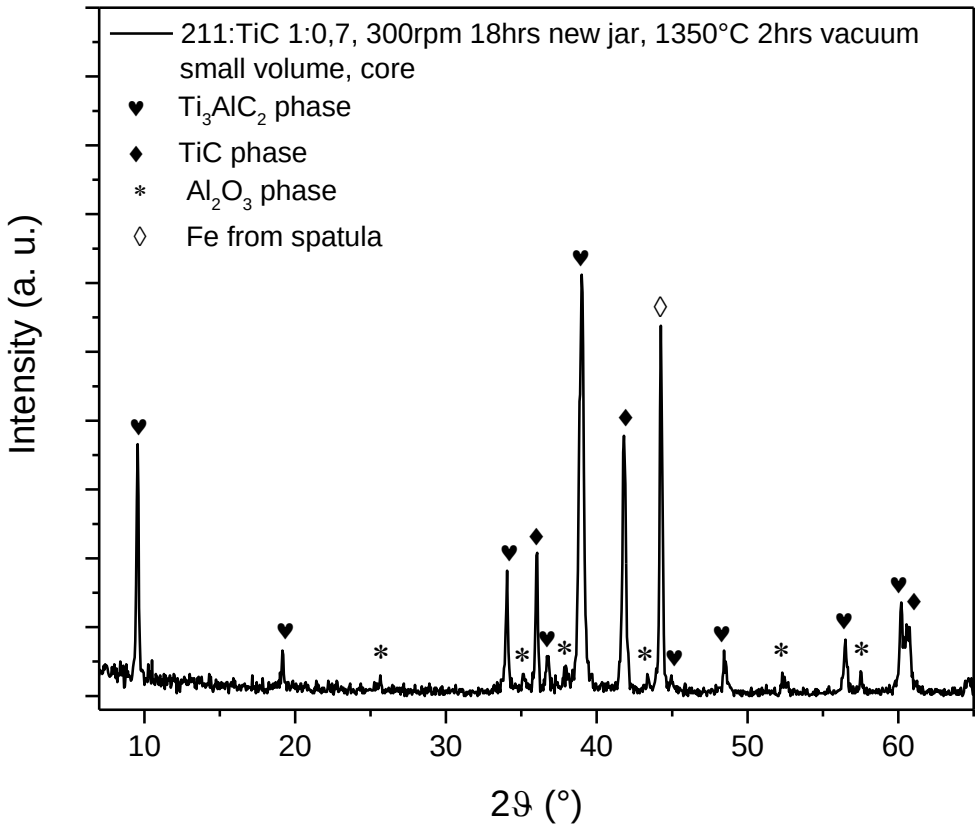

Figure 196, XRD pattern of TiC and Ti_2AlC powders with molar ratio of 1:0.7, ball milled at 300 rpm for 18 hours and sintered at 1350°C for 2 hours with a vacuum stage, core from small volume

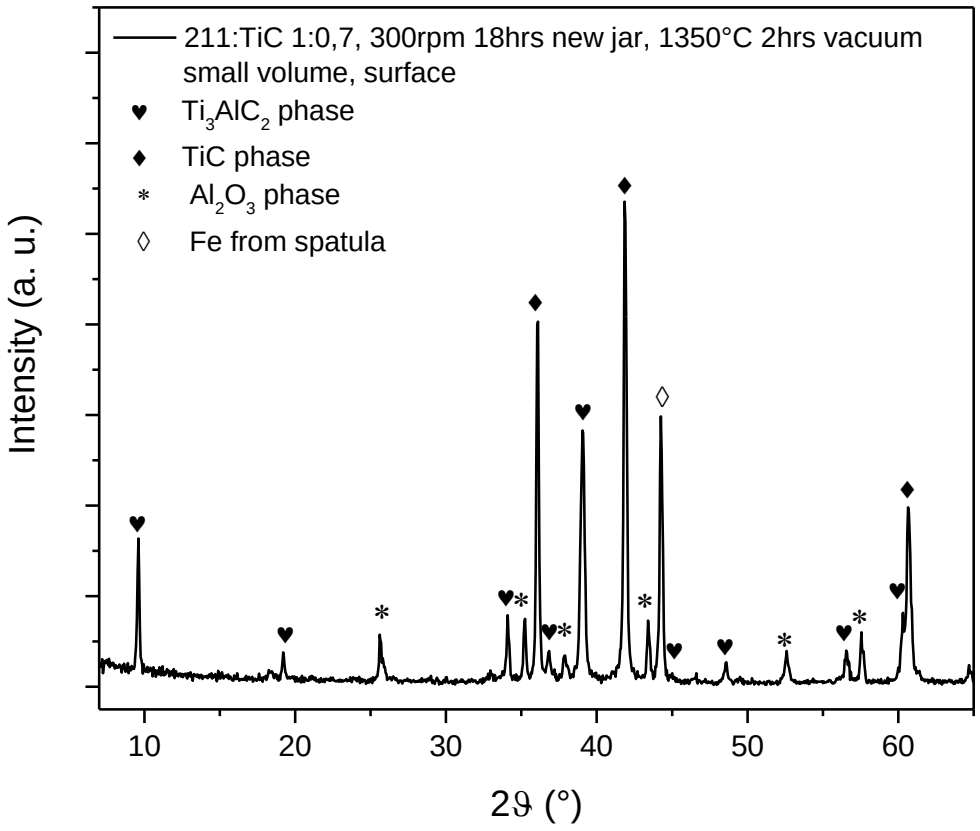

Figure 197, XRD pattern of TiC and Ti2AlC powders with molar ratio of 1:0.7, ball milled at 300 rpm for 18 hours and sintered at 1350°C for 2 hours with a vacuum stage, surface from small volume

The core part of the sample with a big volume was analyzed by SEM to study the morphology of the surface. The images are presented below, in Figure 198, Figure 199 and Figure 200. The layered structure is evident, it is also possible to see bent grains in the second image. There are also small particles (circled in the images) that can be probably ascribed to titanium carbide, albeit it was not possible to confirm it by EDX because the particles are too small to be analyzed one by one.

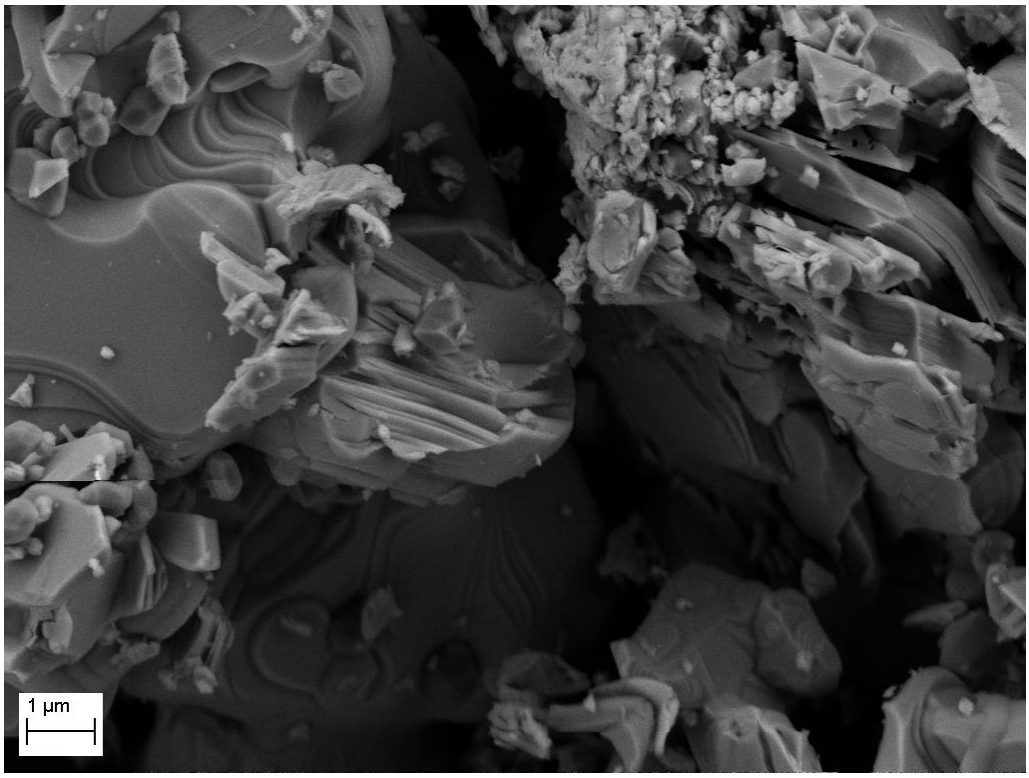

Figure 198, SEM image of the core part of TiC and Ti_2AlC powders with molar ratio of 1:0.7, ball milled at 300 rpm for 18 hours and sintered at 1350°C for 2 hours with a vacuum stage, core from big volume

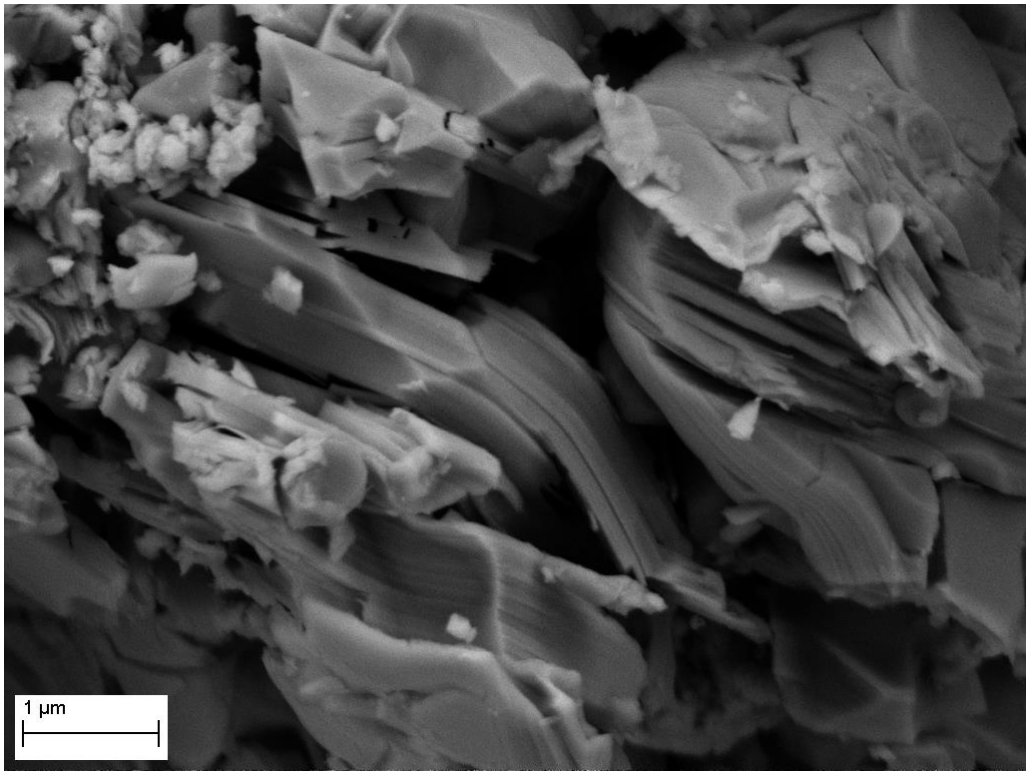

Figure 199, SEM image of the core part of TiC and Ti_2AlC powders with molar ratio of 1:0.7, ball milled at 300 rpm for 18 hours and sintered at 1350°C for 2 hours with a vacuum stage, core from big volume

Figure 200, SEM image of the core part of TiC and Ti_2AlC powders with molar ratio of 1:0.7, ball milled at 300 rpm for 18 hours and sintered at 1350°C for 2 hours with a vacuum stage, core from big volume

After all these considerations, we can say to have found the best parameters to minimize the contamination of TiC, albeit the purity of the samples is not perfect. They can be resumed as follow:

1. Starting stoichiometry: 1 mole of Ti_2AlC + 0.7 mole of TiC
2. Milling: ball milling in polyethylene jar with 5 mm alumina sphere at 300 rpm for 18 hours, weight ratio between powders and sphere of 1:50
3. Sintering: Ar flow of 0.5L/min, vessel fulfilled with the powder, ramp of 10°C/min up to 1350°C, dwell time of 2 hours and natural cooling, discard the surface and use only the core part.

The sintering of all the MAX phases was aimed toward the creation of a suitable anodic support for fuel cells. Unluckily for the study of all the factors that influence the creation of the purest powder we spent an unexpected amount of time, leaving little room for the electrochemical characterization of these

interesting phases. In fact, we were able to test only the feasibility of platinum nanoparticles on the last sample and make a quick characterization in a semicell. The electrochemistry measurements were performed in the lab of Prof. Gaetano Granozzi at the Chemistry Department of our University. We decided to make only platinum nanoparticles and not Pt_xSn because the electrochemical tests would be conducted at room temperature with diluted acid solution. In this conditions Pt has better performances that Pt_xSn and is commonly used.

We used the core part of the Ti_3AlC_2 powder produced with the optimized synthesis for the decoration with platinum nanoparticles. We used the previously described polyol synthesis for the decoration of the Ti_3AlC_2 powder with Pt. Reassuming, in ethylene glycol we put together the support powder and the platinum precursor ($H_2PtCl_6 \cdot 6H_2O$) in the right amount to reach a final 20 mol% of Pt, adjusting the pH to 13 with the addition of NaOH. We heated the suspension at 160°C for 3 hours and, when the temperatures are dropped, the powders are washed with a 1M phosphoric acid solution before the centrifugation, for 3 times. The last wash and centrifugation was done with acetone in order to remove all the traces of EG and let the powder dry at 60°C. At the same time we made the same decoration on the Ensaco 350G, forming a widely and commercial used anode compound, frequently used as standard.

After the synthesis of the NPs we make XRD and SEM analysis to check the formation of them. In Figure 201 and Figure 202 there are the XRD patterns from the two samples, while in Figure 203 there is the comparison of them.

It is easy to see that the peak related to platinum are very similar in the samples, as highlighted also by the comparison. The FWHM of the peaks from the two samples is comparable, signifying that the crystallite sizes are similar.

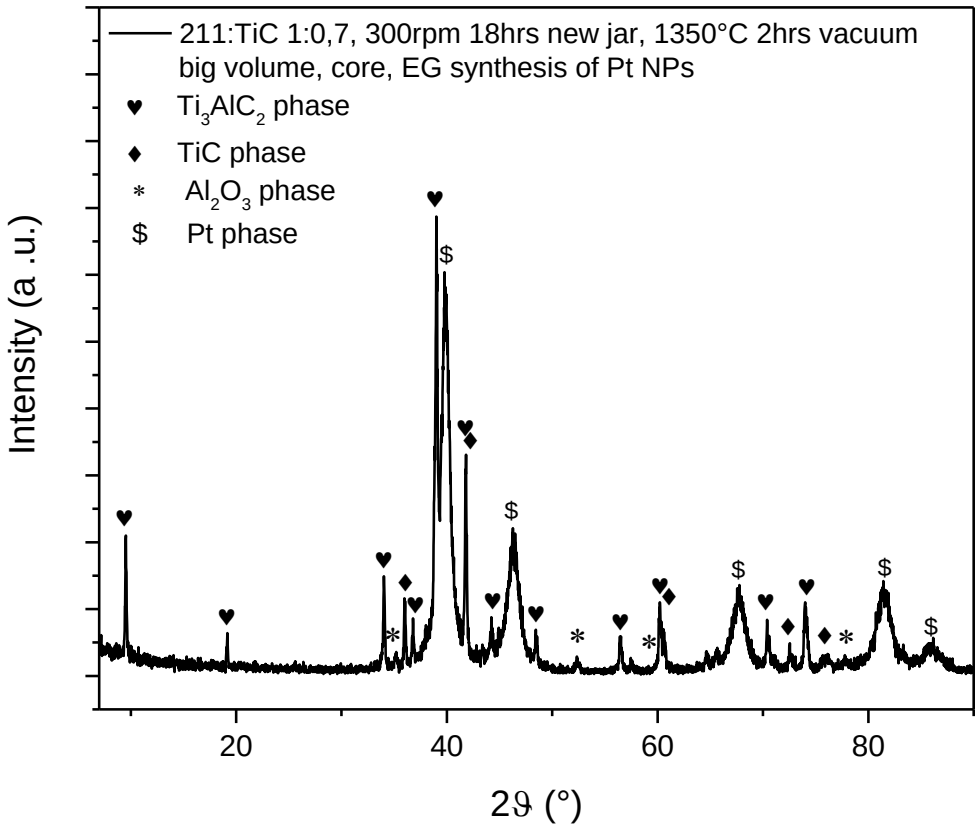

Figure 201, XRD pattern of the powder of the last 312 sample, after the decoration with Pt nanoparticles following the polyol route

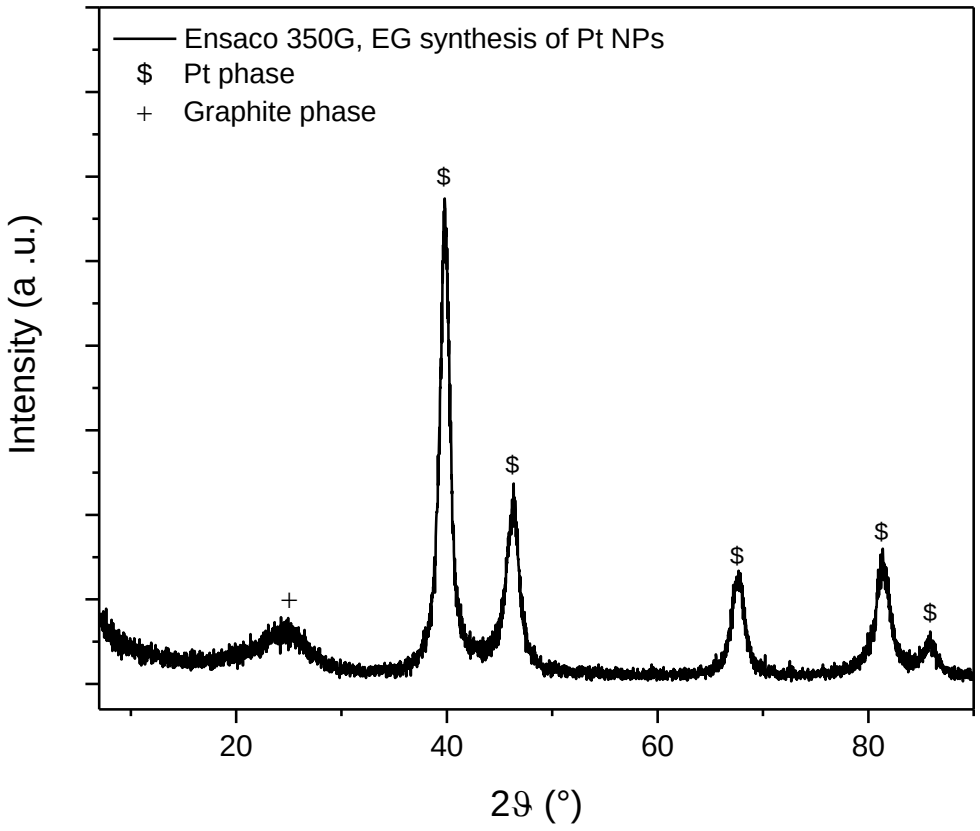

Figure 202, XRD pattern of the powder of Ensaco 350G, after the decoration with Pt nanoparticles following the polyol route

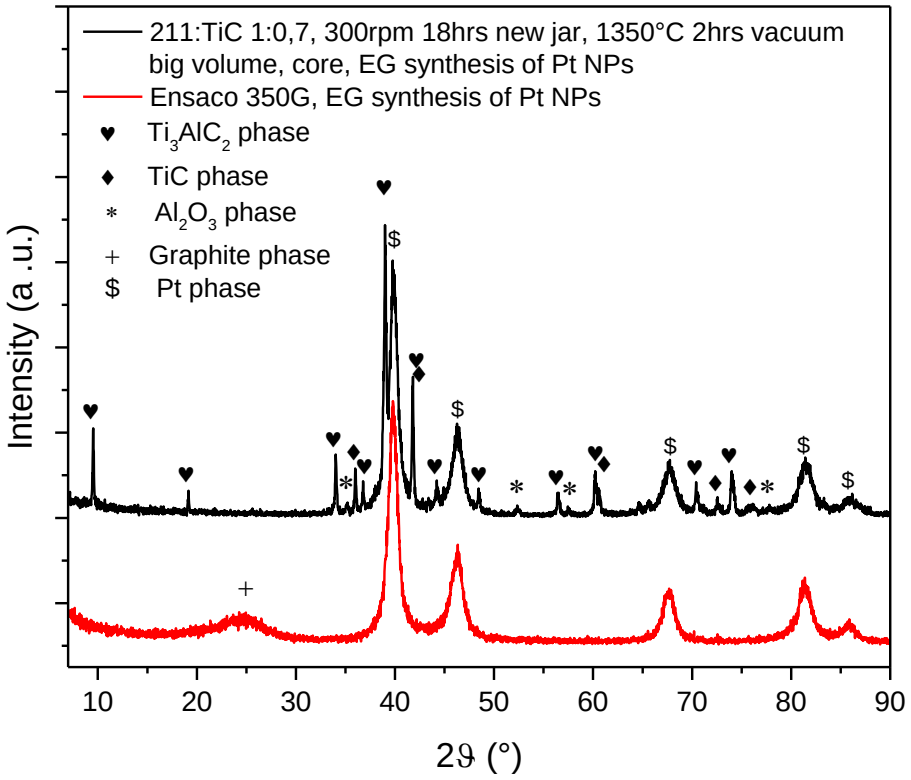

Figure 203, XRD patterns comparison of the powder of the last 312 sample and Ensaco 350G, after the decoration with Pt nanoparticles following the polyol route

To investigate further the shape and the mean dimension of the surface and of the nanoparticles we used SEM analysis. In this case, we investigated first the carbon black, in order to have a benchmark. In Figure 204 and Figure 205 there are the images from this sample. The surface is very sponge-like, with very small bright dots that are the nanoparticles. The distribution of the NPs appears to be not very even, with big agglomerates and few particles standing alone. After these samples, we investigate the Ti_3AlC_2 samples, in Figure 206, Figure 207, Figure 208 and Figure 209.

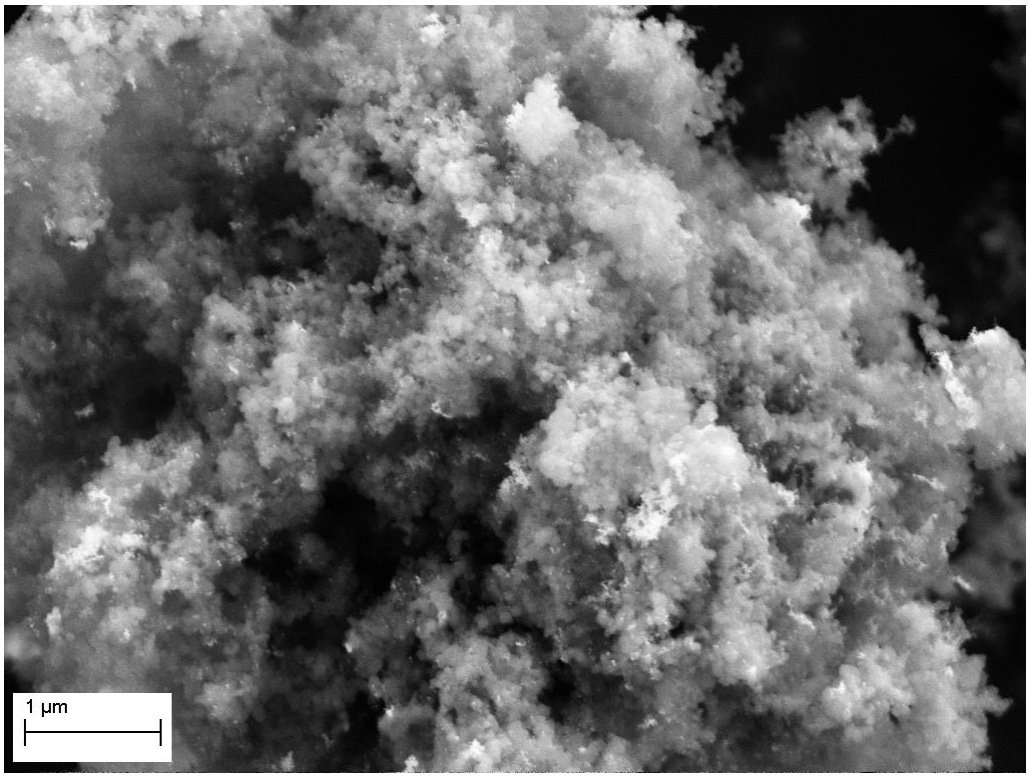

Figure 204, SEM image of the surface of 350G decorated with Pt NPs

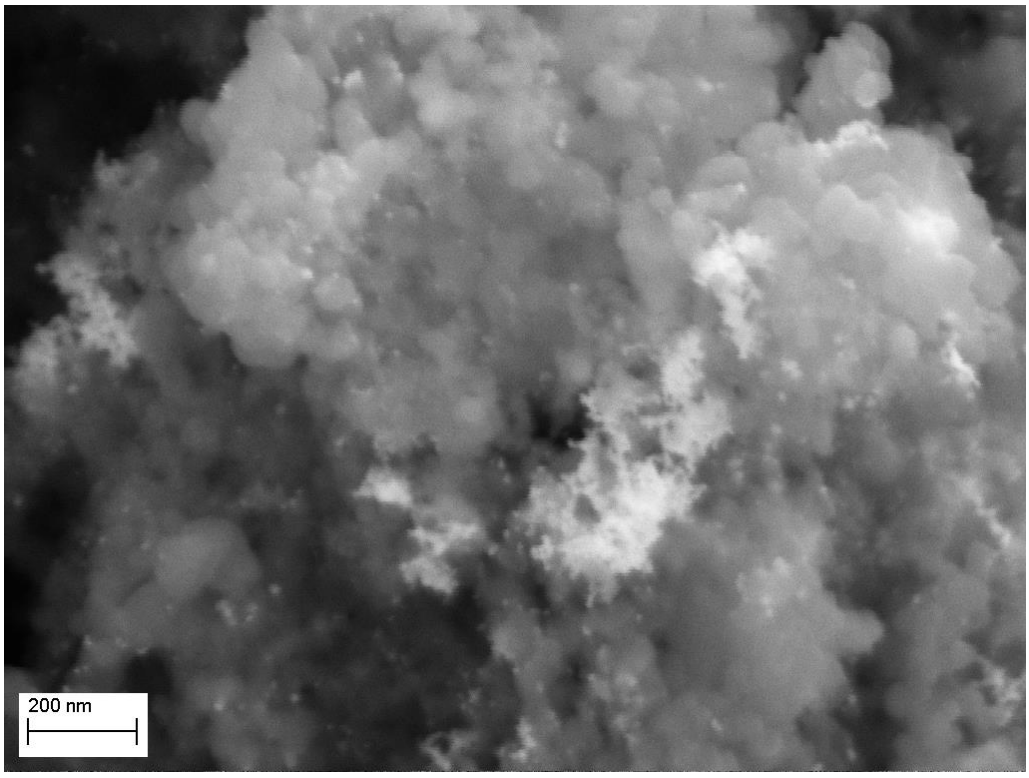

Figure 205, SEM image of the surface of 350G decorated with Pt NPs

Below there are the images from the 312 phase powder.

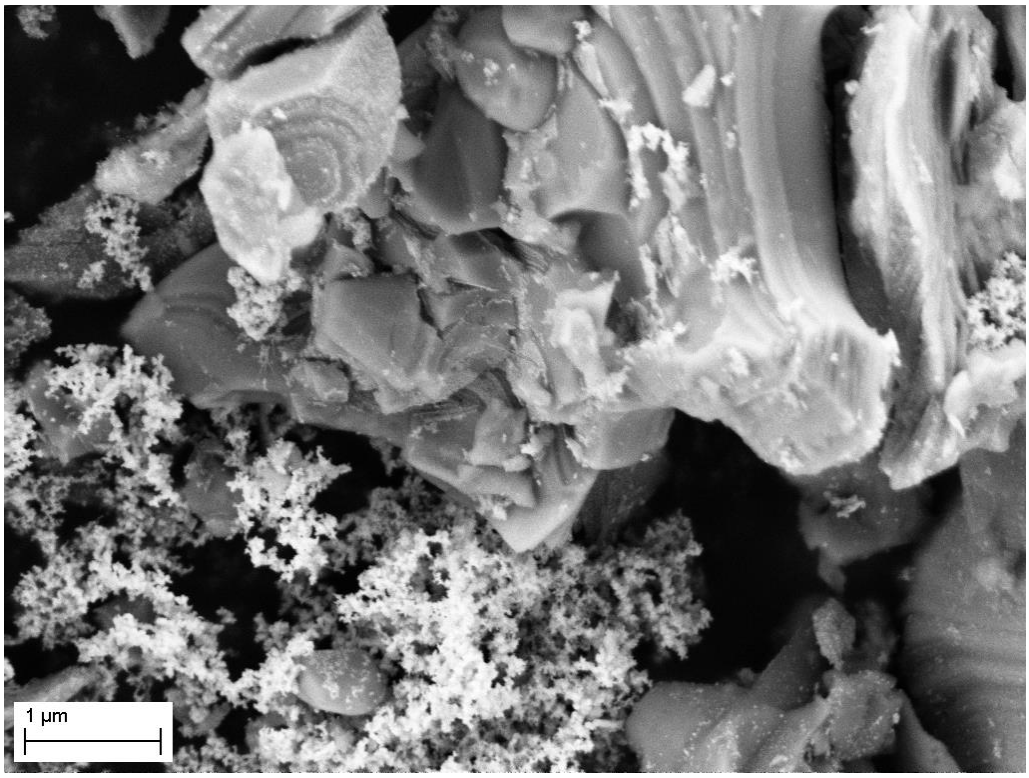

Figure 206, SEM image of the surface of 312 decorated with Pt NPs

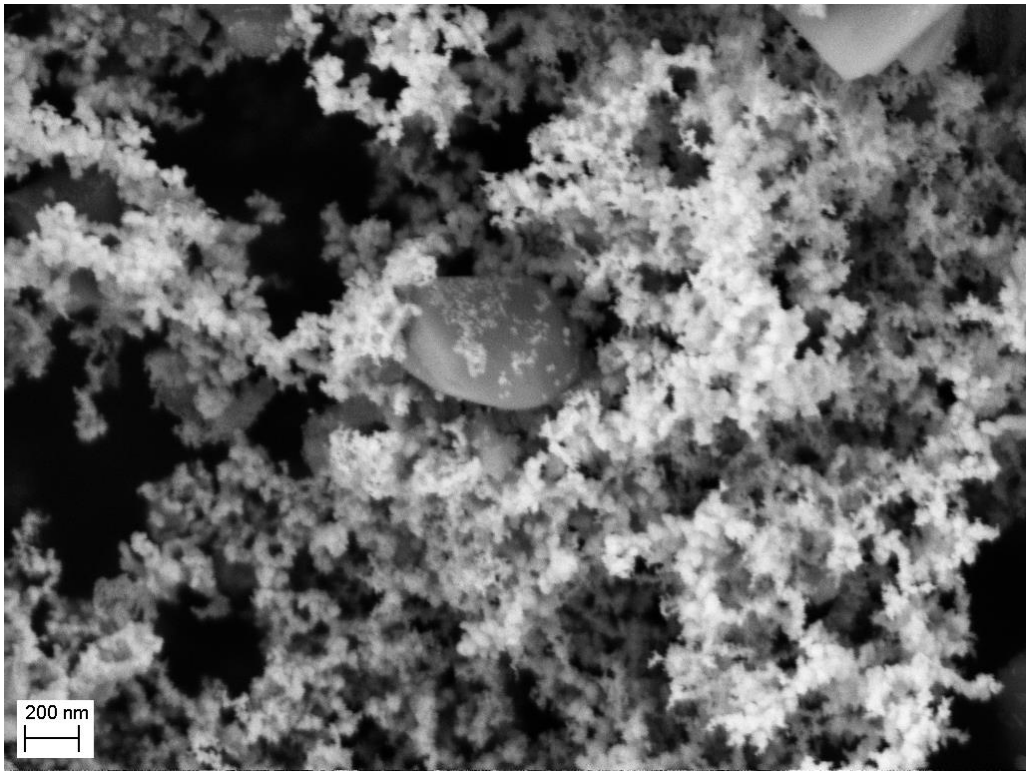

Figure 207, SEM image of the surface of 312 decorated with Pt NPs

Also with this sample the distribution of the particles is not even.

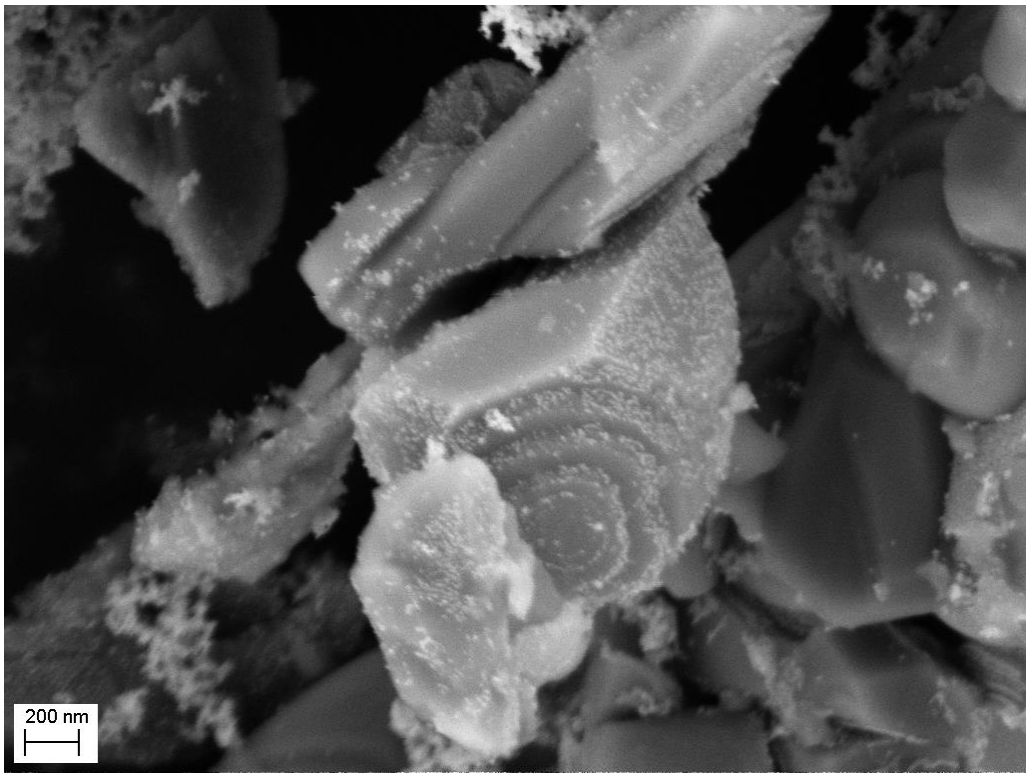

Figure 208, SEM image of the surface of 312 decorated with Pt NPs

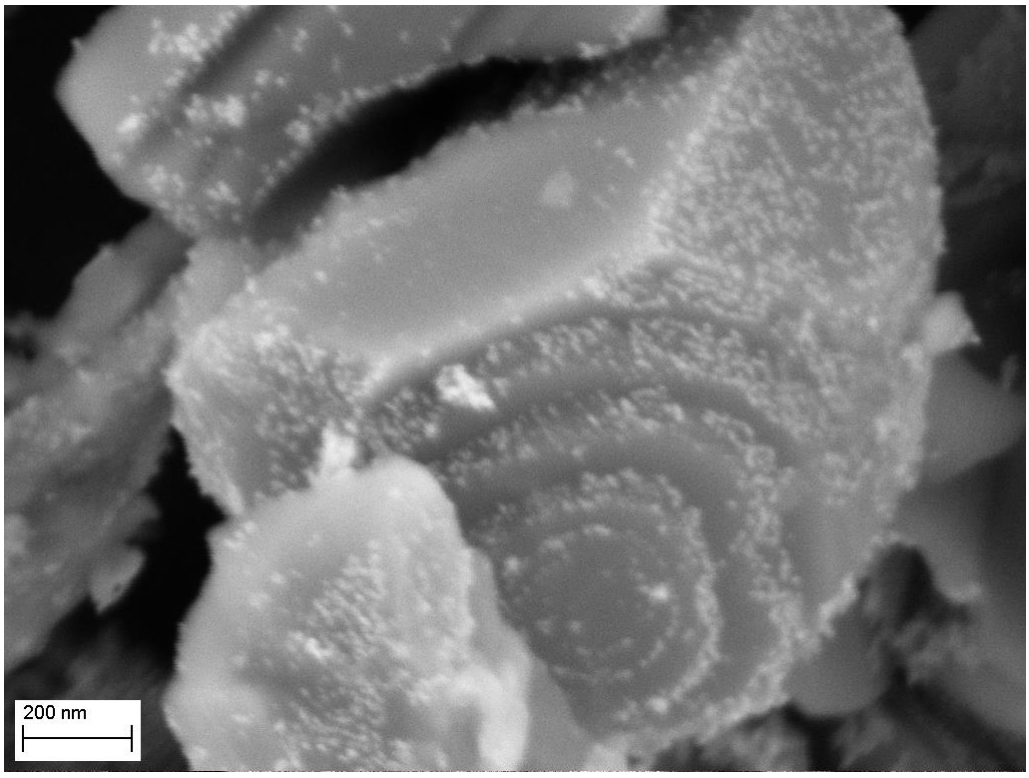

Figure 209, SEM image of the surface of 312 decorated with Pt NPs

Big agglomerates of nanoparticles are still visible, but their distribution on the nanolayered and ordered surfaces is more interesting. As can be seen in the two last images, the nanoparticles grow on a preferential surface, corresponding to a plane perpendicular to the z axis. This exact plane cannot be recognized only with the use of the SEM. The EDX confirmed that the agglomerates are formed primarily by platinum, while the exposed surfaces are Ti_3AlC_2.

4.4. Electrochemistry

After this discovery, worth of future studies, we tested the two powders in the same conditions for the electrochemical characterization. It was only a brief and preliminary study, to check if the MAX phases can work in mild conditions and to justify future researches.

The conditions for both the samples were the same. At room temperature the electrolyte was a 1M phosphoric acid solution. The two anodic supports were suspended in an ethanol/water solution prior the deposition of the same quantity of solution on a small piece of glassy carbon, partially covered with Teflon tape to expose only the coated surface to the electrolyte. As counter electrode we use a platinum wire, while as reference a saturated calomel electrode. We bubbled argon inside the electrolyte to remove the air. For each semicell after the needed stabilization and preliminary cycles, a proper quantity of pure ethanol was added to reach a 0.5M concentration. For all the samples the sweep speed was maintained constant, equal to 0.02V/s.

Firstly, we tested the stability of the 312 phase without nanoparticles in the electrolyte, firstly without ethanol and then with it. The results are below, in Figure 210. It is visible that the curves don't change the shape in a significant way after the addition of ethanol, meaning that the 312 doesn't suffer from degradation in acidic conditions with ethanol. The currents from this sample are very low, in the range of few microamperes.

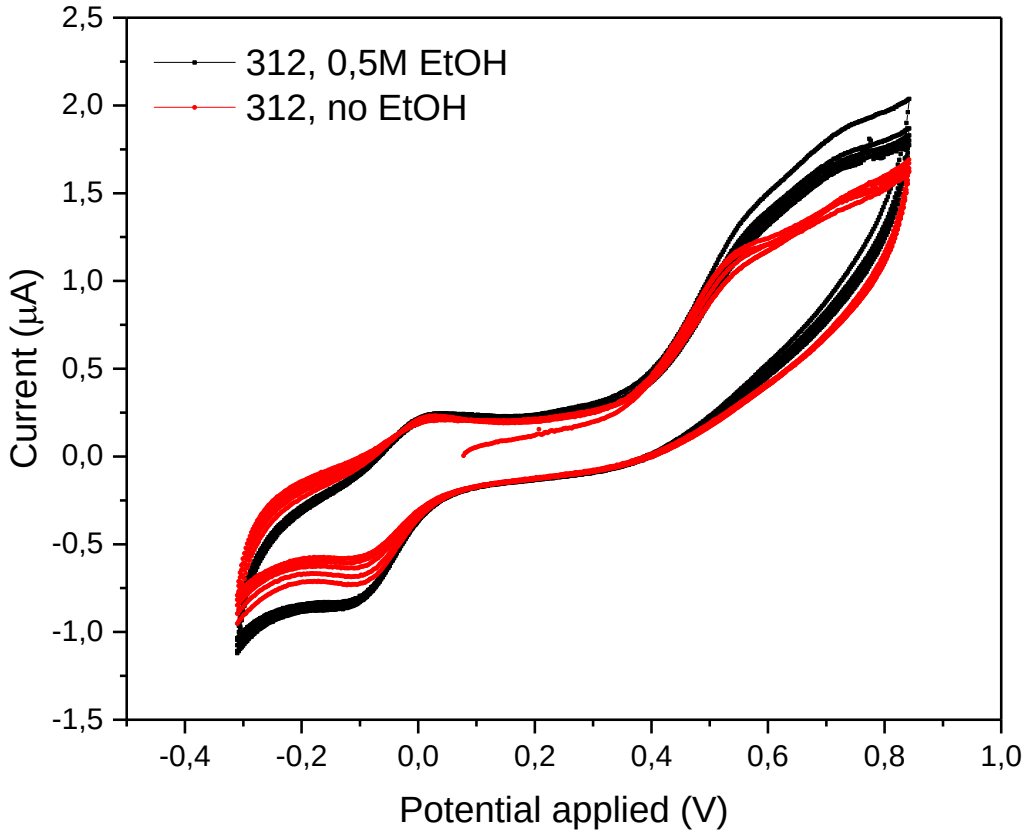

Figure 210, cyclovoltammetries in 1M phosphoric acid with and without EhOH of Ti_3AlC_2 without Pt nanoparticles

Then we tested the carbon black decorated with Pt nanoparticles, to make a benchmark for the following samples, that is the decorated phase.

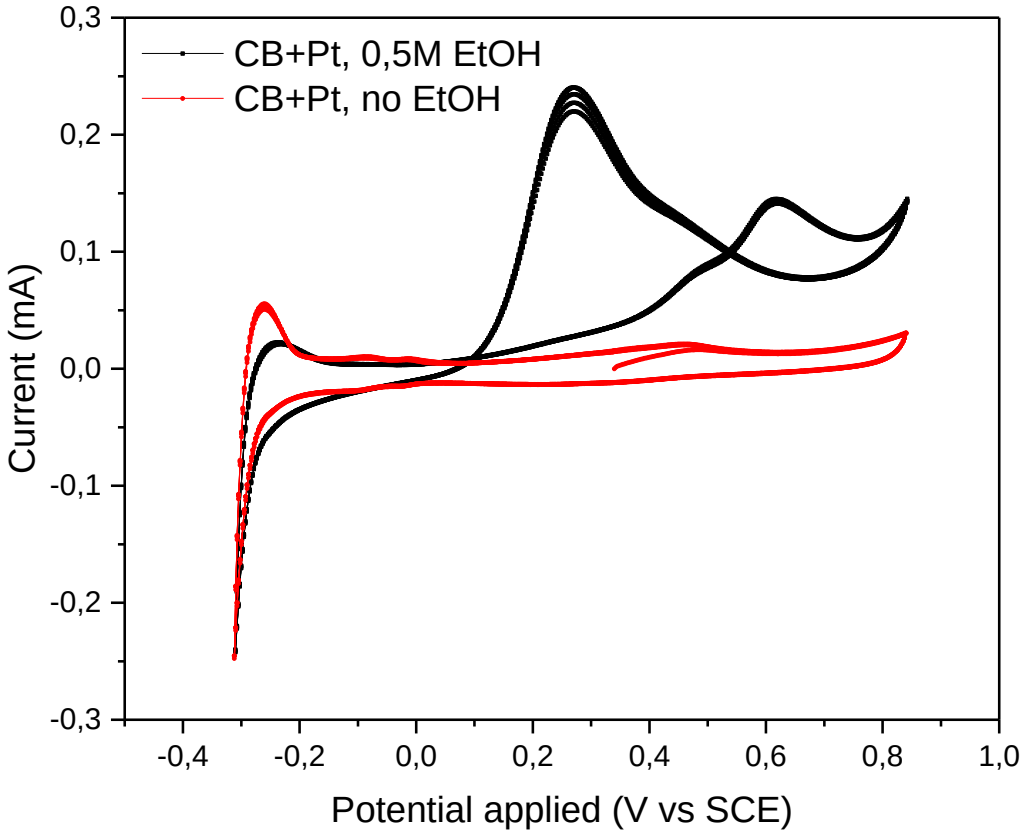

Figure 211, cyclovoltammetries in 1M phosphoric acid with and without EhOH of CB with Pt nanoparticles

In the image above, the peaks from the oxidation of the ethanol by the platinum are evident, at ~0.3V and ~0.65V. This means that at room temperature the platinum on carbon black is already able to oxidize the ethanol and obtain electrons from the reaction. This is the reference pattern from a standard catalyst on a well know support. Our hopes are that the 312 with platinum could at least have half of the current from the oxidation, so further tests at higher temperatures would be justified.

In Figure 212 there is the CVs from the Ti_3AlC_2 sample decorated with nanoparticles. The oxidation of ethanol takes place clearly, with two peaks at ~0.3V and ~0.6V, albeit with different shapes. It is also interesting to note that there is a couple of small peaks around 0V, probably due to the oxidation and reduction of alumina on the surface.

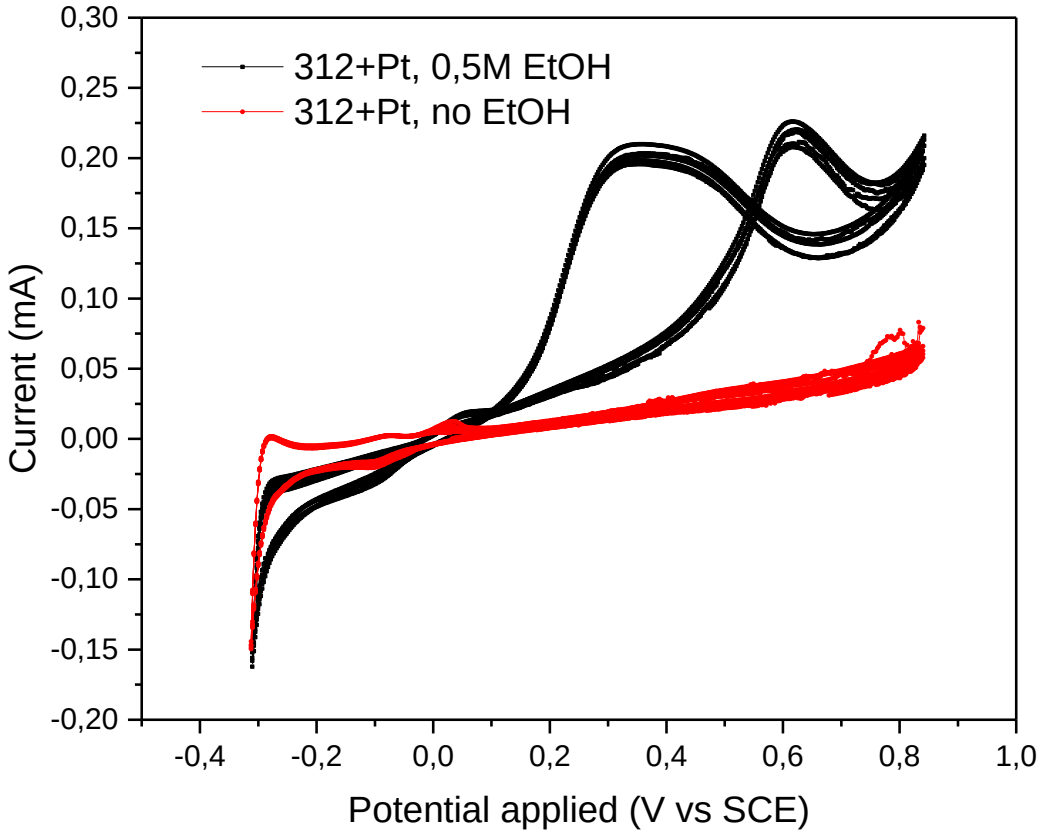

Figure 212, cyclovoltammetries in 1M phosphoric acid with and without EhOH of 312 with Pt nanoparticles

Comparing the last two cyclovoltammetries, in Figure 213, it is clear that the Ti_3AlC_2 works well with platinum for the oxidation of ethanol. The peak of the oxidation of ethanol at ~0.6V for the 312 phase is even higher than the one from CB, meaning that more power can be extracted from the cel. The peaks at ~0.3V for the two samples are pretty different, probably because different mechanisms take place during the oxidation, but with this preliminary work more hypothesis cannot be formulated.

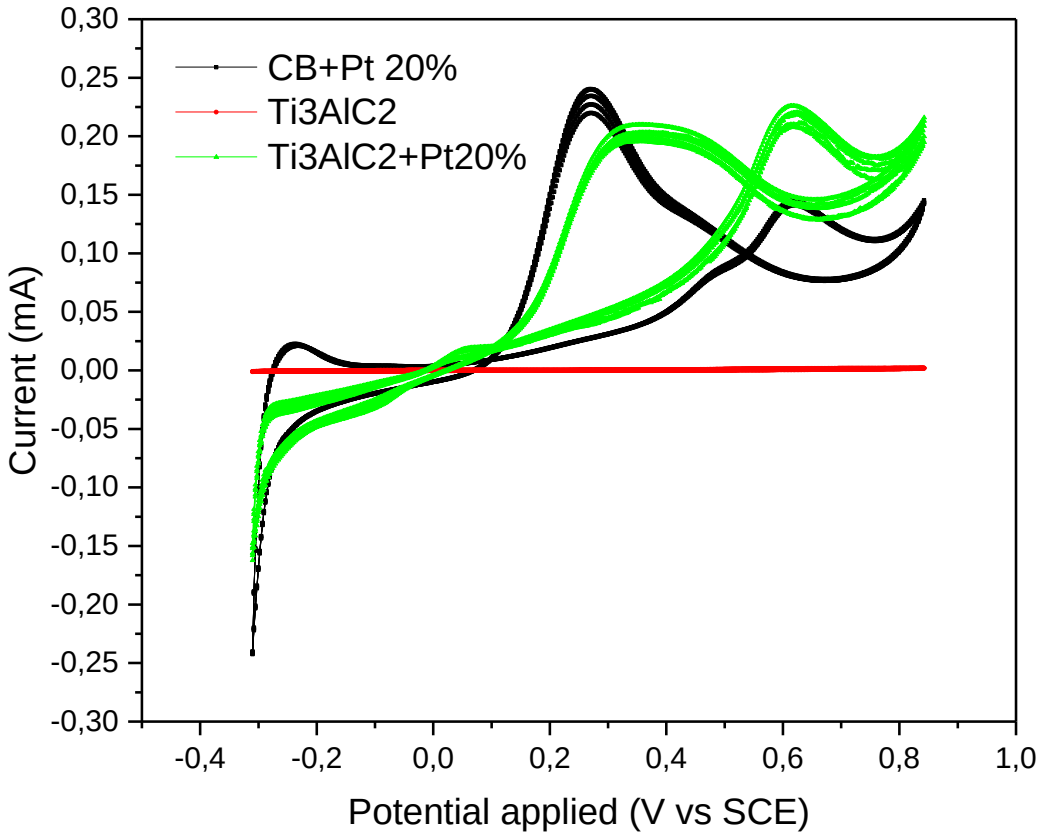

Figure 213, comparison of the cyclovoltammetries in 1M phosphoric acid with and without EhOH of 312 with and without Pt nanoparticles, and CB with Pt nanoparticles

Concluding, albeit these are only preliminary studies, the MAX phases proved themselves to be a valid support for the electrooxidation of ethanol, albeit more in-depth exams are needed to validate these results.

5. Conclusions

In this work we followed two different branches, corresponding to two different types of ceramic powders, to find a valid anodic support for the oxidation of ethanol in a DEFC.

Firstly we investigated the best path to obtain TiOxC1-x powders with defined stoichiometry and large surface area (> 100 m^2g^{-1}). In order to obtain high porosity and an acceptable stoichiometric control, we have adopted two different molecular approaches: one starts from a nanostructured template made of elemental carbon that is impregnated with a titanium dioxide precursor; the other uses organic precursors as the source for both carbon and titanium dioxide. In the first approach the porosity is determined by the carbon template, in the second one by the production of gaseous by-products from the precursors. The carbon template approach, tough it is very simple in preparation and produces samples with a good stoichiometric control, has the main disadvantage of the low final specific surface area because the pores get flooded by the titanium dioxide precursor limiting the total surface area. The organic precursors approach, instead, led to higher surface areas up to ~250 m^2g^{-1} and the final stoichiometry is acceptable, with the main advantage to be reproducible and scalable simply adjusting the carburization parameters.

The obtained powders were decorated with various nanoparticles to study the electrocatalytic behavior and performances during the oxidation of ethanol. The directions for future studies were outlined, minding that the TiOxC1-x powder is a valid anodic support in the harsh working conditions of a DEFT.

The second branch we explored consists in the vast family of MAX phases. We focused our studies on three compositions, trying to synthetize them with high purity and reproducibility. In a first time we tried to adapt the organic precursors used before tailoring them to the new requirements, but this path proved to be unsuccessful because, in the view of using precursors in aqueous solutions, the contaminations of oxygen were not fully removed, but despite the apparent flop, it could represent an interesting future starting point. Later we covered the more conventional path of solid state sintering, adapting the various parameters to our needs. The research of the right parameters proved itself to be very challenging because the interdependence of them but also time consuming. At the end, we obtained good results in pureness, albeit more studies have to be done in order to optimize the process. The obtained powders were decorated with nanoparticles and the electrochemical properties were briefly investigated. It was only a preliminary study to check if the complex system of support and nanoparticles could work together, leaving lot of room for future studies.

Concluding, all the results (and failures) obtained during the Ph.D. period should be considered as a good platform for the realization of unconventional anodic supports, while additional and exhaustive tests are needed to optimize the performances and stability at the operative conditions, searching for the maximum efficiency of new generation DEFC.

6. Literature

1. Badwal, S.P.S., et al., *Direct ethanol fuel cells for transport and stationary applications – A comprehensive review.* Applied Energy, 2015. **145**: p. 80-103.
2. Balat, M., *Production of bioethanol from lignocellulosic materials via the biochemical pathway: A review.* Energy Conversion and Management, 2011. **52**(2): p. 858-875.
3. Kim, S. and B.E. Dale, *Global potential bioethanol production from wasted crops and crop residues.* Biomass and Bioenergy, 2004. **26**(4): p. 361-375.
4. Limayem, A. and S.C. Ricke, *Lignocellulosic biomass for bioethanol production: Current perspectives, potential issues and future prospects.* Progress in Energy and Combustion Science, 2012. **38**(4): p. 449-467.
5. Mielenz, J.R., *Ethanol production from biomass: technology and commercialization status.* Current Opinion in Microbiology, 2001. **4**(3): p. 324-329.
6. Sarkar, N., et al., *Bioethanol production from agricultural wastes: An overview.* Renewable Energy, 2012. **37**(1): p. 19-27.
7. Camargo, A.P.M.C., et al., *Effect of temperature of the electro-oxidation of ethanol on platinum.* Quimica Nova, 2010. **33**(10): p. 2143-2147.
8. Reimer, U., B. Schumacher, and W. Lehnert, *Accelerated Degradation of High-Temperature Polymer Electrolyte Fuel Cells: Discussion and Empirical Modeling.* Journal of the Electrochemical Society, 2014. **162**(1): p. F153-F164.
9. Honji, A., et al., *Agglomeration of Platinum Particles Supported on Carbon in Phosphoric Acid.* Electrochemical Science and Technology, 1988. **135**(2): p. 355-359.
10. *Hydrogen Energy*. Available from: http://www.hydrogen.energy.gov/pdfs/program_plan2011.pdf.
11. Christner, L.G., et al., *Corrosion of Graphite Composites in Phosphoric Acid Fuel Cells.* Corrosion, 1987. **43**: p. 571-575.
12. Bashyam, R.Z., P., *A class of non-precious metal composite catalysts for fuel cells.* Nature, 2006. **443**: p. 63-66.
13. Gasteiger, H.A., et al., *Electrocatalysis and catalyst degradation challenges in proton exchange membrane fuel cells.* Hydrogen and fuel cells. fundamentals, technologies, and applications. Wiley-VCH, Weinheim, 2010: p. 3-16.
14. *DECORE*. Available from: http://decore.eucoord.com/.
15. G. P. Shveikin, B.V.S., *Oxidation of titanium oxycarbides, carbonitrides, and oxynitrides.* Poroshkovaya Metallurgiya, 1970. **2**(86): p. 63-68.
16. *Vulcan XC-72*. Available from: http://www.cabot-corp.com/Specialty-Carbon-Blacks/Products/PR200809231124AM7994/.
17. *Imerys Ensaco 350G*. Available from: http://www.imerys-graphite-and-carbon.com/wordpress/wp-app/uploads/2014/04/Polymer_compounds1.pdf.
18. Neumann, G., R. Kieffer, and P. Ettmayer, *Über das System TiC−TiN−TiO.* Monatshefte fur Chemie, 1972. **103**: p. 1130-1137.
19. Brunauer, S., P.H. Emmett, and E. Teller, *Adsorption of Gases in Multimolecular Layers.* Journal of the American Chemical Society, 1938. **60**(2): p. 309-319.
20. Ignaszak, A., et al., *Titanium carbide and its core-shelled derivative TiC@TiO 2 as catalyst supports for proton exchange membrane fuel cells.* Electrochimica Acta, 2012. **69**: p. 397-405.

21. Calvillo, L., et al., *Electrochemical Behavior of TiOxCy as Catalyst Support for Direct Ethanol Fuel Cells at Intermediate Temperature: From Planar Systems to Powders.* Applied Materials and Interfaces, 2015. **8**(1): p. 716-725.
22. Dewan, M.A.R., G. Zhang, and O. Ostrovski, *Carbothermal Reduction of Titania in Different Gas Atmospheres.* Metallurgical and Materials Transactions B, 2008. **40**(1): p. 62-69.
23. Berger, L.M., *Titanium carbide synthesis from titanium dioxide and carbon black.* Journal of Hard Materials(UK), 1992. **3**(1): p. 3-15.
24. Borovinskaya, I.P., et al., *Self-propagating high-temperature synthesis of ultrafine and nanometer-sized TiC particles.* Inorganic Materials, 2007. **43**(11): p. 1206-1214.
25. Gotoh, Y., et al., *Synthesis of titanium carbide from a composite of TiO2 nanoparticles-methyl cellulose by carbothermal reduction.* Materials Research Bulletin, 2001. **36**: p. 2263-2275.
26. Zhang, H., et al., *Preparation of titanium carbide powders by sol–gel and microwave carbothermal reduction methods at low temperature.* Journal of Sol-Gel Science and Technology, 2008. **46**(2): p. 217-222.
27. Preiss, H., L.M. Berger, and D. Schultze, *Studies on the Carbothermal Preparation of Titanium Carbide from Different Gel Precursors.* journal of the European Ceramic Society, 1999. **19**: p. 195-206.
28. Shin, Y., et al., *Synthesis of Hierarchical Titanium Carbide from Titania-Coated Cellulose Paper.* Advanced Material, 2004. **16**(14): p. 1212-1215.
29. B. Sun, T.F., D. Zhang, *Porous TiC Ceramics Derived from Wood Template.* Journal of Porous Materials, 2002. **9**: p. 275-277.
30. Jiang, B., et al., *Thermodynamic Study of Titanium Oxycarbide.* Metallurgical and Materials Transactions A, 2012. **43**(10): p. 3510-3514.
31. Flaherty, D.W., et al., *Low Temperature Synthesis and Characterization of Nanocrystalline Titanium Carbide with Tunable Porous Architectures.* Chemistry of Materials, 2010. **22**(2): p. 319-329.
32. Borchardt, L., et al., *Preparation and application of cellular and nanoporous carbides.* Chem Soc Rev, 2012. **41**(15): p. 5053-67.
33. Preiss, H., E. Schierhorn, and K.W. Brzezinka, *Synthesis of polymeric titanium and zirconium precursors and preparation of carbide fibres and films.* Journal of Materials Science, 1998. **33**: p. 4697-4706.
34. Shimada, S. and M. Kozeki, *Oxydation of TiC at low temperatures.* Journal of Materials Science, 1992. **27**: p. 1869-1875.
35. Shimada, S., *A thermoanalytical study of oxidation of TiC by simultaneous TGA-DTA-MS analysis.* Journal of Materials Science, 1996. **31**: p. 673-677.
36. Chappé, J.M., et al., *Analysis of multifunctional titanium oxycarbide films as a function of oxygen addition.* Surface and Coatings Technology, 2011. **206**: p. 2525-2534.
37. Popovska, N., et al., *Paper derived biomorphic porous titanium carbide and titanium oxide ceramics produced by chemical vapor infiltration and reaction (CVI-R).* Journal of the European Ceramic Society, 2005. **25**(6): p. 829-836.
38. Zhang, G. and O. Ostrovski, *Reduction of titania by methane-hydrogen-argon gas mixture.* Metallurgical and Materials Transactions B, 2000. **31B**: p. 129-139.
39. Zhang, G. and O. Ostrovski, *Kinetic modeling of titania reduction by a methane-hydrogen-argon gas mixture.* Metallurgical and Materials Transactions B, 2001. **32B**: p. 465-473.
40. Calvillo, L., et al., *Carbothermal Transformation of TiO2 into TiOxCy in UHV: Tracking Intrinsic Chemical Stabilities.* The Journal of Physical Chemistry C, 2014. **118**(39): p. 22601-22610.

41. Wang, Y., et al., *Preparation of Tractable Platinum, Rhodium, and Ruthenium Nanoclusters with Small Particle Size in Organic Media.* Chemistry of Materials, 2000. **12**(6): p. 1622-1627.
42. Zhu, M., G. Sun, and Q. Xin, *Effect of alloying degree in PtSn catalyst on the catalytic behavior for ethanol electro-oxidation.* Electrochimica Acta, 2009. **54**: p. 1511-1518.
43. Zhaolin, L., et al., *Microwave heated polyol synthesis of carbom-supported PtSn nanoparticles for methanol electrooxidation.* Electrochemistry Communication, 2006. **8**: p. 83-90.
44. Brinker, C.J. and G.W. Scherer, *CHAPTER 2 - Hydrolysis and Condensation I: Nonsilicates*, in *Sol-Gel Science*1990, Academic Press: San Diego. p. 20-95.
45. Gao, X., et al., *Preparation and in-Situ Spectroscopic Characterization of Molecularly Dispersed Titanium Oxide on Silica.* The Journal of Physical Chemistry B, 1998. **102**(29): p. 5653-5666.
46. Brantley, L.R. and A.O. Beckman, *The High Temperature Equilibrium of Titanium Dioxide and Carbon with Titanium Carbide and Carbon Monoxide.* Journal of the American Chemical Society, 1930. **52**(10): p. 3956-3962.
47. Fernandes, A.C., et al., *The effect of bombarding conditions on the properties of multifunctional Ti–C–O thin films grown by magnetron sputtering.* Surface and Coatings Technology, 2007. **202**(4–7): p. 946-951.
48. Zhang, L. and R.V. Koka, *A study on the oxidation and carbon diffusion of TiC in alumina–titanium carbide ceramics using XPS and Raman spectroscopy.* Materials Chemistry and Physics, 1998. **57**(1): p. 23-32.
49. Yoshitake, H. and D. Abe, *Raman spectroscopic study of the framework structure of amorphous mesoporous titania.* Microporous and Mesoporous Materials, 2009. **119**(1–3): p. 267-275.
50. Ymeris. *Carbon-based solutions for catalysts - Product portfolio*. 2015; Available from: http://www.imerys-graphite-and-carbon.com/wordpress/wp-app/uploads/2015/09/IMERYS_leaflets_Catalysts.pdf.
51. A. Maitre, D.T., P. Lefort, *Role of some technological parameters during carburizing titanium dioxide.* Journal of the European Ceramic Society, 2000. **20**: p. 15-22.
52. Krabbes, G. and D.V. Hoanh, *Heterogene Gleichgewichte und chemische Transportreaktionen im System Ti-O-C-Cl.* Zeitschrift für anorganische und allgemeine Chemie, 1988. **562**(1): p. 62-72.
53. Patterson, A.L., *The Scherrer Formula for X-Ray Particle Size Determination.* Physical Review, 1939. **56**(10): p. 978-982.
54. Song, S., et al., *Direct ethanol PEM fuel cells: The case of platinum based anodes.* International Journal of Hydrogen Energy, 2005. **30**(9): p. 995-1001.
55. Borbáth, I., et al., *Controlled Synthesis of Pt3Sn/C Electrocatalysts with Exclusive Sn–Pt Interaction Designed for Use in Direct Methanol Fuel Cells.* Topics in Catalysis, 2013. **56**(11): p. 1033-1046.
56. Cantane, D.A. and E.R. Gonzalez, *Chemical Selectivity during the Electro-Oxidation of Ethanol on Unsupported Pt Nanoparticles.* Journal of the Electrochemical Society, 2012. **159**(3): p. B355-B359.
57. Jiang, L., et al., *Structure and chemical composition of supported Pt–Sn electrocatalysts for ethanol oxidation.* Electrochimica Acta, 2005. **50**(27): p. 5384-5389.
58. Jiang, L., et al., *Effects of Treatment in Different Atmosphere on Pt3Sn-C Electrocatalysts for Ethanol Electro-oxidation.* Energy & Fuels, 2004. **18**: p. 866-871.
59. Kim, J.H., et al., *Influence of Sn content on PtSn/C catalysts for electrooxidation of C1–C3 alcohols: Synthesis, characterization, and electrocatalytic activity.* Applied Catalysis B: Environmental, 2008. **82**(1-2): p. 89-102.
60. Léger, J.M., et al., *How bimetallic electrocatalysts does work for reactions involved in fuel cells?* Electrochimica Acta, 2005. **50**(25-26): p. 5118-5125.

61. Lim, D.-H., et al., *A new synthesis of a highly dispersed and CO tolerant PtSn/C electrocatalyst for low-temperature fuel cell; its electrocatalytic activity and long-term durability.* Applied Catalysis B: Environmental, 2009. **89**(3-4): p. 484-493.
62. Liu, B., et al., *A General Protocol for the Synthesis of Pt-Sn/C Catalysts for the Ethanol Electrooxidation Reaction.* Fuel Cells, 2012. **12**(4): p. 670-676.
63. Liu, Z., et al., *Microwave heated polyol synthesis of carbon-supported PtSn nanoparticles for methanol electrooxidation.* Electrochemistry Communications, 2006. **8**(1): p. 83-90.
64. Rodrigues da Silva, M. and A.C.D. Ângelo, *Synthesis and Characterization of Ordered Intermetallic Nanostructured PtSn/C and PtSb/C and Evaluation as Electrodes for Alcohol Oxidation.* Electrocatalysis, 2010. **1**(2-3): p. 95-103.
65. Shen, S.Y., T.S. Zhao, and J.B. Xu, *Carbon supported PtRh catalysts for ethanol oxidation in alkaline direct ethanol fuel cell.* International Journal of Hydrogen Energy, 2010. **35**(23): p. 12911-12917.
66. Wang, Y., et al., *Understanding the electrocatalytic activity of PtxSny in direct ethanol fuel cells.* Journal of Power Sources, 2011. **196**(11): p. 4980-4986.
67. Zhou, W., et al., *Pt based anode catalysts for direct ethanol fuel cells.* Applied Catalysis B: Environmental, 2003. **46**(2): p. 273-285.
68. Zhou, W.J., et al., *Direct ethanol fuel cells based on PtSn anodes: the effect of Sn content on the fuel cell performance.* Journal of Power Sources, 2005. **140**(1): p. 50-58.
69. Zhu, M., G. Sun, and Q. Xin, *Effect of alloying degree in PtSn catalyst on the catalytic behavior for ethanol electro-oxidation.* Electrochimica Acta, 2009. **54**(5): p. 1511-1518.
70. Sun, B., et al., *The synthesis and microstructure of morph-genetic TiC/C ceramics.* Carbon, 2004. **42**(1): p. 177-182.
71. H. Preiss, L.M.B.a.D.S., *Studies on the Carbothermal Preparation of Titanium Carbide from Different Gel Precursors.* Journal of the European Ceramic Society, 1999. **19**: p. 195-206.
72. Preiss, H., *Synthesis of polymeric titanium and zirconium precursors and preparation of carbide fibres and films.* Journal of Materials Science, 1998. **33**: p. 4697-4706.
73. Rimdusit, S., et al., *Biodegradability and property characterizations of Methyl Cellulose: Effect of nanocompositing and chemical crosslinking.* Carbohydrate Polymers, 2008. **72**(3): p. 444-455.
74. Zohuriaan, M.J. and F. Shokrolahi, *Thermal studies on natural and modified gums.* Polymer Testing, 2004. **23**(5): p. 575-579.
75. Bostwick, C.O., *Water Soluble Group IV-A Metal Esters of Amino Alcohols and Their Preparation*, in *18/02/1958*1958: United States of America. p. 3.
76. A. E. Schweizer, G.T.K., *Thermal Decomposition of Hexachloroplatinic Acid.* Inorganic Chemistry, 2326-2327. **17**(8): p. 2326.
77. Barsoum, M.; Available from: http://max.materials.drexel.edu/research-areas/max-phases/.
78. Radovic, M. and M.W. Barsoum, *MAX phases: Bridging the gap between metals and ceramics.* American Ceramic Society Bulletin, 2013. **92**(3): p. 20-27.
79. Sun, Z.M., *Progress in research and development on MAX phases: a family of layered ternary compounds.* International Materials Reviews, 2013. **56**(3): p. 143-166.
80. Högberg, H., et al., *Growth and characterization of MAX-phase thin films.* Surface and Coatings Technology, 2005. **193**(1–3): p. 6-10.
81. Zhou, Y.C., et al., *Electronic and structural properties of the layered ternary carbide Ti3AlC2.* Journal of Materials Chemistry, 2001. **11**(9): p. 2335-2339.
82. Suganuma, K., G. Sasaki, and T. Fujita, *Mechanical properties and microstructures of machinable silicon carbide.* Journal of Materials Science, 1993. **28**: p. 1175-1181.

83. Koc, R., *Kinetics and Phase Evolution During Carbothermal Synthesis of Titanium Carbide from Carbon-Coated Titania Powder.* Journal of the European Ceramic Society, 1997. **17**: p. 1309-1315.
84. Kanthal. *Maxthal Ceramic Engineering Material*. Available from: http://www.kanthal.com/en/products/furnace-products-and-heating-systems/refractory-material/.
85. Hashimoto, S., et al., *Pressureless sintering and mechanical properties of titanium aluminum carbide.* Materials Letters, 2008. **62**(10-11): p. 1480-1483.
86. Lu, X. and Y. Zhou, *Pressureless Sintering and Properties of Ti3AlC2.* International Journal of Applied Ceramic Technology, 2010. **7**(6): p. 744-751.
87. Barsoum, M.W. and T. El-Raghy, *Synthesis and Characterization of a Remarkable Ceramic: Ti3SiC2.* Journal of American Ceramic Society, 1996. **79**(7): p. 1953-1956.
88. Barsoum, M.W., *The M(N+1)AX(N) Phases: A New Class of Solids.* Progress in Solid State Chemistry, 2000. **28**: p. 201-281.
89. Yin, X.H., et al., *Diffusion bonding of Ti3AlC2 ceramic via a Si interlayer.* Journal of Materials Science, 2007. **42**(17): p. 7081-7085.
90. Zhang, Z.F., et al., *Application of pulse discharge sintering (PDS) technique to rapid syntesis of Ti3SiC2 from Ti Si C powders.* Journal of European Ceramic Society, 2002. **22**: p. 2957-2961.
91. Sun, Z., et al., *Synthesis of the MAX Phases by Pulse Discharge Sintering.* International Journal of Applied Ceramic Technology, 2010. **7**(6): p. 704-718.
92. Zhang, Z.F., et al., *Effects of sintering temperature and Si content on the purity of Ti3SiC2 synthesized from Ti/Si/TiC powders.* Journal of Alloys and Compounds, 2003. **352**(1-2): p. 283-289.
93. Palmquist, J.P., et al., *Mn+1AXn phases in theTi−Si−C system studied by thin-film synthesis and ab initio calculations.* Physical Review B, 2004. **70**(16).
94. Wilhelmsson, O., *Synthesis and Characterization of Ternary Carbide Thin Films*, in *Faculty of Science and Technology*2007, Uppsala Universitet.
95. Istomin, P., A. Nadutkin, and V. Grass, *Combustion synthesis of Ti3SiC2-based ceramic matrix composites using non-powder reactant solids.* High Temperature Ceramic Matrix Composites 8, 2014. **248**: p. 515-521.
96. Ma, Y., et al., *Fabrication of MAX-phase-based ceramics by three-dimensional printing.* Journal of Ceramic Science and Technology, 2015. **06**(02): p. 87-94.
97. Ma, Y., et al., *Near-Net-Shape Fabrication of Ti3SiC2-based Ceramics by Three-Dimensional Printing.* International Journal of Applied Ceramic Technology, 2015. **12**(1): p. 71-80.
98. Yin, X., N. Travitzky, and P. Greil, *Three-Dimensional Printing of Nanolaminated Ti3AlC2 Toughened TiAl3-Al2O3 Composites.* Journal of the American Ceramic Society, 2007. **90**(7): p. 2128-2134.
99. Sun, Z. and Y. Zhou, *Fluctuation synthesis and characterization of Ti3SiC2 powders.* Materials Research Innovations, 1999. **2**: p. 227-231.
100. Hendaoui, A., et al., *Synthesis of high-purity polycrystalline MAX phases in Ti–Al–C system through Mechanically Activated Self-propagating High-temperature Synthesis.* Journal of the European Ceramic Society, 2010. **30**(4): p. 1049-1057.
101. Racault, C., F. Langlais, and R. Naslain, *Solid-state synthesis and characterization of the ternary phase Ti3SiC2.* Journal of Materials Science, 1994. **29**: p. 3384-3392.
102. Hwang, S.S., et al., *Synthesis of Ti3SiC2 by infiltration of molten Si.* Journal of Alloys and Compounds, 2011. **509**(35): p. L336-L339.
103. Liu, X., et al., *Characterization and application of porous Ti3SiC2 ceramic prepared through reactive synthesis.* Materials & Design, 2015. **79**: p. 94-98.

7. Ringraziamenti

Arrivare alla conclusione di tre anni di dottorato con qualcosa che avesse senso non è stato semplice.

Devo per questo ringraziare prima di tutto chi ha reso possibile questa esperienza, cioè il prof. Alex Martucci e il prof. Gaetano Granozzi, sia per avermi seguito durante la tesi magistrale sia per avermi accompagnato durante il dottorato.

Di seguito, ma non per meriti minori, devo ringraziare Stu, Angio, il Bersa, Jimmy ed Elena, cioè il gruppo con cui ho condiviso successi e sfighe di laboratorio e ho discusso su quasi tutto, che fosse scientifico o meno. Devo anche ringraziarli per essere stati compagni non solo di laboratorio ma anche di mille avventure, sia dentro che fuori il laboratorio. Un ringraziamento va anche a Jenny, Elisa, Alessandro e Mattia, che mi hanno permesso di velocizzare il lavoro potendo contare su di loro. Ringrazio anche tutte le persone che mi hanno aiutato o consigliato nei vari anni, tra cui Francesco e Laura di chimica e i tecnici Mauro e Sirio. Per non fare torto a nessuno ringrazio l'intero primo (o secondo, per essere fiscali) piano di Ex Fisica Tecnica, sia perché è la sede del mio laboratorio/seconda casa sia perché è pieno di persone da menzionare. Un ringraziamento è dovuto anche al prof. Massimo Guglielmi, il prof. Moreno Meneghetti e la prof. Marina Gobbo.

Beside them (for my non-Italian friend, "ringraziamenti" means aknowledgments) I have to thank prof. Mathias Arenz and the electrochemistry group from the University of Copenhagen. The short period I spent in Denmark was very useful and interesting because of the knowledge you transmitted to me. But Michael, Alessandro and Matteo deserve some special thanks for guiding me in a foreign state and for the extraordinarly well spent free time.

Ovviamente un ringraziamento va anche alla mia famiglia, che è sempre stata di supporto e incoraggiamento. Inserisco tra di loro anche Emanuele e Laura, che a Padova sono stati un po' la seconda famiglia dall'inizio dell'Università.

Parlando di Università un semplice ringraziamento per gli Studenti Associati non rende giustizia, perché quasi dieci anni sono stati mitici grazie a voi. Se potessi, tornerei indietro per rifare tutto da capo.

Per il dottorato devo anche ringraziare il gruppo Mètis Vela, ex Pr3Sailing, per avermi fatto staccare la spina durante i weekend e le molteplici serate di gruppo, per avermi fatto imparare cose nuove e per avermi dato grandissime soddisfazioni, sia personali che sportive.

Anche se non vuole essere citata ringrazio Clara, perché anche in periodi non proprio tranquilli è stata presente.

Se non ho citato tutti non l'ho fatto per cattiveria, ma perché la memoria è più corta della lista di persone da ringraziare.